BNWL-1395
UC-37

[redacted]

PRELIMINARY ANALYSES FOR FFTF HEAT TRANSPORT CONTROL SYSTEMS

R. A. Harvey and S. A. Hunt

September 1970

[redacted]

AEC RESEARCH & DEVELOPMENT REPORT

BNWL-1395

BATTELLE
BATTELLE MEMORIAL INSTITUTE
NORTHWEST
PACIFIC NORTHWEST LABORATORIES
3000 STEVENS DRIVE, P. O. BOX 999, RICHLAND, WASHINGTON 99352

LEGAL NOTICE

This report was prepared as an account of work sponsored by the United States Government. Neither the United States nor the United States Atomic Energy Commission, nor any of their employees; nor any of their contractors, subcontractors, or their employees, makes any warranty, express or implied, or assumes any legal liability or responsibility for the accuracy, completeness or usefulness of any information, apparatus, product or process disclosed, or represents that its use would not infringe privately owned rights.

PACIFIC NORTHWEST LABORATORY
RICHLAND, WASHINGTON
operated by
BATTELLE MEMORIAL INSTITUTE
for the
UNITED STATES ATOMIC ENERGY COMMISSION UNDER CONTRACT AT(45-1)-1830

ERRATA

Page viii: The third line from the bottom should read

A-19 Mixing Plenum A-35

Pages 16 and 17: A dotted arrow should be added to the thermocouple (TC #1 in circle) from the solid line running from the DHX to the SEC PUMPS.

Page 65: The first measurement on the abscissa should be 0.0001.

Page A-16: Equation 9 should read

$$PL_{LR} = \gamma_{LR}\, PL_{N}$$

Page A-17: Equation 17 should read

$$\frac{dT_{f2}}{dl'} \quad \frac{b\alpha\, PL_{F}}{N_{ER}\,(\overline{\rho V'' C})_{f}} \quad \frac{(UA'')}{(\overline{\rho V'' C})_{f}} \left[T_{f2} \quad T_{CTR}\right]$$

3 3679 00061 6872

BNWL-1395
UC-37, Instruments

PRELIMINARY ANALYSES FOR FFTF HEAT TRANSPORT CONTROL SYSTEMS

R. A. Harvey and S. A. Hunt(a)

September 1970

FIRST UNRESTRICTED DISTRIBUTION MADE

BATTELLE MEMORIAL INSTITUTE
PACIFIC NORTHWEST LABORATORIES
RICHLAND, WASHINGTON 99352

(a) Both are now employed by WADCO Corporation, a Subsidiary of Westinghouse Electric Corporation, under AEC Contract No. AT(45-1)-2170

Printed in the United States of America
Available from
Clearinghouse for Federal Scientific and Technical Information
National Bureau of Standards, U.S. Department of Commerce
Springfield, Virginia 22151
Price: Printed Copy $3.00; Microfiche $0.65

BNWL-1395

PRELIMINARY ANALYSES FOR FFTF HEAT TRANSPORT CONTROL SYSTEMS

R. A. Harvey and S. A. Hunt

ABSTRACT

A study was conducted to determine the effect of the Fast Flux Test Facility main heat transport control system on the plant behavior. A high-speed simulation of the facility was used in the study. The study was conducted to gather data concerning plant stability, characteristics of several control configurations and effects of various operating conditions. Transient responses and frequency analysis were used to determine the controlled plant behavior. This report presents the data gathered and draws some conclusions on the basis of the data.

TABLE OF CONTENTS

LIST OF FIGURES

LIST OF TABLES

PRELIMINARY ANALYSES FOR FFTF HEAT TRANSPORT CONTROL SYSTEMS

R. A. Harvey and S. A. Hunt

INTRODUCTION

A study of control systems for the Fast Flux Test Facility heat transport system was started in order to develop a capability for auditing control system designs, develop information useful for safety considerations, and develop information useful during the operational phase of the facility. Also, some of the information should be useful in making design decisions for the facility.

The Fast Flux Test Facility (FFTF) is being designed for the Atomic Energy Commission's Liquid Metal Fast Breeder Reactor Program, a program aimed at developing efficient energy sources for the generation of electric power. The FFTF is being designed with a 400 MW sodium-cooled reactor capable of providing a suitable environment for tests on reactor materials and fuels. The heat transport system has three heat removal circuits, each with a primary sodium cooled loop that supplies heat to a secondary sodium coolant loop through an intermediate heat exchanger. The heat is removed from each secondary loop through a number of sodium-to-air heat exchangers.

The results in this report are from a study of control systems for the heat transport system. The study was made with a high-speed hybrid computer model of the heat transport system using an AD-4 analog computer and a PDP-9 digital computer. The study included three phases as follows:

Comparison of the dynamic responses to disturbances for the following six control configurations:

Configuration Number	Controlled Variables	Manipulated Variables
I (Figure 2)	2.* Pri. Cold Leg Sodium Temp	Air Flow
	3. Pri. Hot Leg Sodium Temp	Pri. Flow
II (Figure 3)	1. Sec. Cold Leg Sodium Temp	Air Flow
	2. Pri. Cold Leg Sodium Temp	Setpoint of 1
	3. Pri. Hot Leg Sodium Temp	Pri. Flow
III (Figure 4)	1. Sec. Cold Leg Sodium Temp	Air Flow
	2. Pri. Cold Leg Sodium Temp	Setpoint of 1
	5. Reac. Sodium Temp Rise	Pri. Flow
IV (Figure 5)	1. Sec. Cold Leg Sodium Temp	Air Flow
	4. Reac. Avg. Sodium Temp	Setpoint of 1
	5. Reac. Sodium Temp Rise	Pri. Flow
V (Figure 6)	1. Sec. Cold Leg Sodium Temp	Air Flow
	2. Pri. Cold Leg Sodium Temp	Sec. Flow
	3. Pri. Hot Leg Sodium Temp	Pri. Flow
VI (Figure 7)	2. Pri. Cold Leg Sodium Temp	Air Flow
	3. Pri. Hot Leg Sodium Temp	Reactivity

- Comparison of the dynamic responses to disturbances for a single control configuration for various different operating condition assumptions for:
  - Power Level (full, 2/3, and 1/3)
  - Primary flow (full, 2/3, and 1/3)
  - Secondary flow (full, 2/3, and 1/3)
  - Air temperature (100 °F, 32 °F, and -25 °F).
- Investigation of trends associated with controller adjustments for a single control configuration.

The purpose of this report is to present the results of the FFTF control systems study along with recommendations relevant to the control system performance. The report includes a summary of results with recommendations; a discussion which includes a description of the performance measures, the model,

---

* *The numbers are controller numbers assigned according to the controlled variables and are consistently used throughout the report.*

control configuration effects, operating condition effects, and controller adjustment effects; and an appendix that describes the model in detail.

CONCLUSIONS AND SUMMARY OF RESULTS

Six different control system configurations, shown in Figures 2 through 7 (pages 14-19), were analyzed for performance in reducing the effects of disturbances. This included a one-third power setback disturbance (other control configurations not considered in this study may merit consideration). On the basis of equal weighting between reactor inlet and outlet temperature transients, Configuration II appears equal to or better than the others for most disturbances. This configuration:

- Controls the secondary cold leg temperature by manipulating air flow.
- Controls the primary cold leg temperature by manipulating the setpoint of the secondary cold leg temperature controller.
- Controls the primary hot leg temperature by manipulating the setpoints of primary flow controllers.

While most of the controllers performed about equally for most disturbances, Configuration II gives equal or superior performance for power setbacks. Configurations III and IV might be considered superior depending upon the desirability of reducing reactor inlet temperature variations at the expense of fuel cladding and reactor outlet temperature variations.

The performance of the controlled system is limited by the large time constants and distance/velocity delays in the secondary loop. A control or operating mode that reduces the secondary sodium flow increases the distance/velocity delays even more and thus degrades the performance of the system. Hence, it is recommended that full secondary sodium flow be maintained even at reduced power in order to provide a control system that most effectively reduces transients caused by disturbances.

Several of the configurations automatically reduce the primary flow in order to maintain the primary hot leg temperature at its setpoint value during a setback. This appears to be the most effective way to reduce the reactor outlet nozzle and primary hot leg temperature transients during the power setback.

Power level changes and air temperature changes cause process gain changes, but do not affect the phase characteristics. Compensating gain changes can be made by adjusting the proportional action setting of the controller that manipulates the air flow. Thus, the capability exists to maintain the system performance for most conditions of power and air temperature by a relatively simple adaptive approach.

Most of the configurations analyzed are relatively easy to control; stability seems to be no problem. There are no prominent differences in ease of control between controlling the primary hot leg temperature or the reactor temperature rise. Also, controlling the reactor average temperature is almost as easy as controlling the primary cold leg temperature. All configurations require that the controllers be adjusted iteratively the first time in order to compensate for the interactions between controllers. Transientsdue to setpoint changes require about 10 min to settle out.

The optimum controller settings are functions of both the plant variable being observed and the type of disturbance. While the data are not complete, it seems that primary cold leg temperature controller settings which most effectively reduce reactor inlet temperature transients are not the most effective settings in reducing process tube outlet temperature transients. Primary hot leg temperature controller settings that are optimum in reducing tube outlet temperature transients

due to setpoint changes are not optimum in reducing the tube outlet transients caused by power level changes. It is recommended that a study be made to determine the best controller adjustment policy, taking into account the likelihood of the disturbances and the affected plant variables.

The following conclusions are made in terms of the specific performance measures and configurations:

- Primary Cold Leg Temperature - Configurations III and IV result in lower primary cold leg temperature transients than do I, II, and V during most transients including power setback. Comparison can be seen in Table 2 (page 22.)
- Fuel Coolant Tube Outlet Temperature - Configurations I, II, and V are superior to III and IV in their ability to reduce tube outlet temperature transients. Configurations II and V are better than I for the slow power setback (one-tenth as fast as the fast power setback).
- Primary Hot Leg Temperature - Configurations I, II, and V are superior to III and IV in their ability to reduce tube outlet temperature transients. Configurations II and V are better than I for the slow power setback (one-tenth as fast as the fast power setback).
- Secondary Hot and Cold Leg Temperatures - Configurations II, III, and IV are superior to I and V in reducing the secondary hot and cold leg temperature transients due to power setbacks. Configuration V is particularly bad in this respect (Table 2).
- IHX Mean Temperature Difference - Sufficient data were not taken to define the IHX mean temperature difference at reduced power levels. The most satisfactory control system performance for low power operation, however, is for an operating mode that has full secondary and full primary

flows as can be seen from Table 5 by comparing run 9 with runs 6, 7, and 8. The low power operating mode that results in the least satisfactory control system performance is to have both primary and secondary flow rate reduced (run 7 for 1/3 power and run 3 for 2/3 power).

- Simplicity - Configuration I is probably easier to operate than all the others. Configuration II appears slightly simpler to operate than Configurations III, IV and V. Configuration V results in the most plant variables changing during a transient.
- Control Rod Motion - Configuration VI, which manipulates a control rod, results in more control rod manipulations than any of the other configurations. All of the other configurations maintain constant reactor inlet and outlet sodium temperature by manipulating flow, and thus no rod manipulation is necessary in order to maintain steady state power.
- Effects on Experiments - A good system is considered as one that holds power level and primary hot and cold leg temperatures constant. Since Configuration II best reduces transient effects from disturbances, it is judged to be the best system.
- Ability to Reduce the Number of Scrams - Configuration II is the most effective system in reducing transients caused by disturbances; Therefore, Configuration II is judged to be the best in reducing the number of scrams.
- Costs - It is assumed that variable flow pumps will be used even if the control system does not require sodium flow manipulation; therefore, no cost penalty is assumed to arise from a requirement for flow manipulation. An operating mode that requires the primary cold leg components to be designed for higher temperatures might impose added

costs. Hence, the mode of controlling average reactor temperature might add to the cost (Configuration IV). The other configurations are about equal with each other.

PERFORMANCE MEASURES

A number of performance measures were established for use in evaluating specific control modes and control configurations for the Fast Flux Test Facility. Some relate to the degree to which the system prevents operating temperatures from exceeding the design values and the degree to which temperature transients are prevented or reduced. The temperatures of specific interest are:

- The primary cold leg temperature is important because of the difficulty in repairing the lower core support structure and because of experimental needs.
- The fuel and fuel cladding temperature must remain low enough to prevent fuel failures. The fuel coolant tube outlet temperature was used to provide an indication of fuel cladding temperature transients.
- The primary hot leg temperature is important because of thermal stresses, particularly at the reactor outlet nozzles and because of experimental needs.
- The secondary hot and cold leg temperature transients are of interest because they give an indication of thermal stresses on all secondary loop components and the margin to blockage due to freezing.
- The intermediate heat exchanger (IHX) mean temperature difference between primary and secondary sides provides a measure of stress on the IHX.

Other performance measures relating to things other than temperature are:

- The simplicity which is important to provide easy operator understanding of what is happening during a transient and to provide high reliability, easy maintenance, and easy adjustments.
- The degree to which control requires reactivity adjustment by control rod motion.
- The effect that the control mode and control configuration have on experiments. Neutron flux and power should be held constant.
- The degree to which the number of scrams is reduced by action of the control system.
- The cost of the control equipment and the additional cost of equipment necessary to meet the control requirements.

An additional index of performance (IP) that was used primarily to define controller adjustment effects is the integral of the error (or deviation from steady state) squared. This penalizes for long time deviations and slow return to steady state as well as for large deviations from steady state.

THE MODEL

A simple model of the reactor and heat transport system was developed for use on a hybrid computer which consisted of an AD-4 analog and a PDP-9 digital computer. The simulation using the model is capable of operating at speeds up to 1000 times faster than the real time system. While the simulation is sufficiently accurate for control studies, it is not intended for use in defining shutdown transients. The phase and magnitude characteristics of the model were adjusted to provide a reasonable match with those from more detailed information (see Appendix A).

In order to gain simplicity and reliability for the high speed simulation, a nodal approach was adopted (see Figure 1)

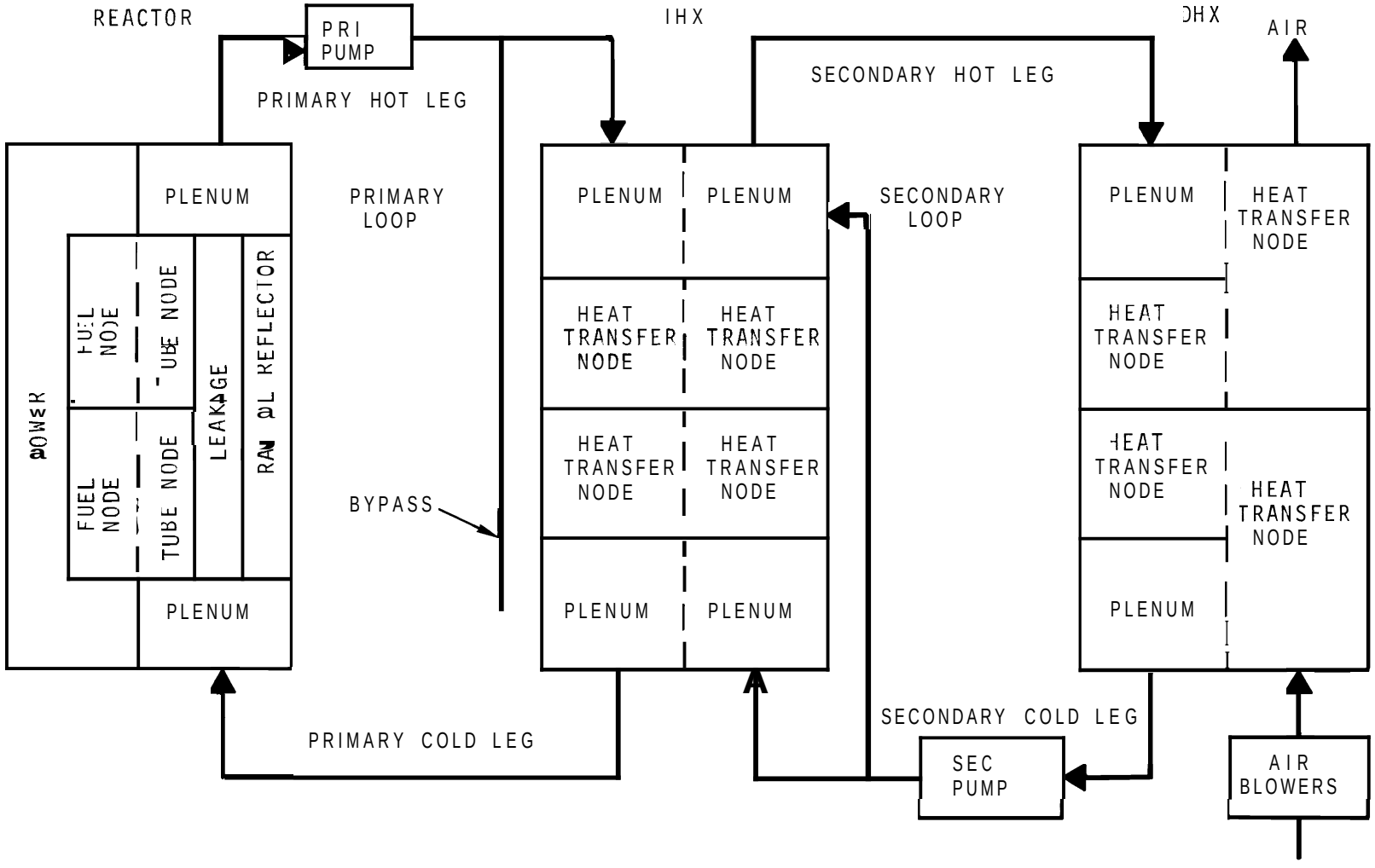

FIGURE 1. **Diagram Showing the Model Nodes and Components in One Heat Removal Circuit. The reactor is common to all heat removal circuits.**

BNWL-1395

which uses as few nodes as possible while maintaining acceptable accuracy. It was determined that two axial nodes would simulate the heat exchange surfaces of the reactor, the IHX, and DHX with sufficient accuracy. Inlet and outlet plena complete the simulation for each of these major components. The reactor kinetics are calculated with three delayed neutron groups and assuming instantaneous prompt neutrons. Doppler feedback from the fuel temperature as well as fission product heat is included. Primary and secondary loop flow dynamic characteristics are simulated by fitting a first order lag that approximates the characteristics from more detailed information. One heat transport system representing all three circuits was simulated.

The reactor vessel inlet plenum model simulates a volume of 975 ft^3 with a first order system time constant that is a function of reactor sodium flow. This inlet volume yields a mixing time constant of about 10 sec at full reactor flow. About 80% of the flow from the inlet plenum passes through the two similar fuel nodes. Approximately 15% of the flow is for vessel and shield cooling and hydraulic holddown where little heat is transferred to the sodium. The remaining 5% of the flow is for radial reflector cooling. The heat from these three flow paths aid in the vessel outlet plenum which has a simulated volume of 1000 ft^3. The outlet plenum is simulated also by a first order system with a time constant that is a function of reactor flow (approximately 10 sec at full flow).

The hot and cold leg pipes are simulated as pure distance/velocity lags on the digital computer with no heat transferred to or from the sodium. The number of nodes are:

Leg	No. of Nodes	Full Flow Time Delay, sec
Primary hot	20	36
Primary cold	8	14
Secondary hot	22	41
Secondary cold	25	47

The first order approximation for the intermediate heat exchanger (IHX) primary inlet plenum has a full flow time constant of 1.5 sec. The IHX primary outlet plenum, also simulated with a first order approximation, has a full flow time constant of about 2 sec.

The heat transfer between the primary and secondary side of the IHX is simulated as two nodes for each side. The first node (in direction of flow) calculation uses a central difference technique while the second node uses the three point back technique. This method of representing the heat transfer process was found to give good dynamic as well as steady-state results under balanced flow conditions. The steady-state results under widely unbalanced flows were not as satisfactory, however. It is not felt that this inaccuracy in steady state is an indication of inaccurate dynamic results. The secondary side of the IHX is similar to the primary side. The only thing that distinguishes one side of the IHX from the other is a small difference in parameters. The time constant for the IHX secondary inlet plenum is about 4 sec, while that for the outlet plenum is about 2 sec. IHX bypass flows of 5% for the primary and 2.5% for the secondary sides are assumed.

The dump heat exchanger (DHX) sodium side calculation has the same form as the IHX primary side calculation, except that the DHX has no bypass flow. However, parameters for the DHX, such as the heat transfer coefficient, are significantly different from those of the IHX. The full flow time constants for the DHX sodium plena, both inlet and outlet, are about 1.5 seconds.

The air side of the DHX uses 100 °F air directly in the heat transfer calculations, unless air temperature is varied as a parameter. No air plena are simulated. The heat transfer calculation for the DHX uses the same finite differencing method as

is used for the IHX and the sodium side of the DHX. The parameters are such that the air side of the DHX has very short time constants in relation to the rest of the process. These time constants are so short in fact that an algebraic solution could be used with no appreciable loss of accuracy.

The frequency response of the primary coolant, coolant pump, and motor were determined from a more detailed simulation. This frequency response demonstrated that a first order lag with a 2.27 sec time constant is sufficiently accurate for the representation of primary flow response from pump motor signal changes. Flow rate of change limitations were not included in the model.

CONTROLLER CONFIGURATION EFFECTS

Five different controller system configurations, as described in the introduction, were studied in order to attain information on control system configurations. A series of computer runs was made to determine if it is desirable to:

- Control the primary cold leg with a cascade system which includes a fast inner loop to control the secondary cold leg temperature (Configurations I and II).
- Control the reactor temperature rise instead of the primary hot leg temperature (Configurations II and III).
- Control the reactor average temperature instead of the primary cold leg temperature (Configurations III and IV).
- Control the primary cold leg temperature by manipulating the secondary flow instead of manipulating the setpoint of controller number 1 (Configurations II and V).

A sixth control configuration was studied to determine if it is desirable from the transient response viewpoint to control the primary hot leg temperature by manipulating the reactivity instead of the primary flow.

The controller configurations are shown in Figures 2 through 7. Figure 2 indicates that the temperature measurement for the primary cold-leg sodium temperature is measured at the primary outlet of the intermediate heat exchanger (IHX). In some of the controller configurations the phase shift added by the primary cold leg distance/velocity lag has noticeable effects, hence for consistency, the IHX primary outlet sodium temperature is used for the primary cold leg temperature for all configurations.

In this preliminary stability study, the use of flow controllers for directly controlling the sodium and air flow rates were not given consideration. They may or may not be used on the actual system. If they are used, the controllers shown in the diagrams simply manipulate the flow controller set points instead of manipulating directly the actuators. It is reasonable to expect, however, that at least the primary flows will be controlled individually by flow controllers.

A consistent method was used to adjust the controllers for all configurations. Controller number one was adjusted first with controller loops two and three open. When proportional action only was used in controller number one, with control loop number one closed, the controller gain* was adjusted until a 10° step increase in setpoint resulted in about a 20% overshoot in response. If a proportional plus integral action controller was used, the integral action was first set at zero, and the proportional gain was adjusted for a 10% overshoot in response. Then the integral action was increased until the

---

* *Throughout the report, the controller gains include amplitude scale factors for the simulation. Since the scale factors remain unchanged, the controller gains (proportional action) are useful for comparison purposes.*

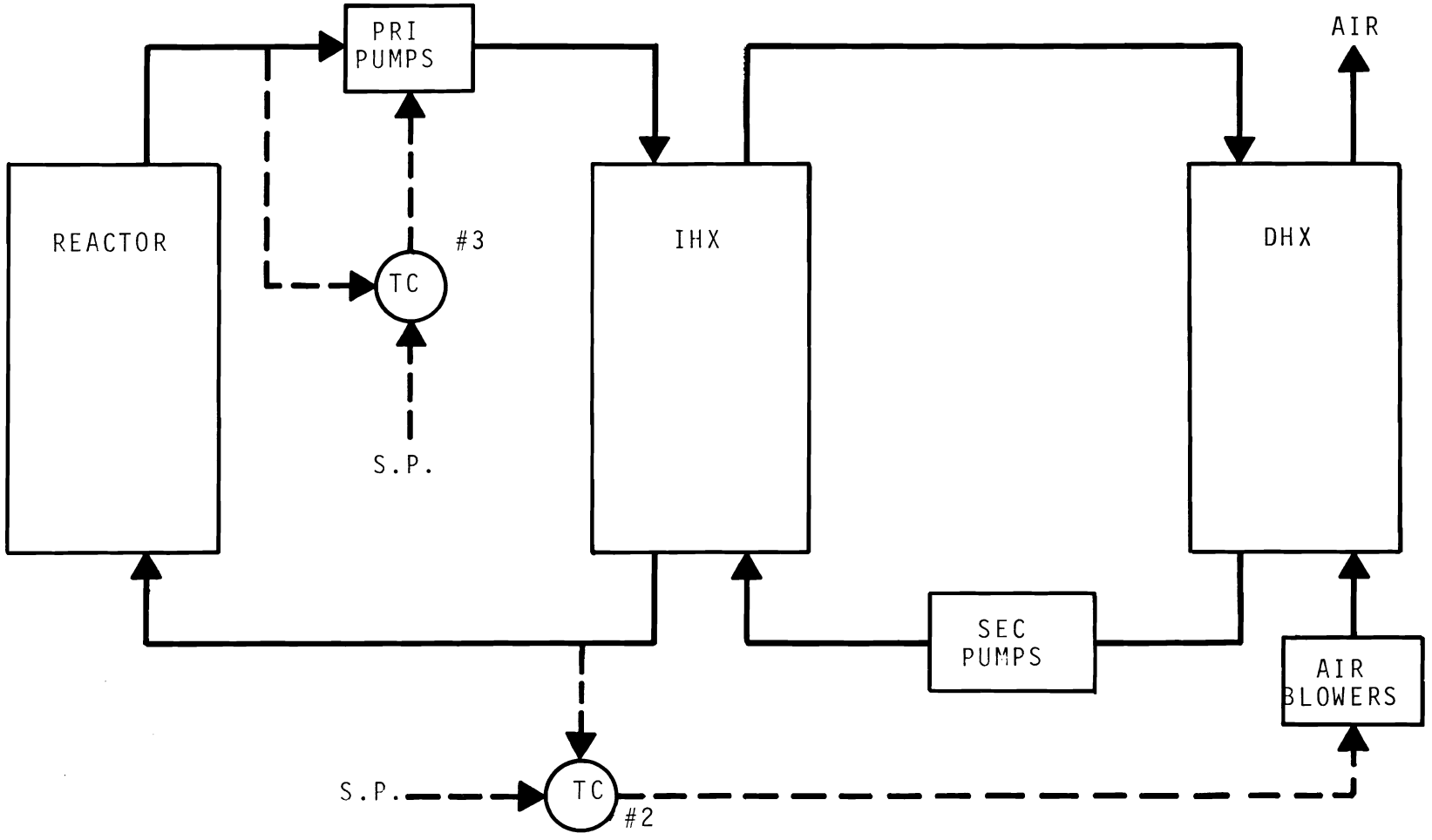

FIGURE 2 Controller Configuration Number I

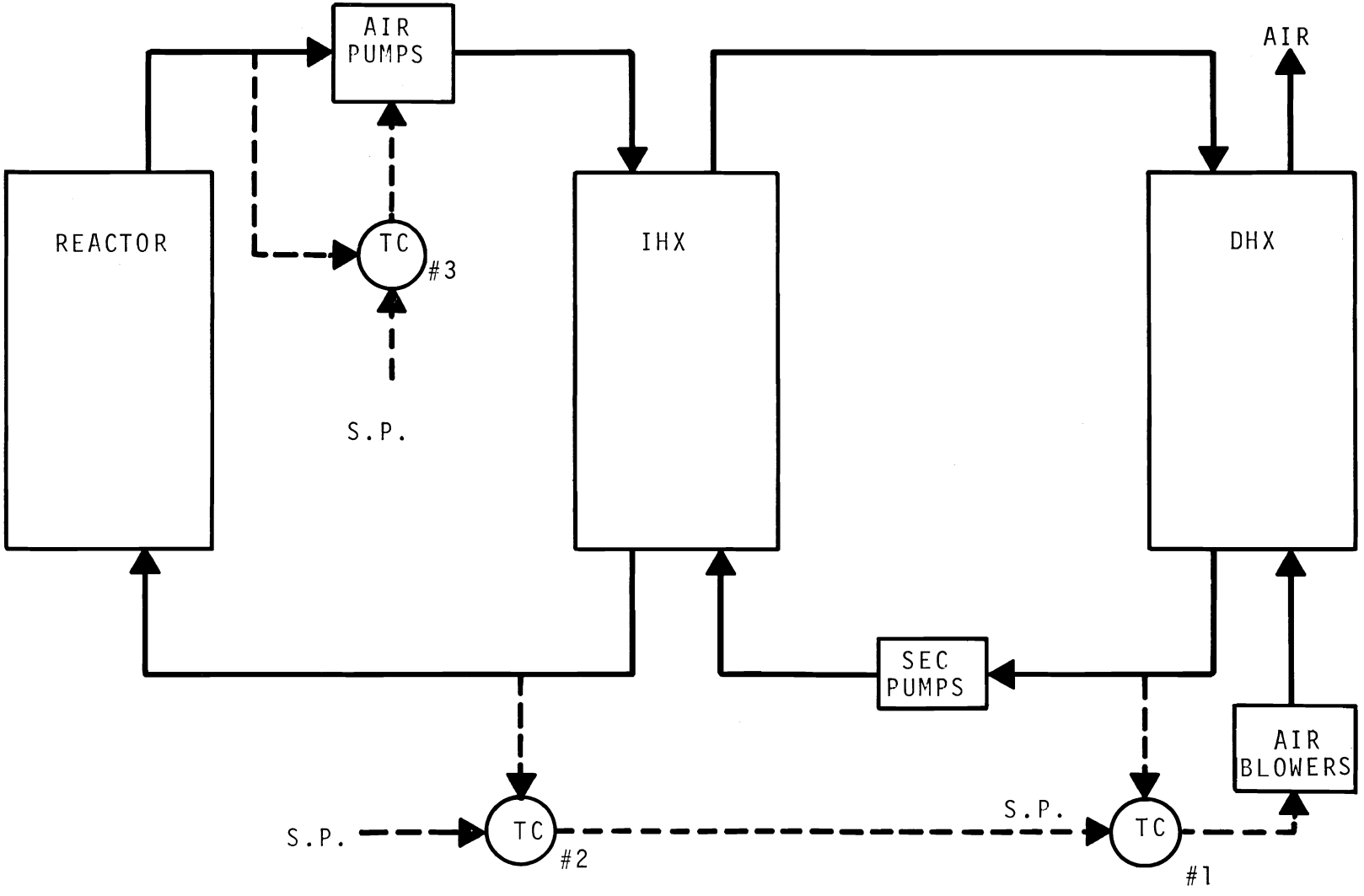

FIGURE 3. Controller Configuration Number II

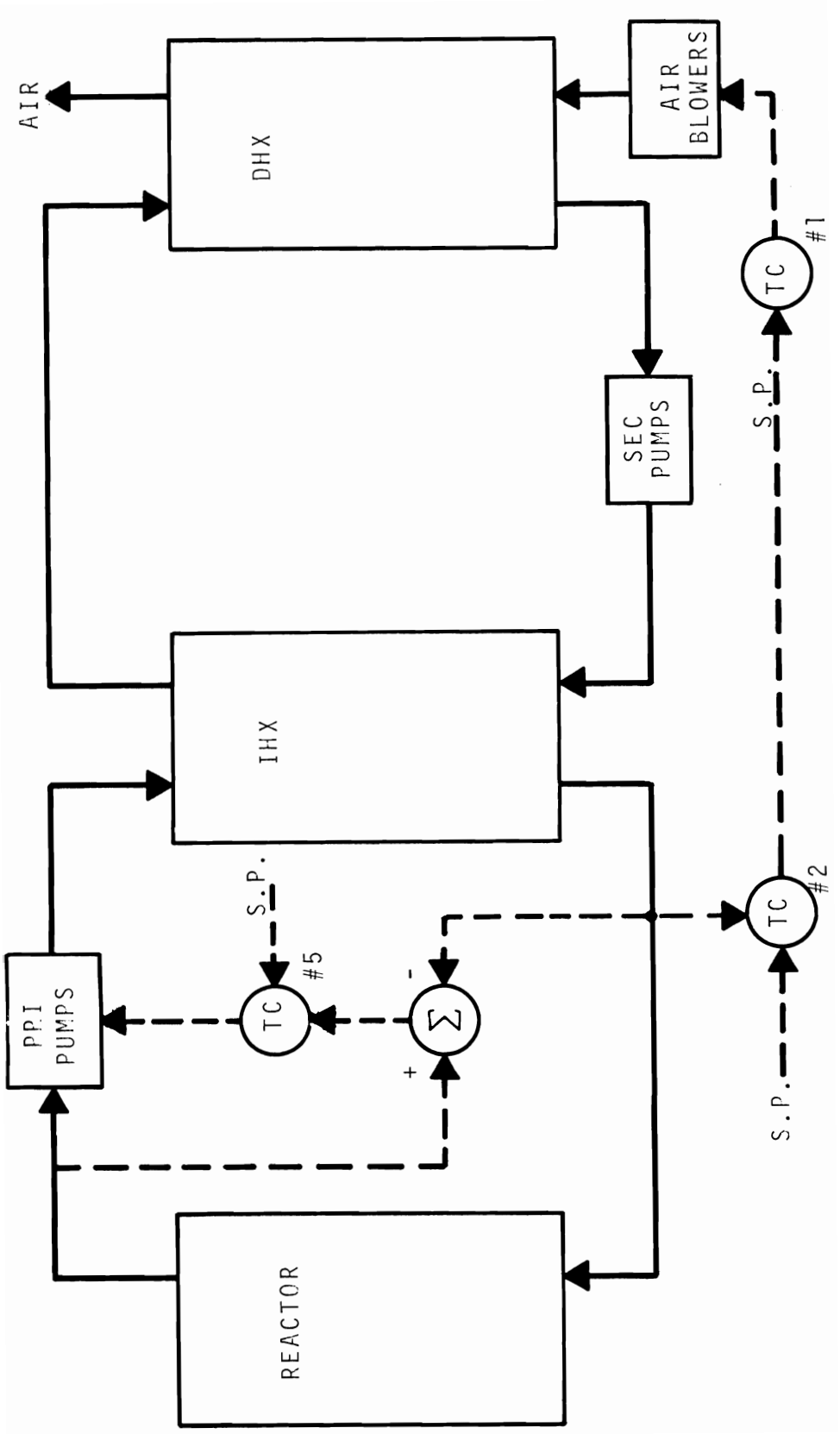

FIGURE 4 Controller Configuration Number III

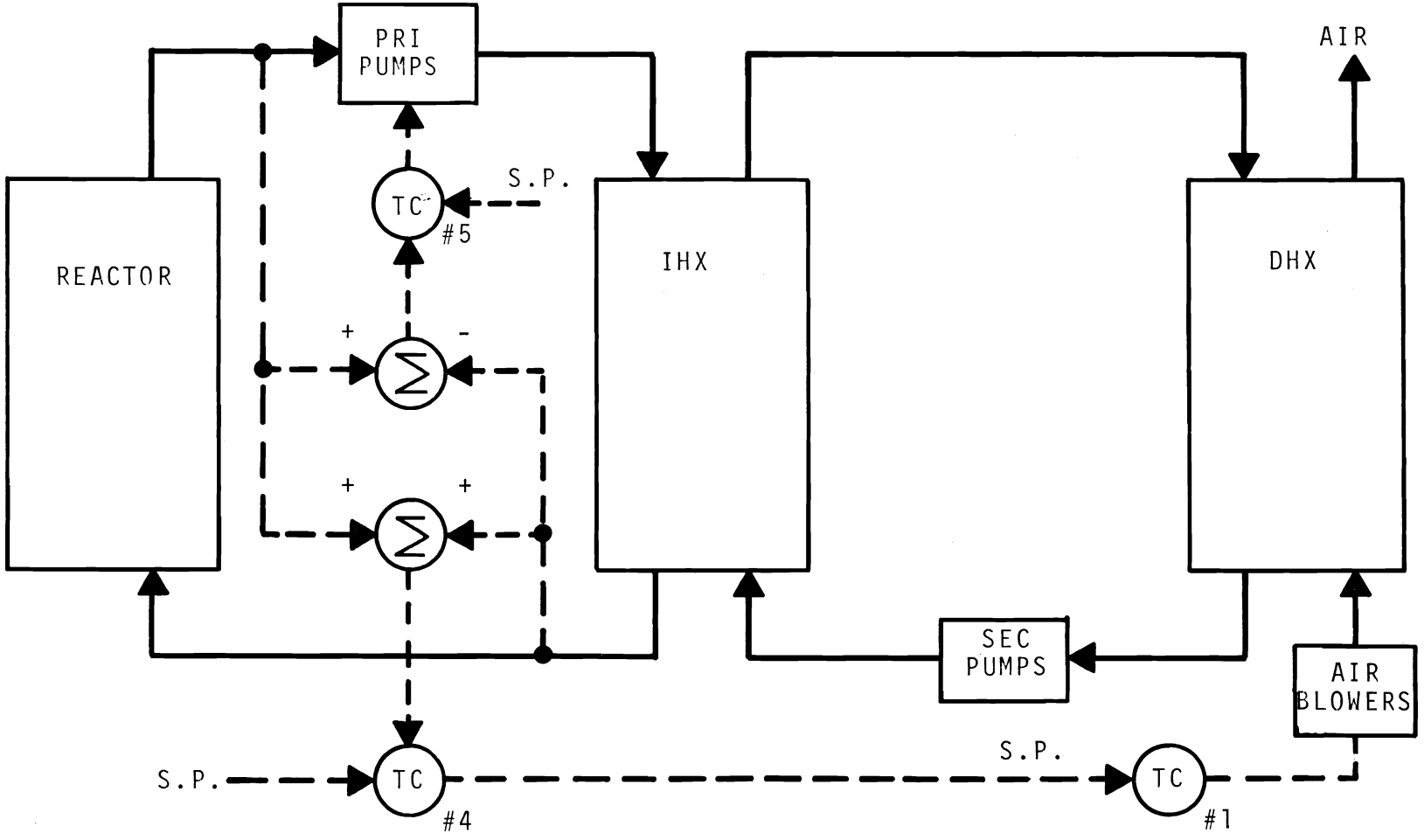

FIGURE 5. Controller Configuration Number IV

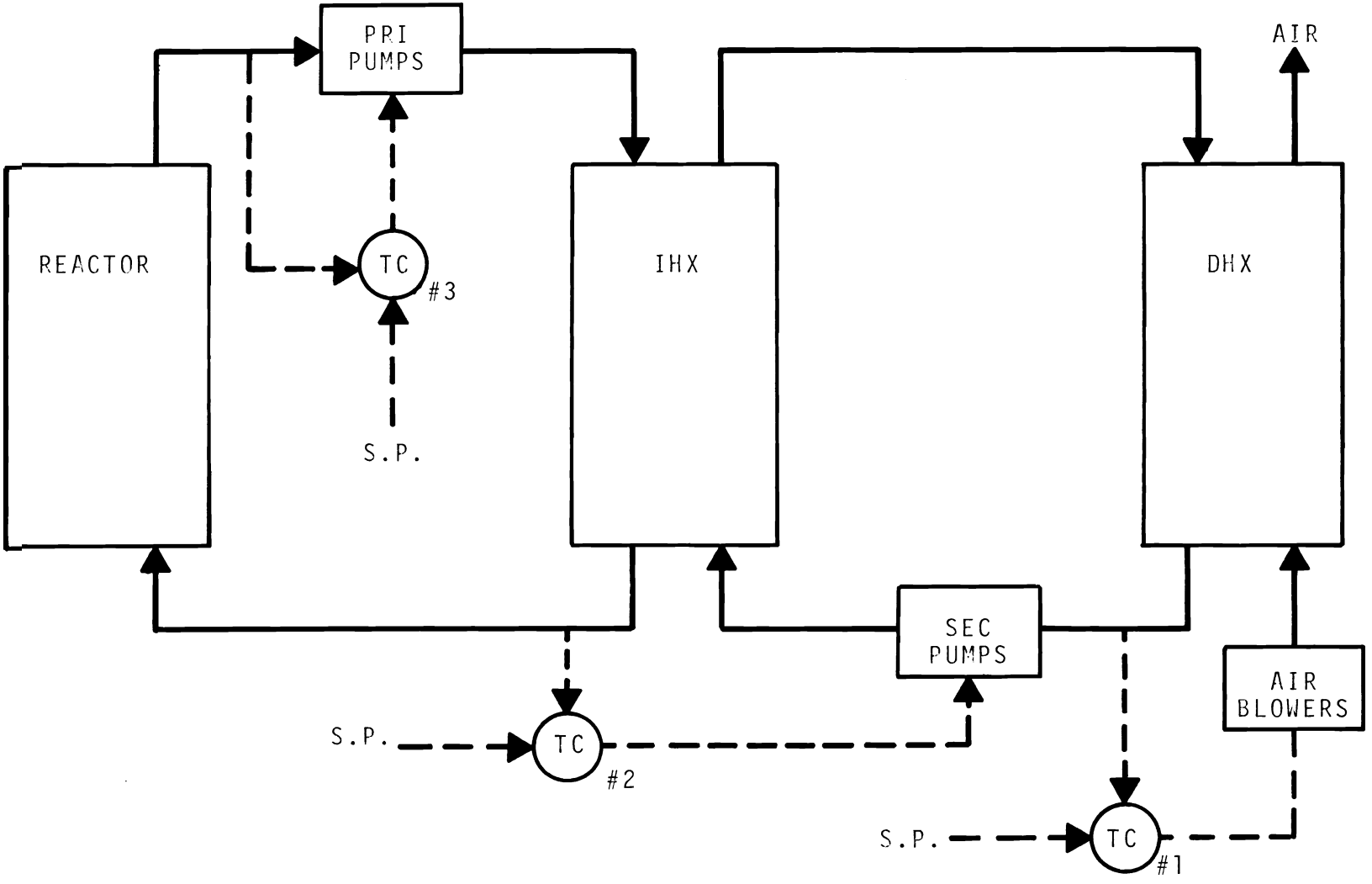

FIGURE 6 Controller Configuration Number V

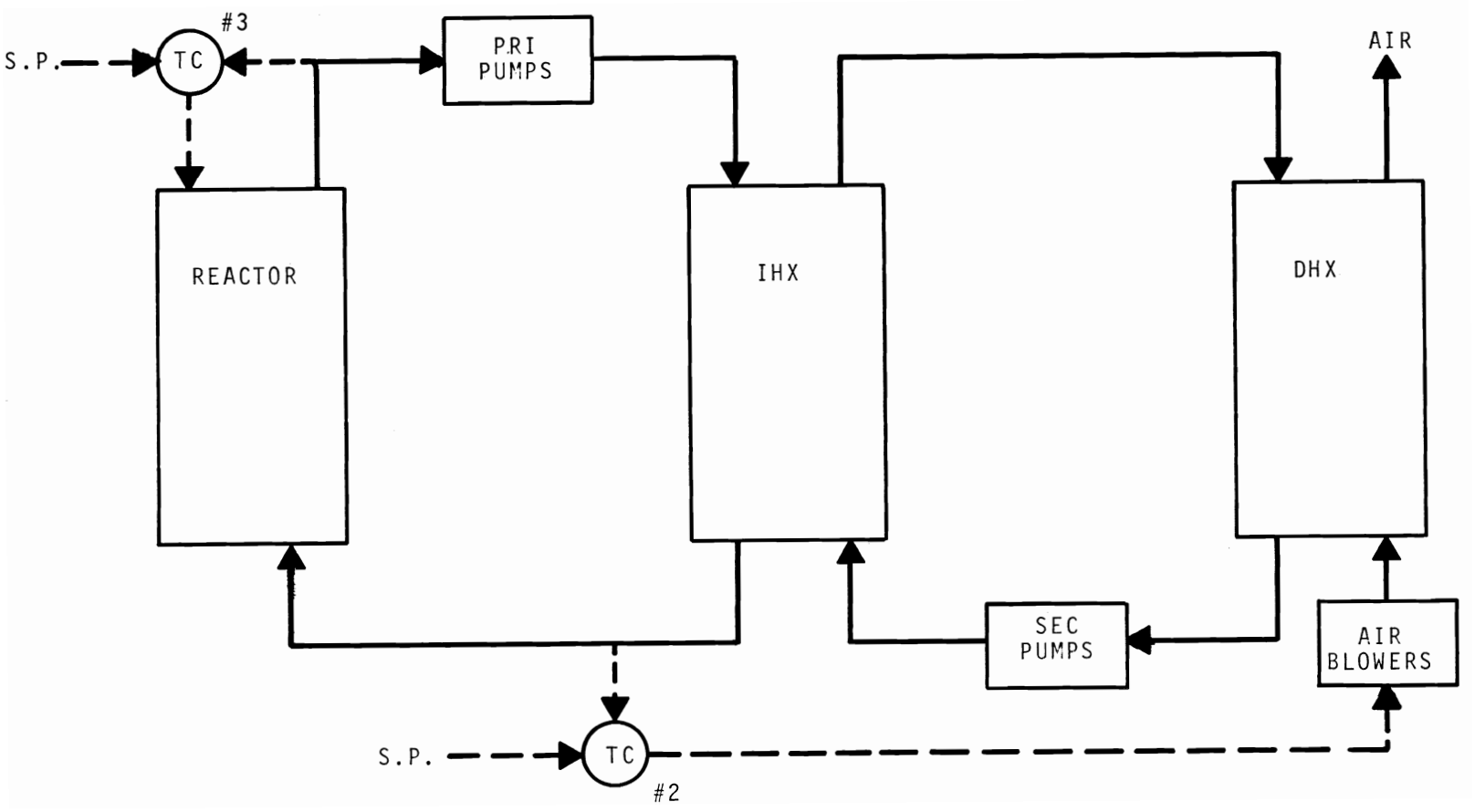

FIGURE 7 Controller Configuration Number VI

response to the step setpoint change resulted in a 20% overshoot. Next, leaving controller loop one closed and adjusted, controller loop two was closed and the controller proportional and integral action settings were adjusted in a manner similar to that for controller loop one. Next, with controller loops one and two closed and adjusted, controller loop three was closed and adjusted in the same manner. Interactions between controller loops require that with all loops closed, readjustments be made until the loops respond to setpoint changes with a 20% overshoot. In the power setback transients, the final power level and primary flow were at two-thirds of full power. Prior to the power setback the controllers were readjusted to give 20% overshoot to setpoint step changes at the reduced power level instead of at full power (for configuration comparison purposes only). The controller settings thus determined were:

TABLE 1. Controller Settings

Configuration	Controller Number	Controller Settings			
		Full Power		2/3 Power	
		P	I	P	I
I	2	7	0.005	2.6	0.0035
	3	12	0.1	10	0.075
II	1	30	0	10	0
	2	0.75	0.015	0.7	0.019
	3	12	0.1	10	0.075
III	1	30	0	10	0
	2	1.2	0.017	1	0.022
	5	1.5	0.27	1.5	0.16
IV	1	30	0	10	0
	4	1.3	0.017	1.2	0.015
	5	1.5	0.27	1.5	0.16
V	1	25	0.01	2	0.002
	2	2.5	0.06	1	0.04
	3	12	0.1	10	0.075

The following disturbances were applied to each configuration:

- Air temperature slow 32 °F decrease. (This disturbance is an air temperature decrease with a time constant of 1000 sec to approximate realistic extremes in rate and magnitude of temperature change.)
- Air temperature step 32 °F increase.
- Air flow step 8% decrease (to approximate sudden loss of one blower).
- Primary flow step 10% decrease.
- Power 15 MW increase (caused by a step change in rod reactivity).
- Controller number 2 or 4 setpoint 10° step increase.
- Controller number 3 or 5 setpoint 10° step increase.
- Fast 1/3 power setback (rod reactivity decrease rate of one cent per second).
- Slow 1/3 power setback (rod reactivity decrease of one-tenth cent per second).

The initiating events are shown on strip chart recordings in Figure 13. The resulting temperature transients for process tube outlet temperature and both primary and secondary loop hot and cold leg temperatures are shown in Figures 8 through 12. Additional parameters for power setback including power level, reactivity, primary flows, and air flow are also shown in Figures 8 through 12. Table 2 summarizes peak temperature transient values for all configurations.

Configurations I and II can be compared to determine if there is an advantage is using the cascade control system. In general, the cascade system results in better performance, particularly in the power setback transients (Table 2). While Configuration II is already superior to I for the fast power setback, the improvement in performance is even greater in going to the slower power setback, particularly in the tube

TABLE 2 Transient Peaks for Configurations I, II, III, IV, and V

Measured Parameter	Configuration Number	Disturbances: Air Temp Slow 32 °F Decrease	Air Temp Step 32 °F Increase	Air Flow Step 8% Decrease	Pri Flow Step 10% Decrease	Power 15 MW Increase	Controller 2 and 4 10° Setpoint Increase	Controller 3 and 5 10° Setpoint Increase	Fast One-Third Power Setback	Slow One-Third Power Setback
Tube	I	0.5°	-3°	-2°	18°	4°	-2°	36°	19°	17°
	II	0	-0.5	0	18	4	-2	34	13	7
Outlet	III	0	3°	1	22	5	13	13	-56	-29
	IV	0	3	1	22	5	16	11	-54	-28
Temp	V	0	-0.5	0	18	4	-2	35	15	6
Primary	I	0	1	0.5	5	1	0.5	12	-8	-3
	II	0	0	0	5	1	0	12	-7	-2
Hot Leg	III	0	2	1	8	4	12	10	-50	-28
	IV	0	2	1	9	4	13	7	-46	-26
Temp	V	0	0	0	5	1	0.5	12	-7	-2
Primary	I	-3	14	8	-6	8	12	-12	-95	-86
	II	0	3	2	-6	7	12	-12	-67	-36
Cold Leg	III	0	2	1	-8	4	12	-6	-41	-23
	IV	0	2	1	-8	4	12	-5	-7	-22
Temp	V	0	3	1	-5	3	12	-12	-70	-60
Secondary	I	-2	7	4	-3	5	6	-7	-82	-77
	II	0	2	1	-3	5	6	-7	-56	-34
Hot Leg	III	0	2	1	-5 & +4	5	11	-3 & +5	-56	-37
	IV	0	2	1	-5 & +4	4	12	-3	-53	-37
Temp	V	0	-3	-2	4	-9	13	14	150	145
Secondary	I	-1	12	7	1	-7	10	8	80	80
	II	0	4	2	2	-7	10	11	82	80
Cold Leg	III	0	5	2	10	-8	19	-8	84	80
	IV	0	5	2	2	-8	21	1	80	80
Temp	V	0	5	2	1	3	-3	-3	Z05	-190

outlet and the primary cold leg temperatures. Table 2 shows that all of the configurations (II, III, IV and V) employing controller one (controls secondary cold leg temperature by manipulating air flow) are better than Configuration I for air disturbances, but not necessarily for the other disturbances. The improvement is expected since the control loop one is faster acting due to the relatively small time delays as compared with control loop two. Configurations I and II are easy to stabilize and easy to adjust. Configuration I is simpler than II since it has one less controller to adjust in each of the three heat transport circuits; however, Configuration II is considered generally superior to Configuration I because of the greater effectiveness in reducing transients due to the controlled power reduction.

A comparison can be made between results from Configurations II and III to determine the desirability of controlling the reactor temperature rise instead of the primary hot leg temperature by manipulating the primary flow. In Table 2, the expected tendency of Configuration III to increase primary hot leg temperature transients (and tube outlet temperature transients) over Configuration II and decrease primary cold leg temperature transients is evident. Close comparison of the transient timing in Figures 9 and 10 also reveals that some of the Configuration III transients are slower than comparable Configuration II transients. Weighting reactor inlet and outlet temperature variations equally, a degradation in overall system performance appears to result from controlling the reactor temperature rise instead of the primary hot leg temperature. The power setback peak transient increase in the primary hot leg is greater than the decrease in the primary cold leg. Both are easily stabilized. Configuration II is

probably simpler for setpoint adjustments than III because primary cold leg and hot leg temperatures can be set independently. In Configuration III, an operator may be concerned with the outlet temperature in addition to the temperature rise, so that the cold leg temperature must be set first.

A comparison of Configuration III and IV transient responses reveals the effects of controlling the reactor average temperature instead of the primary cold leg temperature. There appears to be a trend for Configuration IV to result in slightly lower setback transients than III. The transient response times are not noticeably different.

The effectiveness of manipulating the secondary loop sodium flow instead of the number one controller setpoint can be determined by comparing Configuration V with II. A major difference exists in the secondary loop temperature transients that result from the power setbacks; Configuration II appears considerably better than V. There are small differences in the remaining responses except that in V, the secondary cold leg transients are reduced at the expense of the hot leg temperature transients. Configuration II is simpler because fewer process variables change during a transient. Comparison of the improvement that Configuration II gives over V in going from fast setback to slow setback indicates that II has a greater potential.

A comparison was made between Configuration I and VI, where VI is similar to I except that the reactivity instead of the primary flow is manipulated to control the primary hot leg temperature (Figure 7). No limitations were put on the control reactivity magnitudes or rates of change. When Configuration VI controllers were adjusted in the manner of the other configurations, very large tube outlet temperature transients resulted. Hence, the adjustment was made for 20% overshoot in the tube outlet temperature instead of the primary hot

leg temperature in response to a setpoint step change in number three controller. In order to provide a fair comparison, Configuration I controllers were adjusted also for 20% overshoot in tube outlet temperature response. The controller settings used for the transients summarized in Table 3 were:

Configuration	P_2	I_2	P_3	I_3
I	7	0.0065	2.5	0.08
VI	5	0.025	0.6	0.08

The transients for Configuration VI are shown in Figure 13. Although the two configurations are comparable, the results slightly favor Configuration VI. If reactivity variations are permissible for control, and if the rates and magnitudes of reactivity variations are not constrained, then reactivity is a slightly better variable to manipulate than the primary flow. Although the difference does not appear great, it seems easier to satisfy safety criteria by manipulating the primary sodium flow rather than the reactivity.

TABLE 3 Transient Peaks for Configurations and VI

Measured Parameter	Configuration Number	Disturbances: Air Temp Slow 32 °F Decrease	Air Temp Step 32 ° Increase	Air Flow Step 8% Decrease	Pri Flow Step 10% Decrease	Power 15 MW Increase	Controller #2-10° Setpoint Increase	Controller #3-10° Setpoint Increase
Tube Outlet Temp	I	0	+2,-3	-2	20	5	-3	14
	VI	0	±3	-1	15	4	-4	13
Primary Hot Leg Temp	I	0	2	1	11	3	2	11
	VI	0	2	0	8	3	2	11
Primary Cold Leg Temp	I	-2	11	7	-9	8	12	-8
	VI	-1	8	5	-16	0	13	3

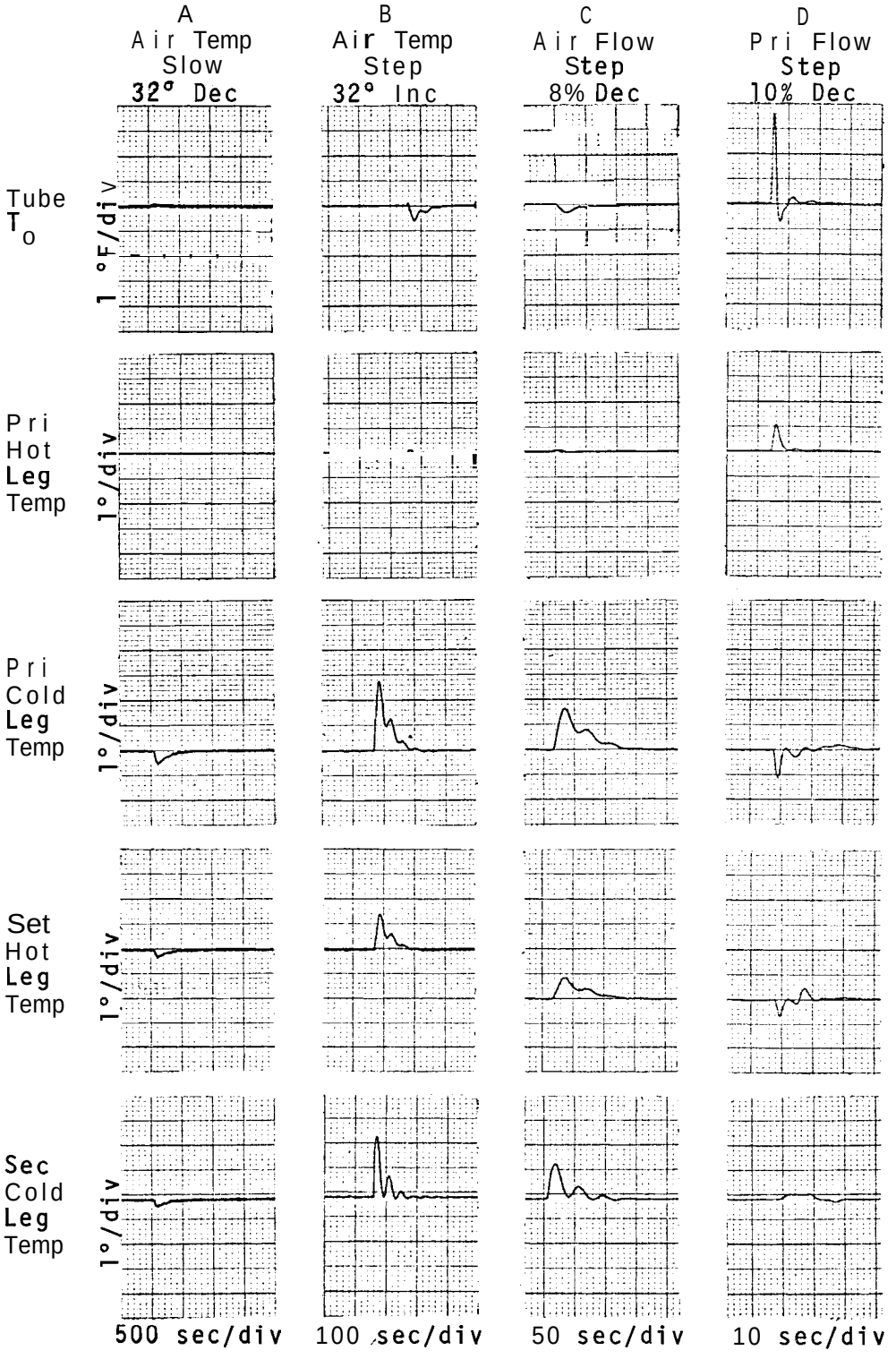

FIGURE 8. Controller Configuration Number I Transients

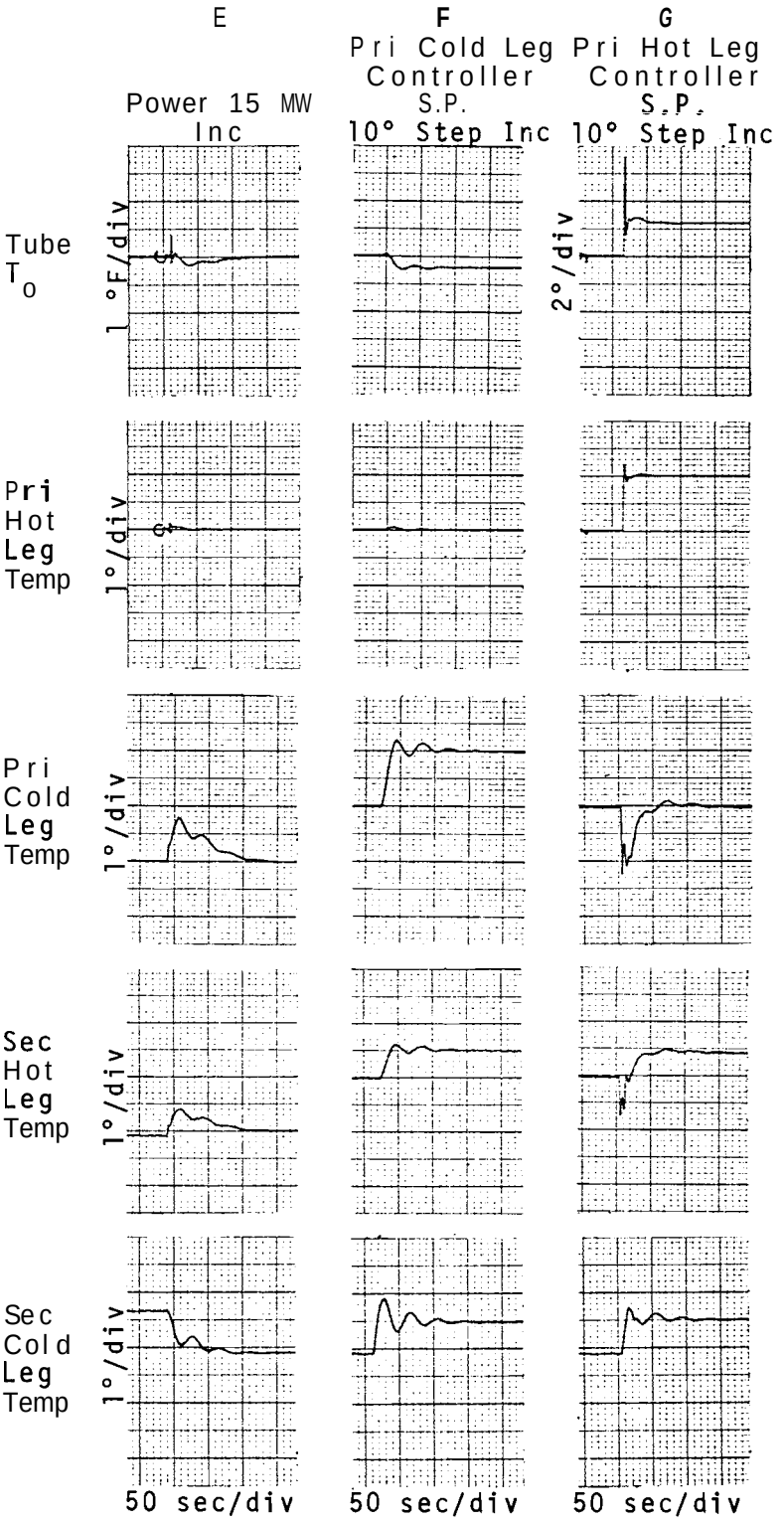

FIGURE 8. **(contd)**

H
Fast 1/3 Power Setback
(Rod reactivity decrease rate of 1¢/sec)

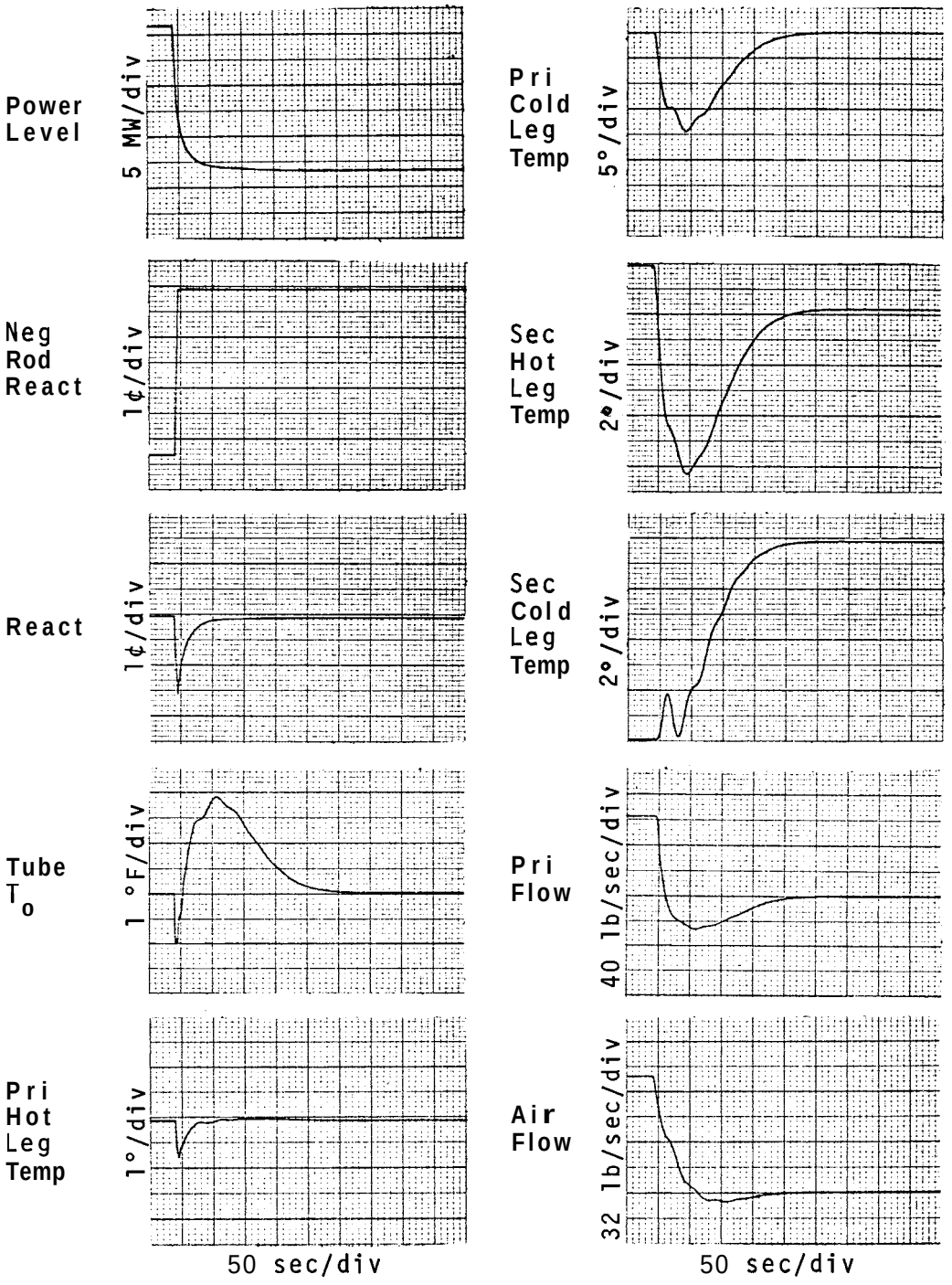

FIGURE 8. **(contd)**

I

Slow 1/3 Power Setback
(Rod reactivity decrease rate of 0.1¢/sec)

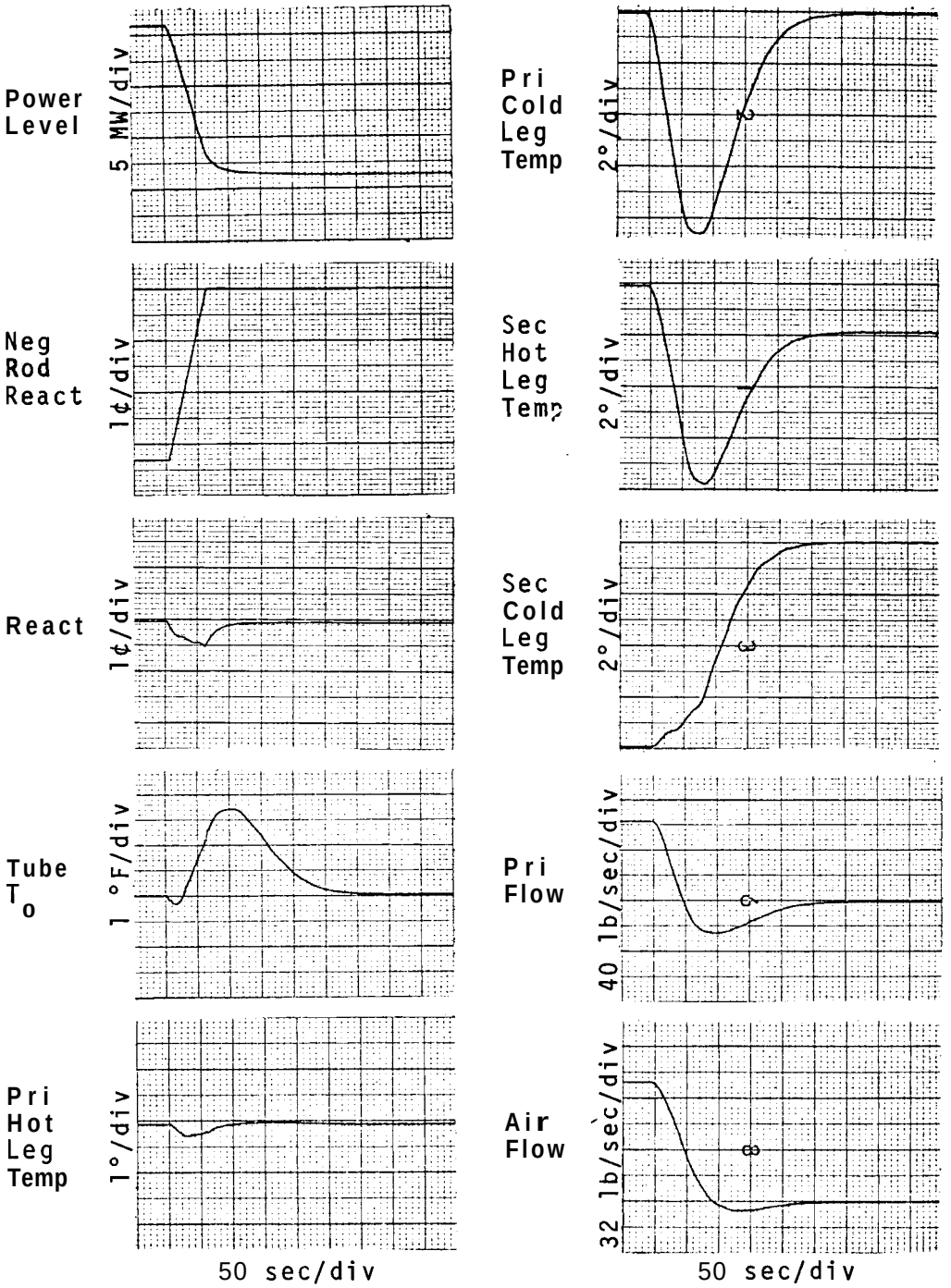

FIGURE 8. (contd)

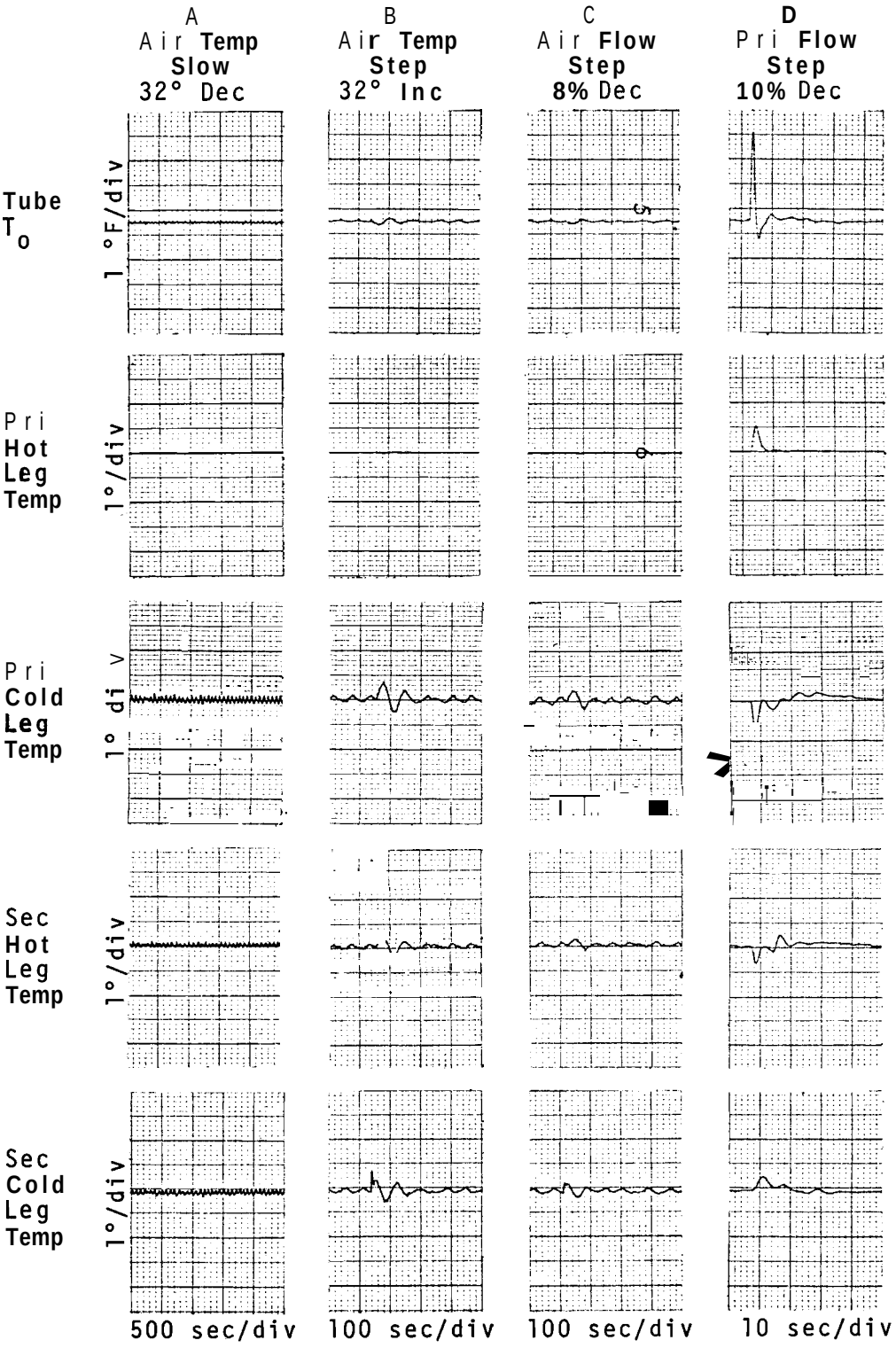

FIGURE 9. Controller Configuration Number II Transients

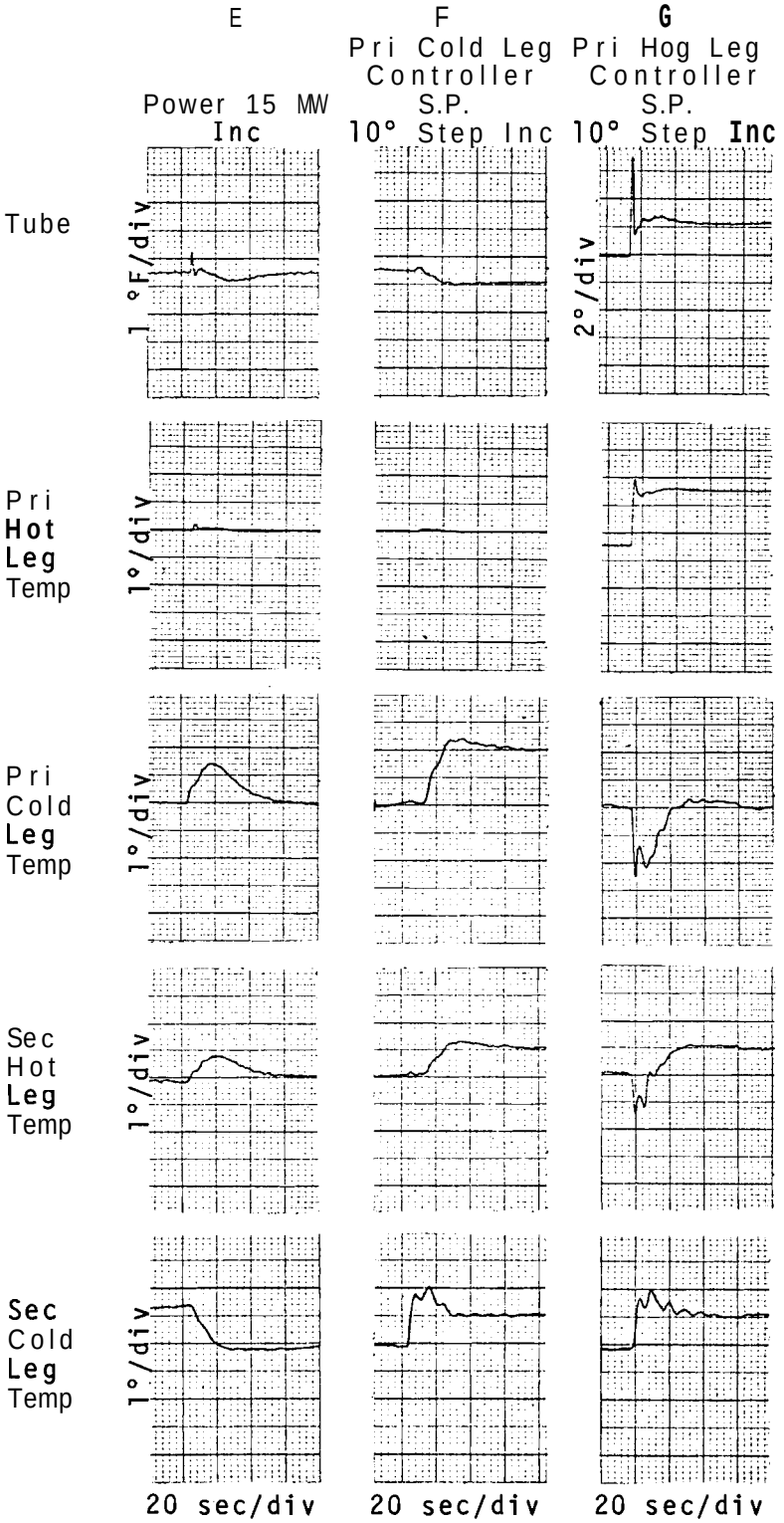

FIGURE 9. (contd)

H

Fast 1/3 Power Setback

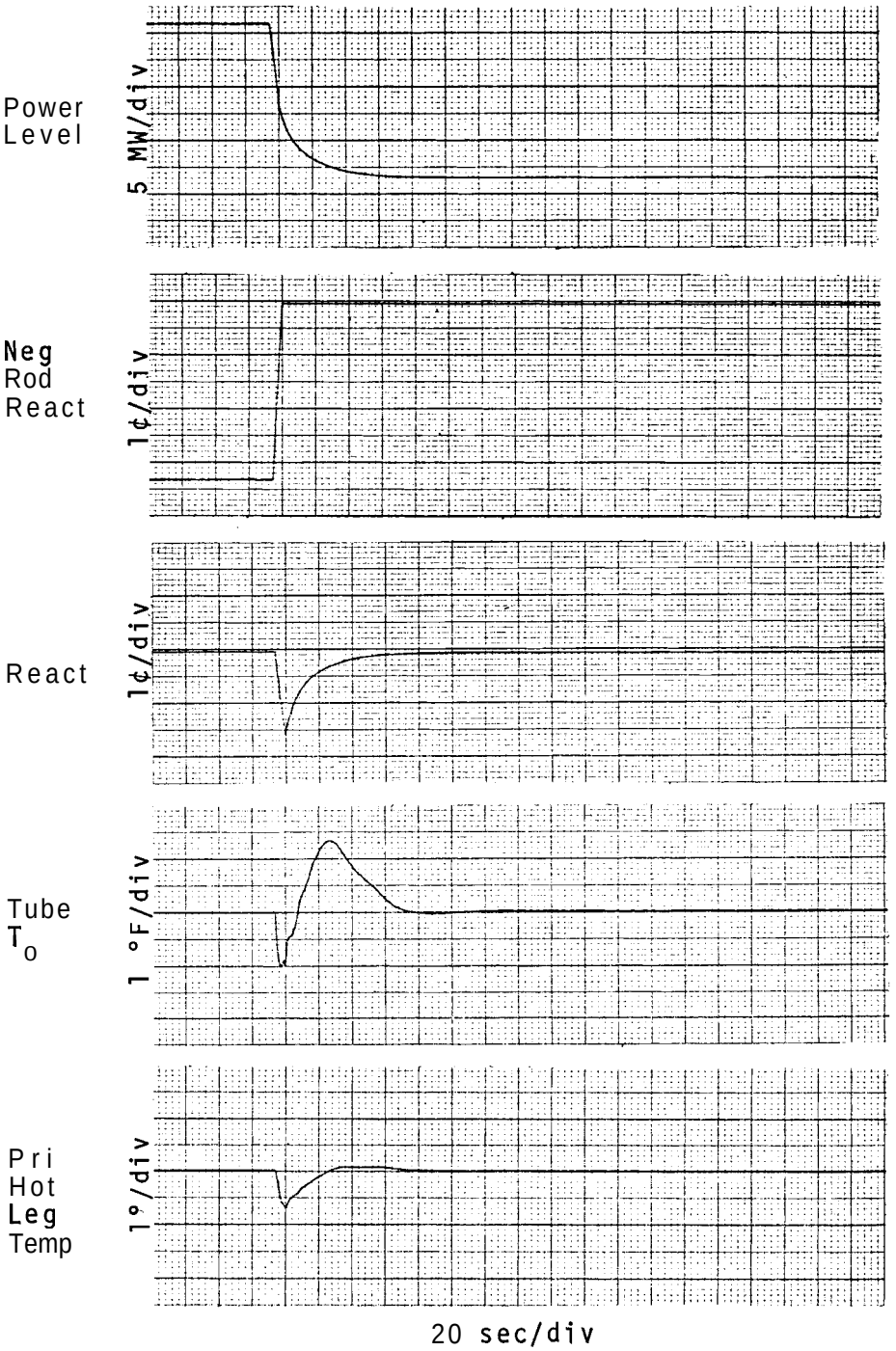

FIGURE 9. **(contd)**

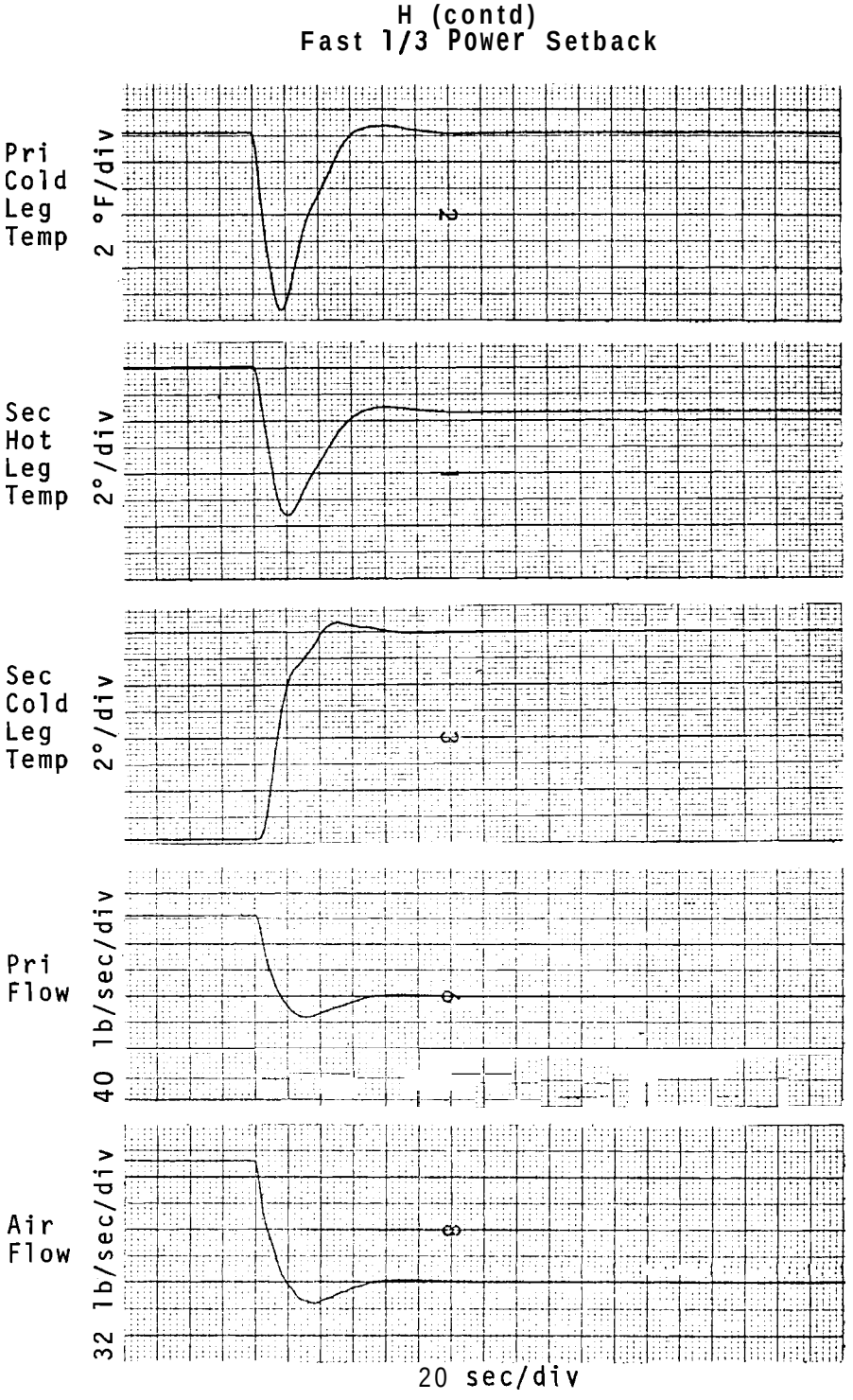

FIGURE 9. (contd)

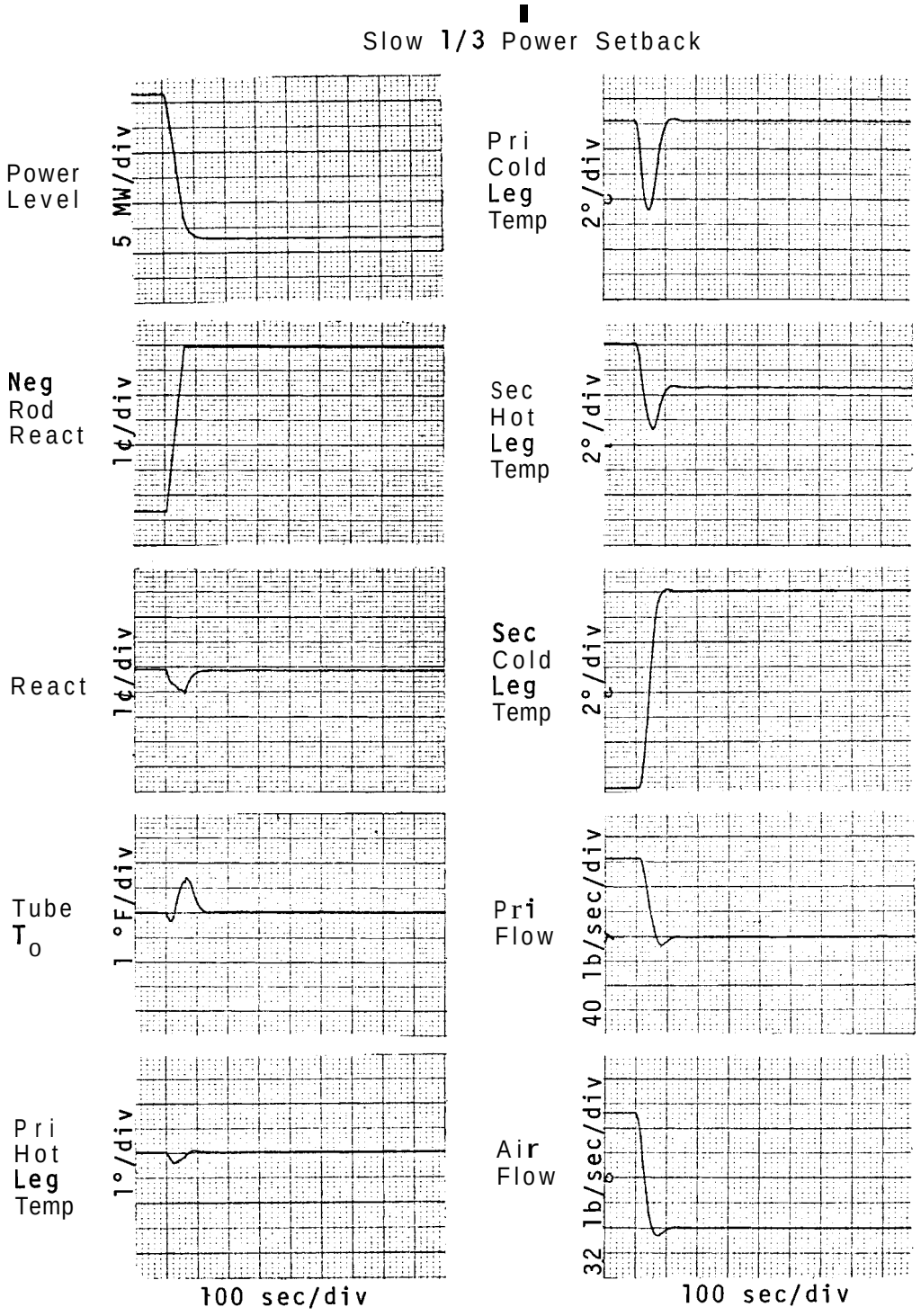

FIGURE 9. **(contd)**

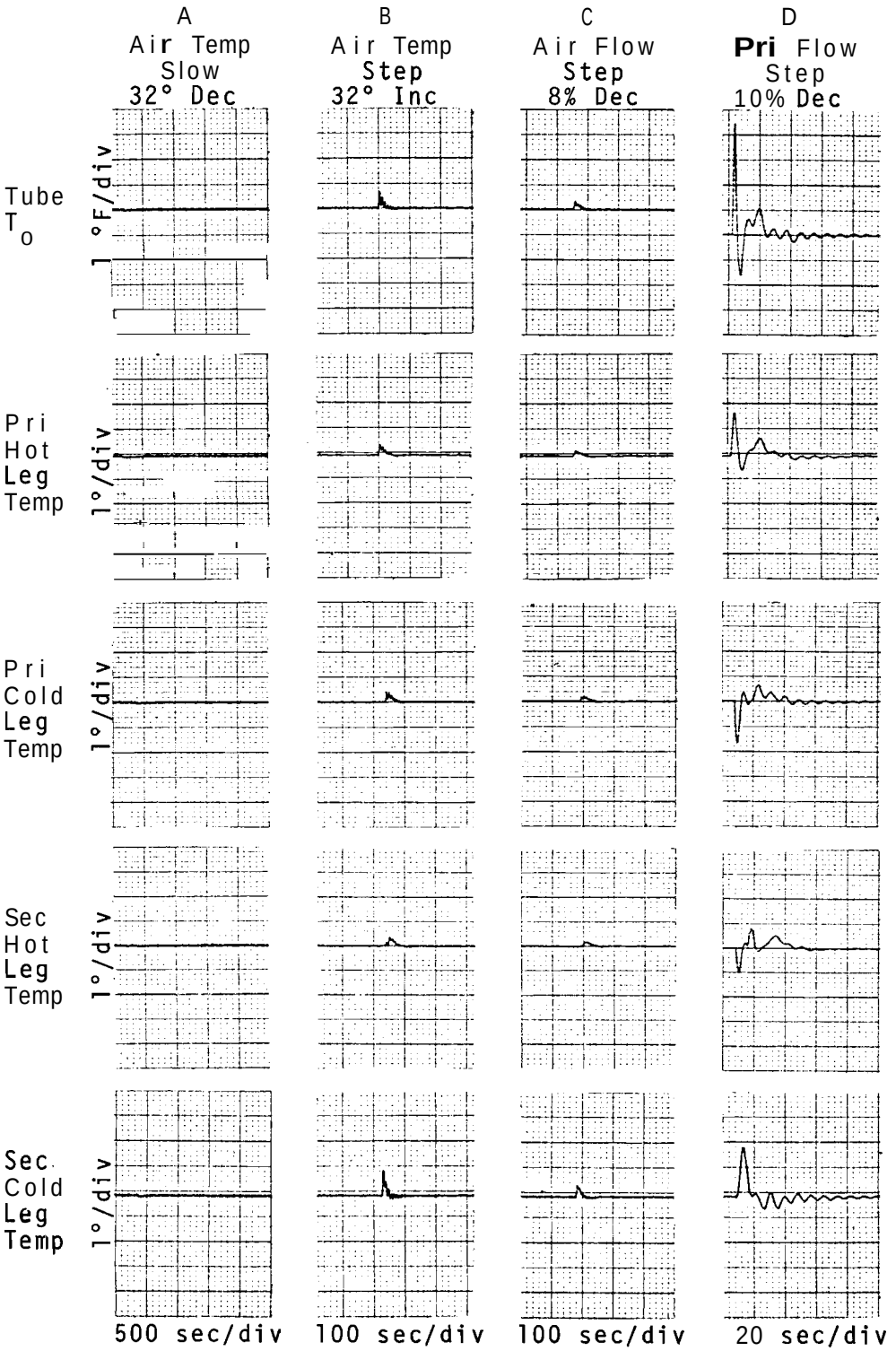

FIGURE 10. Controller Configuration Number III Transients

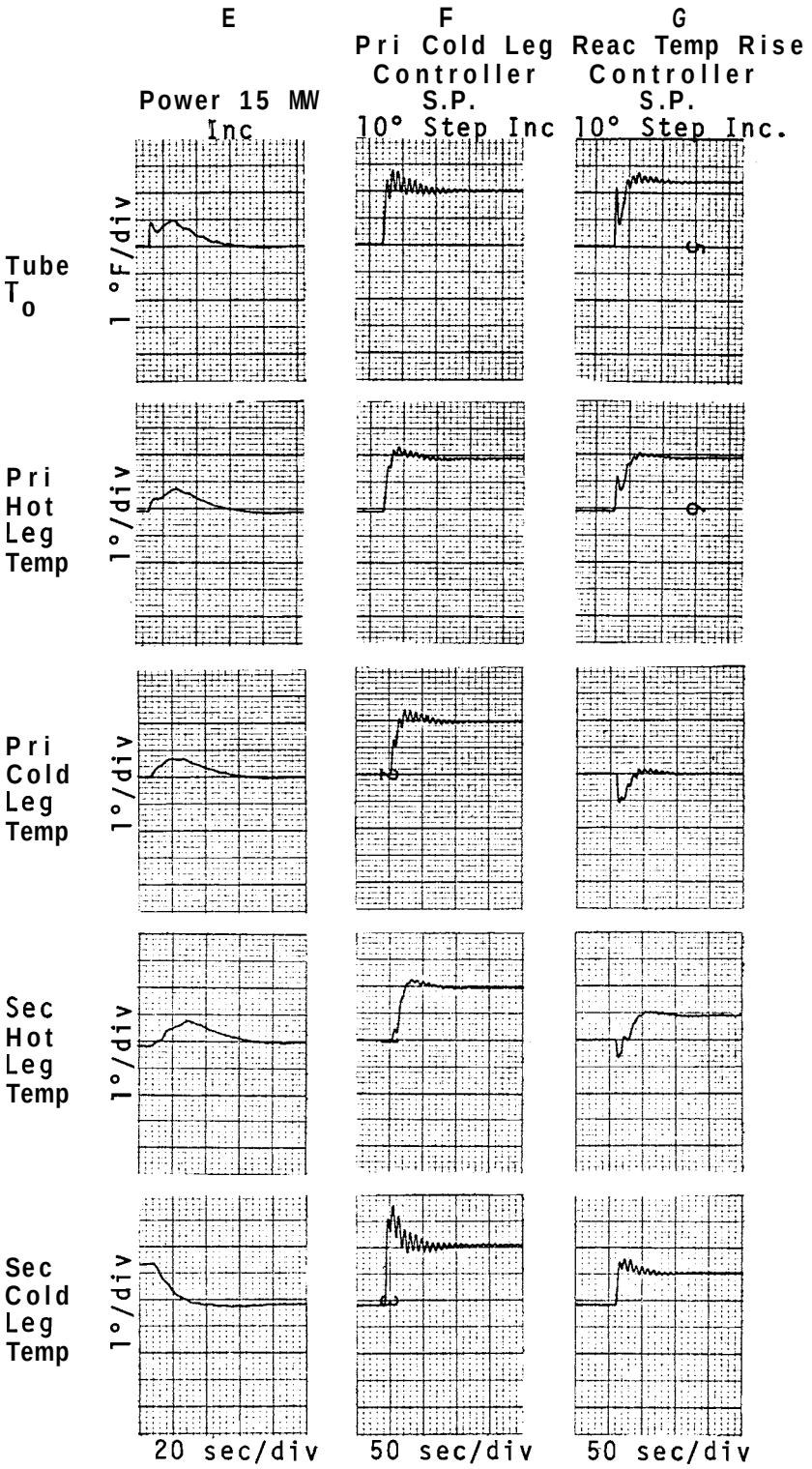

FIGURE 10. (contd)

H
Fast 1/3 Power Setback

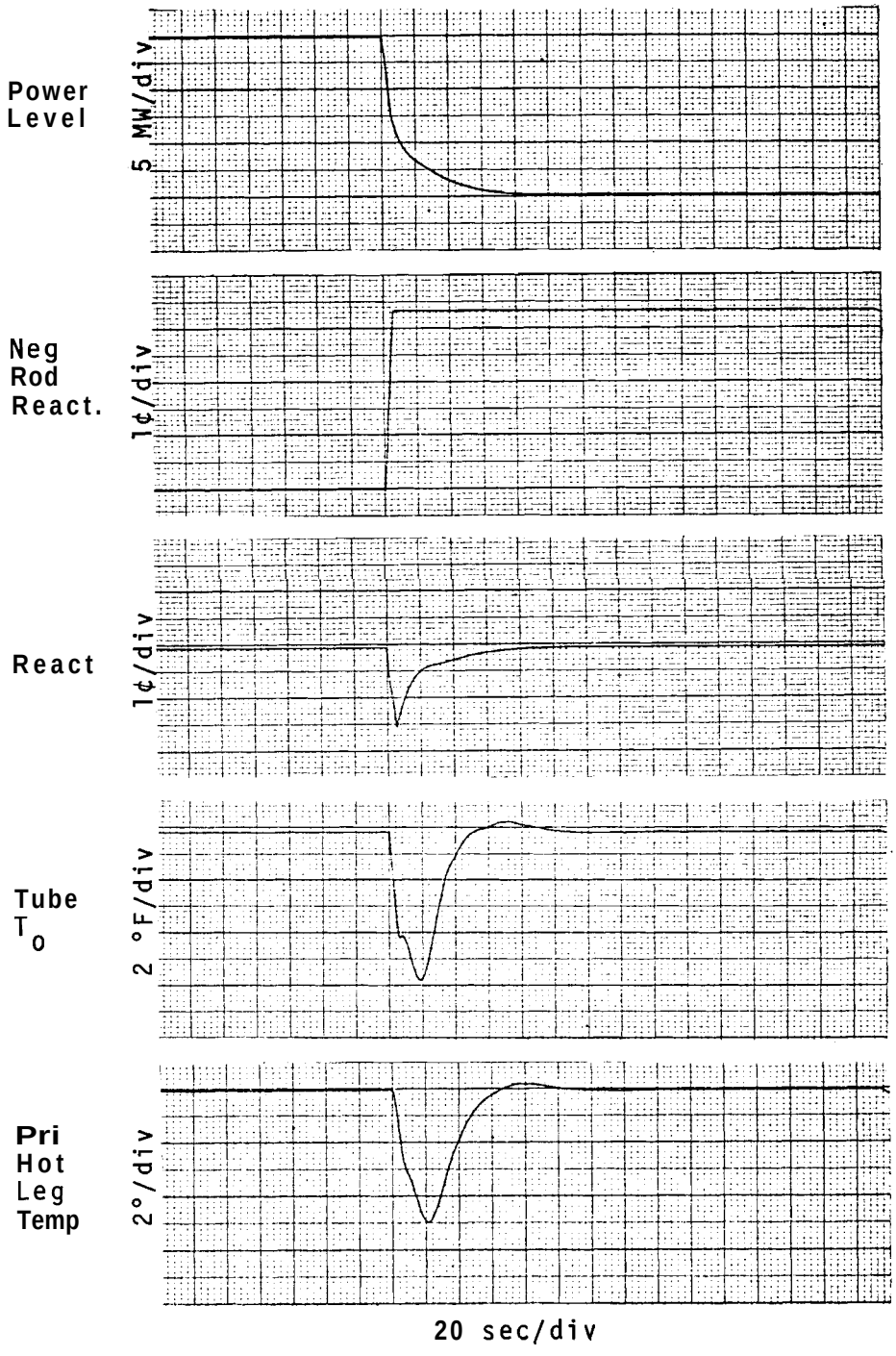

FIGURE 10. (contd)

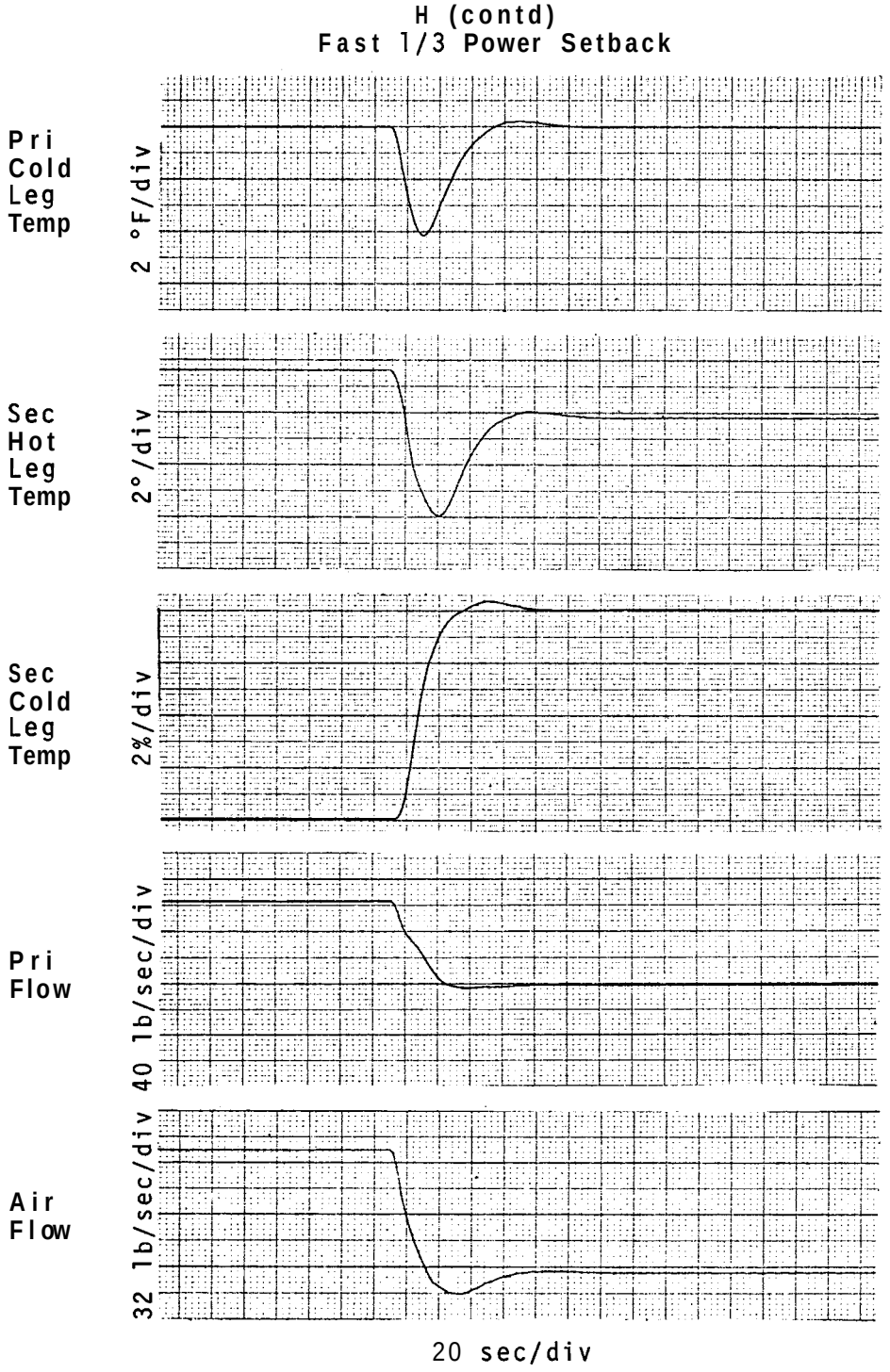

FIGURE 10. (contd)

I

Slow 1/3 Power Setback

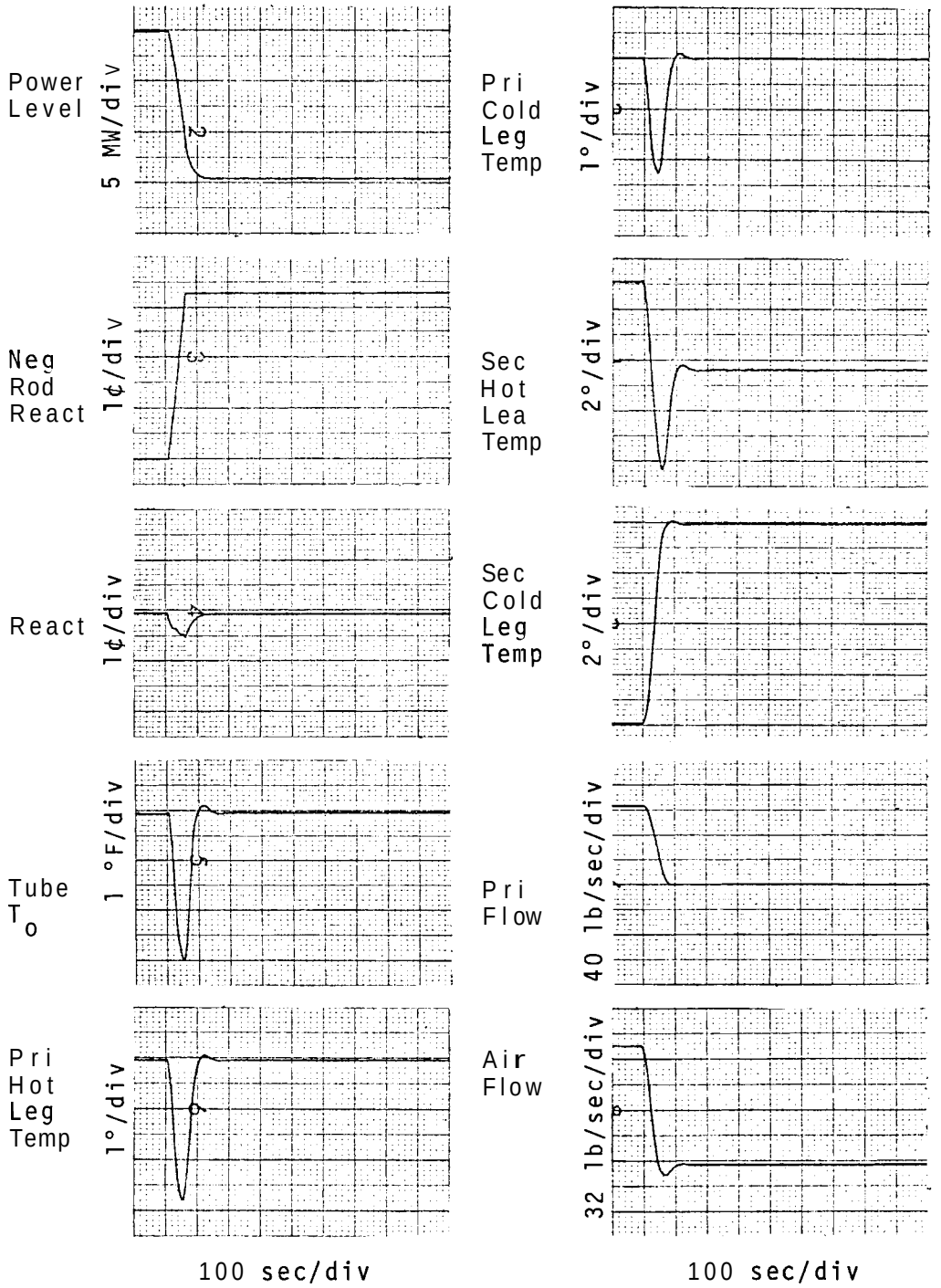

FIGURE 10. **(contd)**

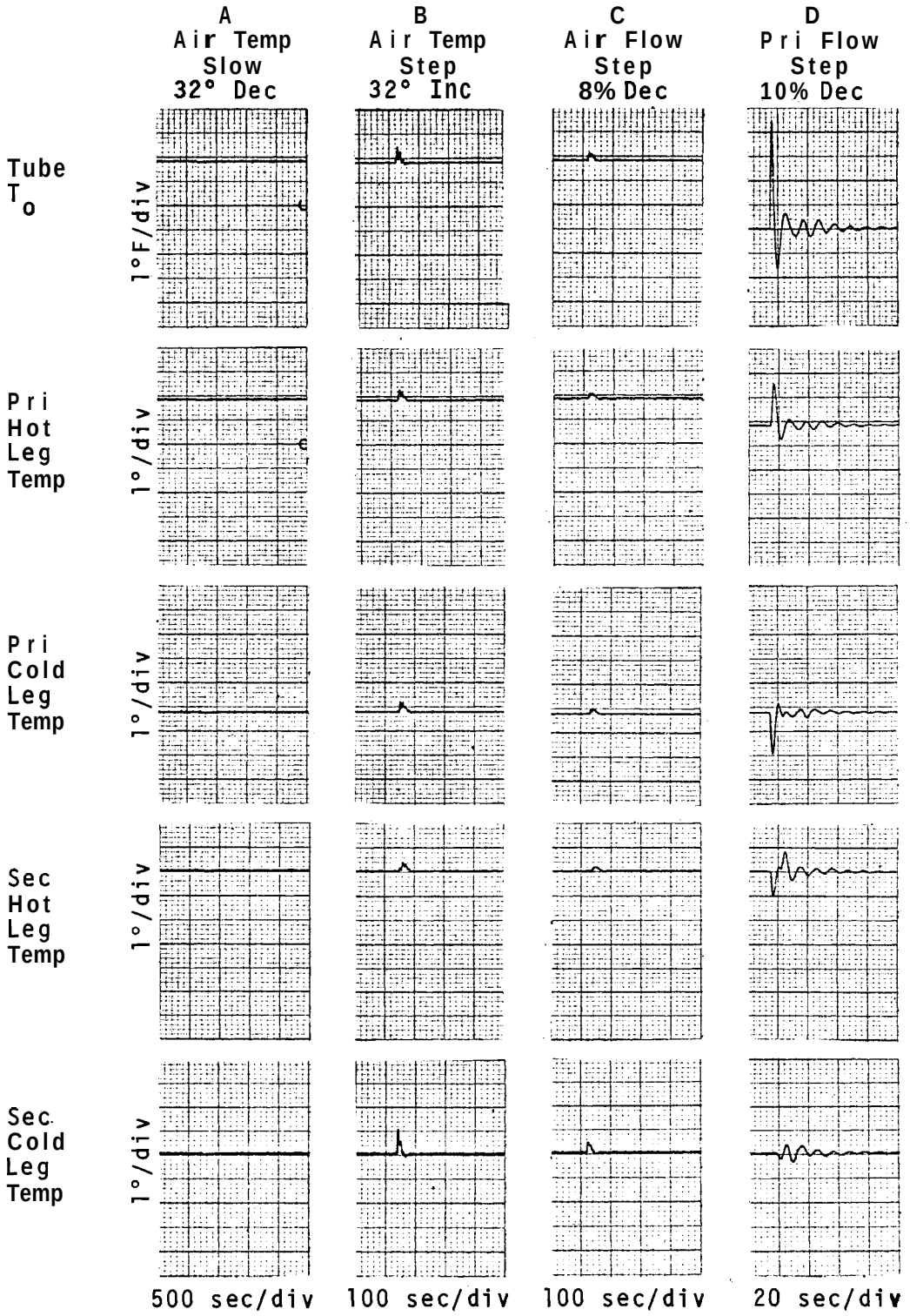

FIGURE 11. Controller Configuration Number IV Transients

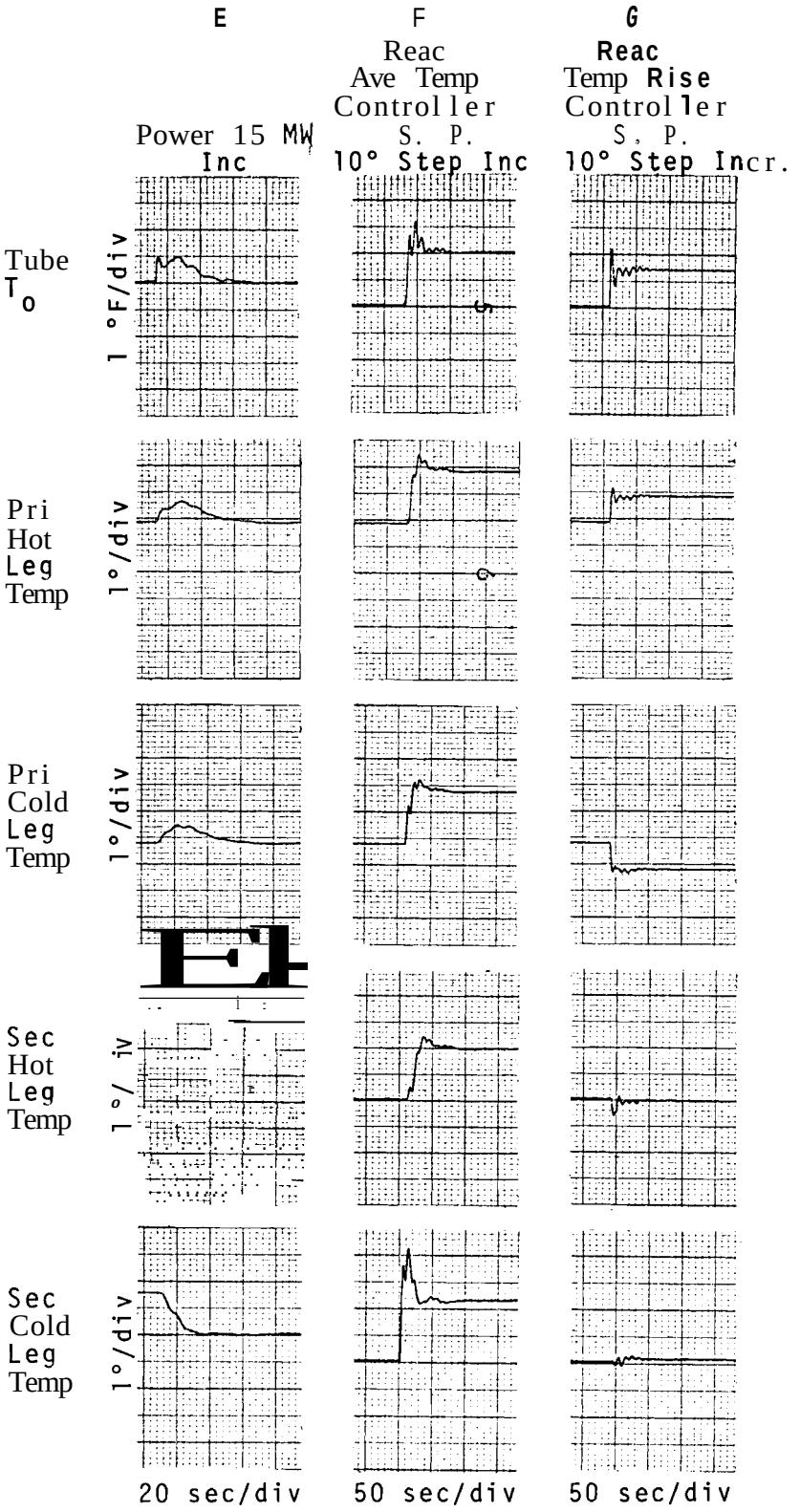

FIGURE 11. (contd)

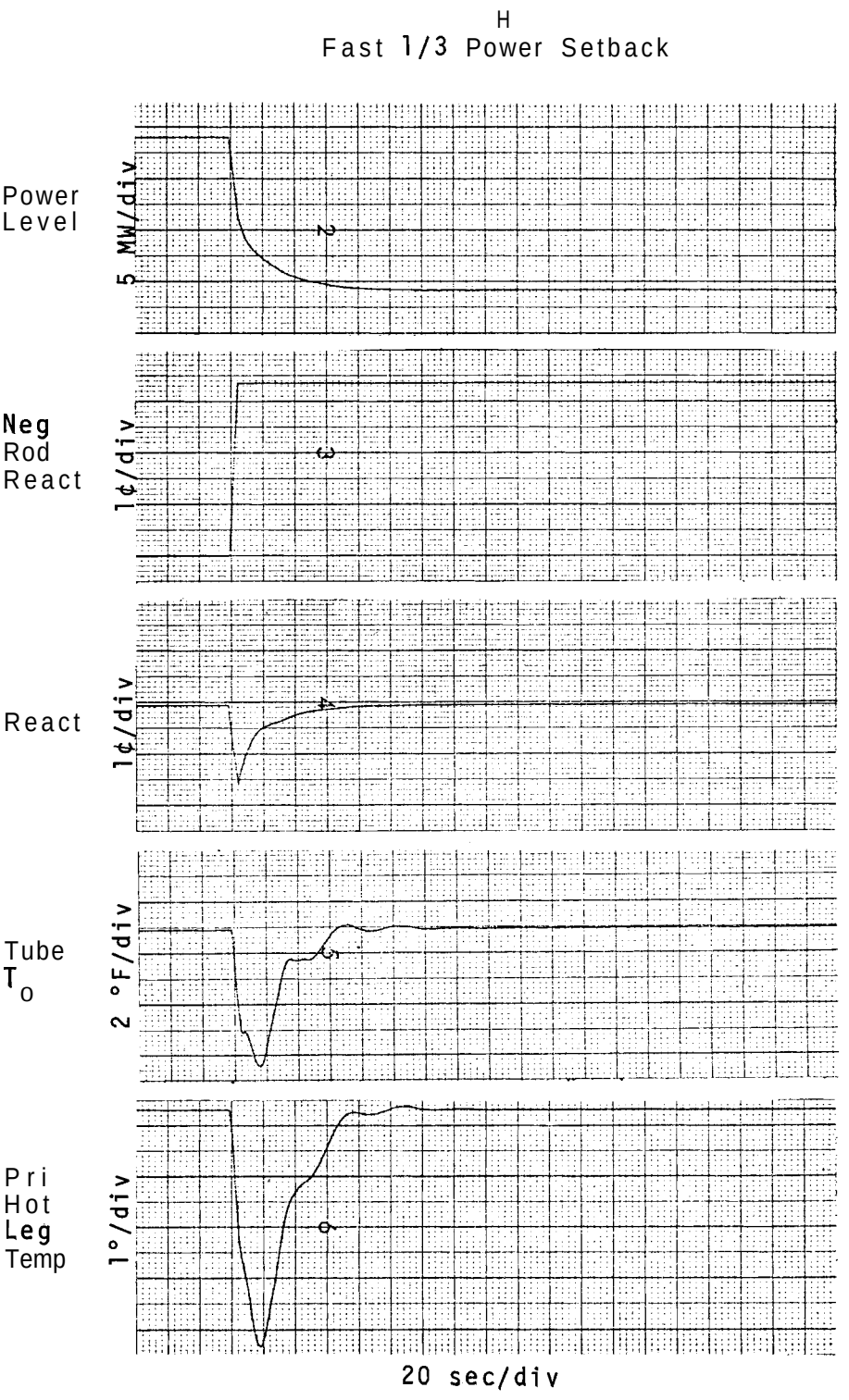

FIGURE 11. (contd)

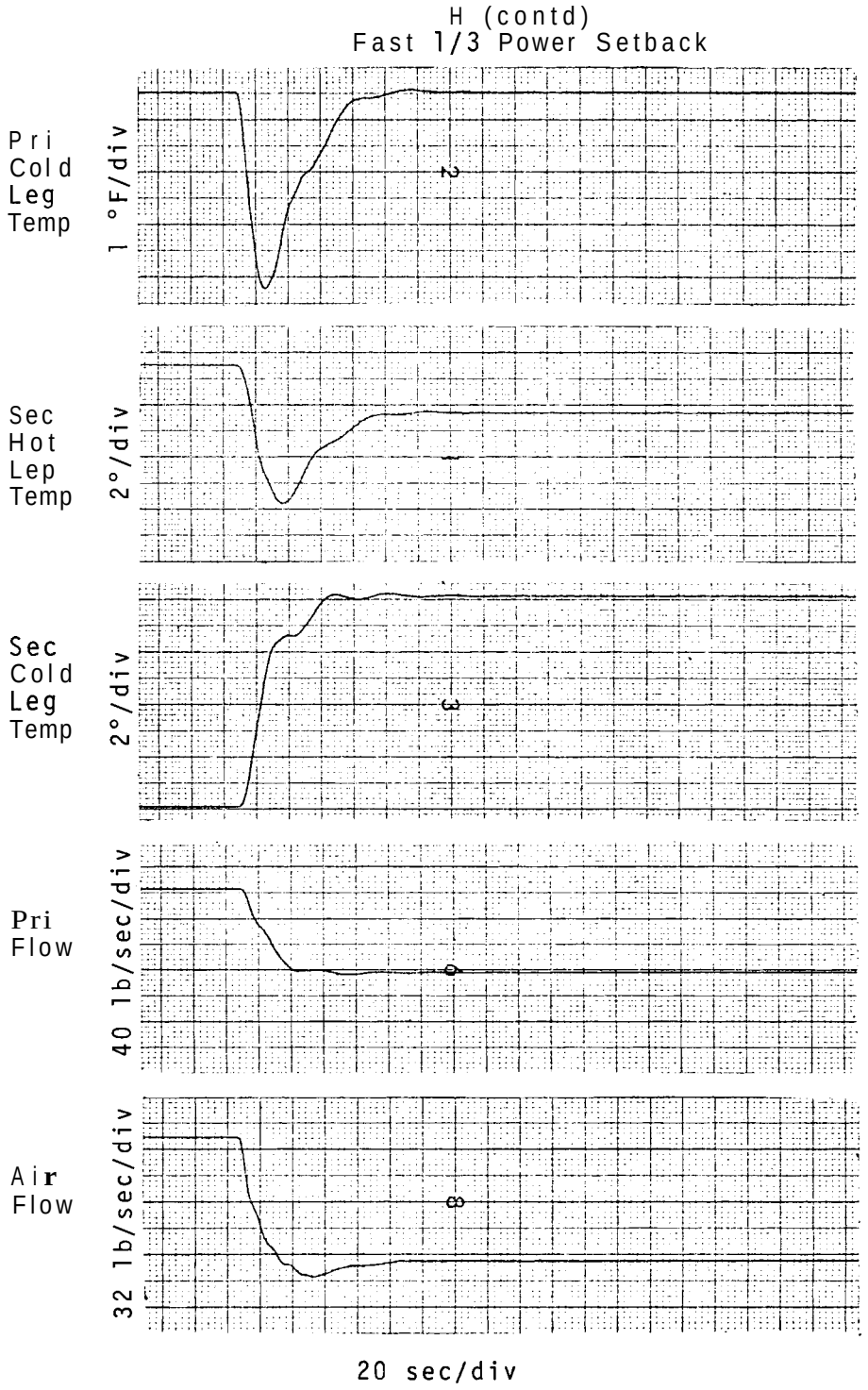

FIGURE 11. (contd)

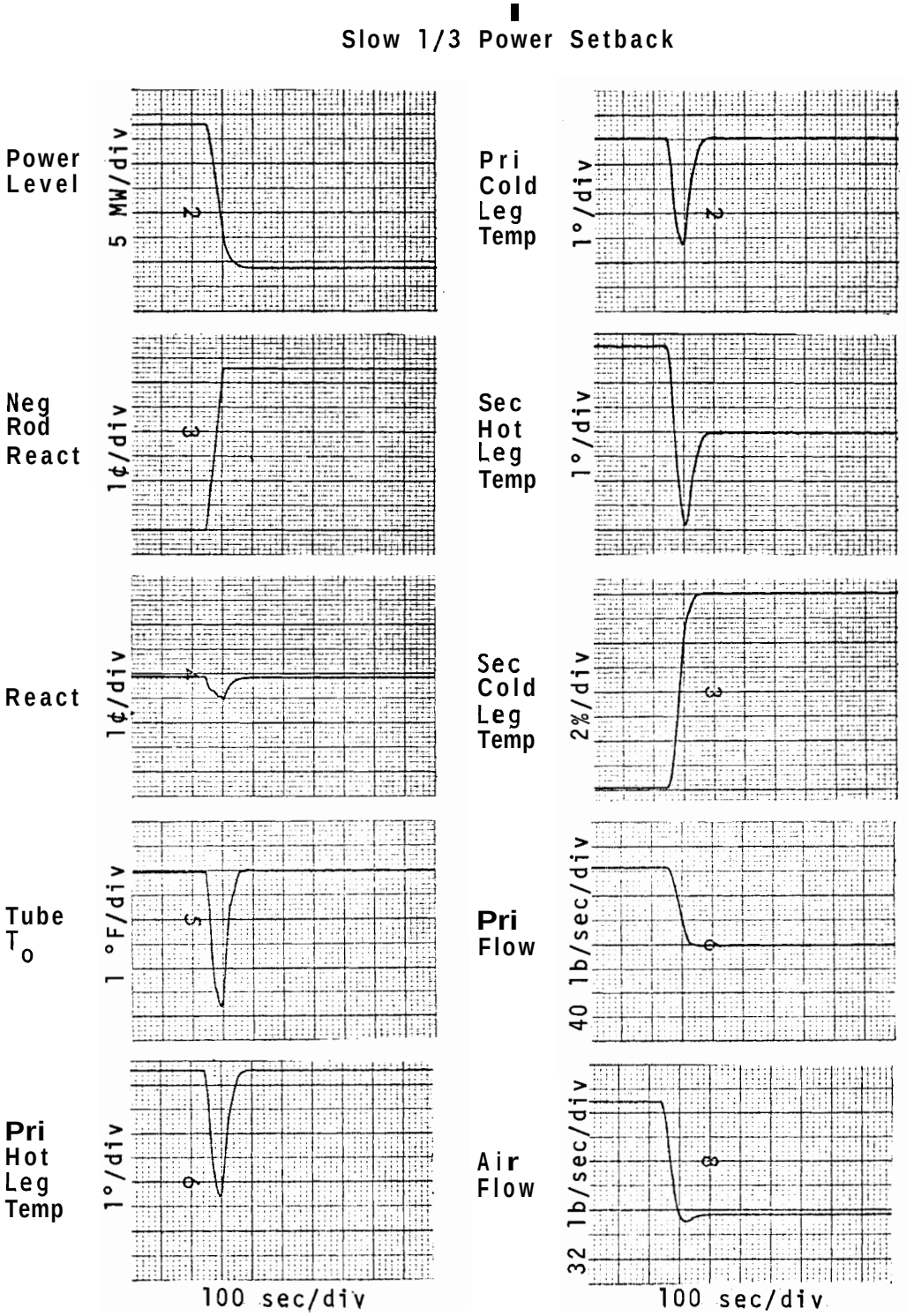

FIGURE 11. (contd)

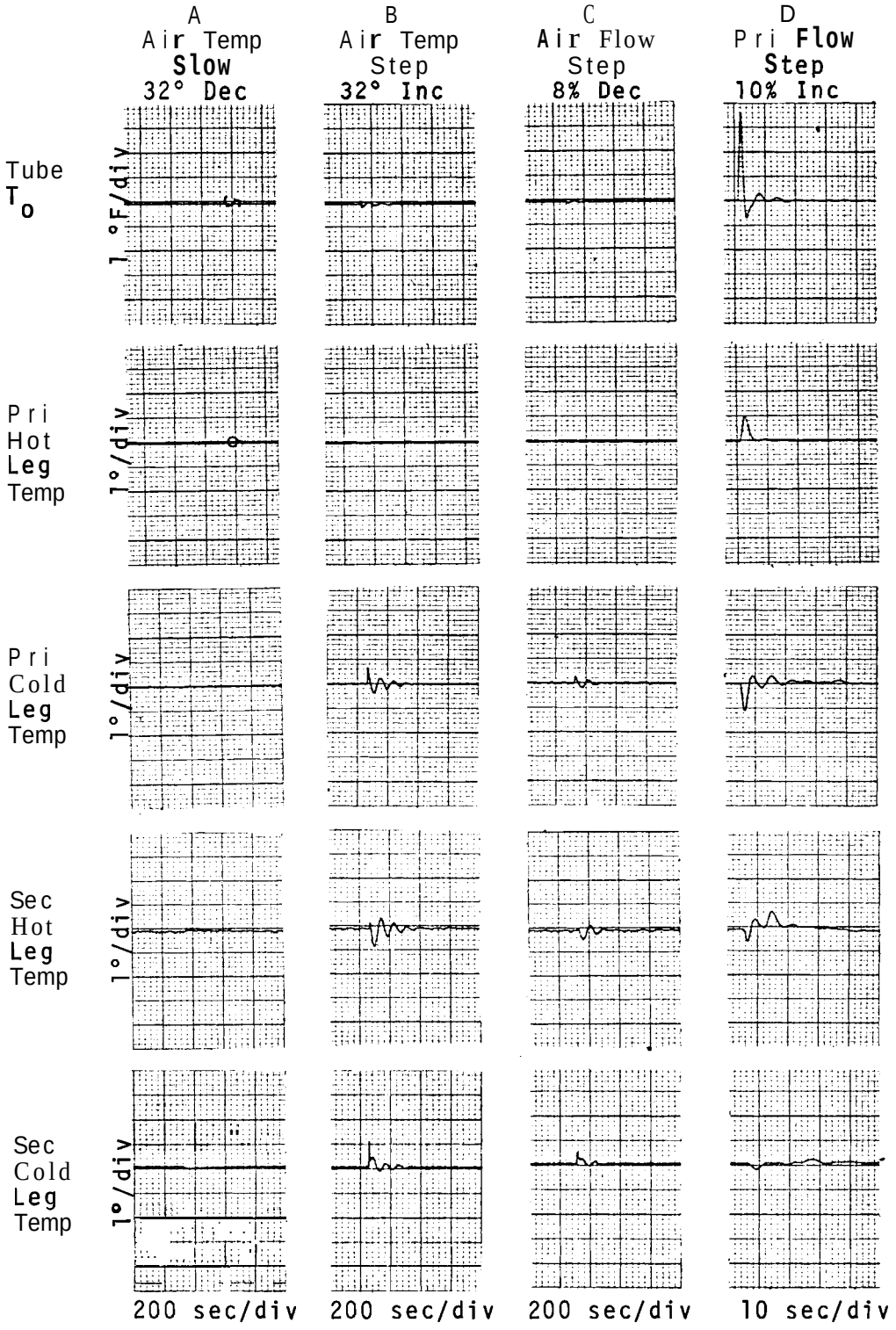

FIGURE 12. Controller Configuration Number V Transients

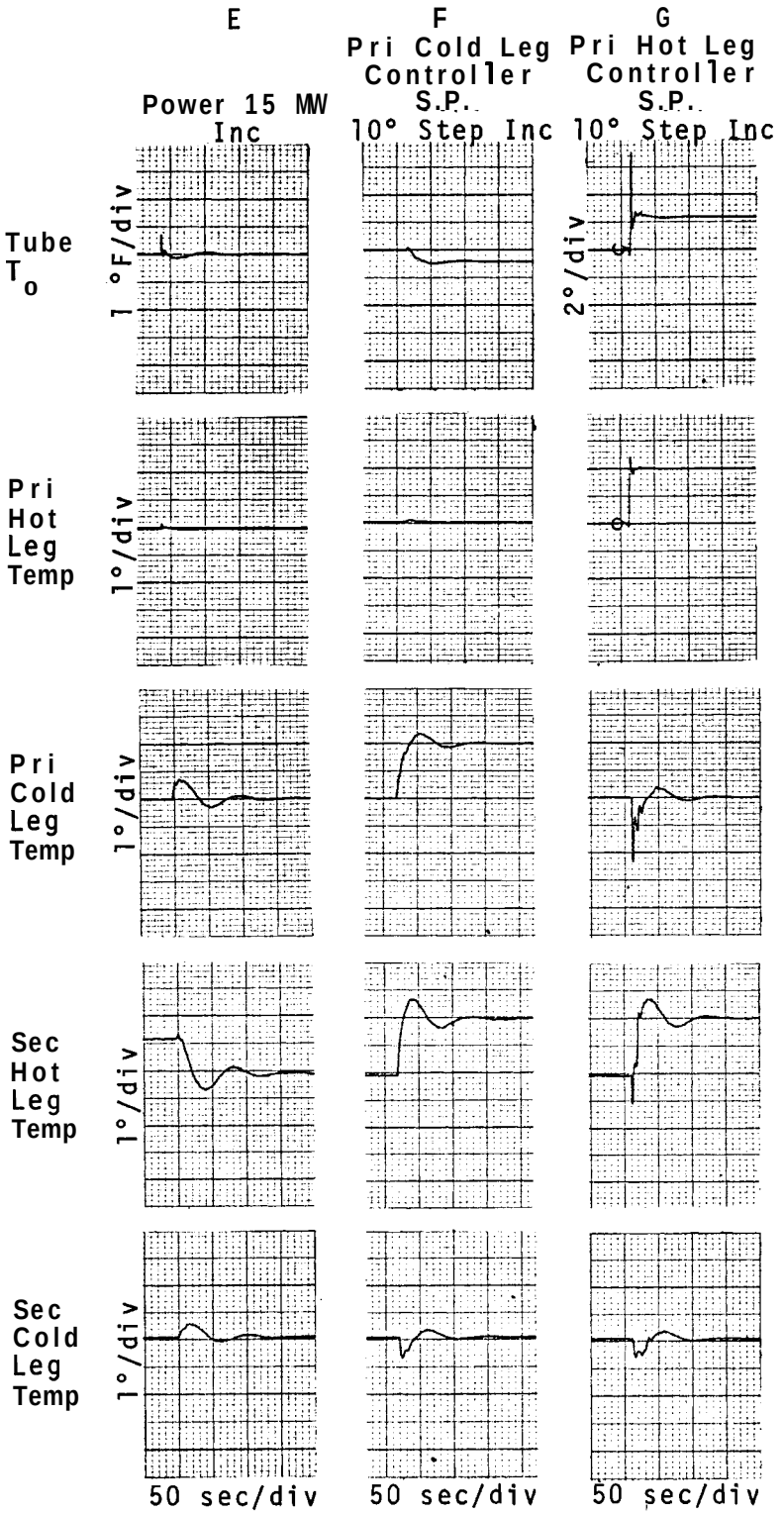

FIGURE 12. (contd)

H
Fast 1/3 Power Setback

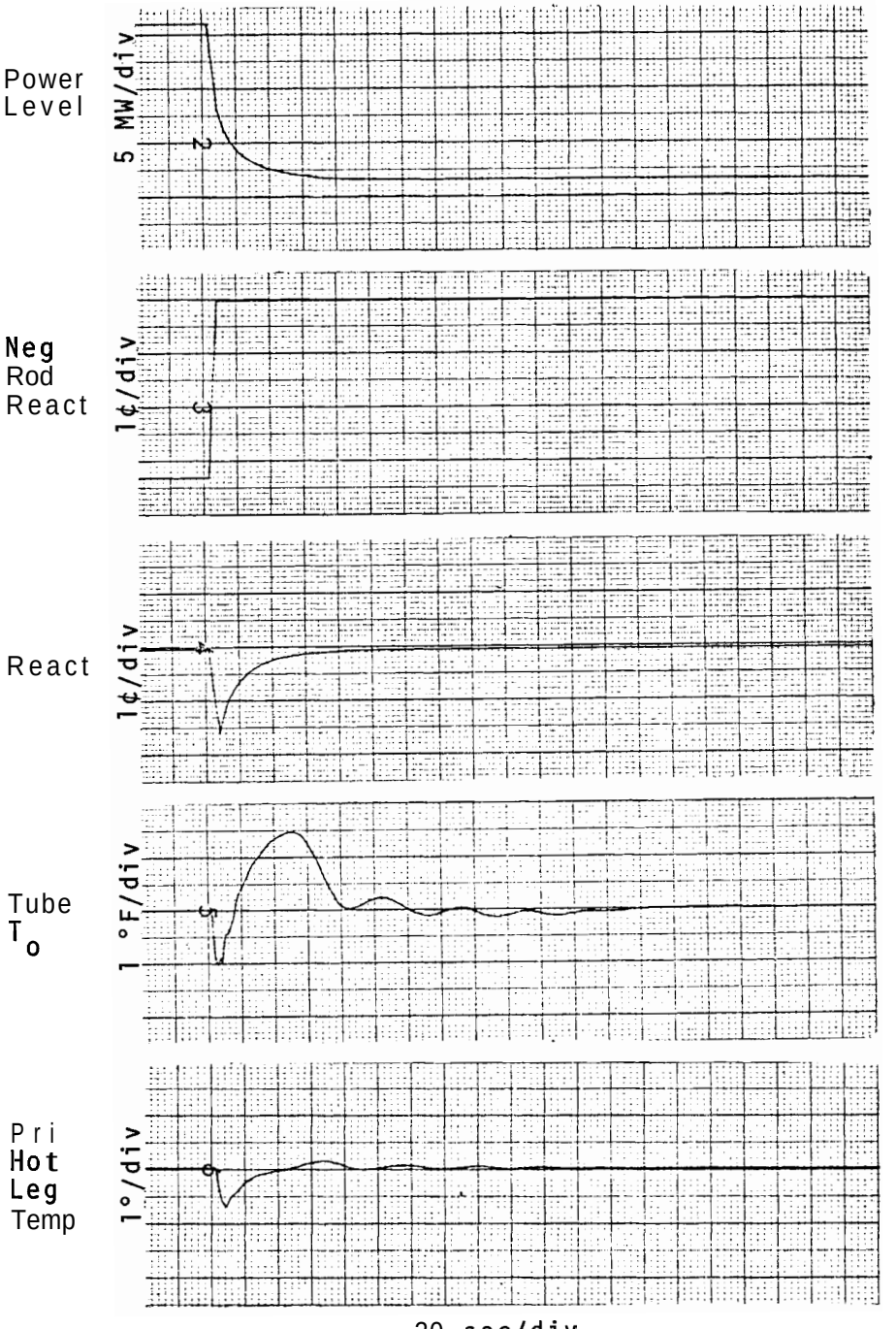

FIGURE 12. (contd)

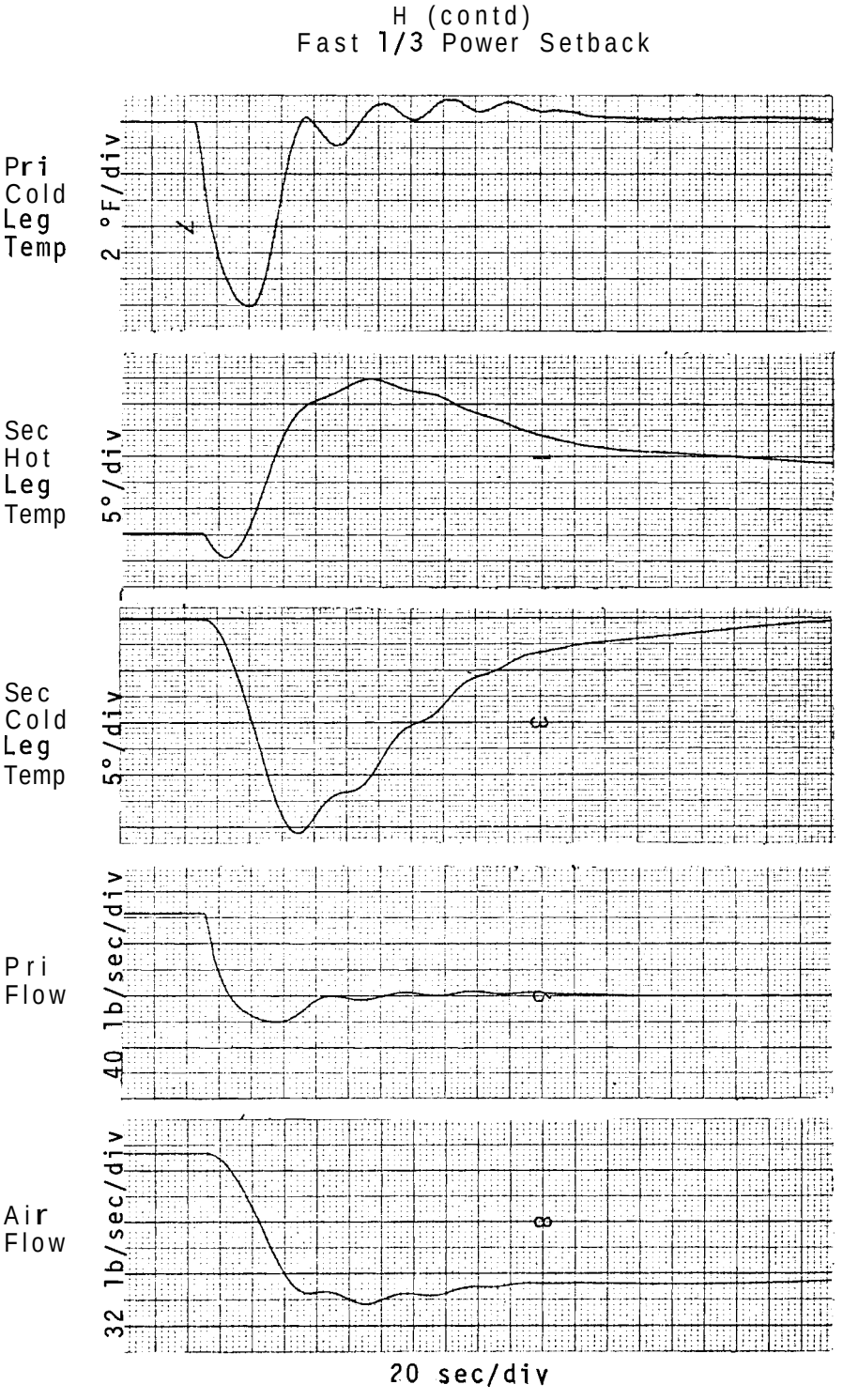

FIGURE 12. (contd)

Slow 1/3 Power Setback

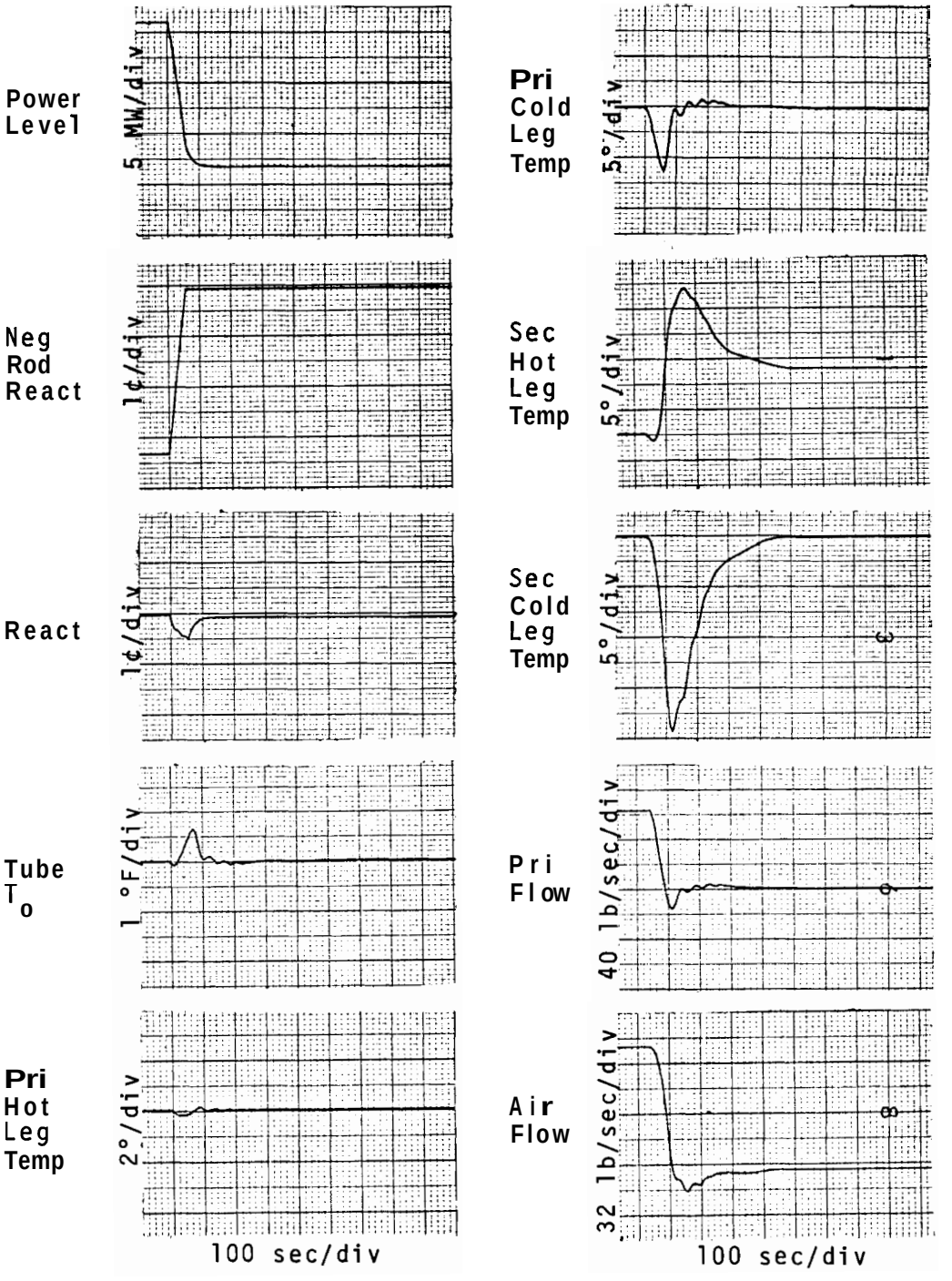

FIGURE 12. (contd)

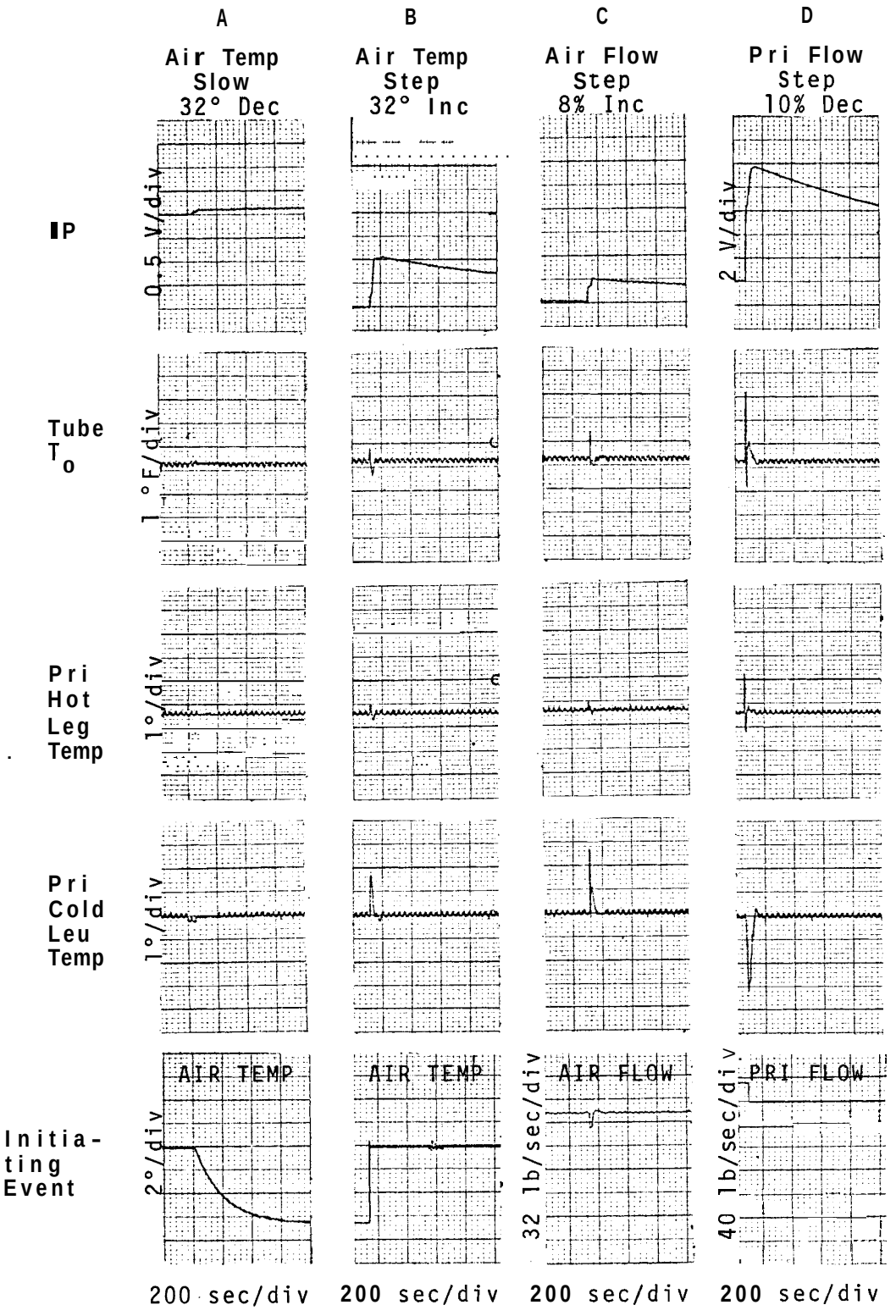

FIGURE 13. Controller Configuration Number VI Transients

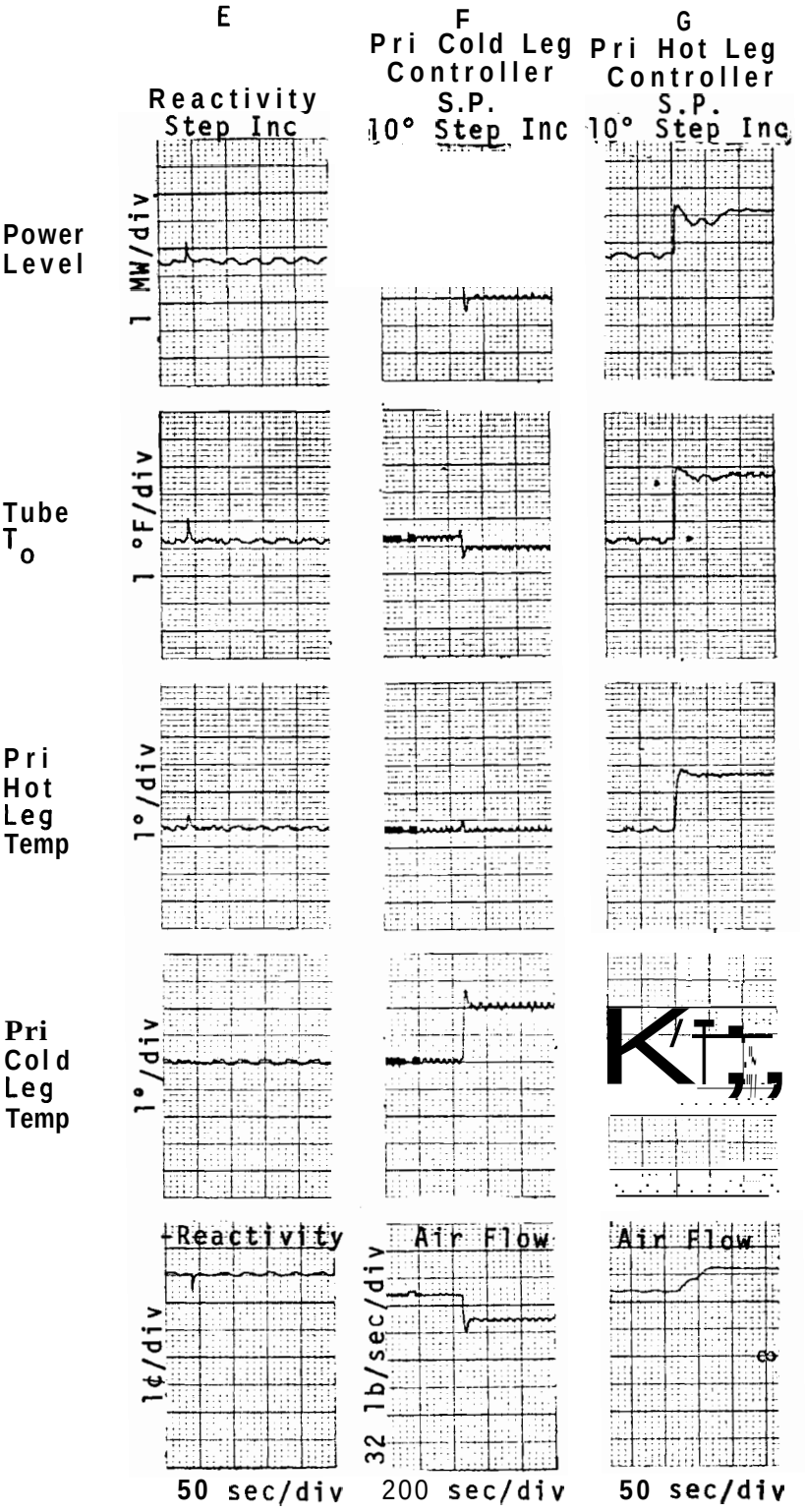

FIGURE 13. (contd)

OPERATING CONDITION EFFECTS

A series of computer runs were made to gain understanding of the effects of operating conditions on control system performance. Control Configuration I was used for this series of runs because it is a simple configuration and because it is relatively straightforward to interpret the effects for other configurations.

The performance of the controlled system is affected by power level, primary and secondary sodium flow rates, and by the cooling air inlet temperature. The controlled system performance was studied to define the process gain and phase changes as well as the effects on transient responses caused by disturbances for the various operating conditions. Table 4 lists the set of eleven runs that include combinations of three operating power levels (full, two-thirds, and one-third) primary flow rates, secondary flow rates, and air inlet temperatures. Also included in Table 4 are the controller settings that resulted in approximately 20% overshoot to 10° setpoint step changes when both control loops are closed.

Three kinds of information obtained in order to study the overall operating condition effects include:

- Open loop frequency responses
- Controller settings for 20% overshoot
- Transient responses.

The frequency responses for each run include a primary cold leg temperature controller open loop frequency response (Figure 14-1 through 14-11), and a primary hot leg temperature controller open loop frequency response (Figure 15-1 through 15-11). The frequency response for the primary cold leg controller was taken in all runs with the hot leg control loop open. The

TABLE 4. Operating Conditions with Controller Settings for 20% Overshoot to Setpoint Changes for Configuration I

Run	Power Level	Pri Flow	Secon Flow	Air in Temp., °F	Controller Settings P_2	I_2	P_3	I_3
1	full	full	full	100	7	0.005	12	0.1
2	2/3	2/3	full	100	2.6	0.0035	10	0.075
3	2/3	2/3	2/3	100	1.5	0.003	10	0.07
4	2/3	full	2/3	100	1.65	0.0035	15	0.11
5	2/3	full	full	100	2.75	0.005	13	0.12
6	1/3	1/3	full	100	1.5	0.0035	5.5	0.05
7	1/3	1/3	1/3	100	0.5	0.002	6	0.045
8	1/3	full	1/3	100	0.8	0.00026	12	0.01
9	1/3	full	full	100	2	0.002	25	0.1
10	full	full	full	32	4	0.006	13	0.09
11	full	full	full	-25	3	0.005	12	0.1

sine wave output from a signal generator was applied to the air flow, and the primary cold leg temperature was recorded. The frequency response for the primary hot leg temperature controller was taken in all runs with the primary cold leg control loop closed and adjusted for 20% overshoot to setpoint changes and with the hot leg control loop open.

Important information on the effects of operating condition changes is contained in the controller settings, (Table 4) that were found to result in 20% overshoot when 10° step setpoint changes were made. The method of repeatedly adjusting the controllers for 20% overshoot when both control loops were closed was the same as for the runs on controller configuration effects.

The third kind of information is the transient responses in the process tube outlet temperature, the primary hot and

cold leg temperatures, and the secondary cold leg temperature when various disturbances are introduced into the system. The transient responses for balanced IHX flows only are shown in Figures 16-1 through 6. The peak magnitudes for all runs are given in Table 5.

POWER LEVEL EFFECTS

The effects on the controlled system of changing the power level only is seen by comparing Runs 1, 5, and 9 which all have full flows and 100 °F air temperature. The cold leg control open loop frequency responses for these runs show that little phase differences of significance appears, but there is an increase in the process gain (db) as the reactor power level decreases. One would expect that a compensating decrease in primary cold leg controller proportional action (P_2) would result, since for each run the controllers were adjusted to give approximately the same overshoot for step setpoint changes.

The frequency responses for the primary hot leg controller open loop were taken with the cold leg controller loop closed. Since interaction exists between the two control loops, the hot leg controller frequency responses have some phase and magnitude changes that occur at about the cutoff frequency for the primary cold leg controller. These vary widely depending upon the primary cold leg control loop characteristics. A primary hot leg control open loop frequency response taken with the primary cold leg temperature held completely constant did not show any sharp phase and magnitude changes occurring just below the frequency of 0.01 H_z. For most runs, the phase and magnitude effects due to the interaction are ignored and the characteristics at higher and lower frequencies are considered.

TABLE 5. Transient Peaks – Configuration I – Varying Operating Conditions

Measured Parameter	Run	Power Level	Pri Flow	Sec Flow	Air Temp., °F	Disturbances a: Air Temp. Slow 32 °F Decrease	b: Air Temp. Step 32 °F Increase	c: Air Flow Step 8% Decrease	d: Pri Flow Step 10% Decrease	e: Power 15 MW Increase	f: Pri Cold Leg 10° Setpoint Increase	g: Pri Hot Leg 10° Setpoint Increase
Tube Outlet Temp.	1	full	full	full	100	0°	-3°	-2°	18°	4°	-3°	35°
	2	2/3	2/3	full	100	0	-2.5	-5	19	5.5	-3	46
	3	2/3	2/3	2/3	100	1	-3	-8	19	7	-3	44
	4	2/3	full	2/3	100	1	-6.5	-4	12	3	-2.5	34
	5	2/3	full	full	100	0	-2.5	-6	13	3.5	-2.5	31
	6	1/3	1/3	full	100	0	-1	-3	19	5	-2.5	52
	7	1/3	1/3	1/3	100	1	-3		19	6	-2.5	56
	8	1/3	full	1/3	100	1.5	-3.5	-3	8	-3	-3	15
	9	1/3	full	full	100	0	-1.5	-3	6	2	-2.5	34
	10	full	full	full	32	0.5	-3.5	-4	17	3.5	-2.5	37
	11	full	full	full	-25	0	2.5	-3.5	17	3.5	-2.5	36
Primary Hot Leg Temp.	1	full	full	full	100	0	0	0	5	1	0	12
	2	2/3	2/3	full	100	0	0	1	4.5	1	0.5	12
	3	2/3	2/3	2/3	100	0	0.5	-1	4.5	1.5	0.5	12
	4	2/3	full	2/3	100	0	-1	-1	4	1.0	0	12
	5	2/3	1/3	full	100	0	-0.5	-2	4	1.0	0	12
	6	1/3	1/3	full	100	0	0	1	4	1	0.5	12
	7	1/3	1/3	1/3	100	0	0.5	1.5	4	1.5	0	12
	8	1/3	full	1/3	100	-1	4.5	3	3.5	3.5	3	11.5
	9	1/3	full	full	100	0	0	0.5	2	0.5	0.5	12
	10	full	full	full	32	0	0.5	0.5	5	0.5		
	11	full	full	full	-25	0	-0.5	0.5	3	1	0	12
Primary Cold Leg Temp.	1	full	full	full	100	-2	13	8	-5	8	12	12
	2	2/3	2/3	full	100	-2	10	23	-4	8.5	12	-8.5
	3	2/3	2/3	2/3	100	-3.5	13.5	19.5	-4.5	15	12	-10
	4	2/3	full	2/3	100	-5	22.5	23	-5	19	12	-14
	5	2/3	full	full	100	-1.5	12.5	15	-4	10	12	-11
	6	1/3	1/3	full	100	0	7	16.5	0	6	12.5	-5
	7	1/3	1/3	1/3	100	-4	14.5	18/60	-2	17	12	-10
	8	1/3	full	1/3	100	-9.5	17.5	15	-7	15	13	-19.5
	9	1/3	full	full	100	-1	6.5	13	2.5	5.5	11.5	-10
	10	full	full	full	32	-3	15	17	-5	8	12.5	-12.5
	11	full	full	full	-25	2	-12	17	-6	8.5	11.5	-12
Secondary Cold Leg Temp.	1	full	full	full	100	-1	11	7	0.5	-9	11	9
	2	2/3	2/3	full	100	-1.5	9	20	1	-9	9.5	6
	3	2/3	2/3	2/3	100	-2	2.5	15	1	-13	9	7
	4	2/3	full	2/3	100	-2	12.5	11.5	0	-16	8.5	11
	5	2/3	full	full	100	-1	10	8	1	-11	9	8
	6	1/3	1/3	full	100	0	6.5	17	0	-3	10	-3
	7	1/3	1/3	1/3	100	-3	13	50	0	-29	9	9
	8	1/3	full	1/3	100	-2	15	11	2	-12.5	9	20
	9	1/3	full	full	100	-1	7	10	1	-7	10	8
	10	full	full	full	32	-1	11	12	0	-8	10	7.5
	11	full	full	full	-25	1	-10	15	1	-8	10	7

Comparison of the open loop frequency responses for the primary hot leg control system shows that, as with the cold leg, the phase differences are not significant. However, process gain decreases; one would therefore expect an increased controller gain as power decreases in order to compensate for the process gain change.

Finally, since all effects of power level change occurs in process gain and not in the phase, we would expect to see little difference in transient responses to disturbances, provided that controller gain adjustments are made to compensate for process gain changes.

Comparison of the controller settings showed that the primary cold leg controller proportional action decreased as expected, and the primary hot leg controller proportional action increased, as expected. Also, comparison of the transients show that there are no major differences. There appears to be no degradation of the controlled system performance as a function of the power level only, provided that compensating proportional action adjustments are made.

PRIMARY SODIUM FLOW RATE EFFECTS

The effects of decreasing only the primary sodium flow rate can be compared at various conditions of power level and secondary flow as follows:

- Run 5 versus Run 2 for 2/3 power and full secondary flow.
- Run 4 versus Run 3 for 2/3 power and 2/3 secondary flow.
- Run 9 versus Run 6 for 1/3 power and full secondary flow.
- Run 8 versus Run 7 for 1/3 power and 1/3 secondary flow.

Inspection of the frequency responses show that in the primary cold leg control loop there are no effects on the phase and only slight increase of the process gain. The primary hot leg control loop shows an increased process gain and an increased phase lag as the primary flow decreases. The increased phase

lag in the hot leg loop is expected since lower flow causes longer mixing and transport times. Also, the hot leg loop process gain increase results from the longer time that the sodium is influenced by the reactor heat. The controller settings for the 20% overshoot are summarized in Table 6.

TABLE 6. Controller Settings to Show the Effect of Primary Flow Changes

Run	Pri Flow	P_2	I_2	P_3	I_3	
5	full	2.75	0.085	13	0.12	2/3 power, full sec flow
2	2/3	2.6	0.0035	10	0.075	
4	full	1.65	0.0035	15	0.11	2/3 power, 2/3 sec flow
3	2/3	1.5	0.003	10	0.07	
9	full	2	0.002	25	0.1	1/3 power, full sec flow
6	1/3	1.5	0.0035	5.5	0.05	
8	full	0.8	0.0026	12	0.01	1/3 power, 1/3 sec flow
7	1/3	0.5	0.002	6	0.045	

Table 6 shows that in all cases, as the primary flow decreases, the primary cold leg controller proportional action (P_2) decreases slightly to compensate for the process gain increase, and the primary hot leg controller gain (P_3) decreases to compensate for the process gain increase. There is no consistent effect on cold leg controller integral action, but the hot leg controller integral action was reduced as a result of the increased process phase lag.

There appears to be a minor degradation of the transient performance, as is expected due to the increased phase lag effects. In summary, the primary hot leg control system

characteristics and performance appear slightly degraded when the primary flow is reduced. This mostly results from the lengthening of transit and mixing times. The proportional action in the primary hot leg controller must be increased as the flow is decreased in order to retain system performance.

SECONDARY SODIUM FLOW RATE EFFECTS

The runs that demonstrate the effects of changing only the secondary flow are:

- Run 2 versus Run 3 for 2/3 power and 2/3 primary flow
- Run 5 versus Run 4 for 2/3 power and full primary flow
- Run 6 versus Run 7 for 1/3 power and 1/3 primary flow
- Run 9 versus Run 8 for 2/3 power and full primary flow.

The frequency responses show that the process phase and gain for the primary hot leg control system are essentially unchanged as the secondary flow is changed. The primary cold leg control system, however, shows increased phase lag as the secondary flow is decreased. This is as expected because of the long distance/velocity delays inherent in the secondary loop. The process gain for the primary cold leg system open loop remains essentially unchanged as the secondary flow is reduced.

Table 7 presents the controller settings to show the effects of the secondary flow rate.

The characteristics of the primary cold leg control system open loop are such that the increased phase lag caused by reduced secondary flow requires that the overall control loop gain must be decreased, thus causing a degradation in control system performance. Study of the transient peaks from Table 5 reveals that the system performance is degraded as the secondary flow decreases. The secondary flow is a major factor in establishing the performance of the primary cold leg temperature controller. We expect that the same effect is present on other control configurations.

TABLE 7. Controlled Settings to Show the Effect of Secondary Flow Changes

Run	Sec. Flow	P_2	I_2	P_3	I_3	
2	full	2.6	0.0035	10	0.075	2/3 power, 2/3 primary flow
3	2/3	1.5	0.003	10	0.07	
5	full	2.75	0.005	13	0.12	2/3 power, full primary flow
4	2/3	1.65	0.0035	15	0.11	
6	full	1.5	0.0035	5.5	0.05	1/3 power, 1/3 primary flow
7	1/3	0.5	0.002	6	0.045	
9	full	2	0.002	25	0.1	1/3 power, full primary flow
8	1/3	0.8	0.00026	12	0.01	

It appears that the secondary flow produces the most severe of the effects with regard to the control system performance. The operating philosophy that gives the best control system performance at reduced power is to maintain full primary and secondary flows. Table 8 shows a comparison of the transient responses in an order that demonstrates the effect that coolant flows have on the system performance. The best cases of full primary and full secondary flows for reduced power are shown on top, and the worst case of low primary and low secondary flows are next. The unbalanced cases of primary and secondary flows (not included) are in between the best and worst cases on Table 8. All cases with low secondary flow appear unfavorable, however, regardless of what the primary flow is.

TABLE 8 Transient Peaks Arranged to Emphasize Effects of Flow Changes

Measured Parameter	Run No.	Power Level	Pri. Flow	Sec. Flow	Air Temp., °F	Disturbances a: Air Temp Slow 32 °F Decrease	b: Air Temp Step 32 °F Increase	c: Air Flow Step 8% Decrease	d: Pri. Flow Step 10% Decrease	e: Power 15 MW Increase	f: Pri. Cold Leg 10° Setpoint Increase	g: Pri. Hot Leg 10° Setpoint Increase
Tube Outlet Temp.	1	full	full	full	100	0 °a	-3°	-2°	18°	4°	-3°	35°
	5	2/3	full	full		0	-2.5	-6	13	3.5	-2.5	31
	9	1/3	full	full		0	-1.5	-3	6	2	-2.5	34
	3	2/3	2/3	2/3		1	-3	-8	19	7	-3	44
	7	1/3	1/3	1/3		1	-3		19	6	-2.5	56
Primary Hot Leg Temp.	1	full	full	full		0	0	0	5	1	0	12
	5	2/3	full	full		0	-0 5	-2	4	1.0	0	12
	9	1/3	full	full		0	0	0.5	2	0.5	0.5	12
	3	2/3	2/3	2/3		0	0.5	-1	4.5	1.5	0.5	12
	7	1/3	1/3	1/3		0	0.5	1 5	4	1.5	0	12
Primary Cold Leg Temp.	1	full	full	full		-2	13	8	-5	8	12	12
	5	2/3	full	full		-1 5	12.5	15	-4	10	12	-11
	9	1/3	full	full		-1	6.5	13	2.5	5 5	11.5	-10
	3	2/3	2/3	2/3		-3 5	13.5	19.5	-4.5	15	12	-10
	7	1/3	1/3	1/3		-4	14.5	18/≤0	-2	17	12	-10
Secondary Cold Leg Temp.	1	full	full	full		-1	11	7	0.5	-9	11	9
	5	2/3	full	full		-1	10	8	1	-11	9	8
	9	1/3	full	full		-1	7	10	1	-7	10	8
	3	2/3	2/3	2/3		-2	25	15	1	-13	9	7
	7	1/3	1/3	1/3		-3	13	50	0	-29	9	9

AIR TEMPERATURE EFFECTS

Runs 1, 10, and 11 demonstrate the effects of temperature variations in the cooling air. Inspection of the frequency responses show that as the air gets colder, the phase does not change, but the process gain increases for the primary cold leg temperature control system. Neither the phase nor the magnitude of the primary hot leg temperature control loop are affected by the air temperature change.

Inspection of the controller settings on Table 4 reveals that the primary cold leg controller proportional action is decreased to compensate for the increased process gain. None of the other controller settings are appreciably changed. The transients in Table 5 show no significant differences except for the air flow disturbance.

The use of configurations that control the secondary cold leg by manipulating the air flow (such as II and V) would show the open loop process gain change in the system that manipulates air flow. In Configuration II, one would expect no appreciable effect in the primary cold leg control loop.

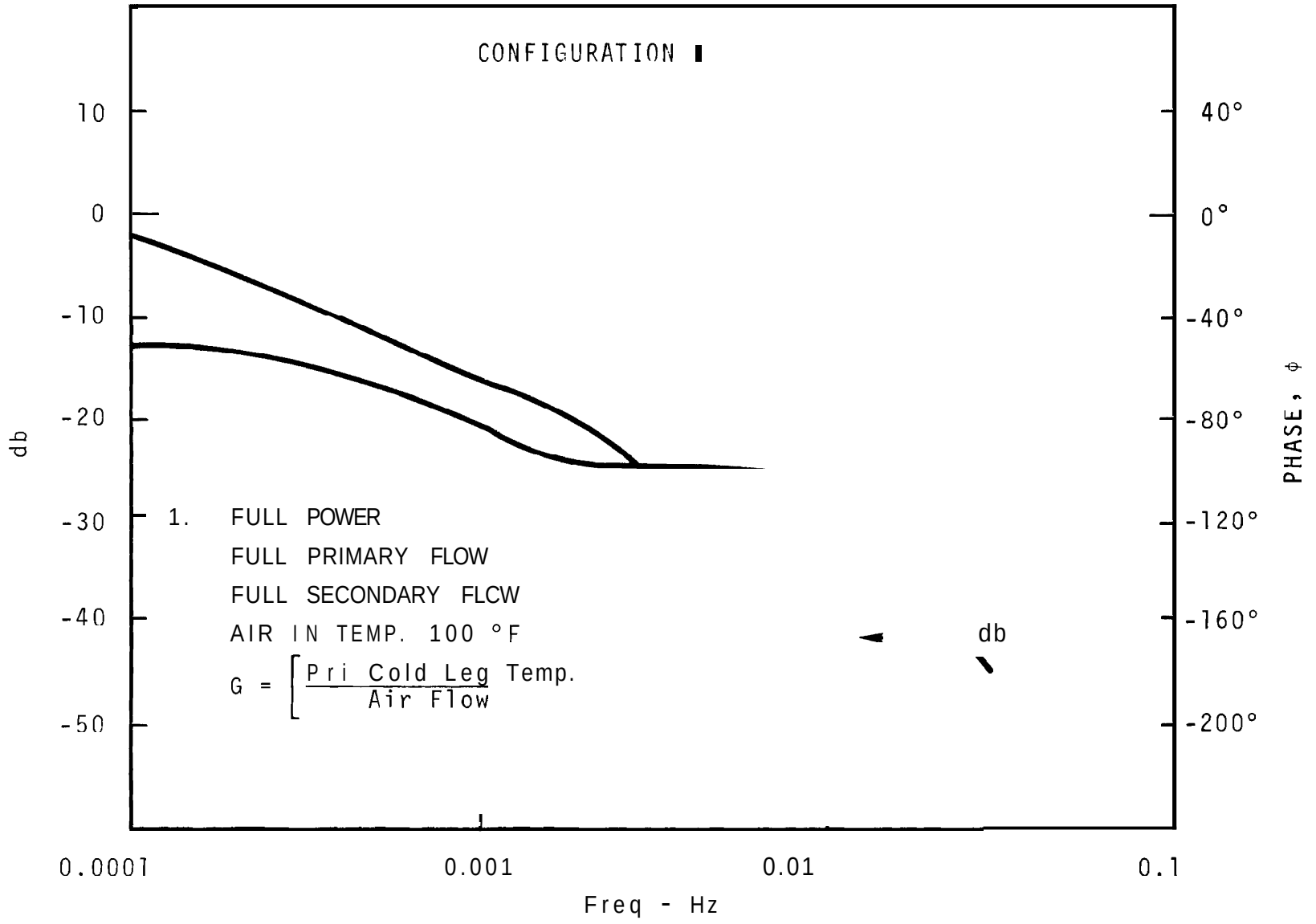

FIGURE 14-1. Primary Cold Leg Controller Open Loop Frequency Response

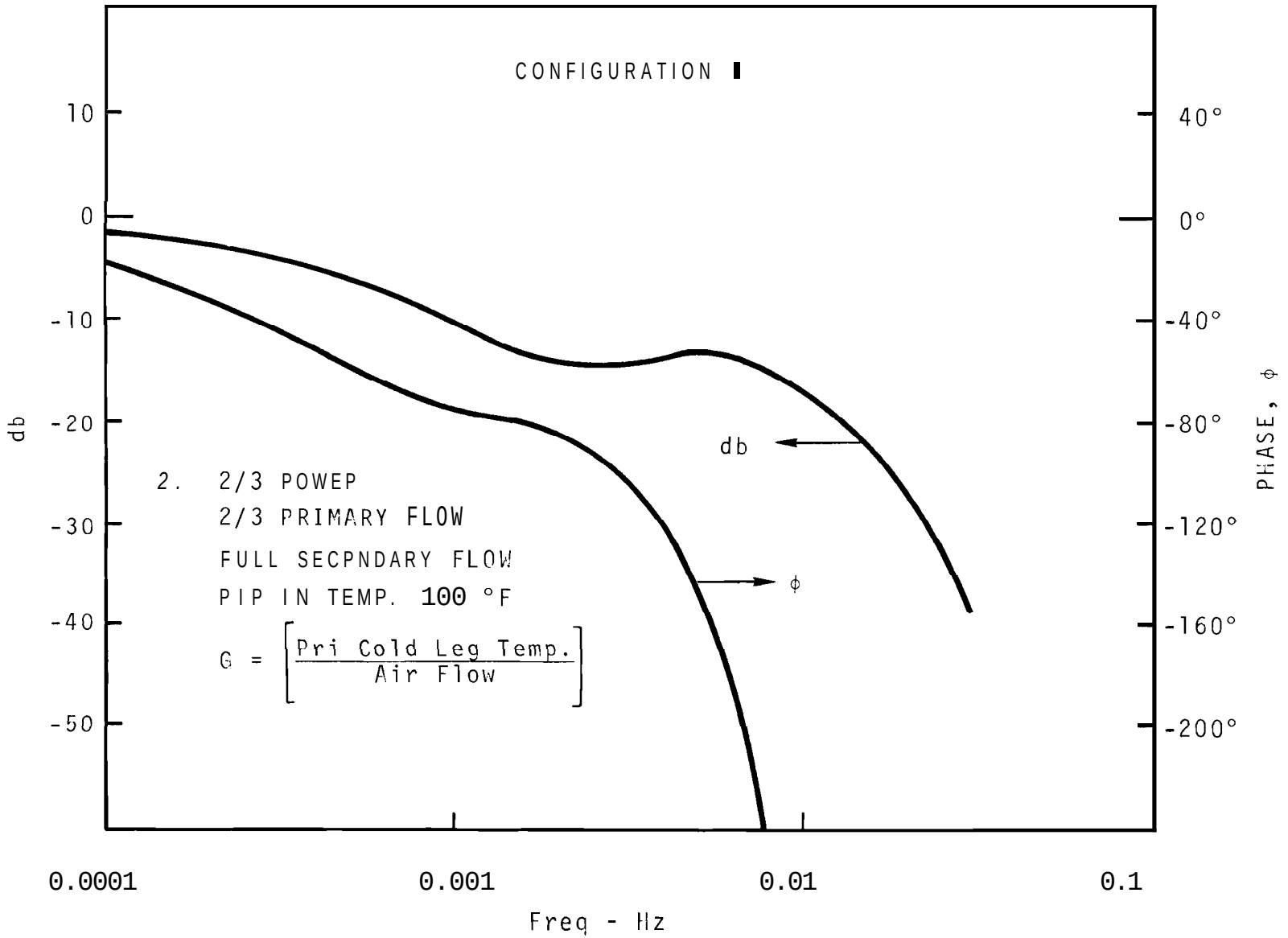

FIGURE 14-2. Primary Cold Leg Controller Open Loop Frequency Response

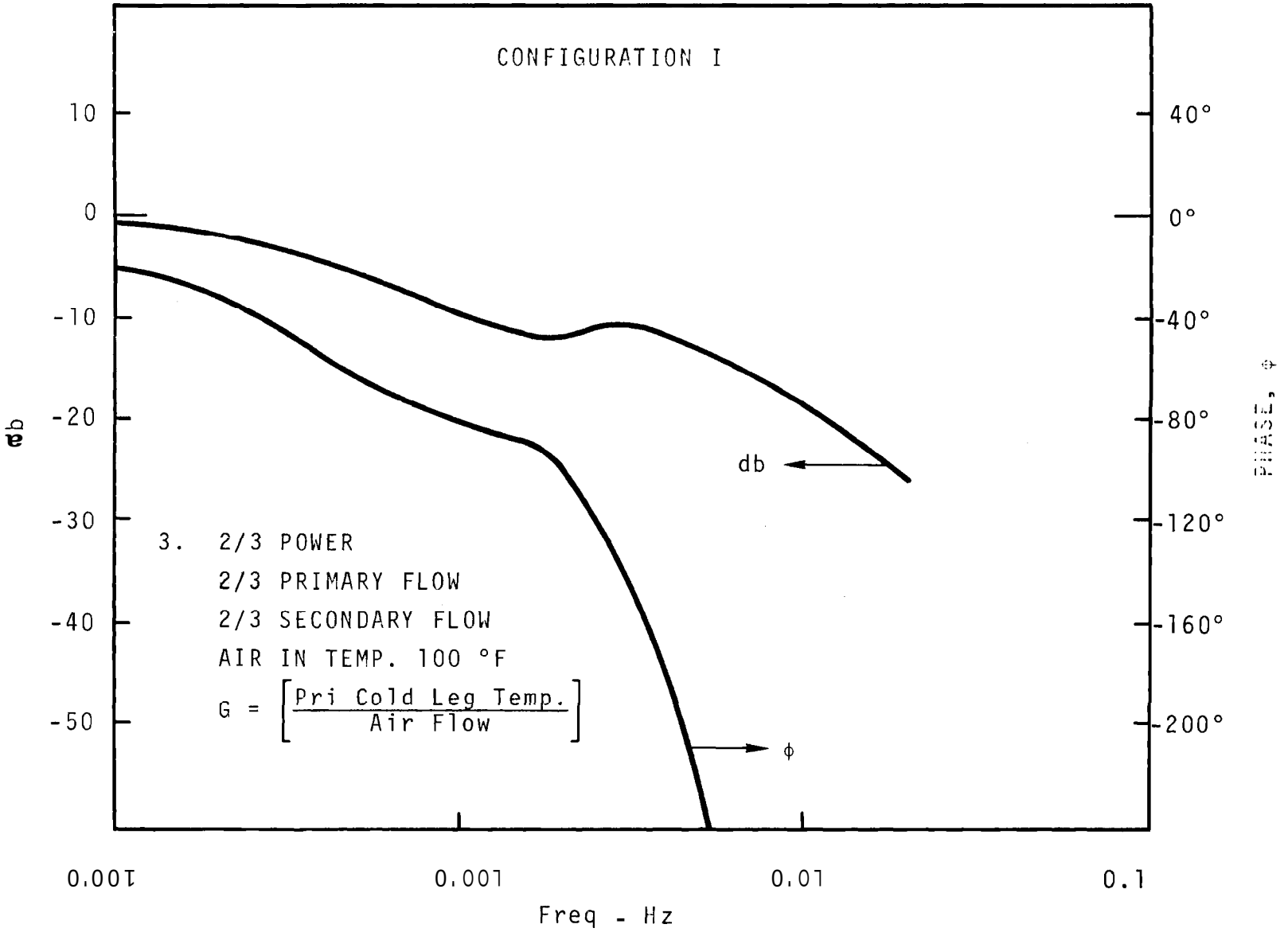

FIGURE 14-3. Primary Cold Leg Controller Open Loop Frequency Response

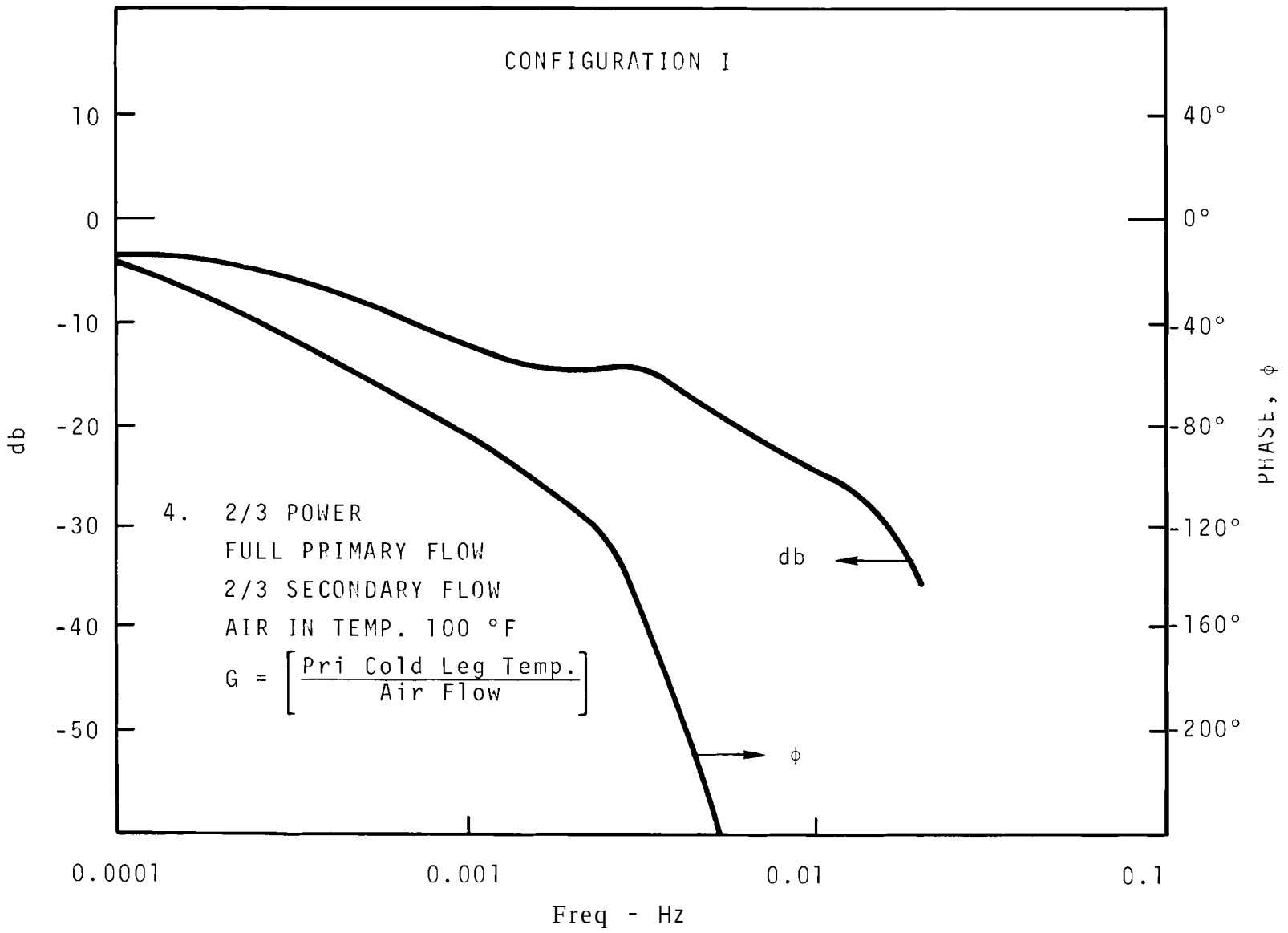

FIGURE 14-4. Primary Cold Leg Controller Open Loop Frequency Response

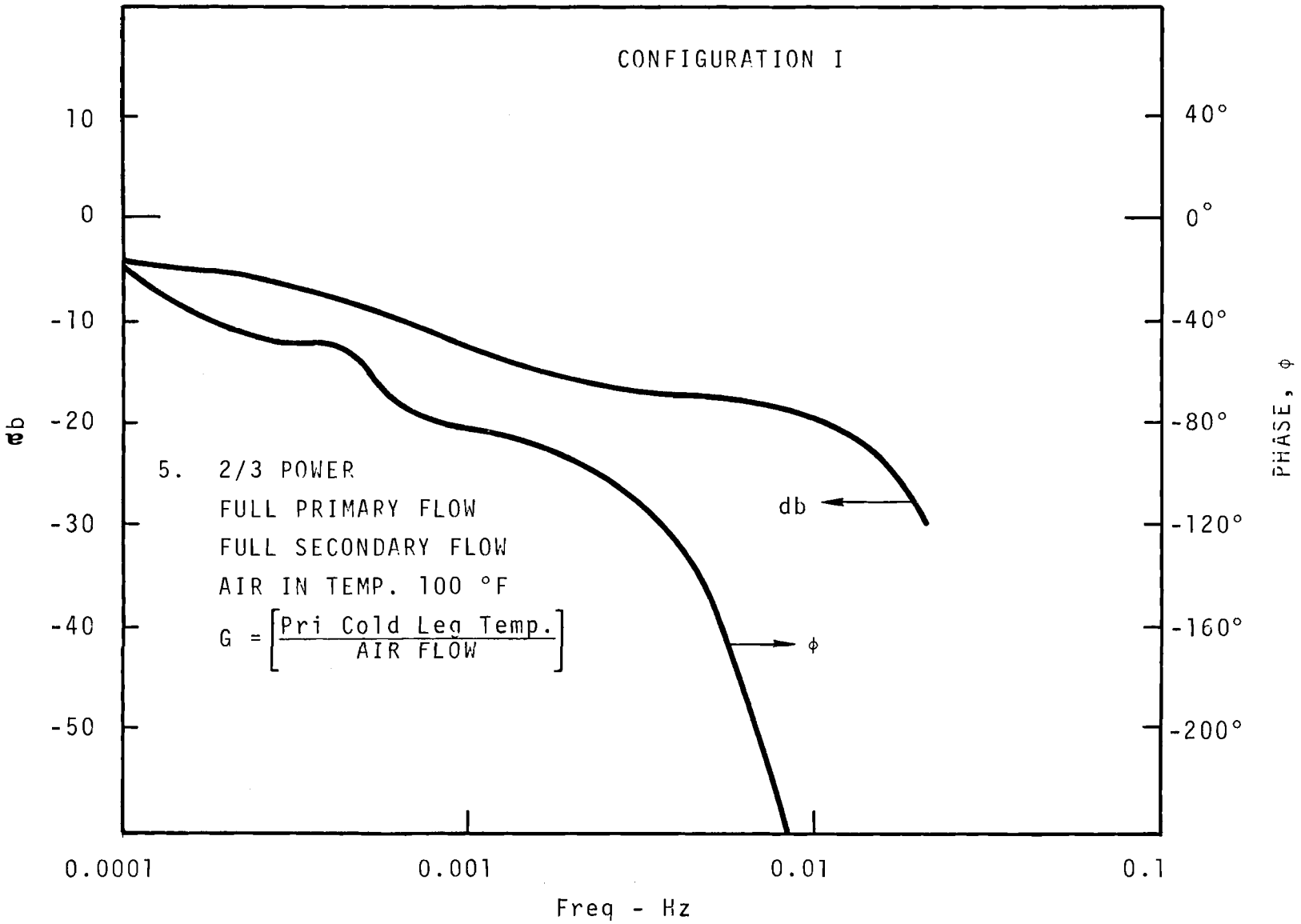

FIGURE 14-5. Primary Cold Leg Controller Open Loop Frequency Response

L-1395

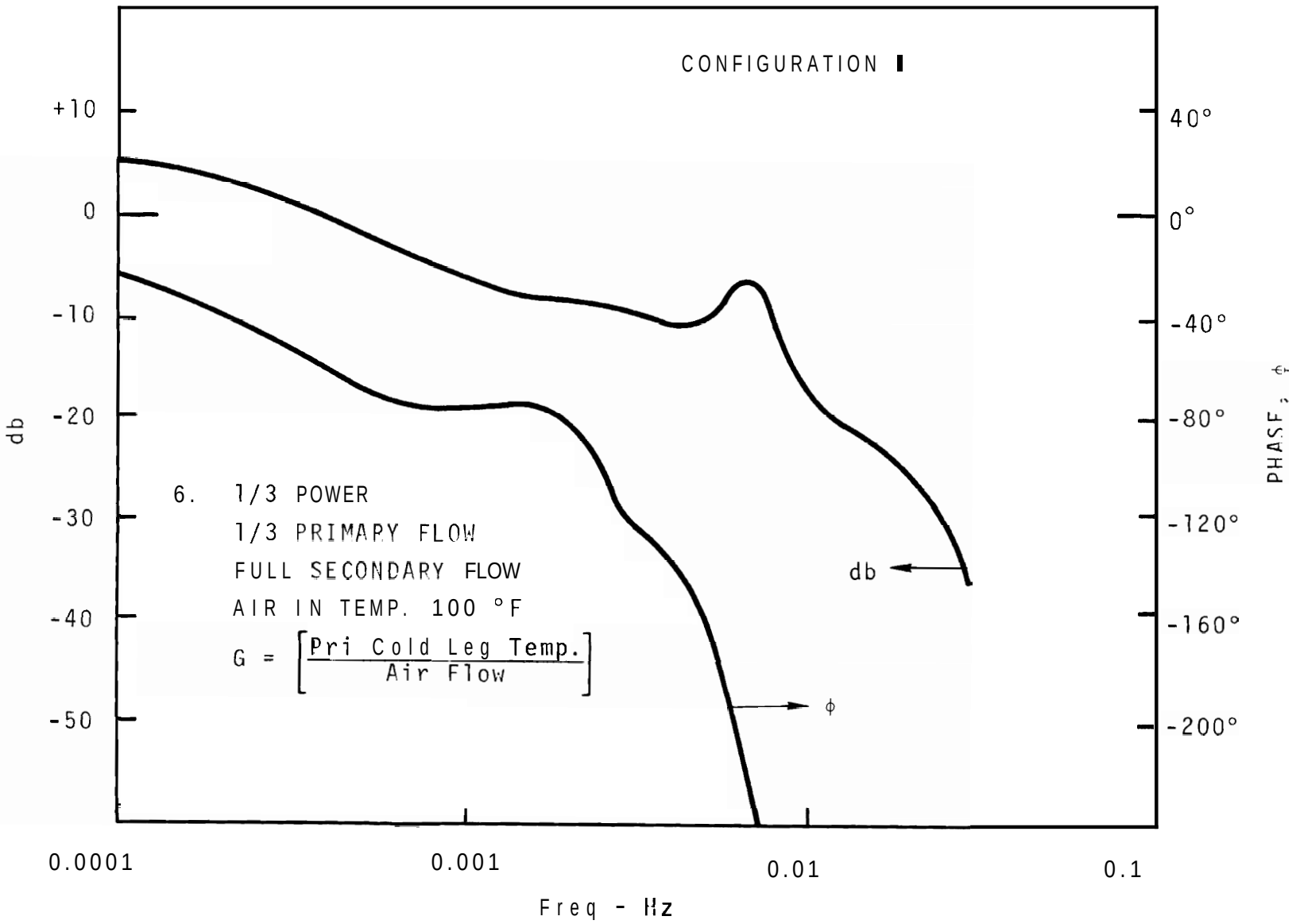

FIGURE 14-6. Primary Cold Leg Controller Open Loop Frequency Response

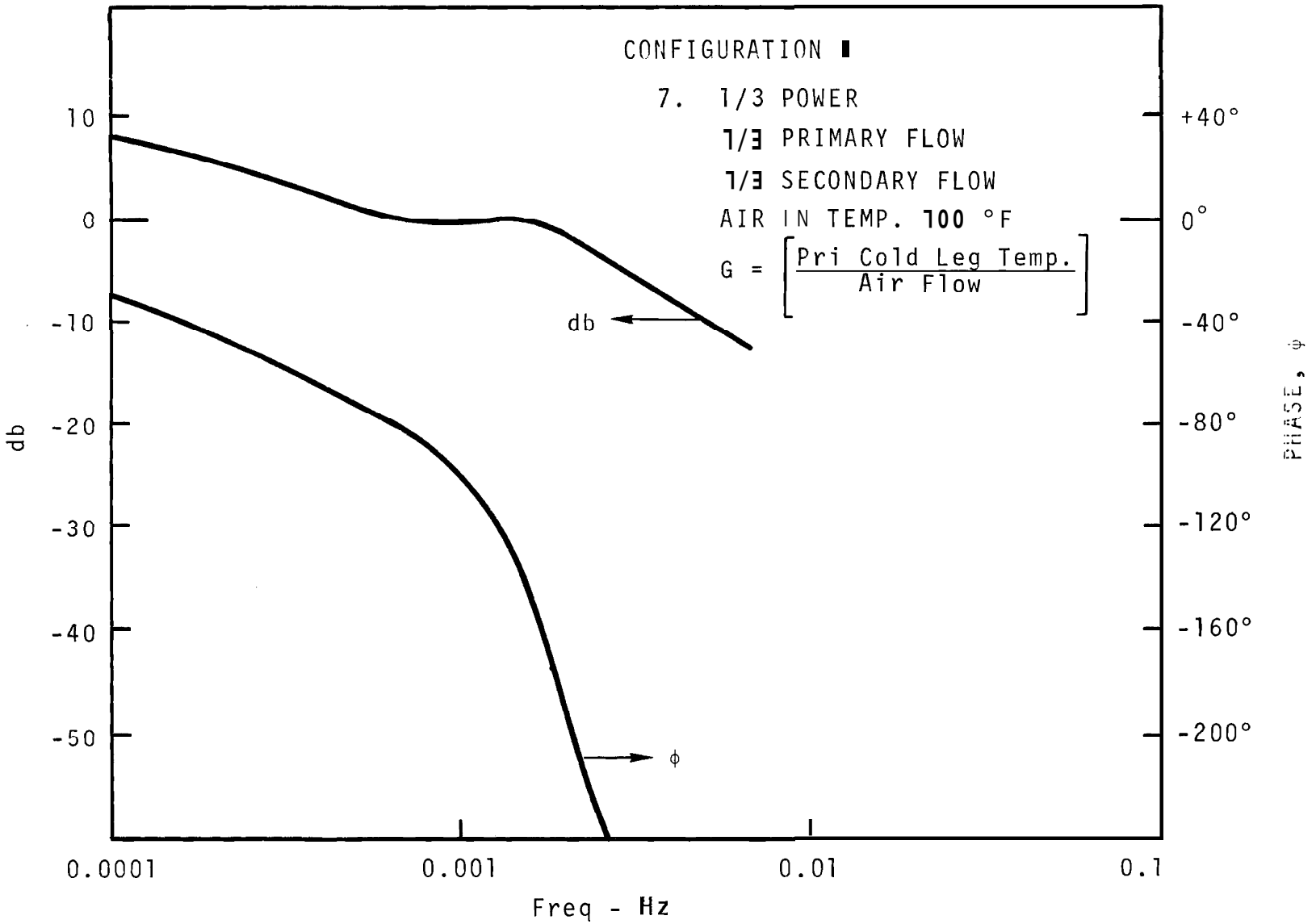

FIGURE 14-7. Primary Cold Leg Controller Open Loop Frequency Response

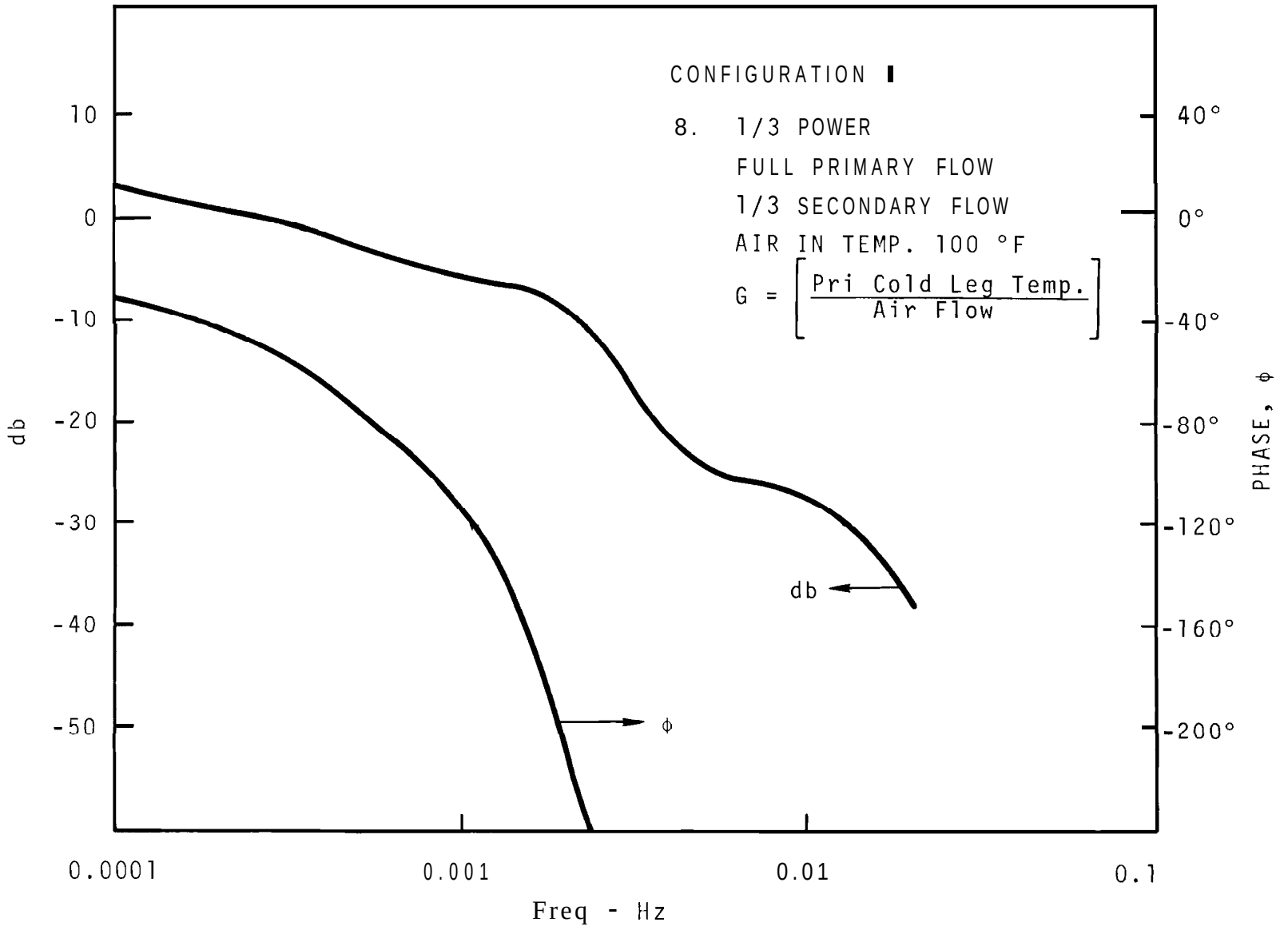

FIGURE 14-8. Primary Cold Leg Controller Open Loop Frequency Response

BNWL

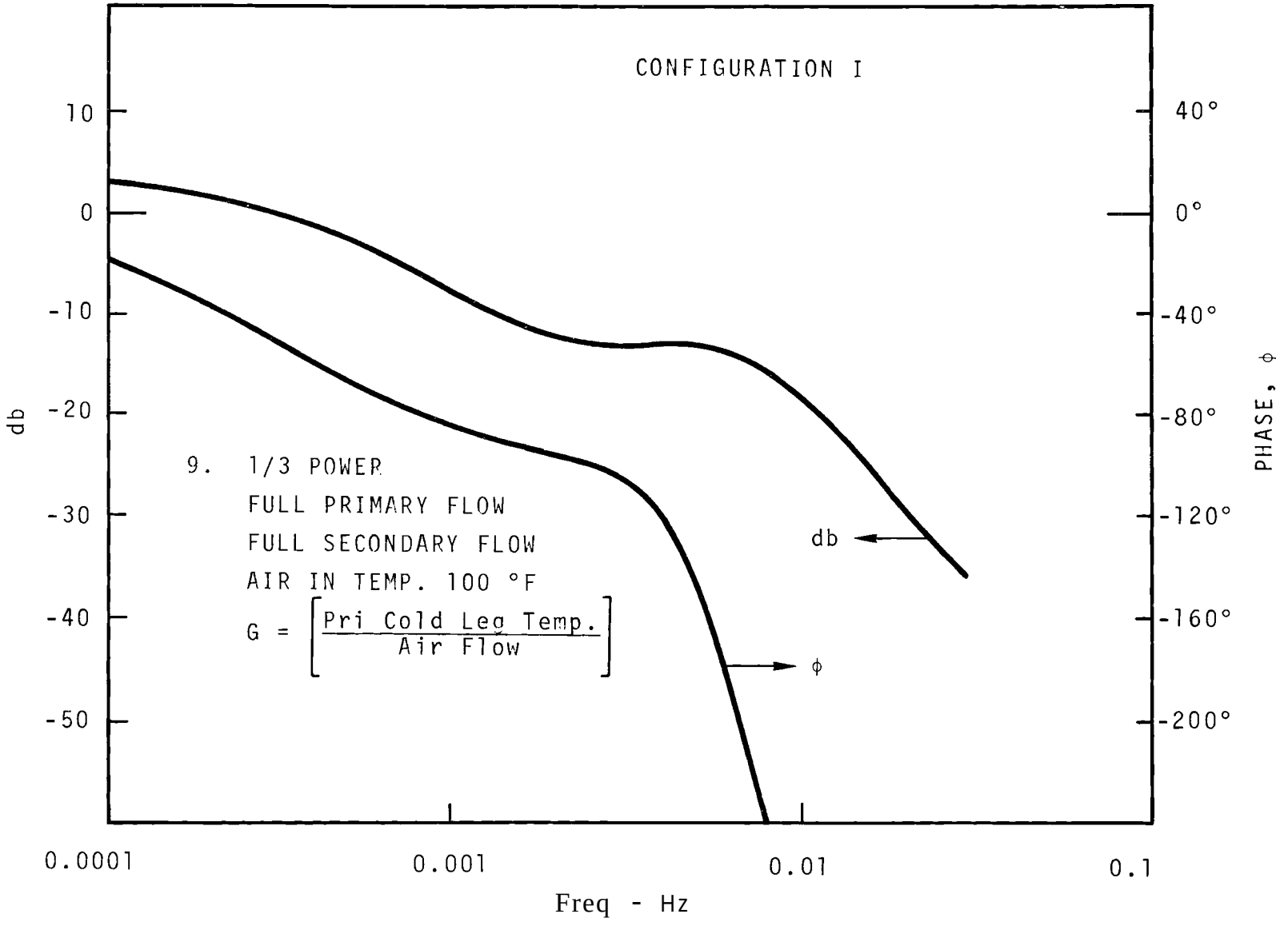

FIGURE 14-9. Primary Cold Leg Controller Open Loop Frequency Response

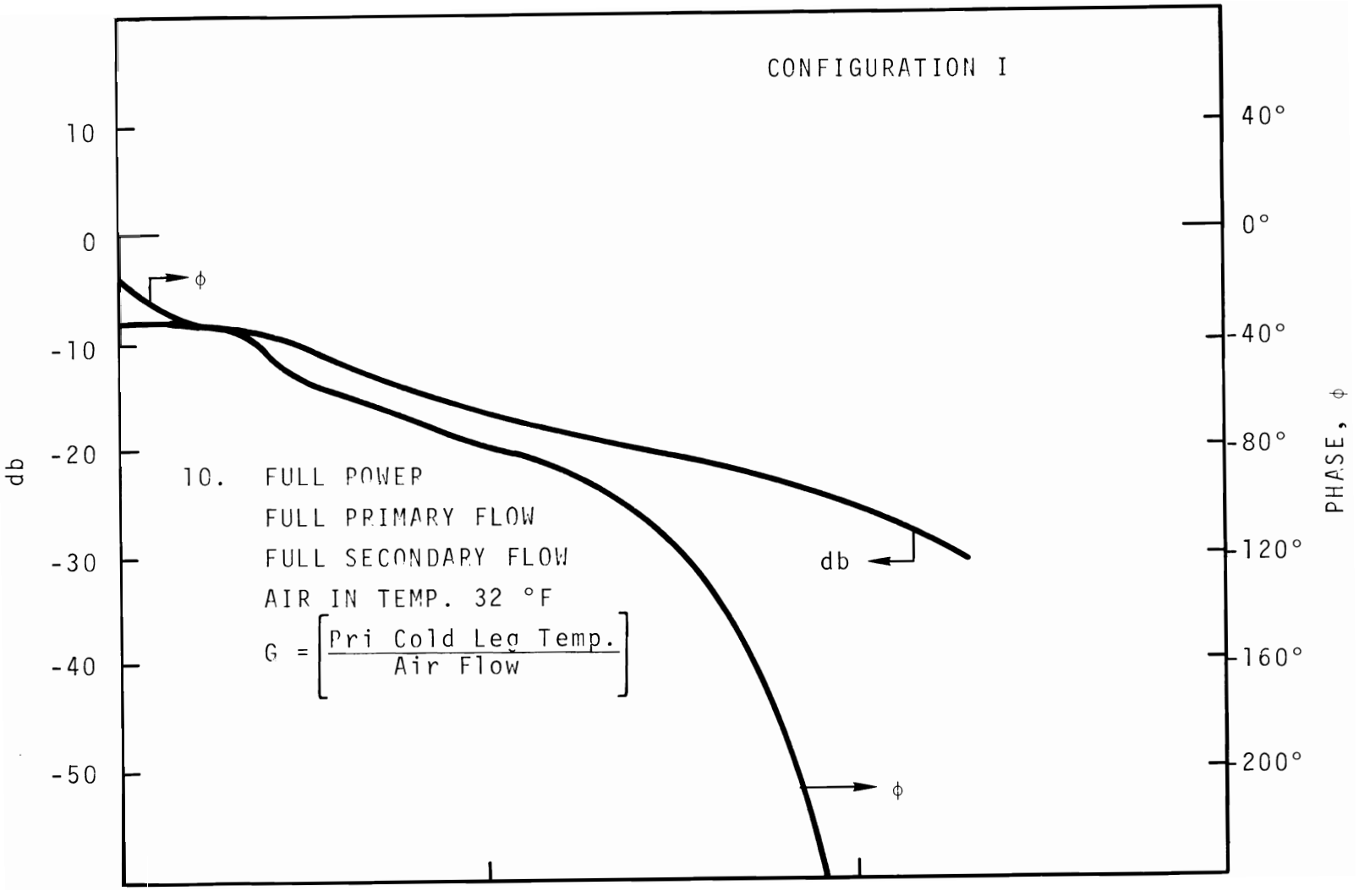

FIGURE 14-10 Primary Cold Leg Controller Open Loop Frequency Response

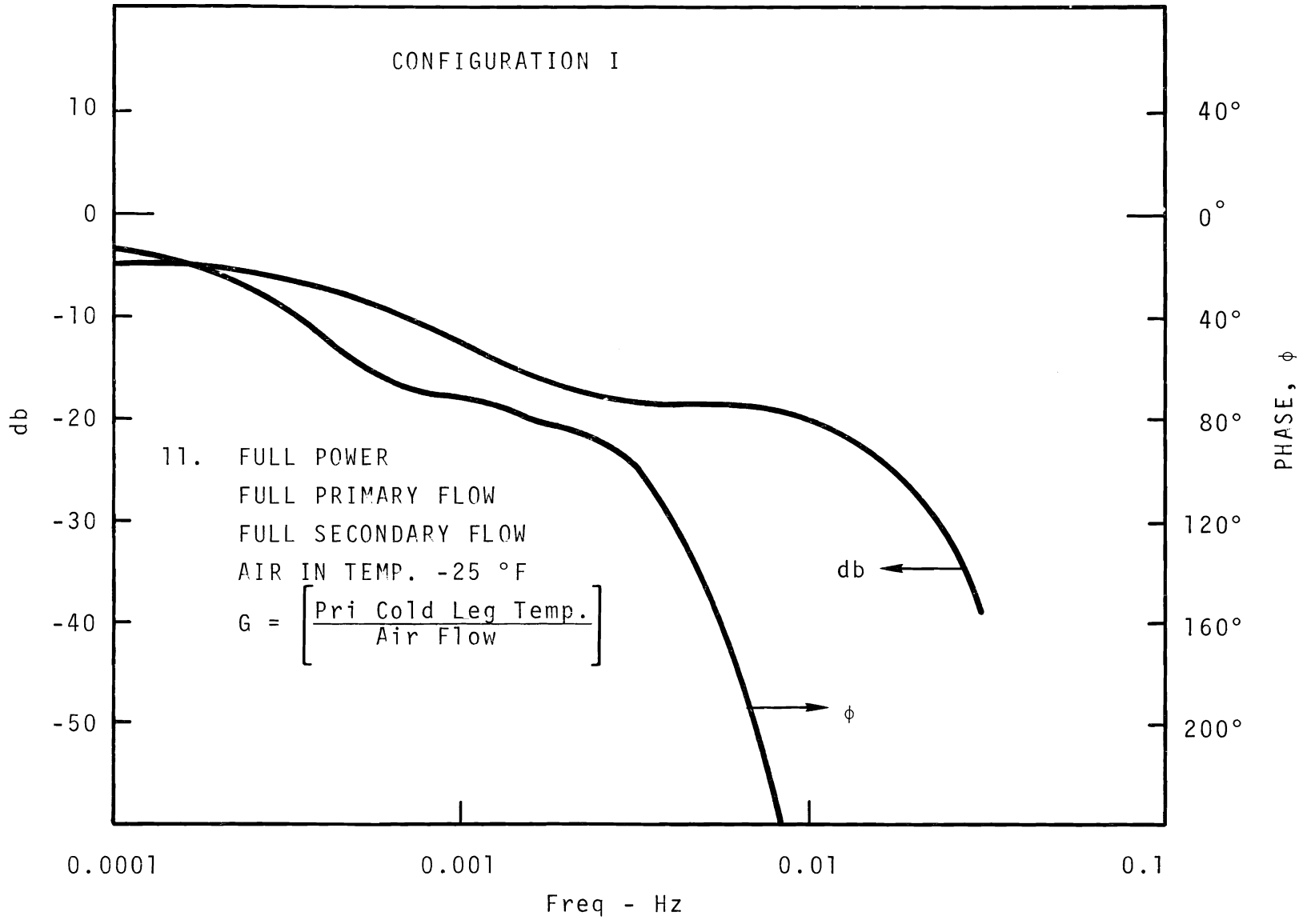

FIGURE 14-11. Primary Cold Leg Controller Open Loop Frequency Response

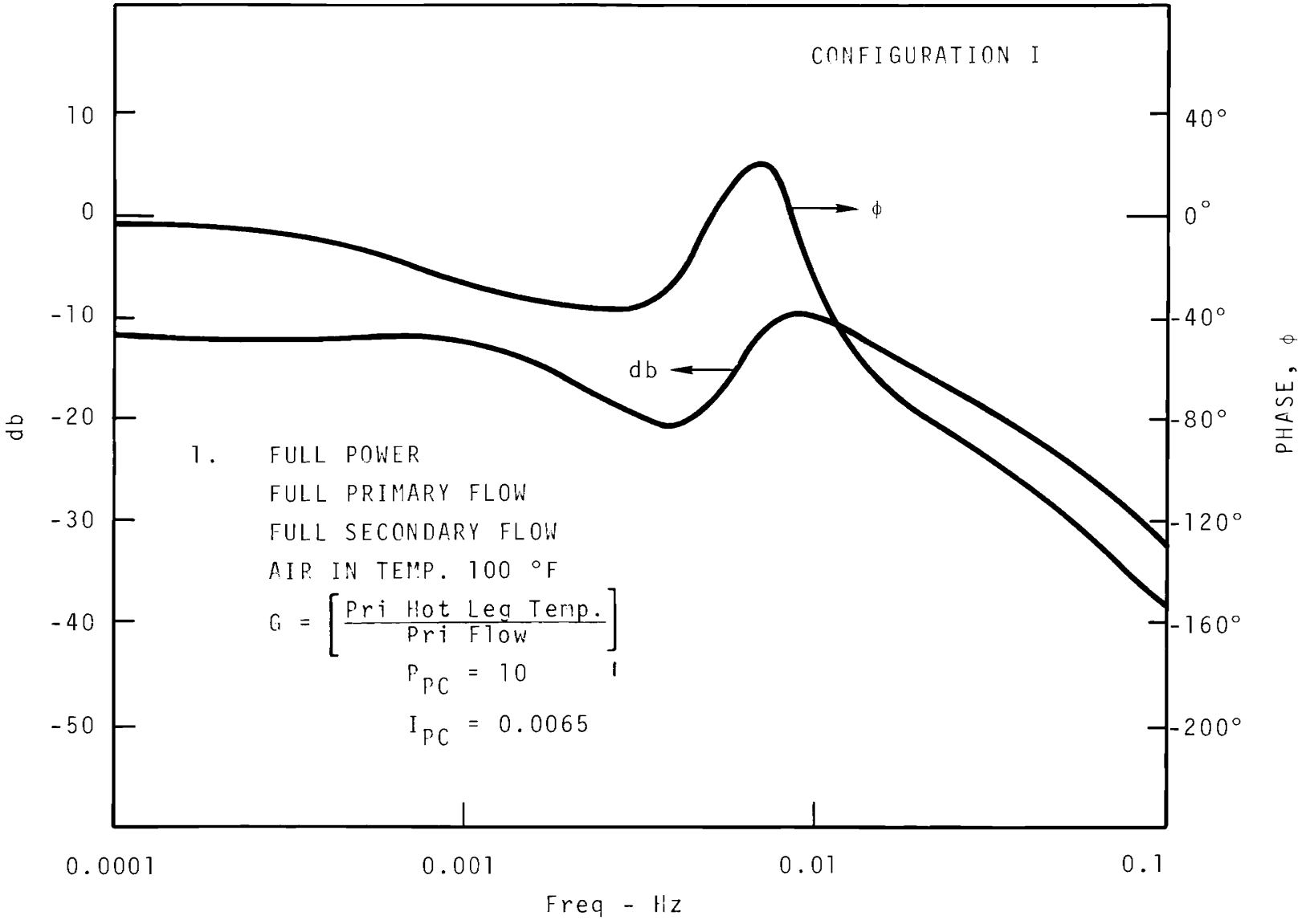

FIGURE 15-1. Primary Hot Leg Temperature Controller Open Loop Frequency Response

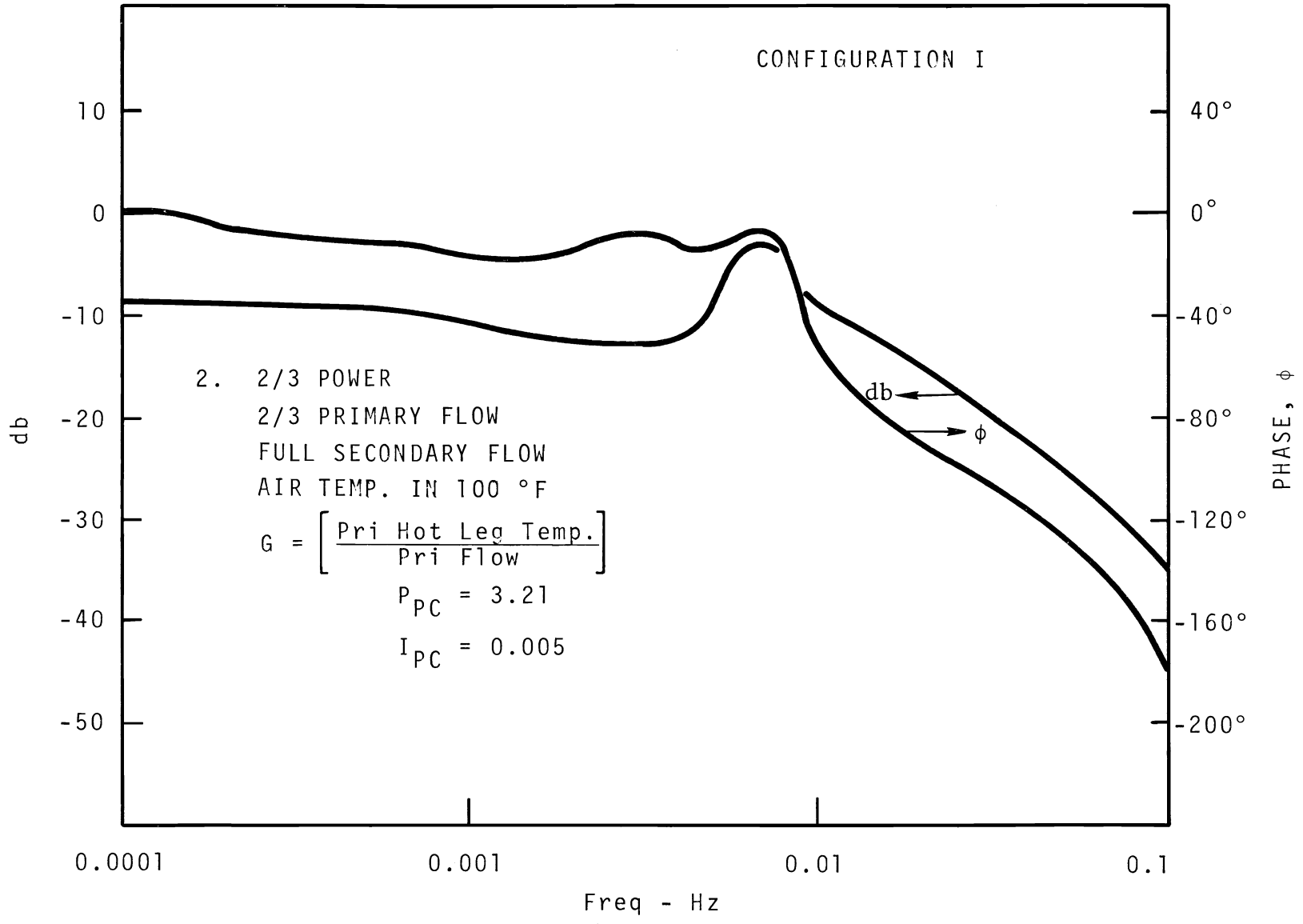

FIGURE 15-2. Primary Hot Leg Temperature Controller Open Loop Frequency Response

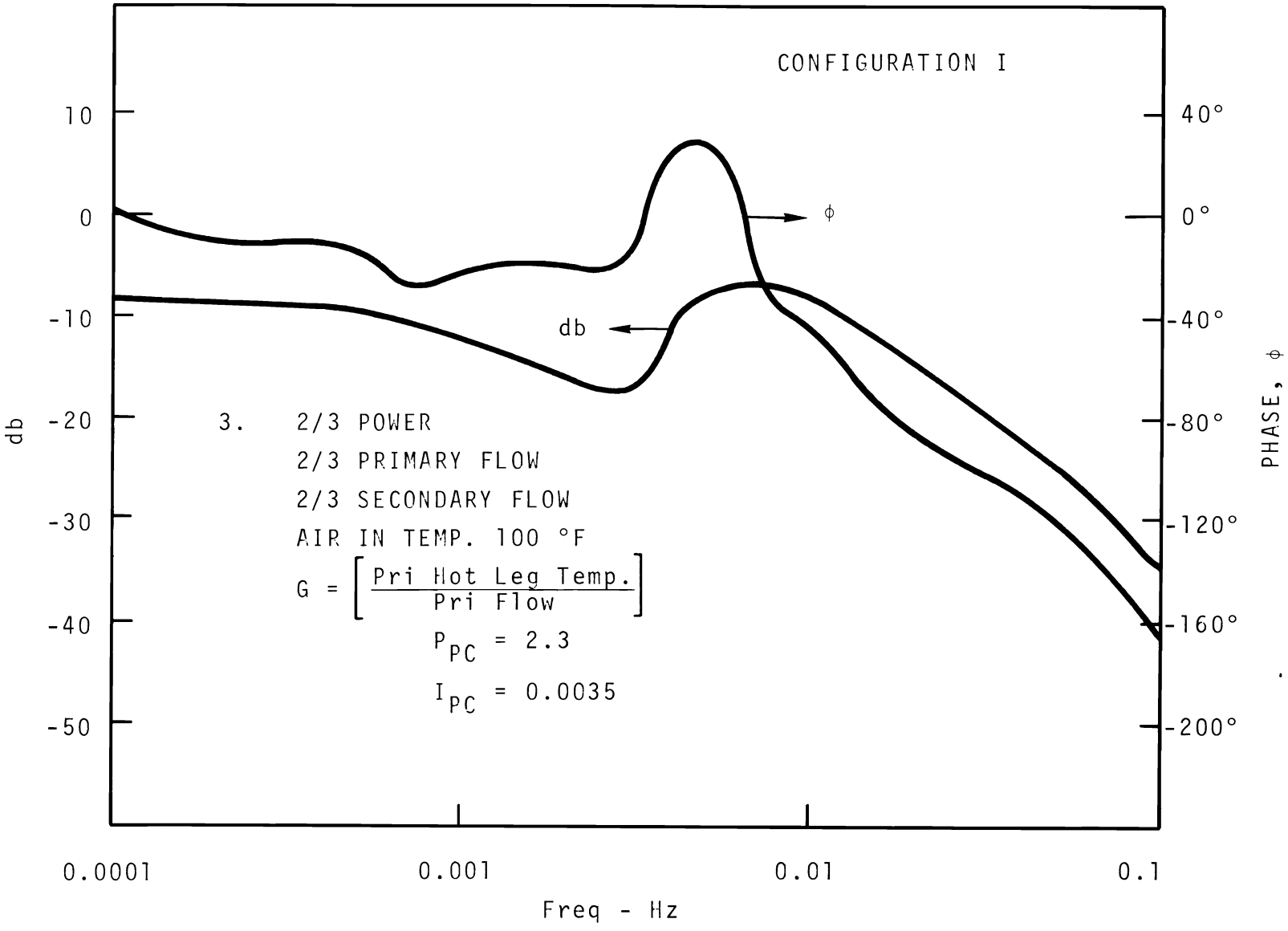

FIGURE 15-3 Primary Hot Leg Temperature Controller Open Loop Frequency Response

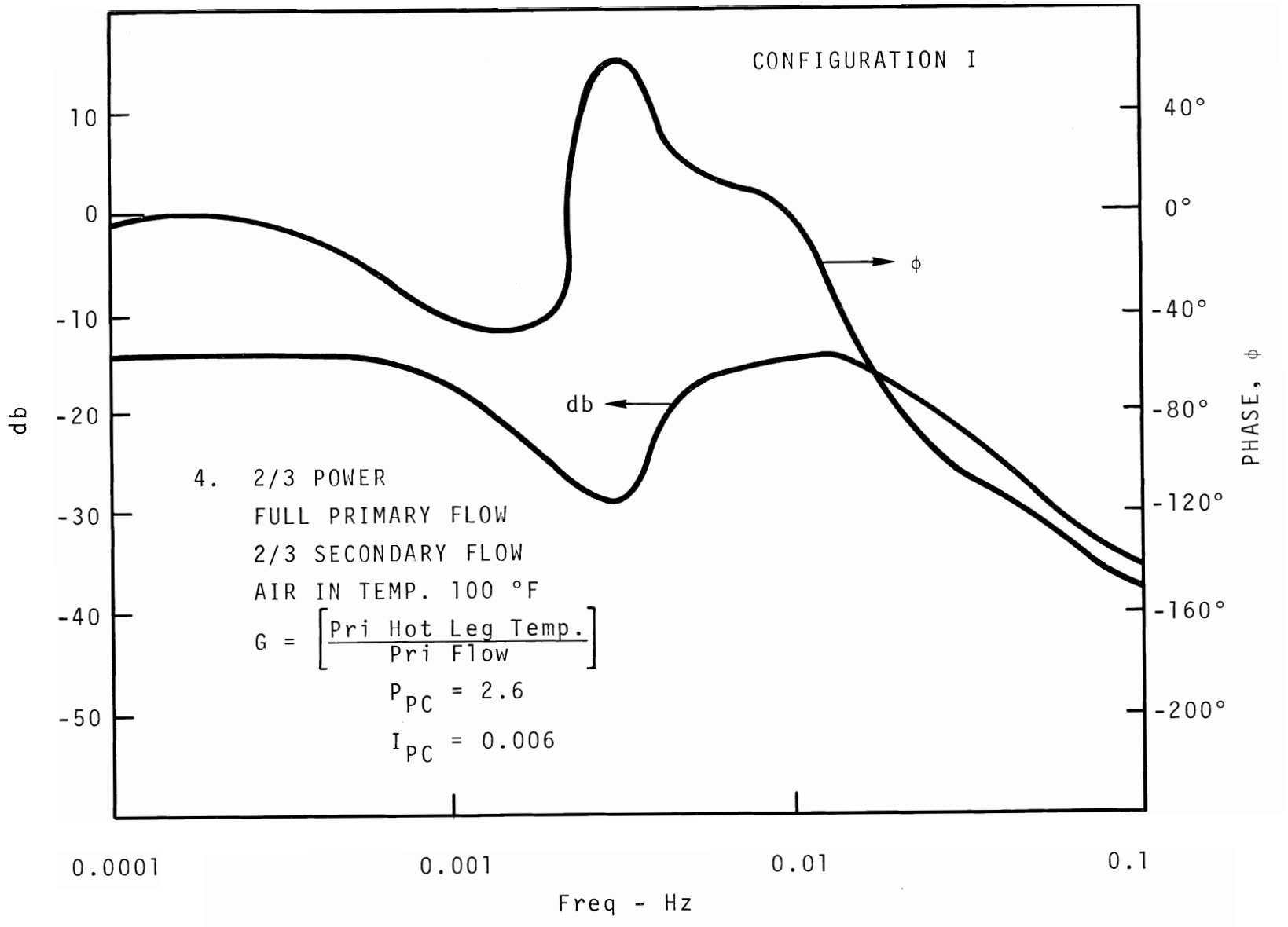

FIGURE 15-4 Primary Hot Leg Temperature Controller Open Loop Frequency Response

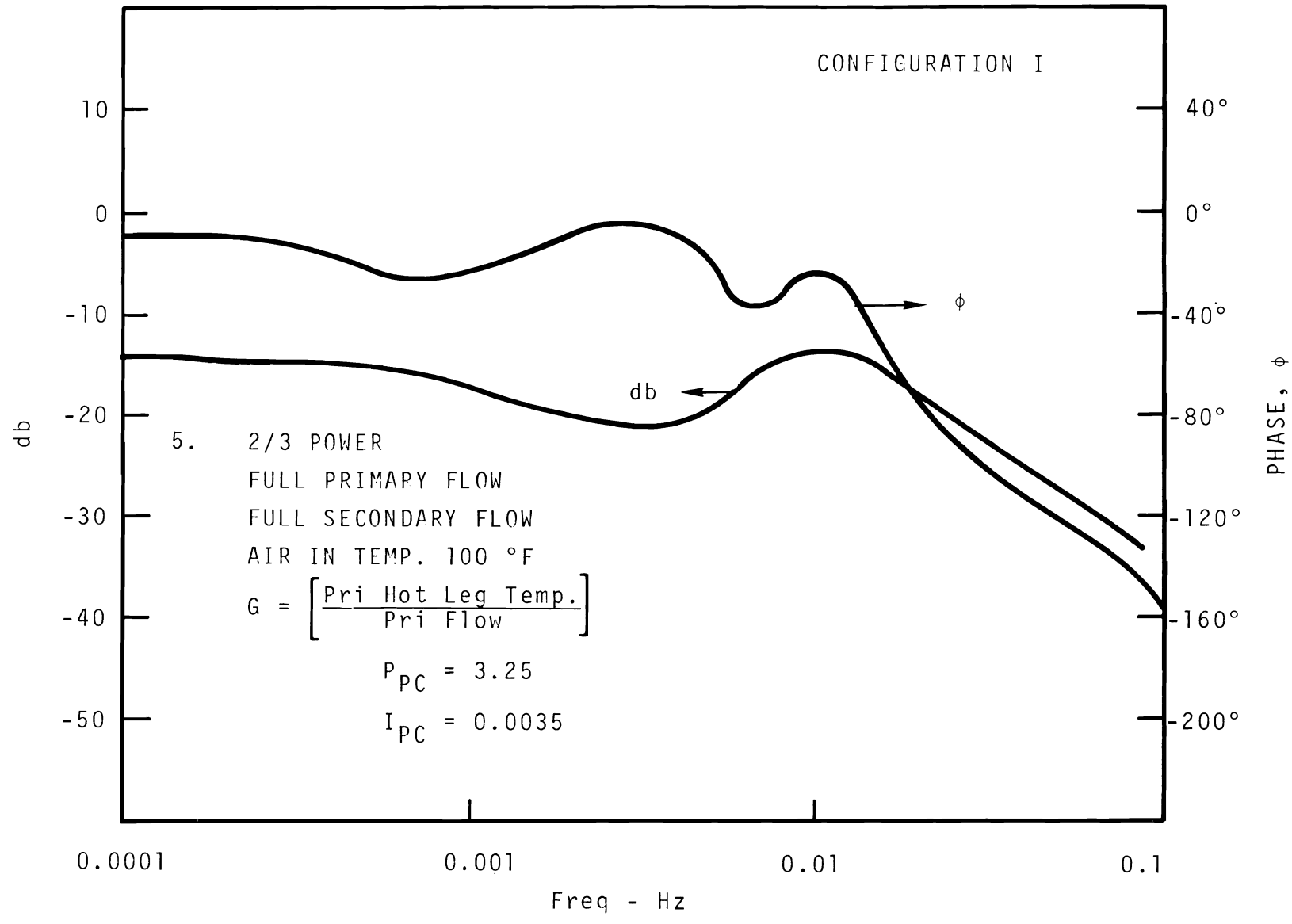

FIGURE 15-5 Primary Hot Leg Temperature Controller Open Loop Frequency Response

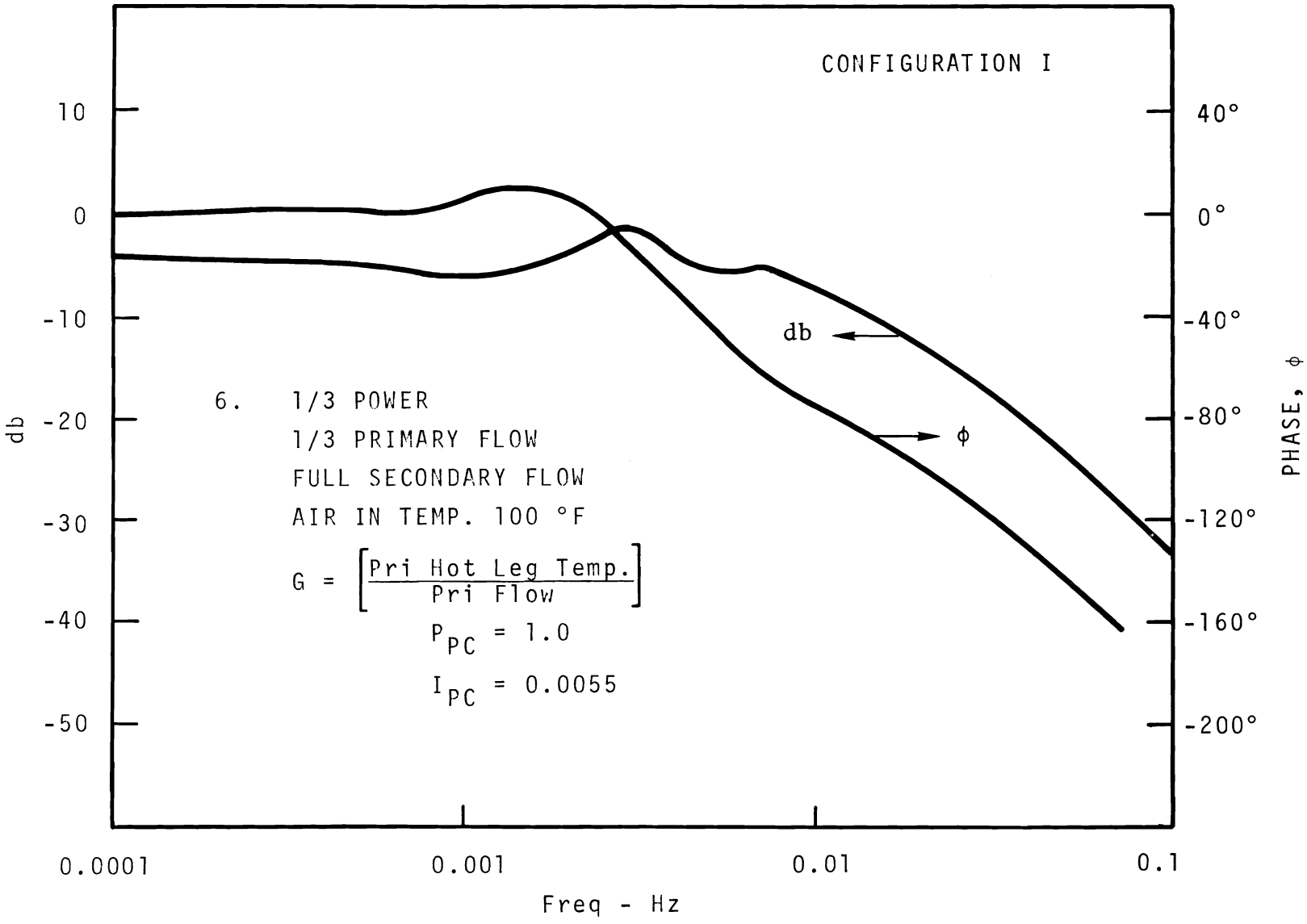

FIGURE 15-6. Primary Hot Leg Temperature Controller Open Loop Frequency Response

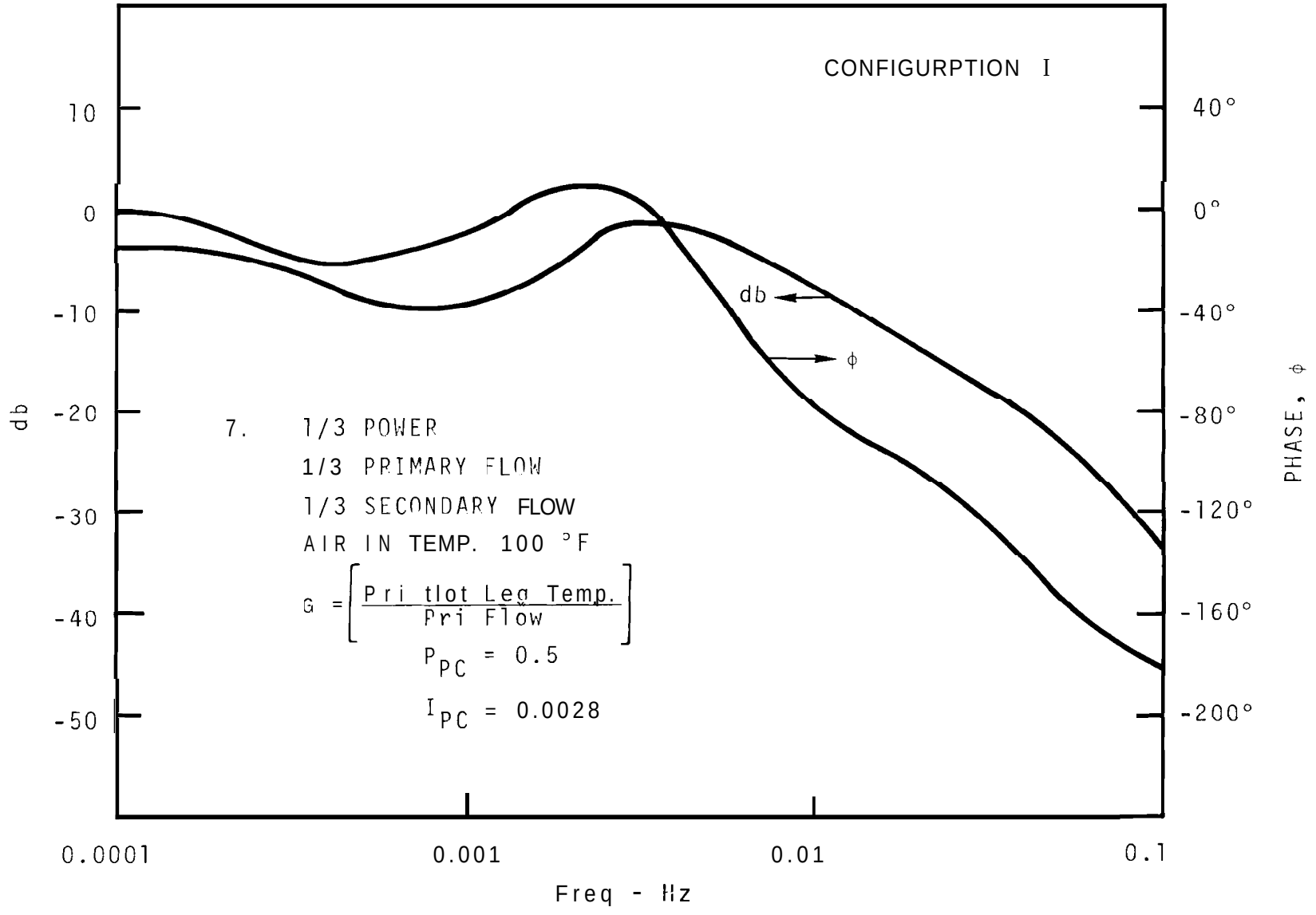

FIGURE 15-7. Primary Hot Leg Temperature Controller Open Loop Frequency Response

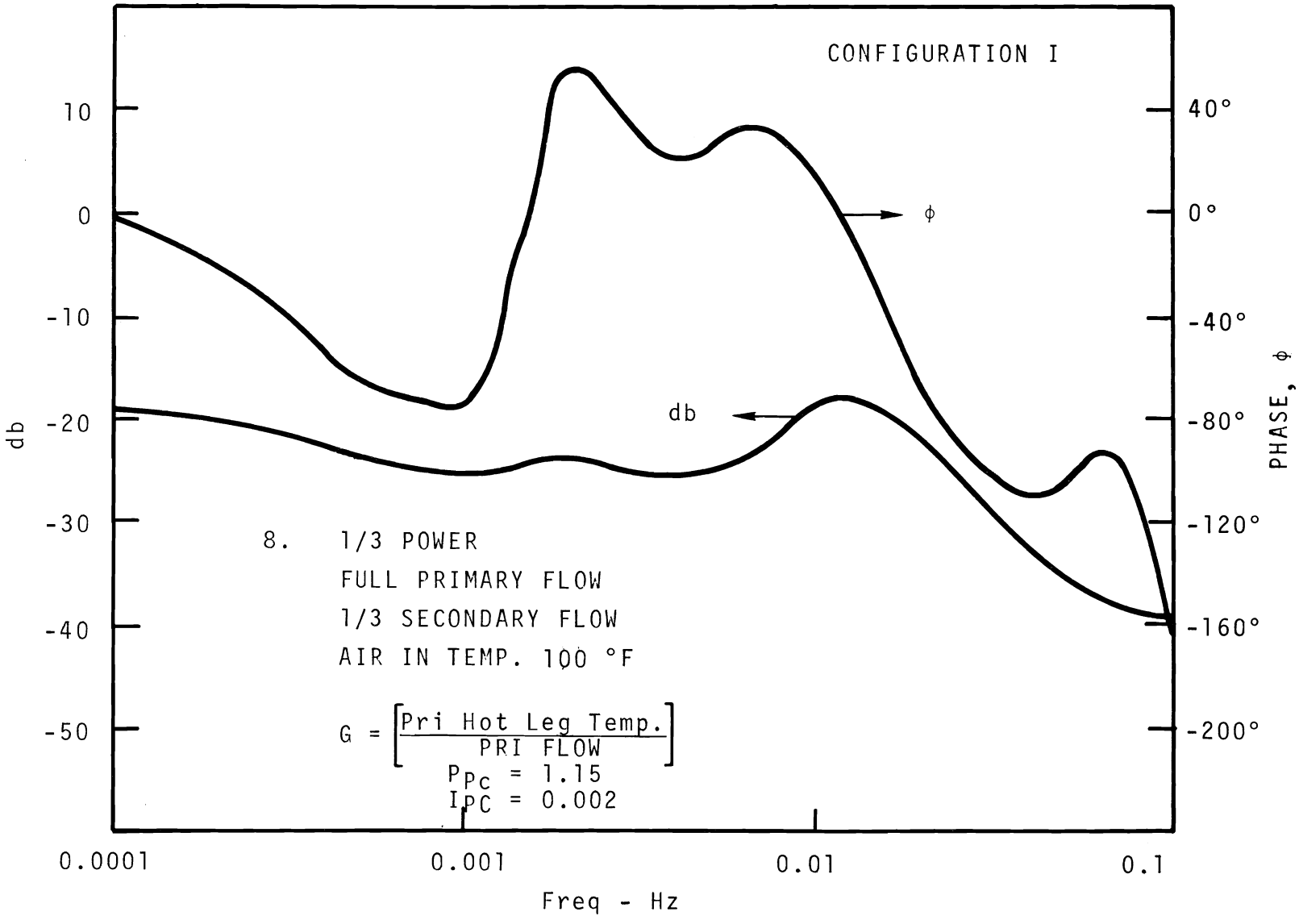

FIGURE 15-8. Primary Hot Leg Temperature Controller Open Loop Frequency Response

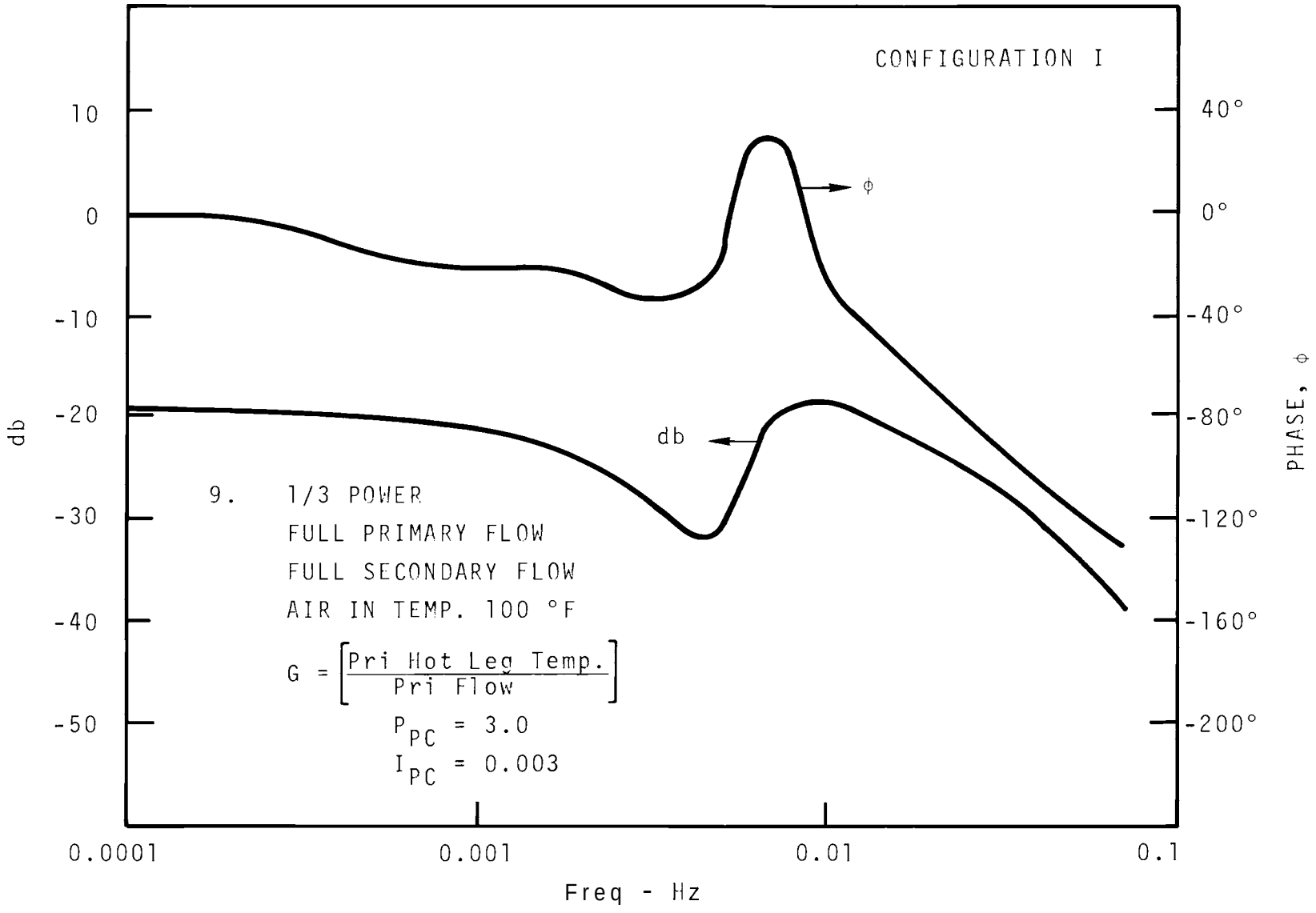

FIGURE 15-9. Primary Kot Leg Temperature Controller Open Loop Frequency Response

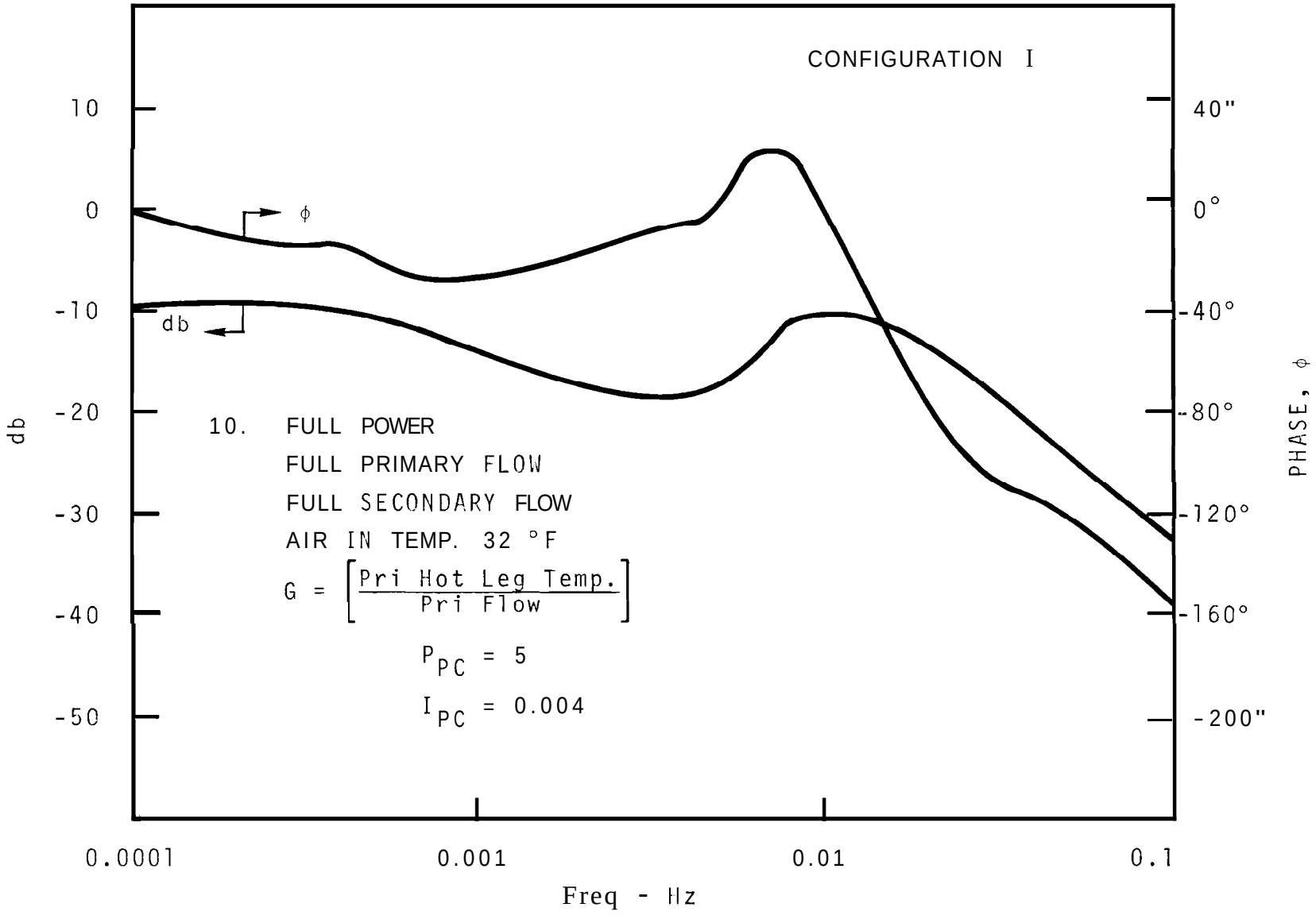

FIGURE 15-10. Primary Hot Leg Temperature Controller Open Loop Frequency Response

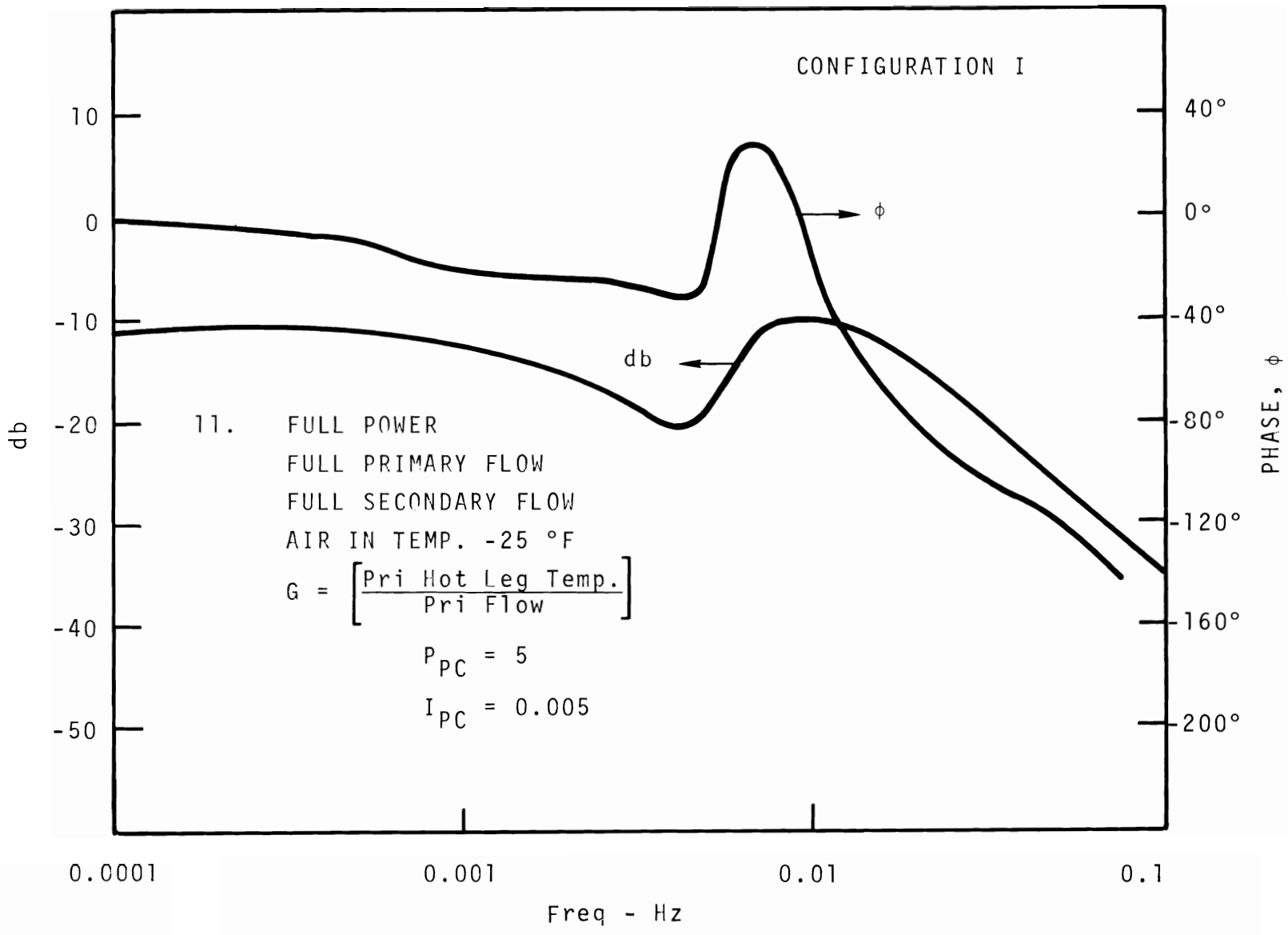

FIGURE 15-11 Primary Hot Leg Temperature Controller Open Loop Frequency Response

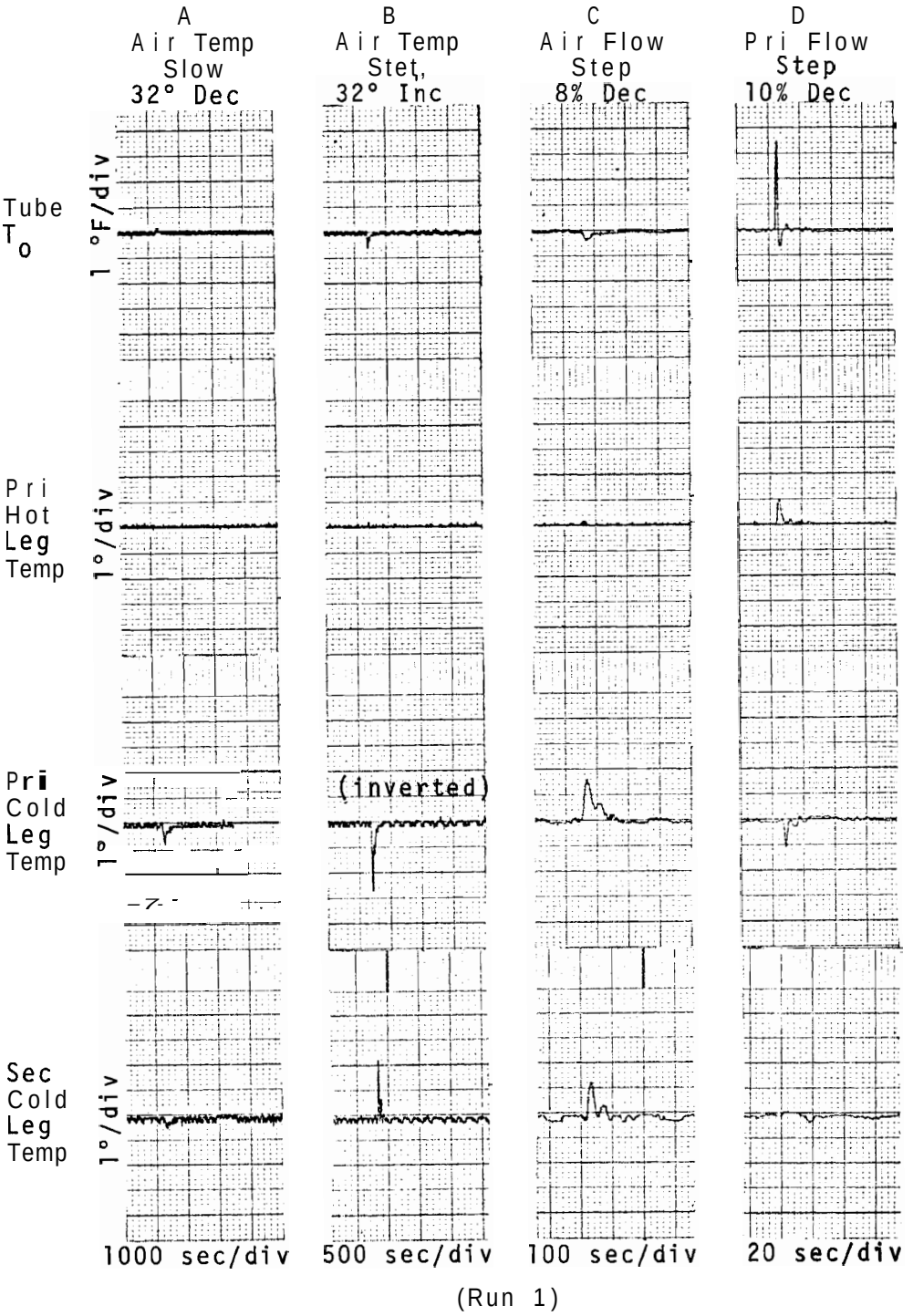

FIGURE 16-1. **Controller Configuration Number I Transients. Full power, full primary and secondary flows, air in at 100 °F.**

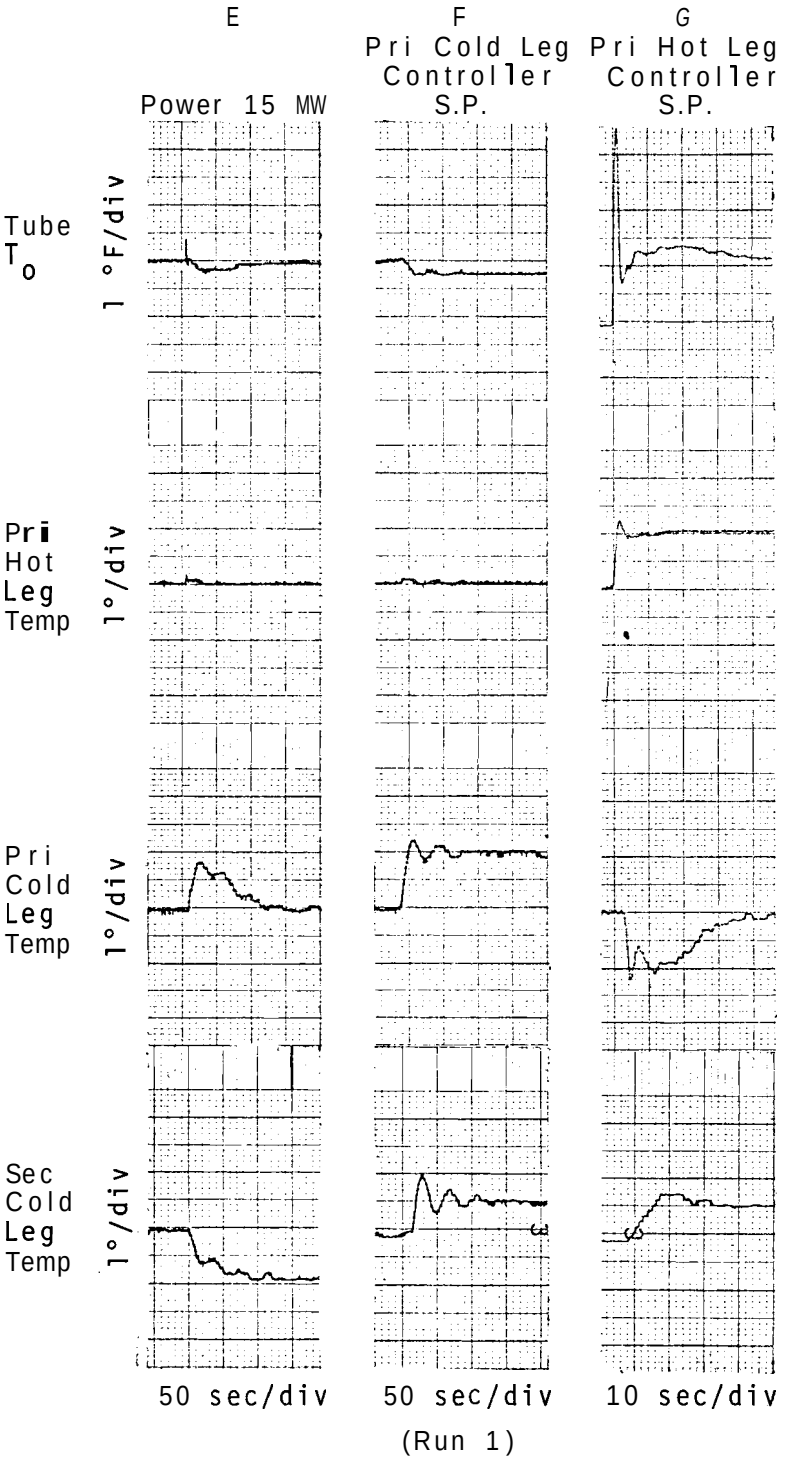

FIGURE 16-1. (contd)

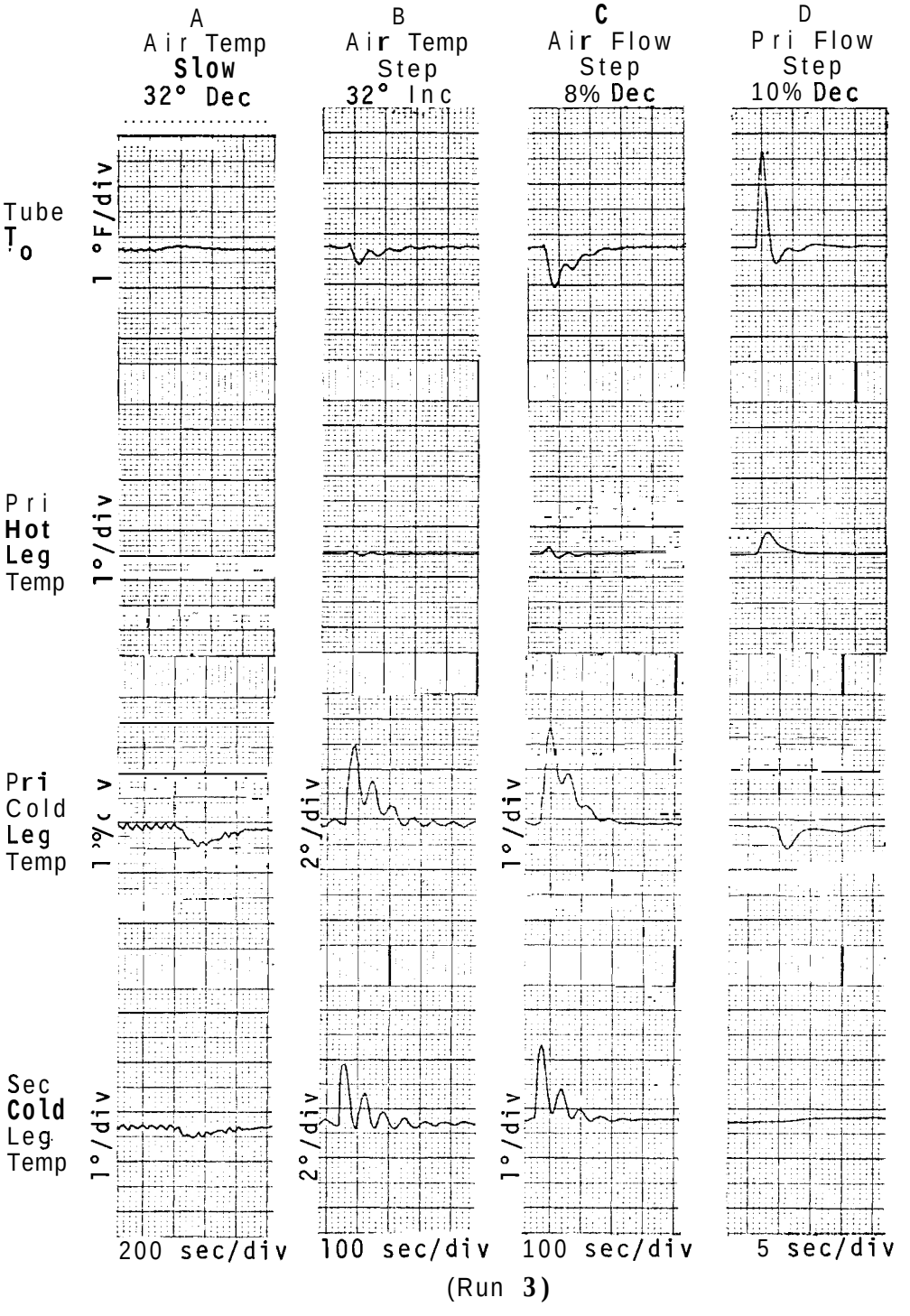

FIGURE 16-2. Controller Configuration Number I Transients. 2/3 Power, 2/3 primary flow, 2/3 secondary flow, air in at 100 °F.

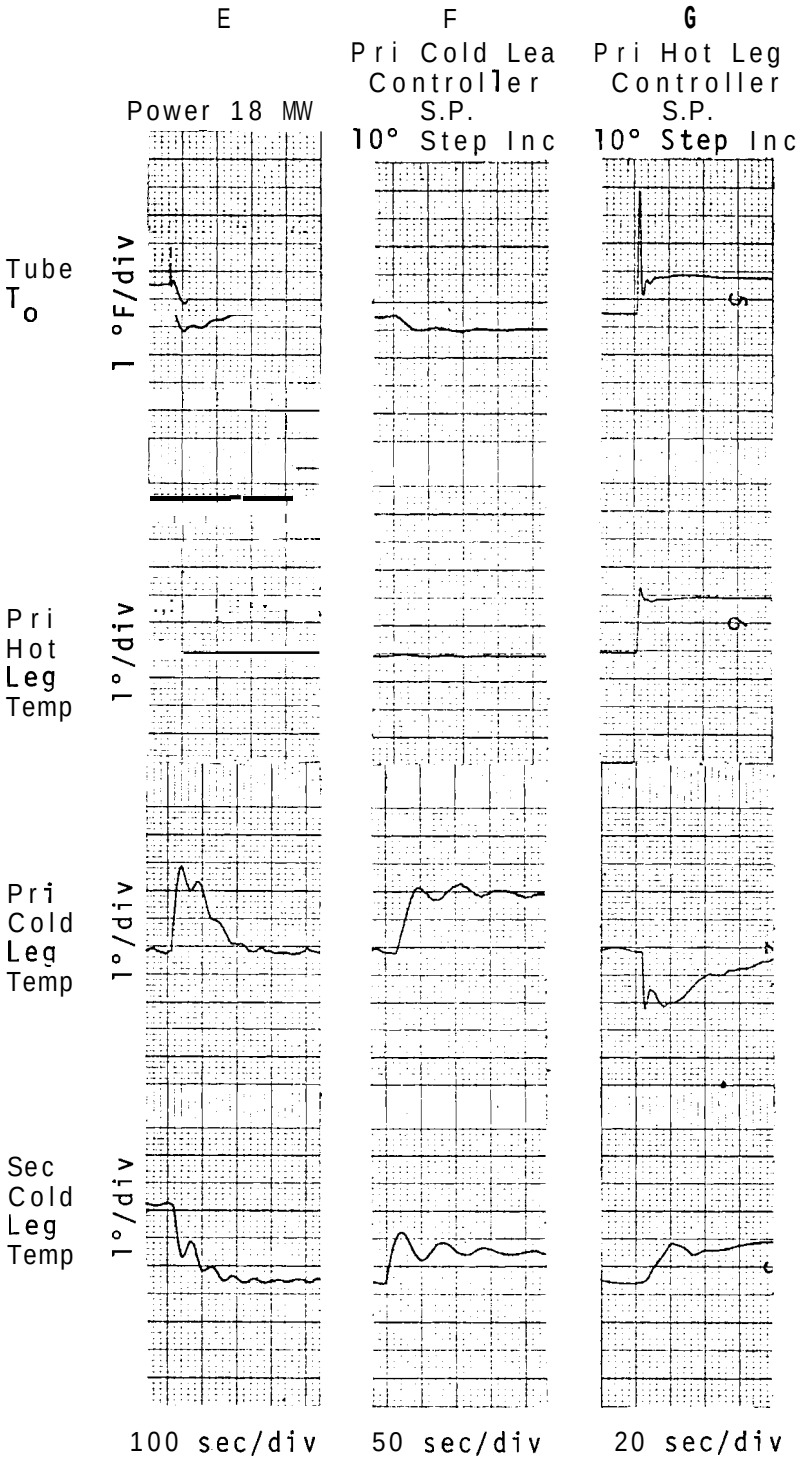

FIGURE 16-2. (contd)

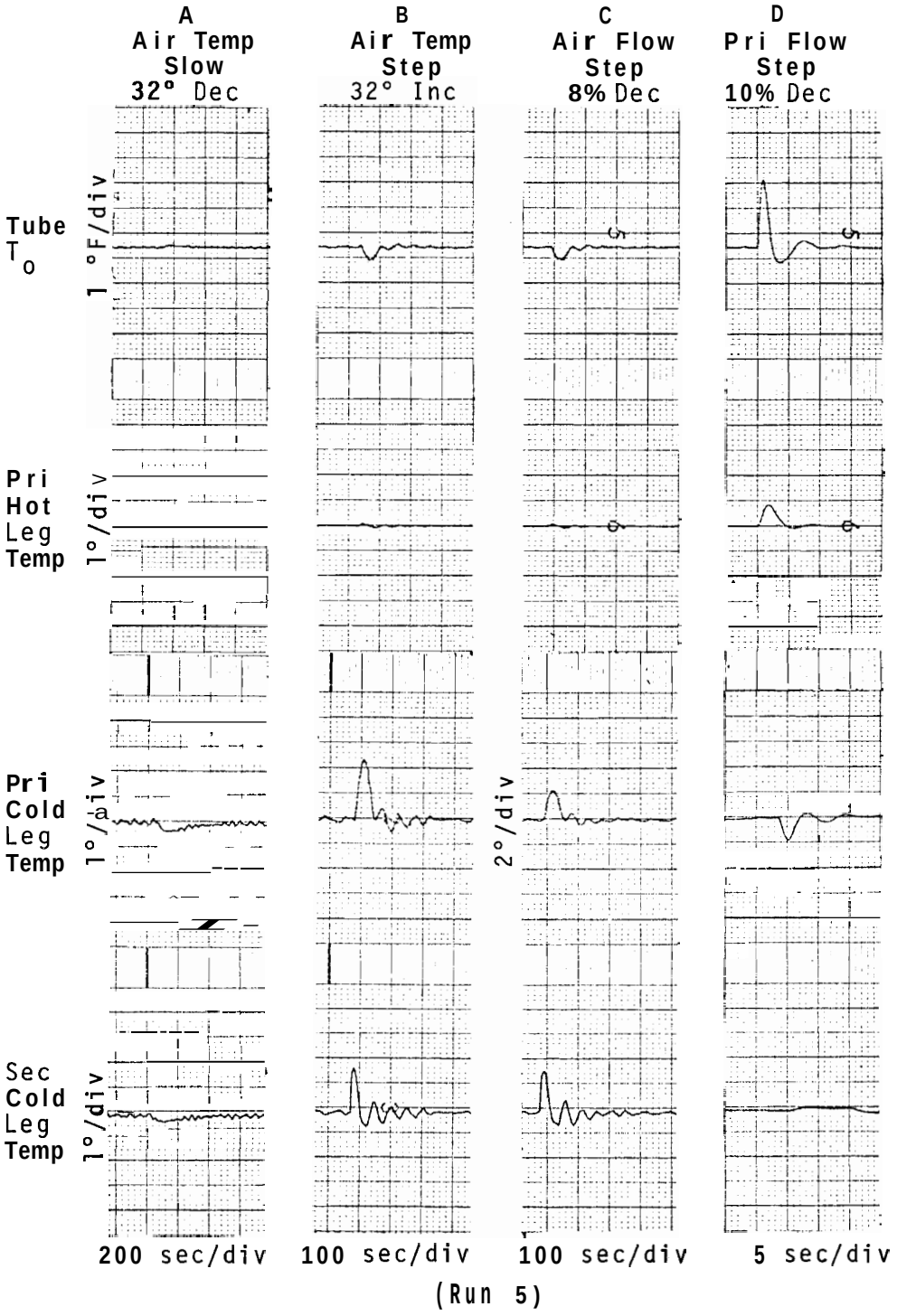

FIGURE 16-3. Controller Configuration Number I Transients. 2/3 Power, full primary and secondary flows, air in at 100 °F.

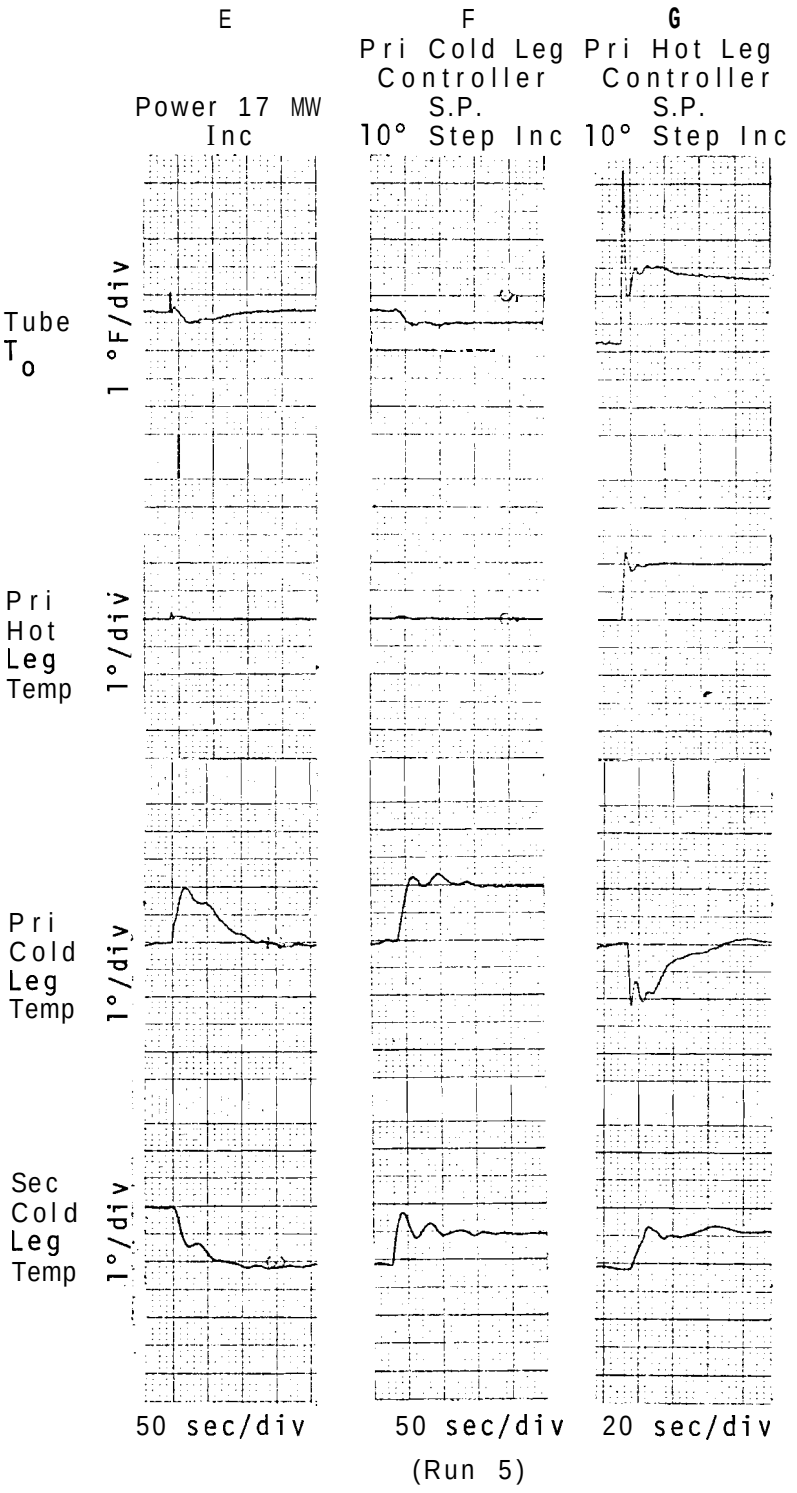

FIGURE 16-3. (contd)

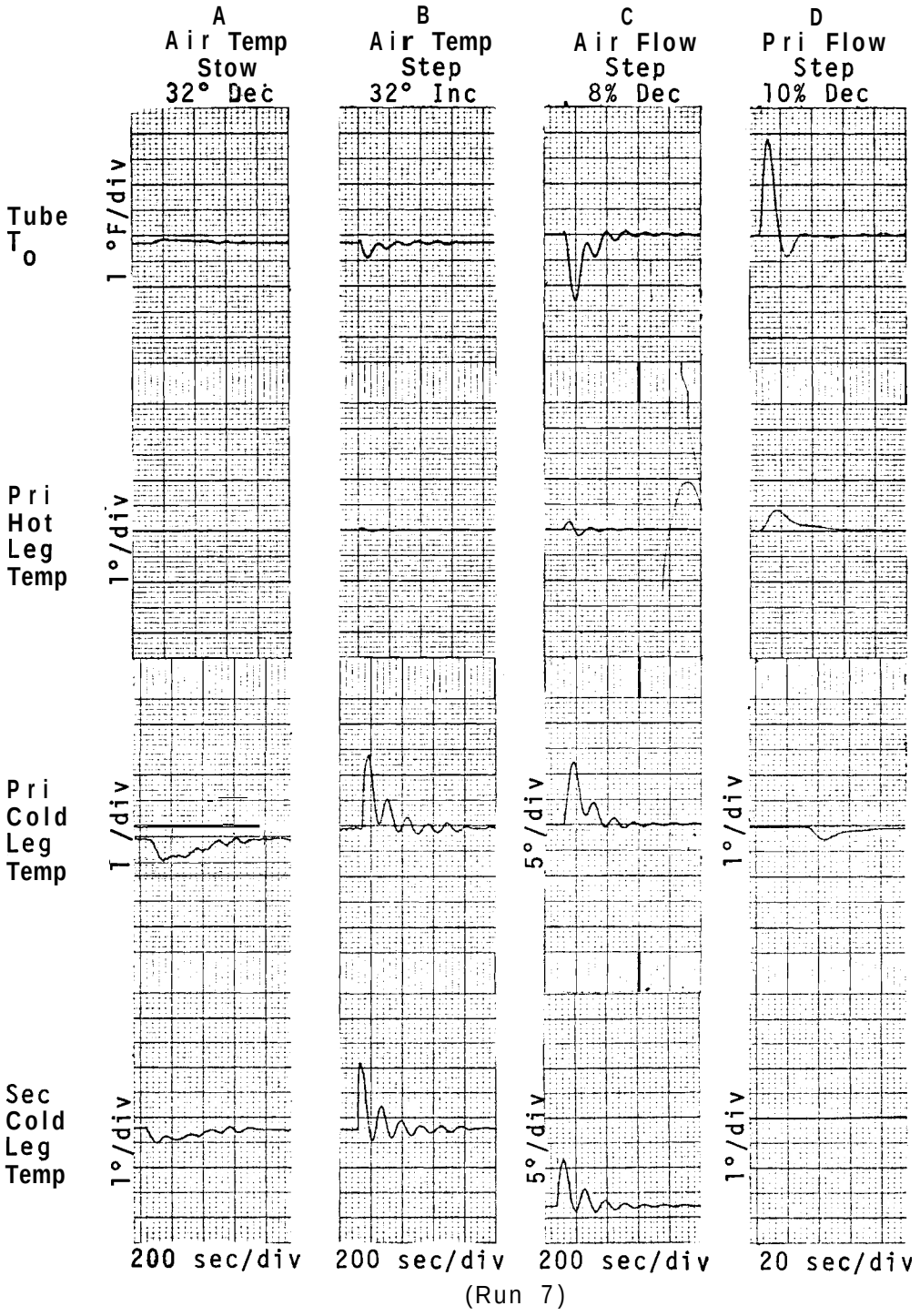

FIGURE 16-4. **Controller Configuration Number I Transients. 1/3 Power, 1/3 primary and secondary flows, air in at 100 °F.**

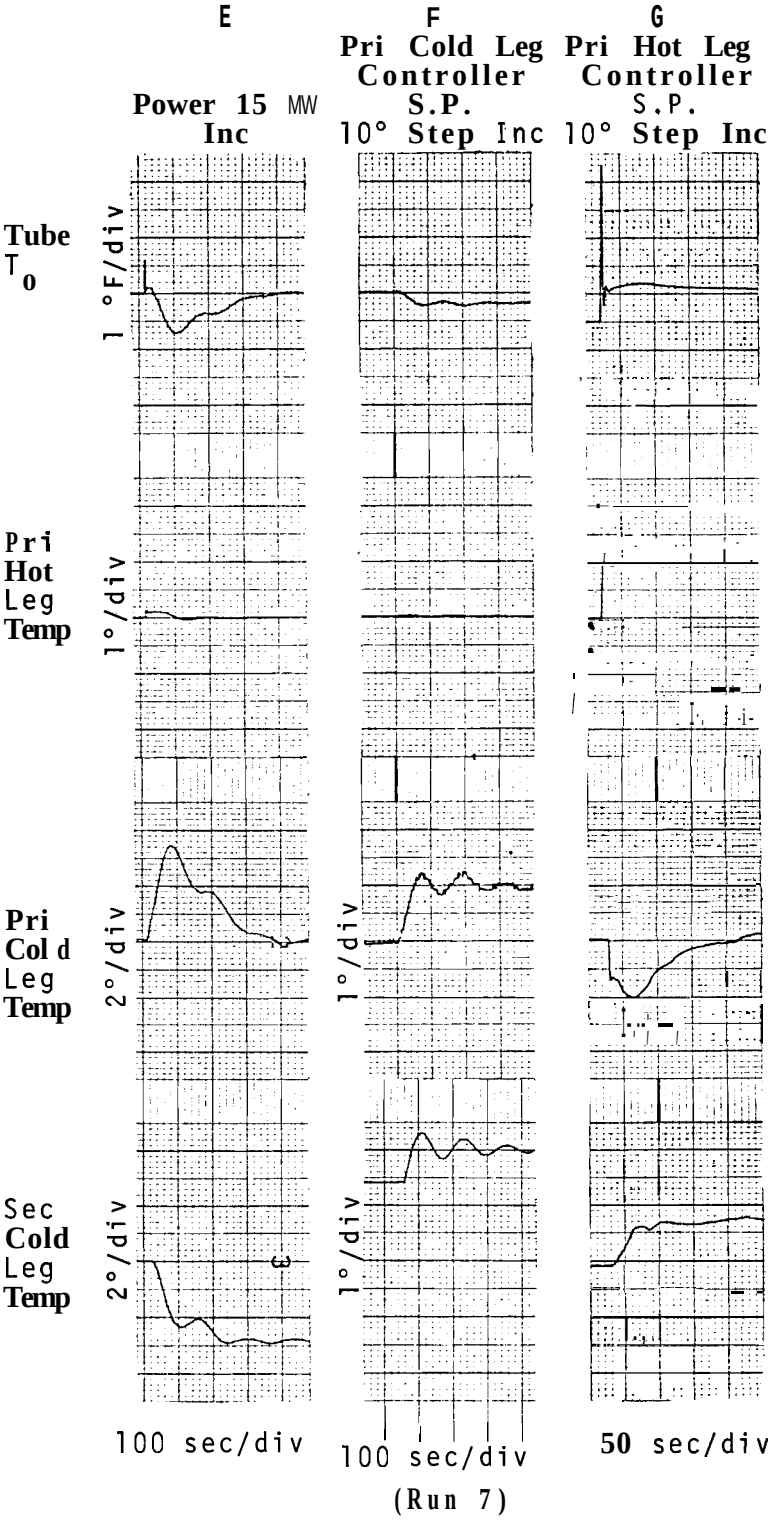

FIGURE 16-4. (contd)

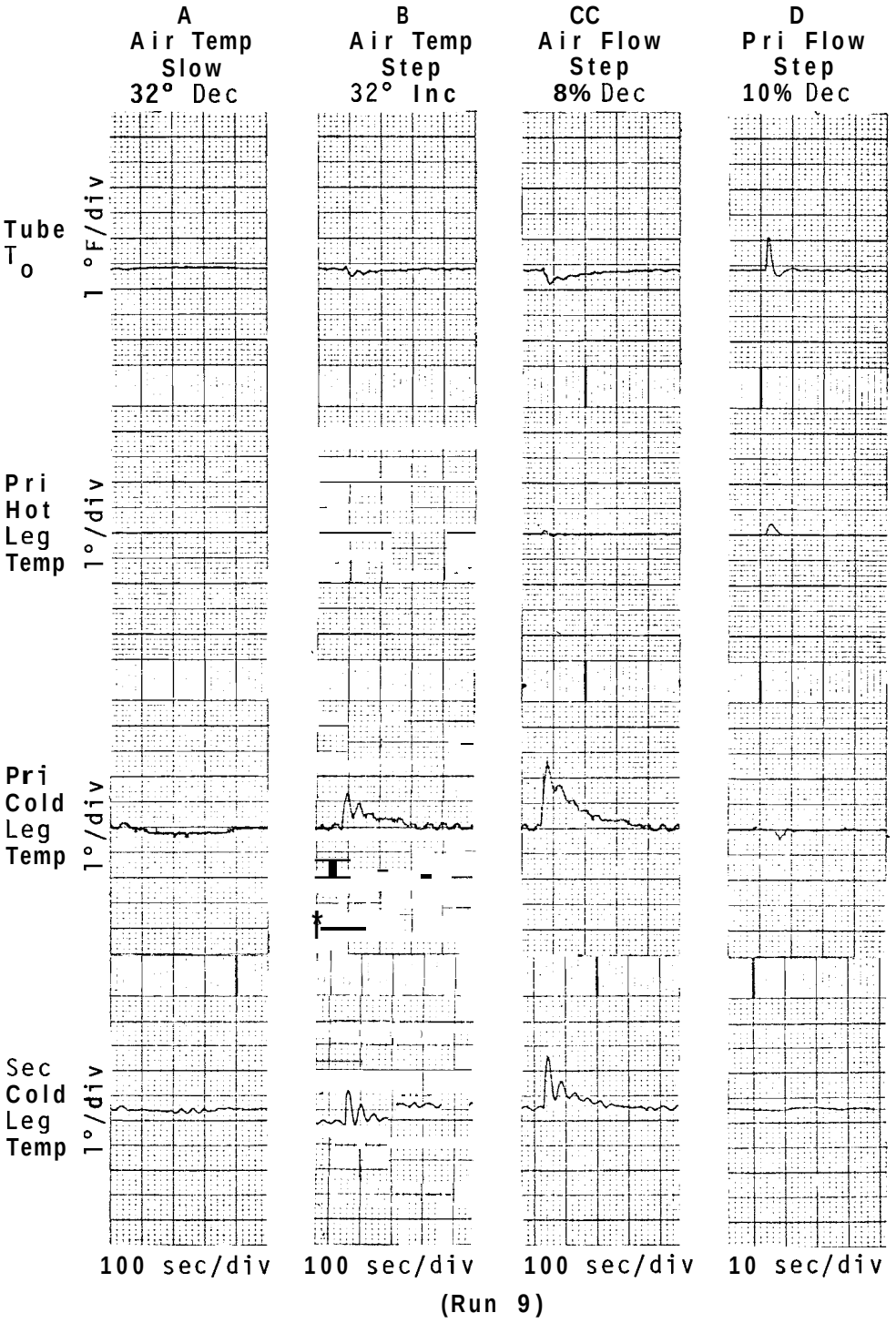

FIGURE 16-5. Controller Configuration Number I Transients. 1/3 Power, full primary and secondary flows, air in at 100 °F.

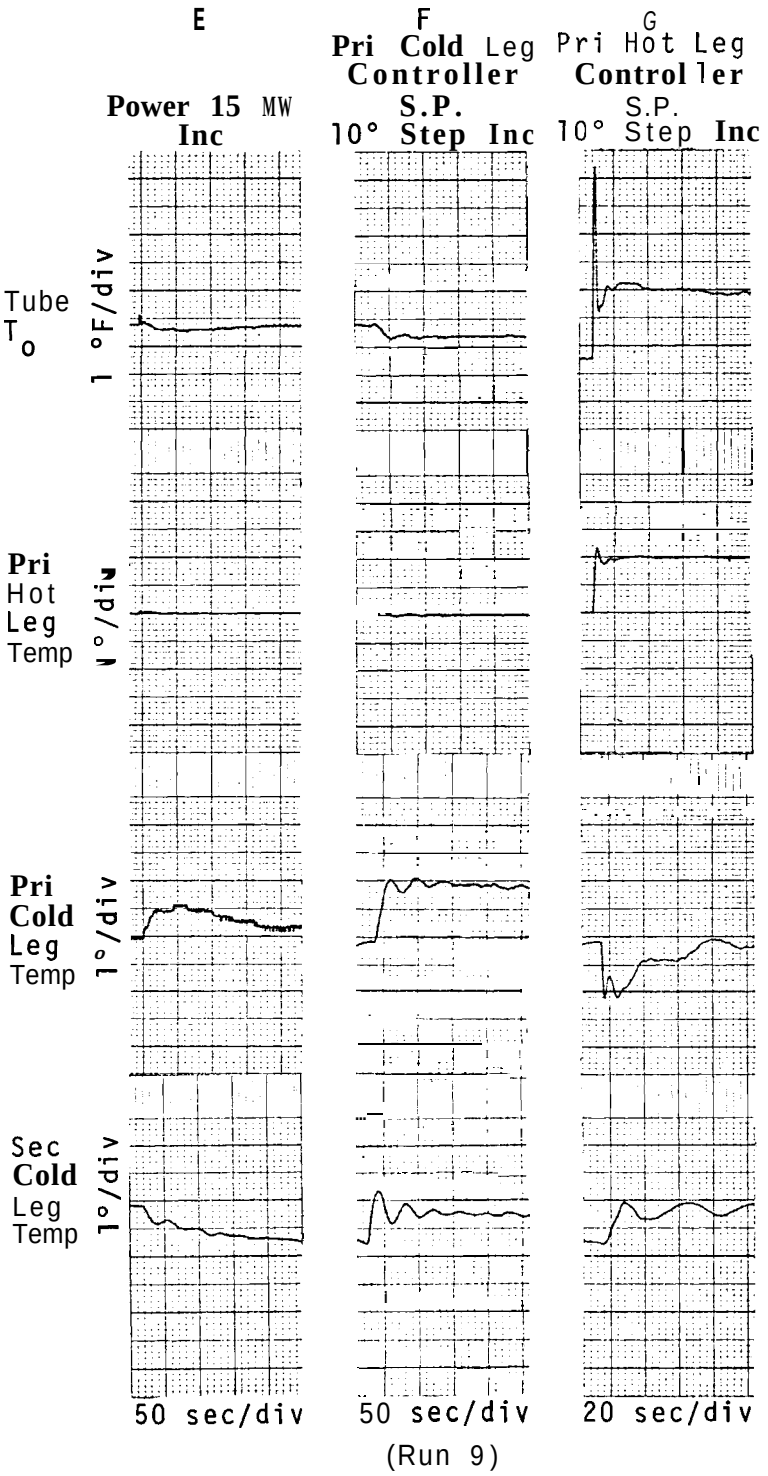

FIGURE 16-5. (contd)

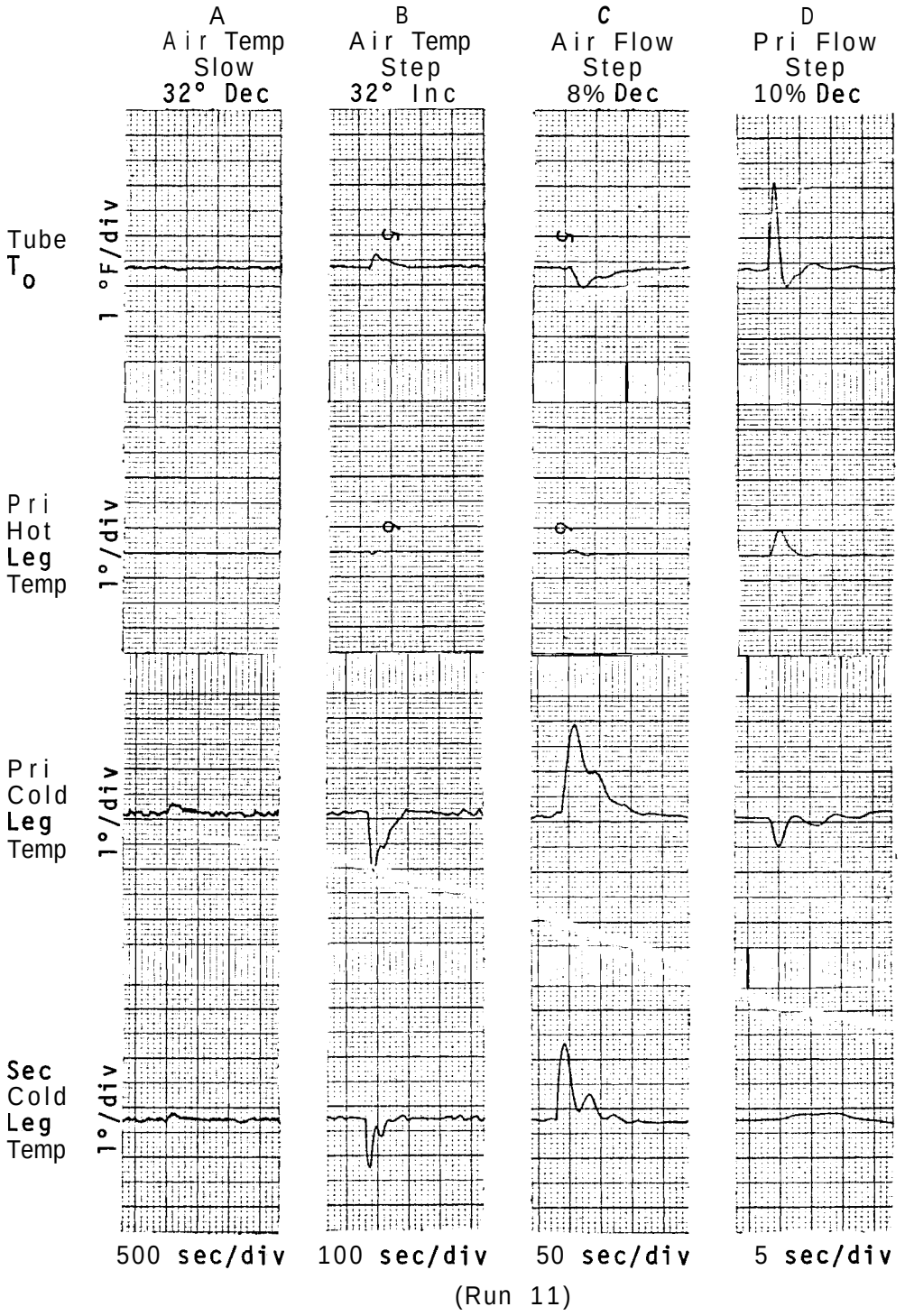

FIGURE 16-6. Controller Configuration Number I Transients. Full power, full primary and secondary flows, air in at -25 °F.

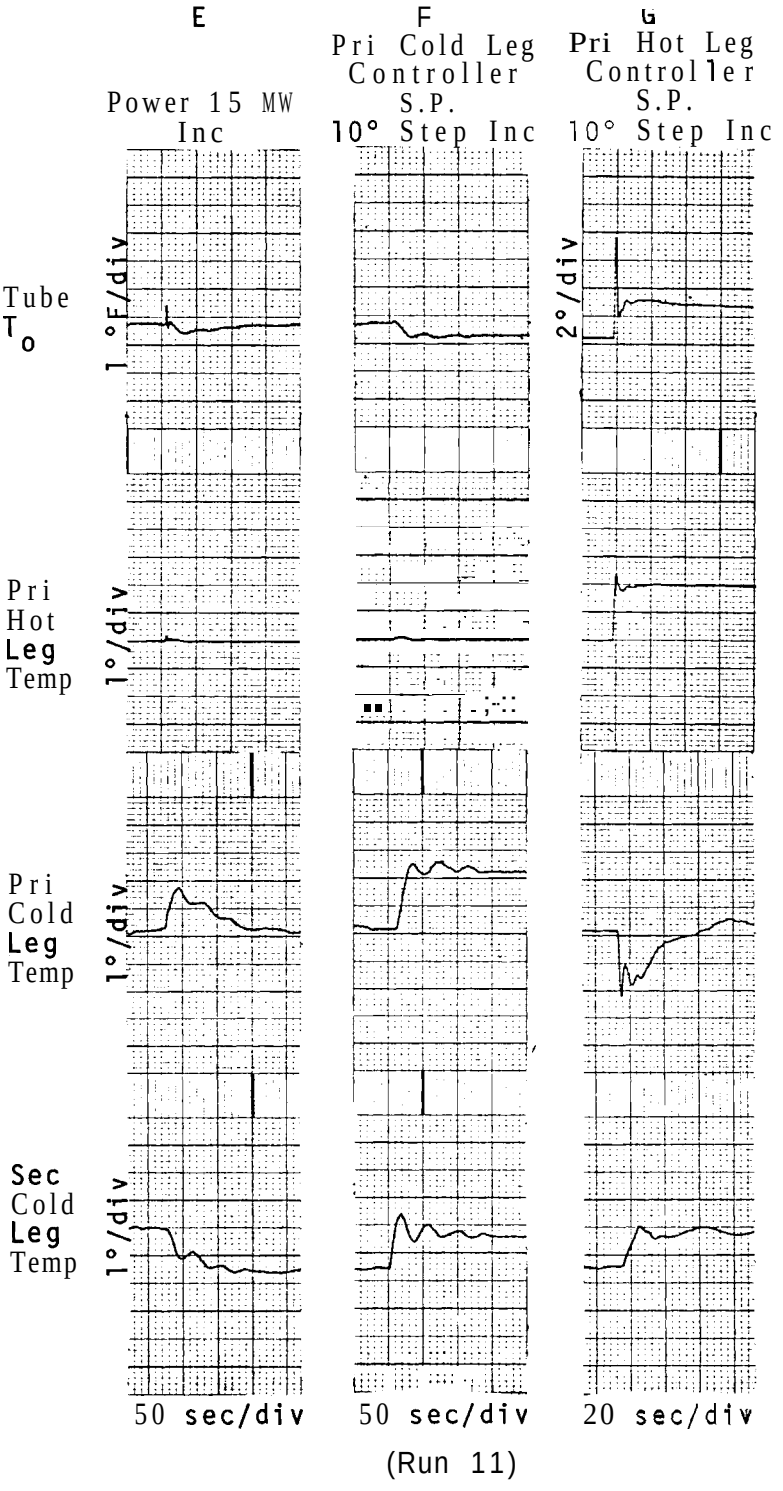

FIGURE **16-6. (contd)**

TRENDS WITH CONTROLLER SETTINGS

A series of computer runs were taken early in the study to define the effects of controller setting adjustment changes on the performance of the controlled systems. All of the information on this set of runs is for a control Configuration II in which proportional plus derivitive action was used for the secondary cold leg temperature controller. The results were influenced by the lack of limits on the air and primary sodium flow rates, but the results are still considered as indicative of the trends.

The indices of performance (IP) for the runs are all of the integral-error-squared type. Where the IP was taken from the controlled variable, such as the secondary cold leg temperature, the error was the difference between the setpoint value and the measured value of the controlled variable. In some runs, however, the IP was taken from the reactor process tube outlet temperature. In these cases, the error is taken as the difference between tube outlet temperature and the final steady-state value.

SECONDARY COLD LEG CONTROLLER

A frequency response of the secondary cold leg system open loop is shown in Figure 17. Figures 18 and 19 show stability limits and contours of constant index of performance as functions of the controller settings.

The frequency response shows that at 180° phase shift, the gain is down by 44 db. Thus the system is expected to oscillate if the controller gain is greater than about 150 (44 db). Figure 18 shows that the stability limit for zero derivitive action is about 150. The addition of the derivative action introduces a phase lead which stabilizes the system and permits higher proportional action. The stability limit for various values of proportional and derivative action is defined

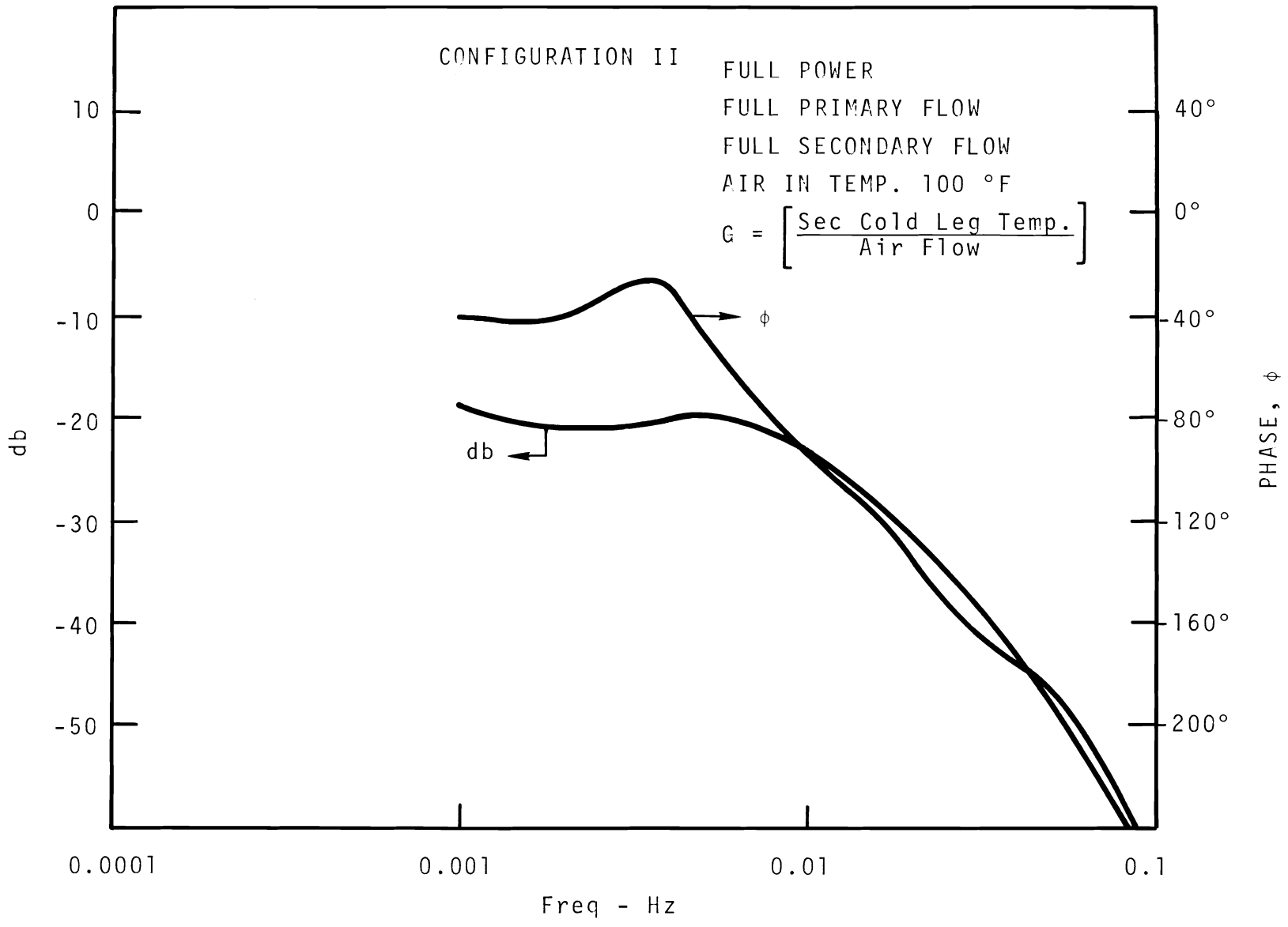

FIGURE 17. Secondary Cold Leg Temperature Controller Open Loop Frequency Response

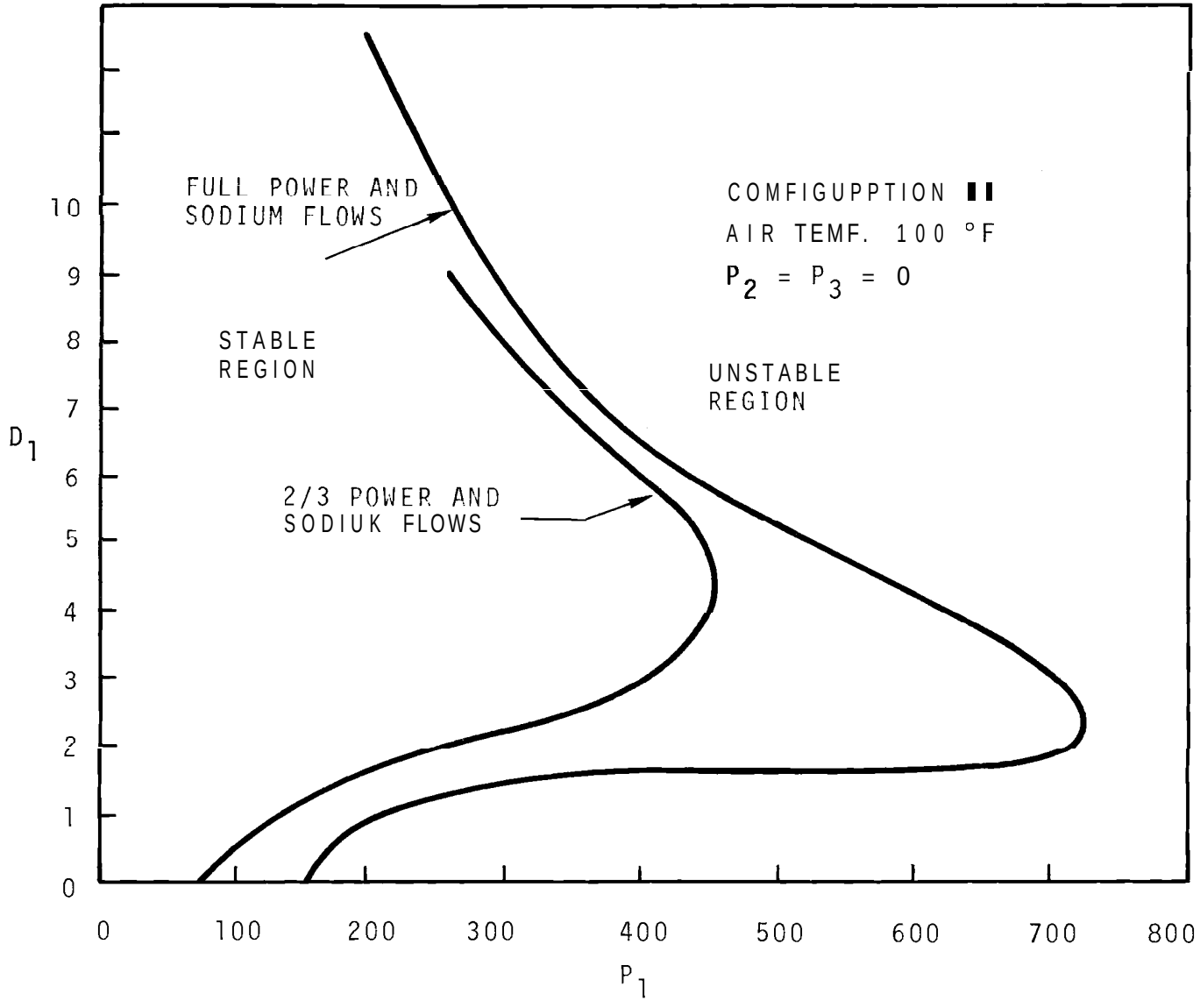

FIGURE 18. Graph Showing the Stability Limits for the Secondary **Cold** Leg Temperature Controller

in Figure 18 for both the full-power full-flow condition and two-thirds/two-thirds flow condition. It can be seen that operation at reduced power and sodium flow rates decreases the area of the stable region.

Figure 19 shows relationships between the index of performance and the controller settings for derivitive (D_1) and proportional (P_1) action for both the full-power, full-flow condition (Figure 19-1) and the two-thirds power/two-thirds sodium flow condition (Figure 19-2). The contours define the limit of stability. The dotted lines on Figure 19-1 show the values of P_1 and D_1 used for later runs in this same set of runs. At a different time when the runs for the configuration effects were made, D_1 was set to zero and P_1 of 30 gave an approximately 20% overshoot. It is apparent from Figure 19, however, that improved control system performance can be obtained over the proportional only action if the improved performance benefits the entire system. At the time of this writing, we believe that the overall heat transport system would not be improved appreciably by using the derivitive action. The long time and distance/velocity lags in the remaining part of the primary cold leg temperature control loop provides a dominating effect that cannot be negated by improving the secondary cold leg temperature control system performance. The use of reset action is not considered beneficial when the outer loop of a cascade control system has reset action.

PRIMARY COLD LEG TEMPERATURE CONTROLLER

Figure 20 shows the primary cold leg temperature controller stability limits for the two conditions of full power and sodium flows and for one-third power and sodium flows. The region to the right of each line is unstable for the pertinent conditions, and to the left of each line is stable. The trend with power and sodium flow levels is the same as for the

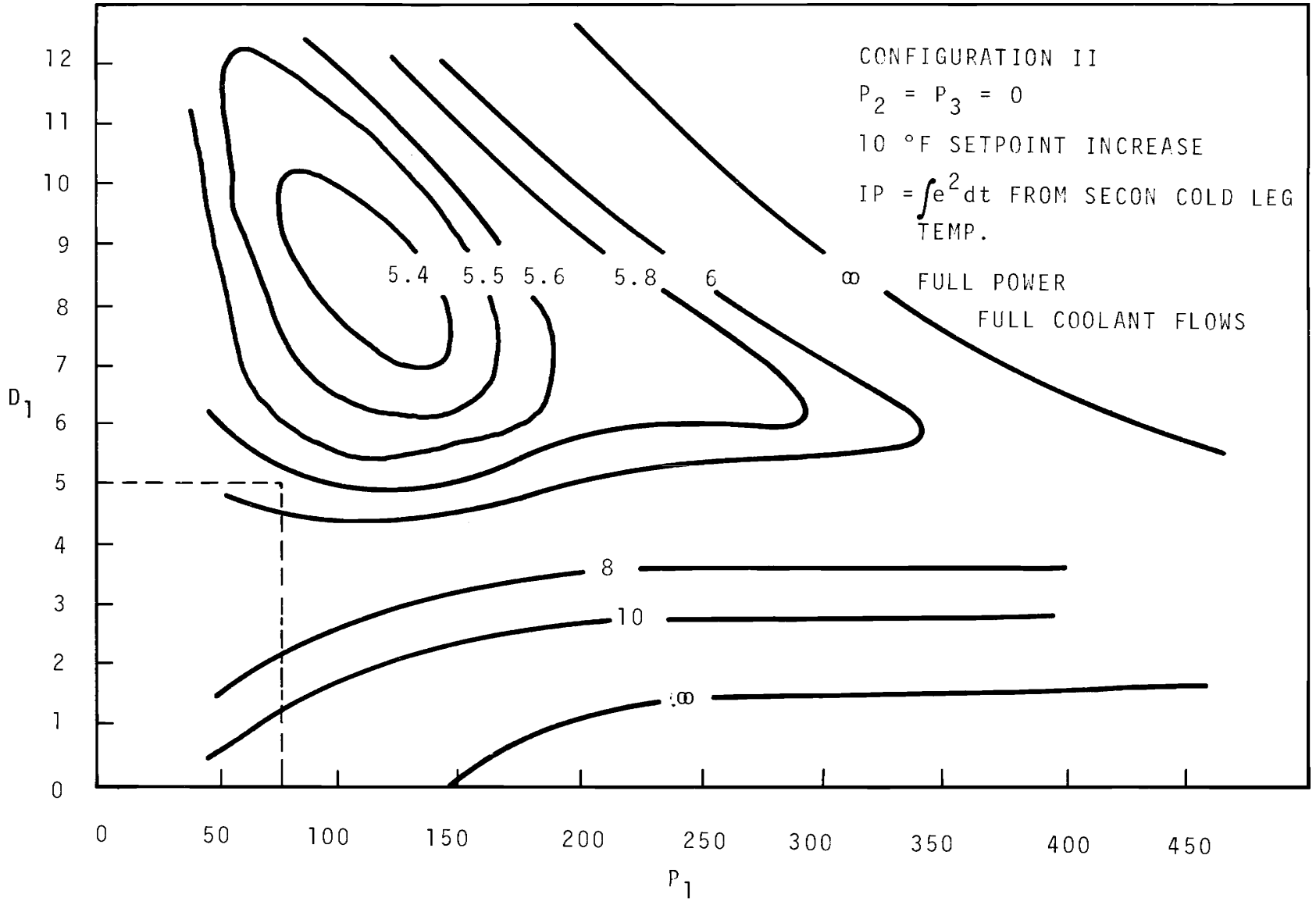

FIGURE 19-1. Contours of Constant Performance Index (IP) as a Function of the Secondary Cold Leg Temperature Controller Settings of Proportional Action (P_1) and Derivitive Action (D_1).

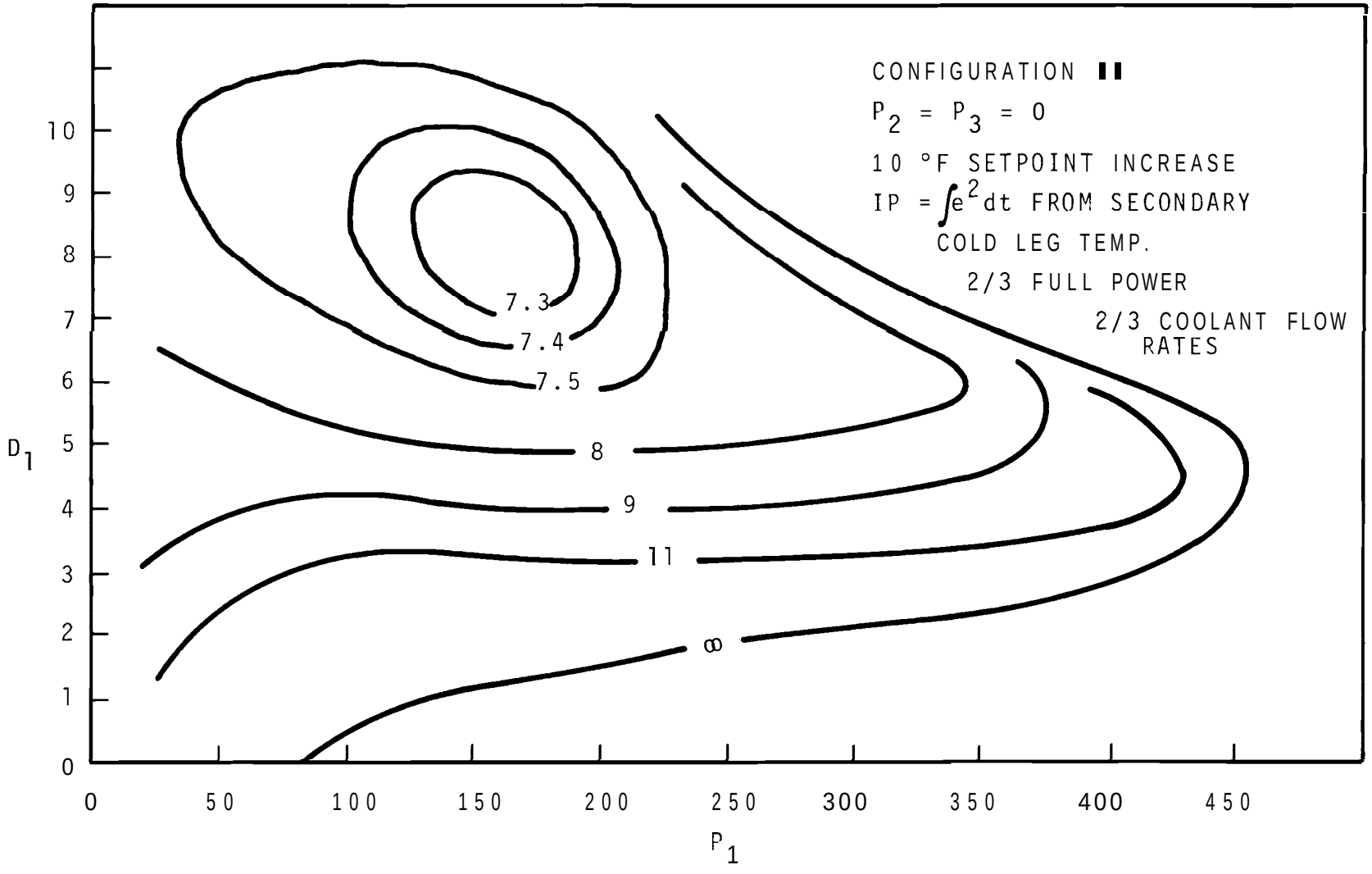

FIGURE 19-2. Contours of Constant Performance Index (IP) as a Function of the Secondary Cold Leg Temperature Controller Settings of Proportional Action (P_1) and Derivitive Action (D_1).

secondary cold leg temperature controller stability limits. Reducing power and flow reduces the area of the stable region.

The effect of the integral action is different from the derivitive action in that the integral action decreases stability instead of increasing it. This can be seen from the need to reduce proportional gain as reset action increases in order to maintain system stability.

The index of performance contours for setpoint changes are shown in Figure 21, where Figure 21-1 is for the IP from the primary cold leg temperature, and Figure 21-2 is for the IP from the process tube outlet sodium temperature. The dotted lines indicate that the controller settings used to study the other controllers in this same set of runs. The method of adjusting for about 20% overshoot with setpoint changes (as described previously in this report) results in an integral action setting of about 0.005. Comparison of Figure 21-1 with 21-2 illustrates that the optimum adjustments for tube outlet sodium temperature are different than for primary cold leg temperature. Figure 22 shows the IP contours from process tube outlet temperature for a power disturbance. Comparison of Figure 22 with Figure 21-2 shows that the shape of the contours is also a function of the type of disturbance. The numbers on the contours giving the value of the IP are related to other contours on the same graph but should not be interpreted between graphs. In general, the right side of a contour is less stable than the left side. Thus, a greater stability margin is realized by using low, rather than high values for the proportional action setting. The low values of integral action settings produce a high IP because the system is slow to reach the steady-state condition. Very low values of proportional action settings make the system respond slowly and results in a high error; thus, the result is a high IP.

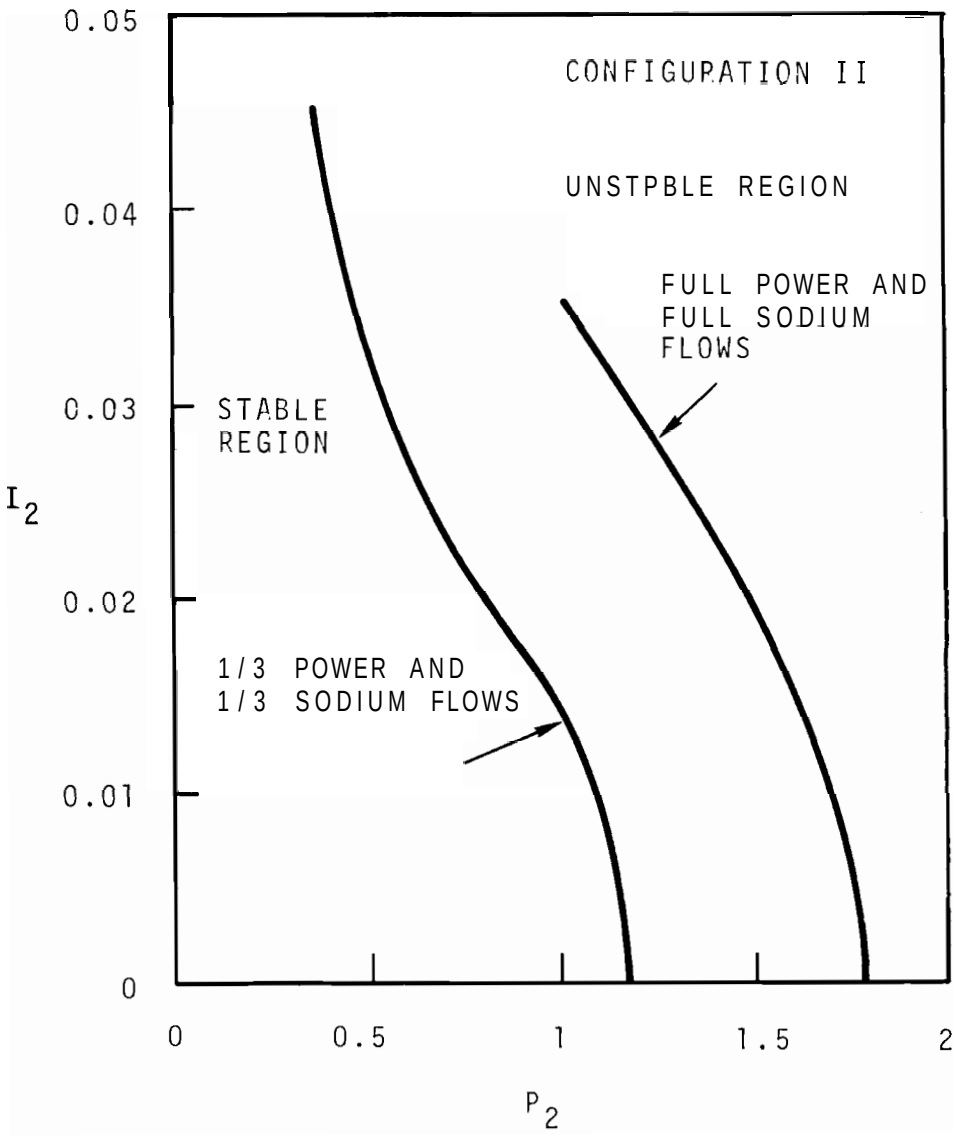

FIGURE 20. Stability Limits for the Primary Cold Leg Temperature

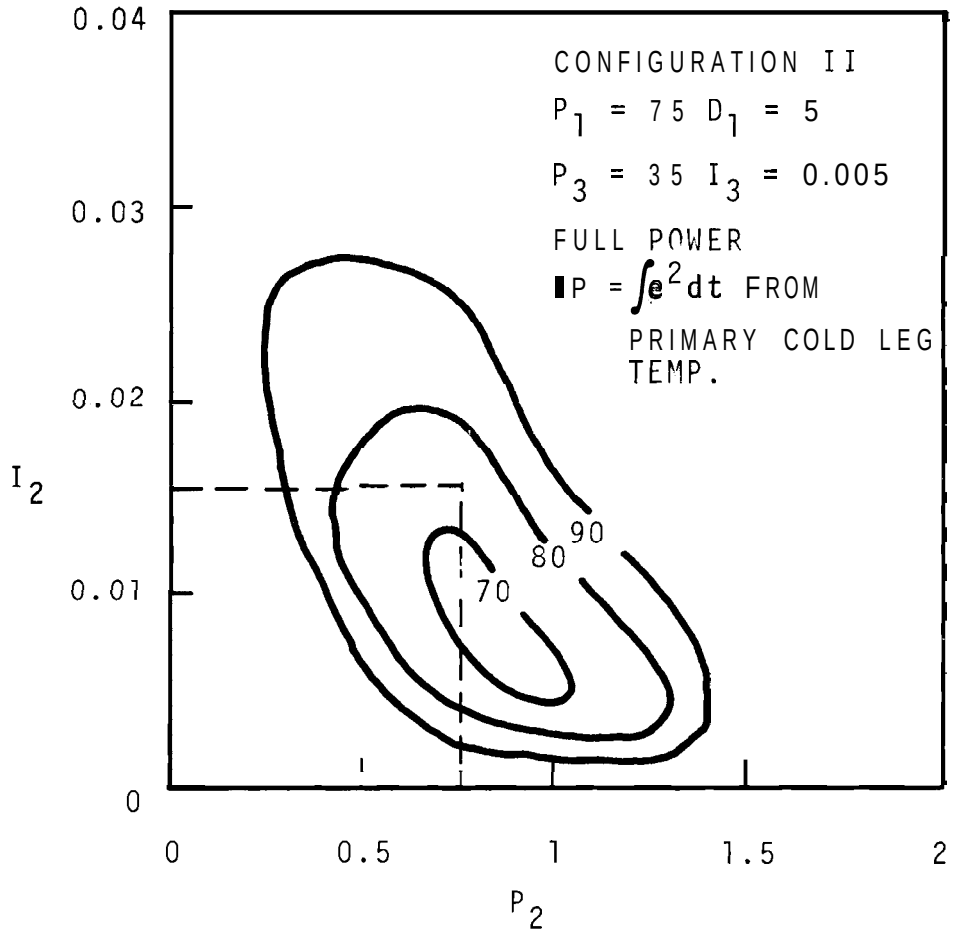

FIGURE 21-1. **Contours of Constant IP for the Primary Cold Leg Temperature Controller with a 10° Set-point Step Increase**

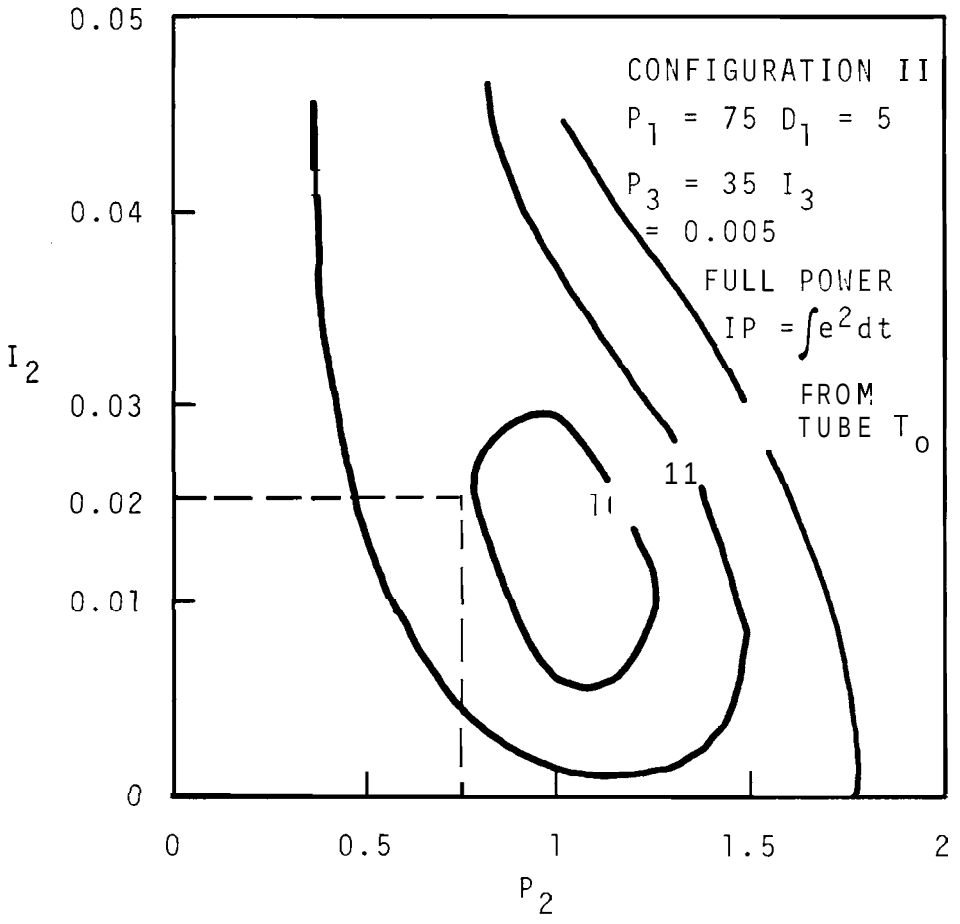

FIGURE 21-2. **Contours of Constant IP for the Primary Cold Leg Temperature Controller with a** 10° Setpoint **Step Increase**

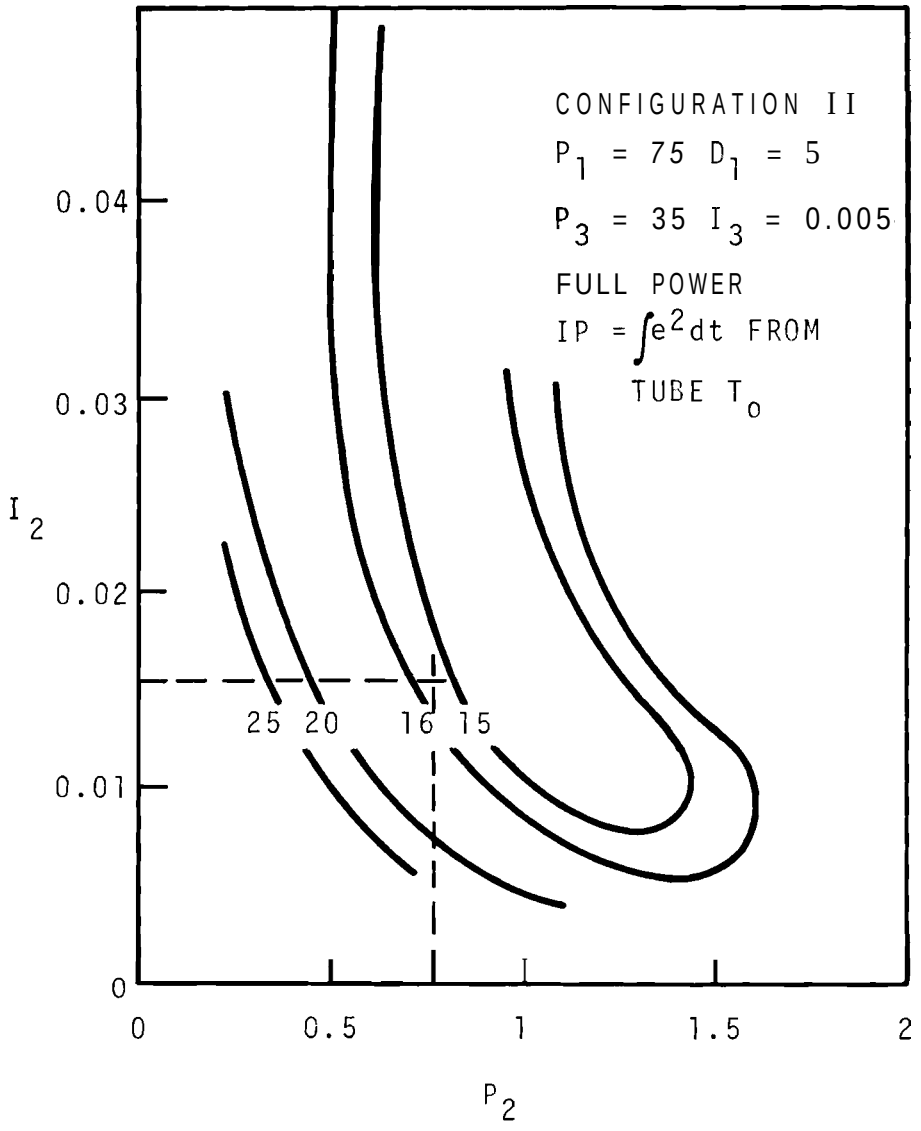

FIGURE 22. Contours of Constant IP for the Primary Cold Leg Temperature Controller with a Power Disturbance of 15 Megawatts Increase

PRIMARY HOT LEG TEMPERATURE CONTROLLER

The trends for the primary hot leg temperature controller settings are shown in Figures 23 and 24 for setpoint and power disturbances, respectively. Figure 23-1 shows the full-power-full-flow condition, and Figure 23-2 shows the one-third power, one-third sodium flow condition, both with the IP from the primary hot leg temperature. Figure 23-3 shows the IP contours from the process tube outlet temperature.

A general trend can be seen by comparing Figure 23-1 for full power and flows with Figure 23-2 for one-third power and flows. The location of the optimum moves to lower values of proportional and integral action settings for conditions with lower power and sodium flows. The settings of $P_3 = 35$ and $I_3 = 0.005$ were used for other full power-full sodium flow runs. The settings for 20% overshoot, as used in the runs showing trends with operating conditions, result in values for proportional and integral action settings of 12 and 0.1., respectively.

Comparison of Figure 23-1 for the IP from primary hot leg temperature with Figure 23-3 for the IP from tube outlet temperature emphasizes the differences that show up in different plant variables. Since the index of performance from tube temperature gets worse (increases) as proportional action setting increases, the desirability of using low settings is obvious. Figure 23-1 shows that the system may be on the inside contour line by having either high or low proportional action settings. Figure 23-3 indicates that the low settings should be used.

Comparison of Figures 23-3 and 24 shows another difference. Both figures use tube outlet temperature for the index of performance, but the disturbances are different. Figure 23-3 is for a setpoint disturbance, while 24 is for a

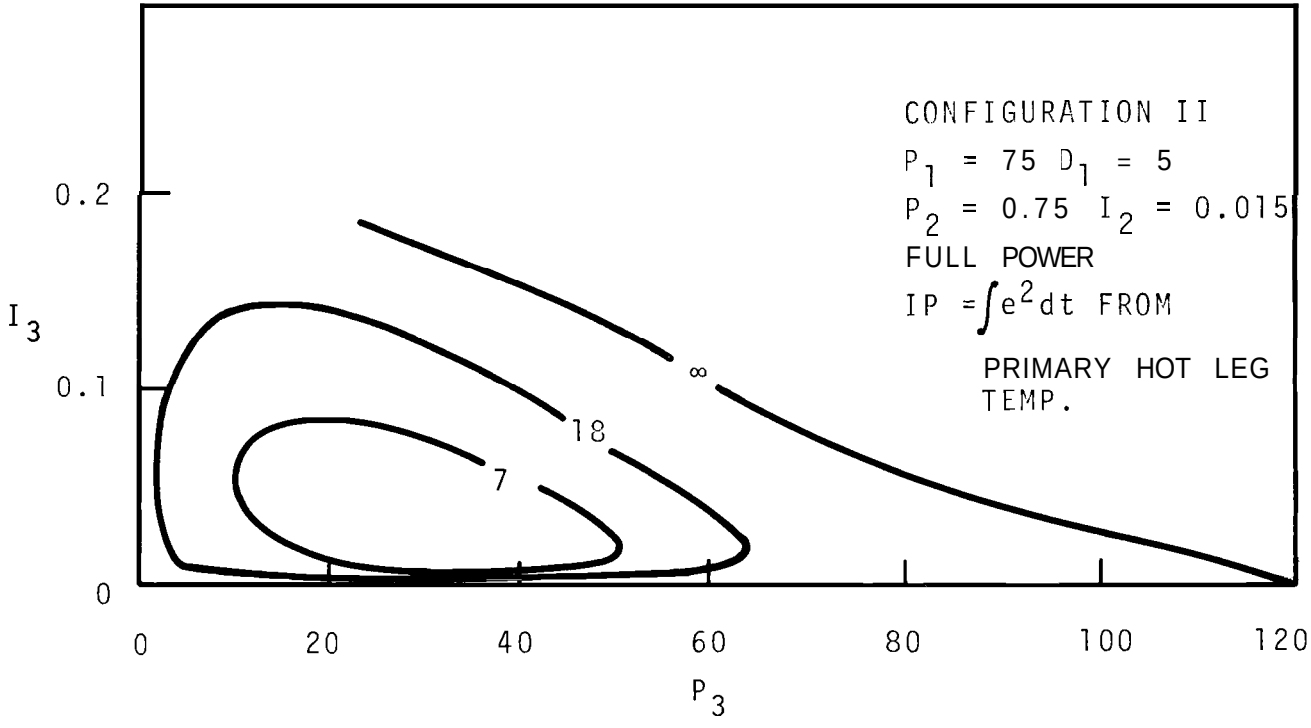

FIGURE 23-1. **Contours of Constant IP for the Primary Hot Leg Temperature Controller with a 10° Step Increase in** Setpoint

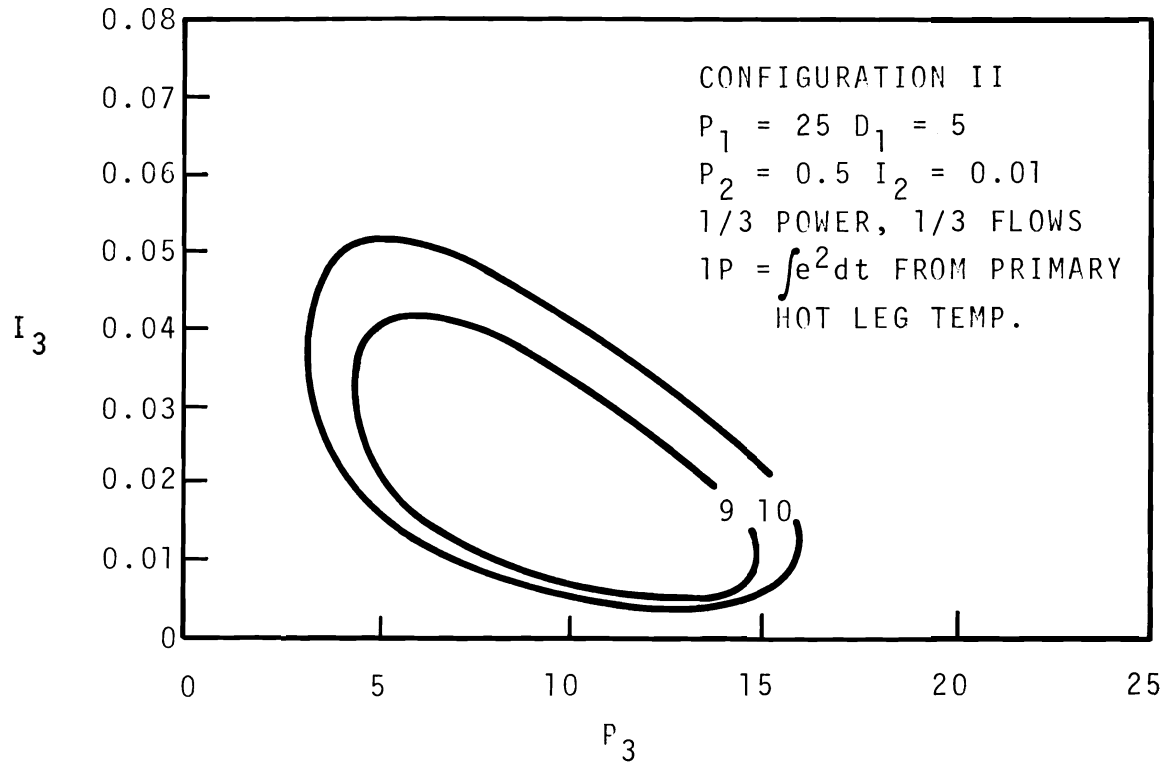

FIGURE 23-2 Contours of Constant IP for the Primary Hot Leg Temperature Controller with a 10° Step Increase in Setpoint

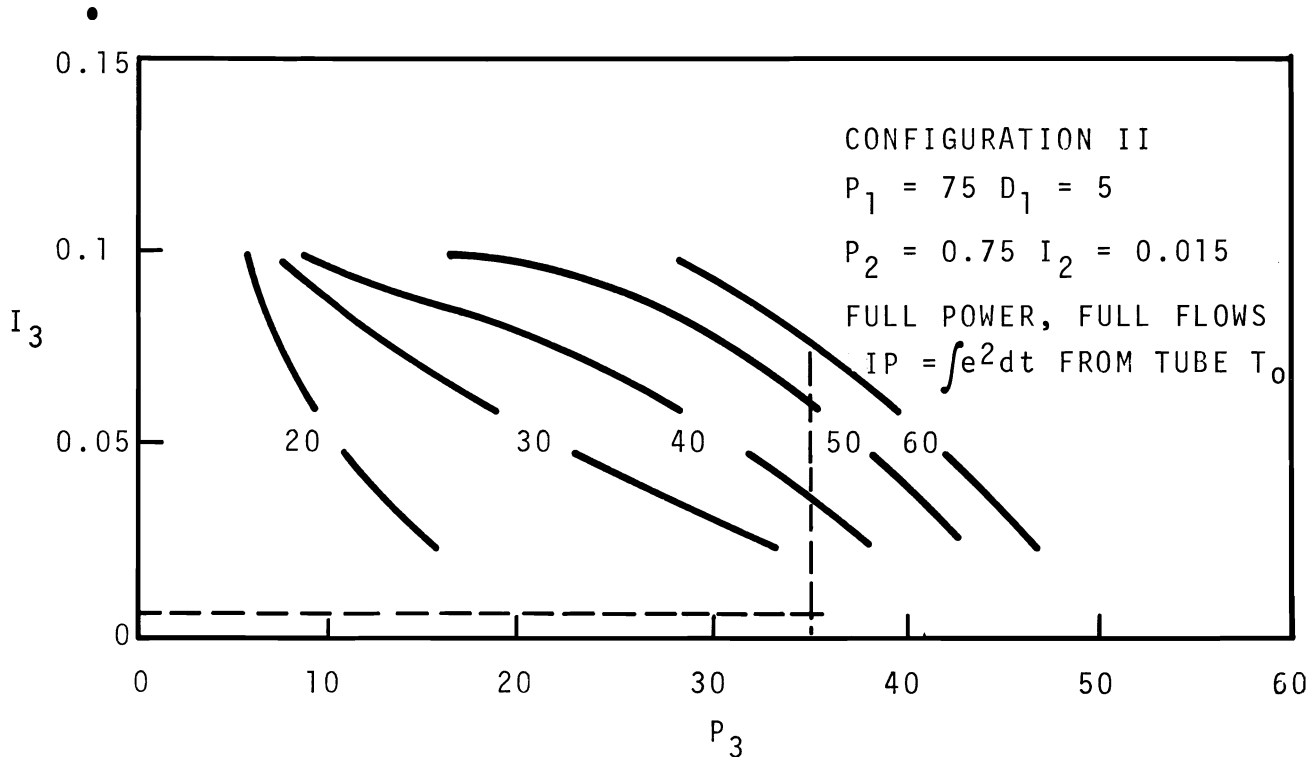

FIGURE 23-3 Contours of Constant IP for the Primary Hot Leg Temperature Controller with a 10° Step Increase in Setpoint

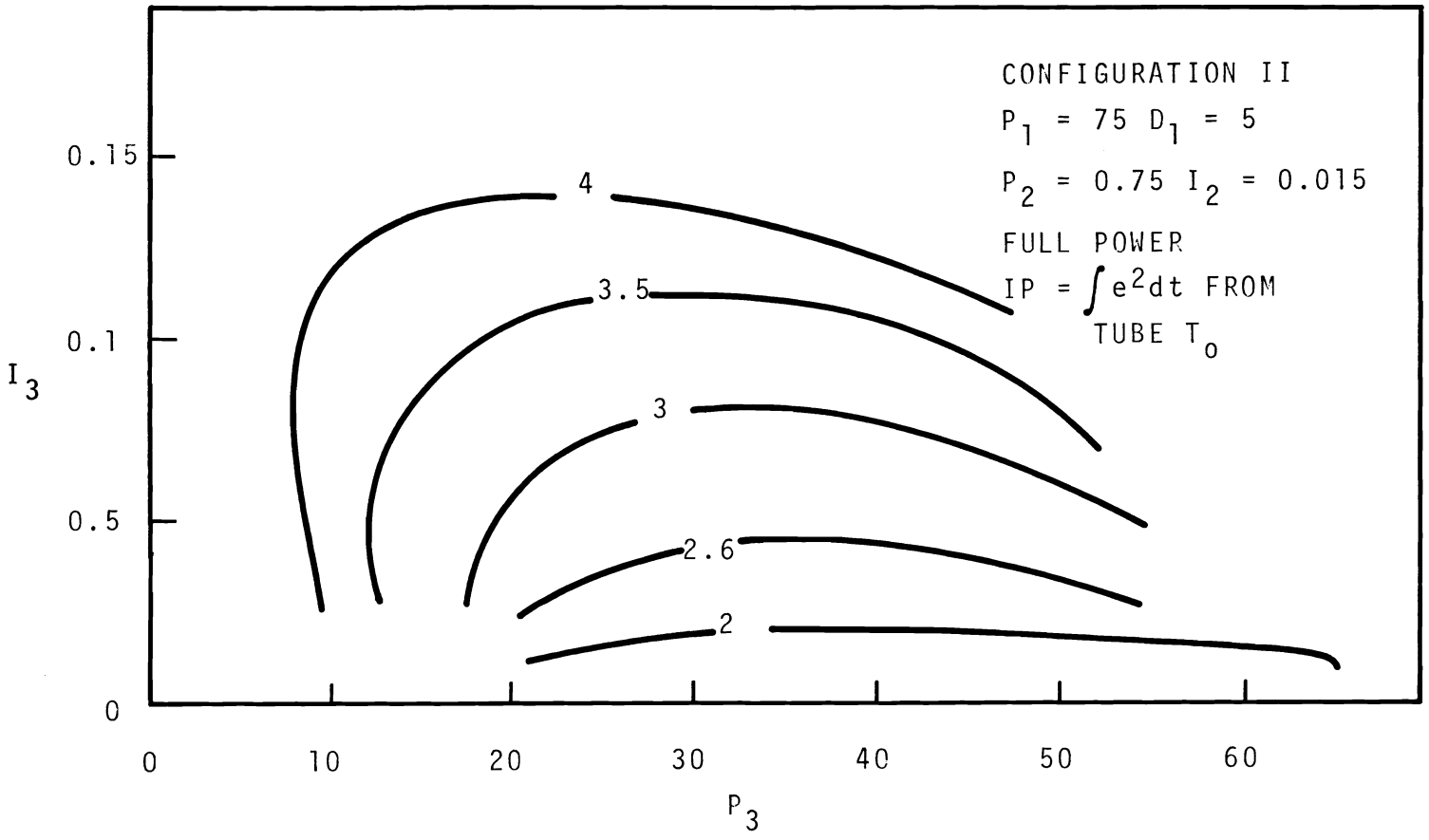

FIGURE 24 Contours of Constant IP for the Primary Hot Leg Temperature Controller with a 15 Megawatt Increase Power Disturbance

power disturbance. The power disturbance indicates that a low integral action setting is desirable with a relatively high proportional action setting.

The above trends make it apparent that controllers can be adjusted to decrease the effects of disturbances at a particular point and for particular disturbances. This however, is often at the expense of the effects for other disturbances and for other temperatures. We believe, however, that study of these trends with controller adjustments can result in a better overall understanding and lead to more knowledgeable adjustment procedures.

APPENEIX A

THE SIMULATION

APPENDIX A

THE SIMULATION

A simplified, high-speed dynamic simulation of the FFTF reactor and heat transport system was developed for use in control studies. The simulation which provides solutions of the dynamic equations, represents the reactor and one heat transport circuit of the FFTF. The simulation can operate as fast as 1000 times real time. The simplified simulation is based on a more detailed hybrid simulation called HYSIM-2A. HYSIM-2A is the present generation of the simulation described by Flowers, et al.[1] Many of the simulation techniques and all of the system parameters used in the simplified simulation were previously developed for HYSIM-2A.

The HYSIM-2A model and intermediate generations of the model were compared with detailed digital codes and found to provide sufficient accuracy for system transients and preliminary heat transport design studies.[2] We conclude that this model is sufficiently accurate to serve as a basis for the simplified model for control studies.

Frequency responses from the simplified model were compared with those from the HYSIM-2A model for each plant component (Reactor, IHX, and DHX) using both flow and temperature variations. As a criterion for acceptable accuracy, the simplified simulation, under full power and flow conditions, had to produce reasonably accurate ($\sim\pm5$ db) magnitude and ($\sim\pm30°$) phase results up to the frequency where the phase shift was 180°. Also, all full power and flow steady-state values had to be reasonably accurate ($\sim5\%$). The comparison frequency responses are included in Figures A-1 through A-12. The simplified simulation frequency response characteristics are shown using a solid line and the detailed simulation characteristics are superimposed using open circles for the phase and filled-in circles for the db.

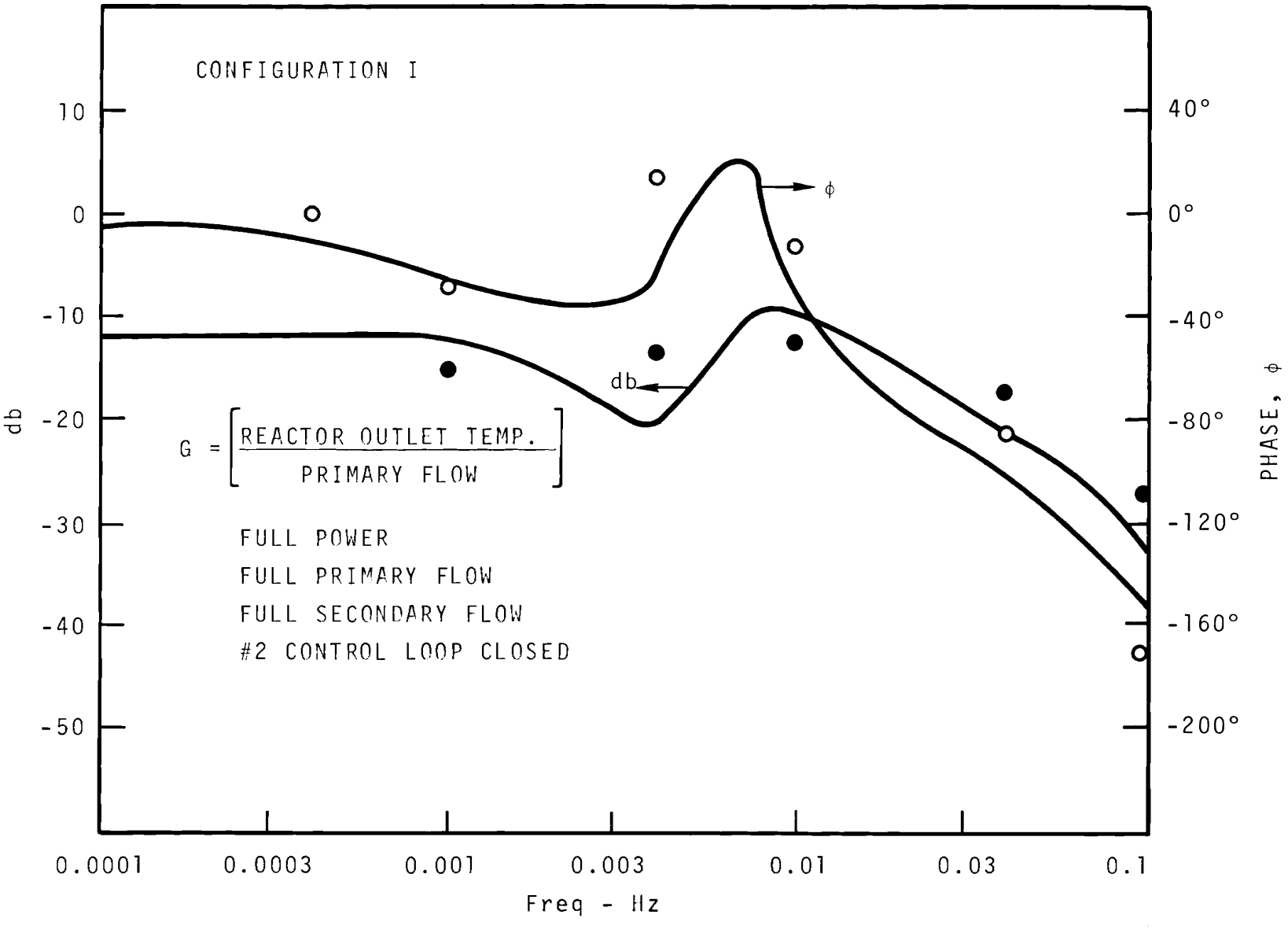

FIGURE A-1. Reactor Frequency Response Characteristics

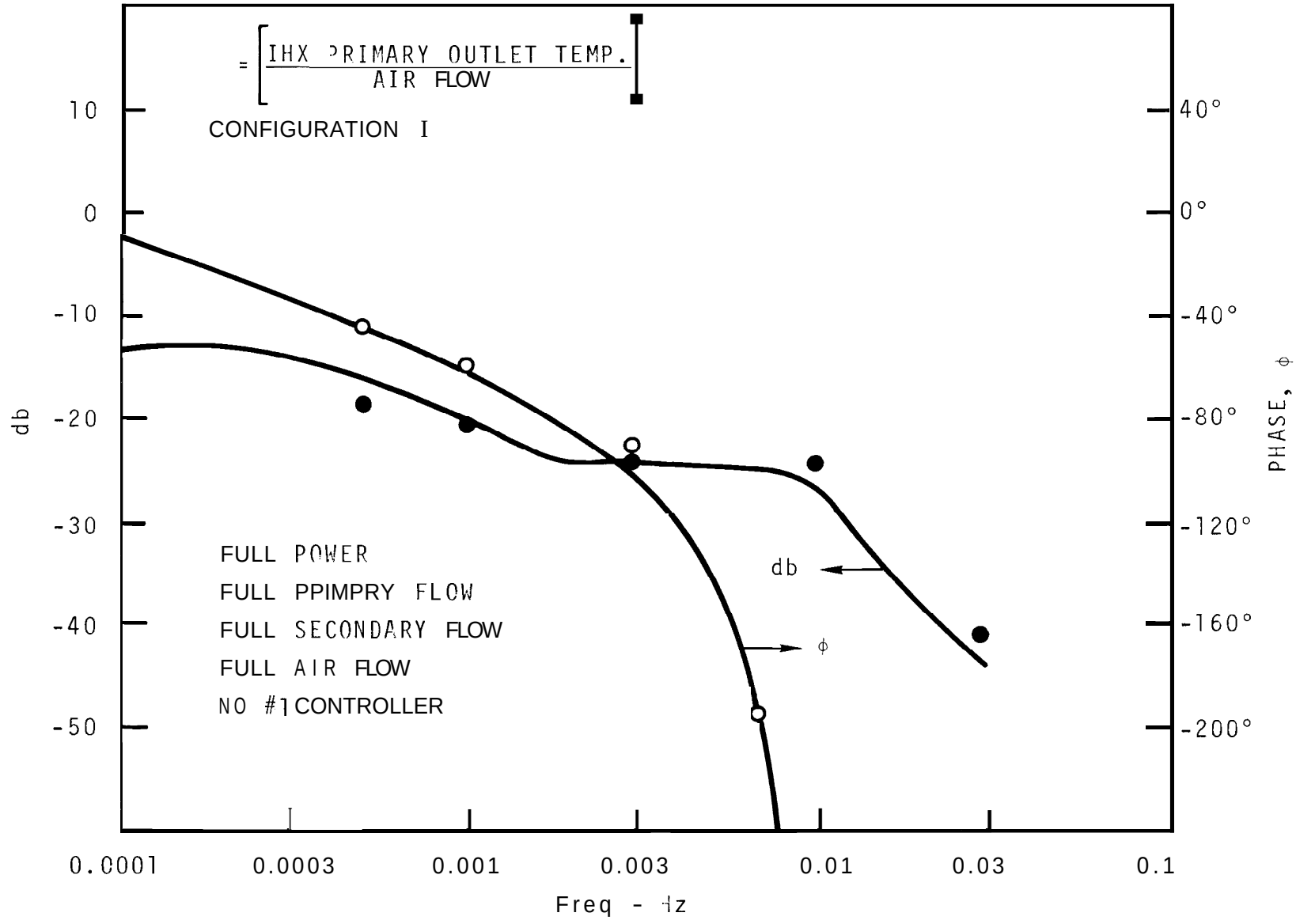

FIGURE A-2. Control Loop No. 2 Frequency Response

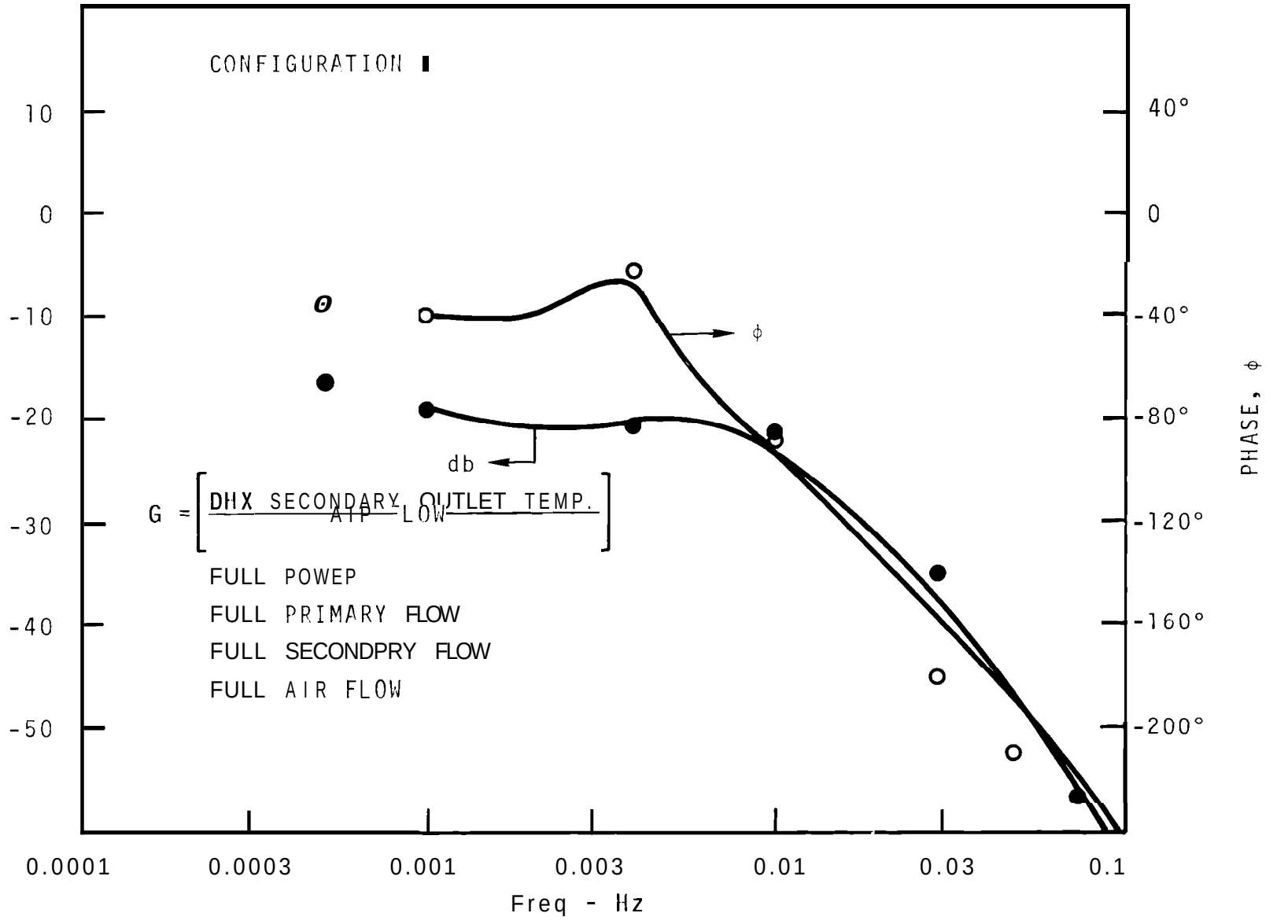

FIGURE **A-3.** Control Loop No. 1 Frequency Response

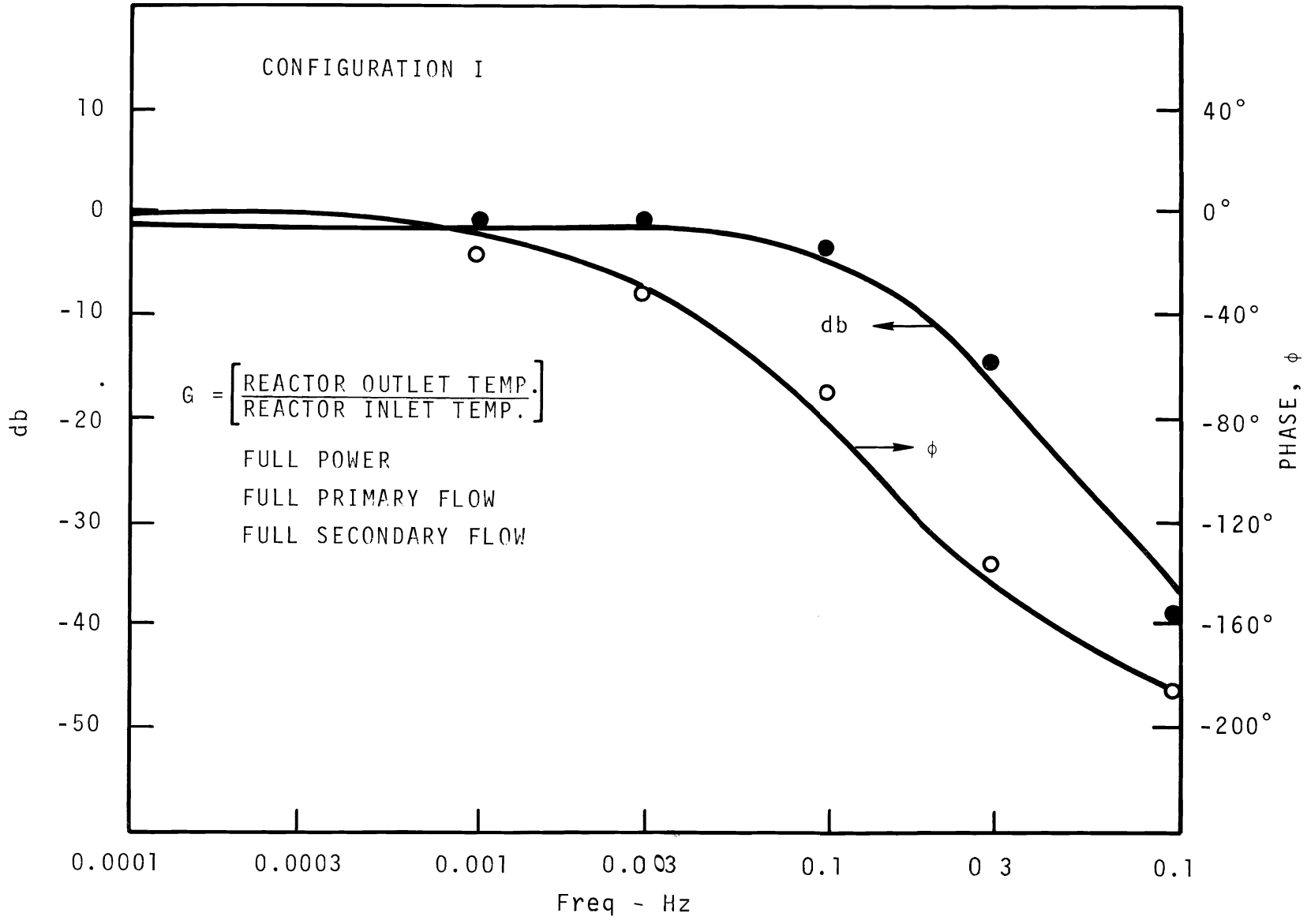

FIGURE A-4. Reactor Frequency Response Characteristics

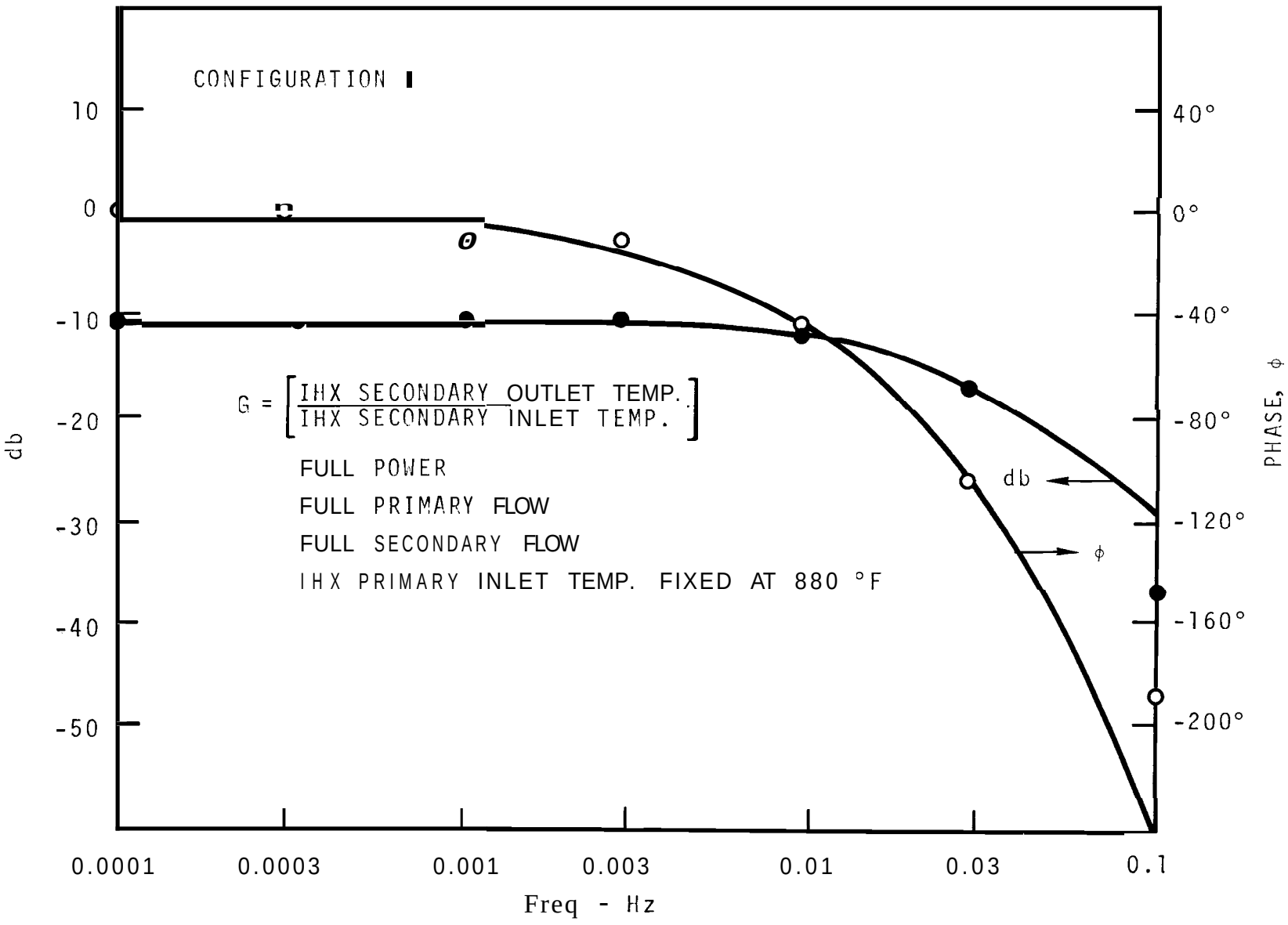

FIGURE A-5. IHX Frequency Response Characteristics

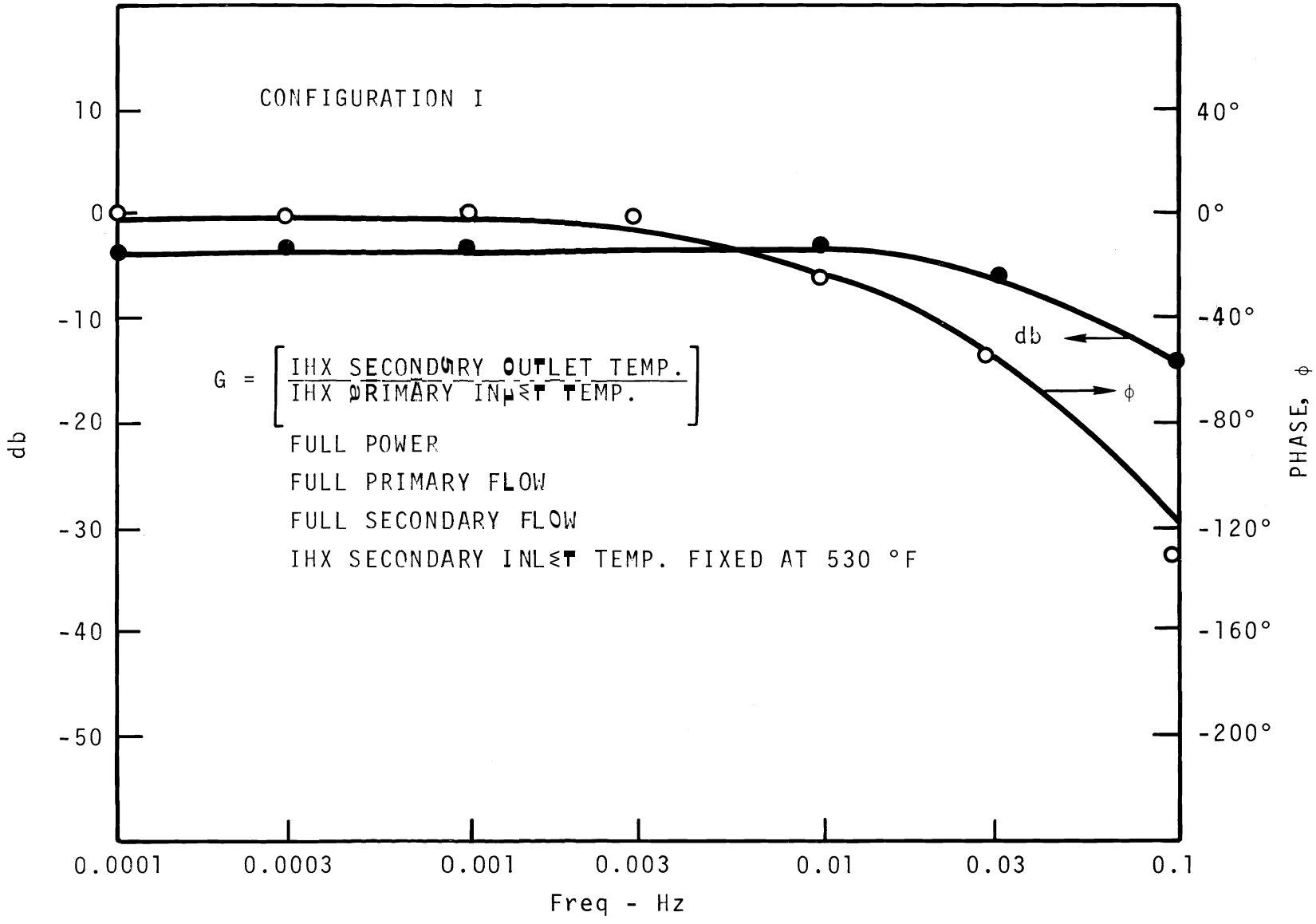

FIGURE A-6. IHX Frequency Response Characteristics

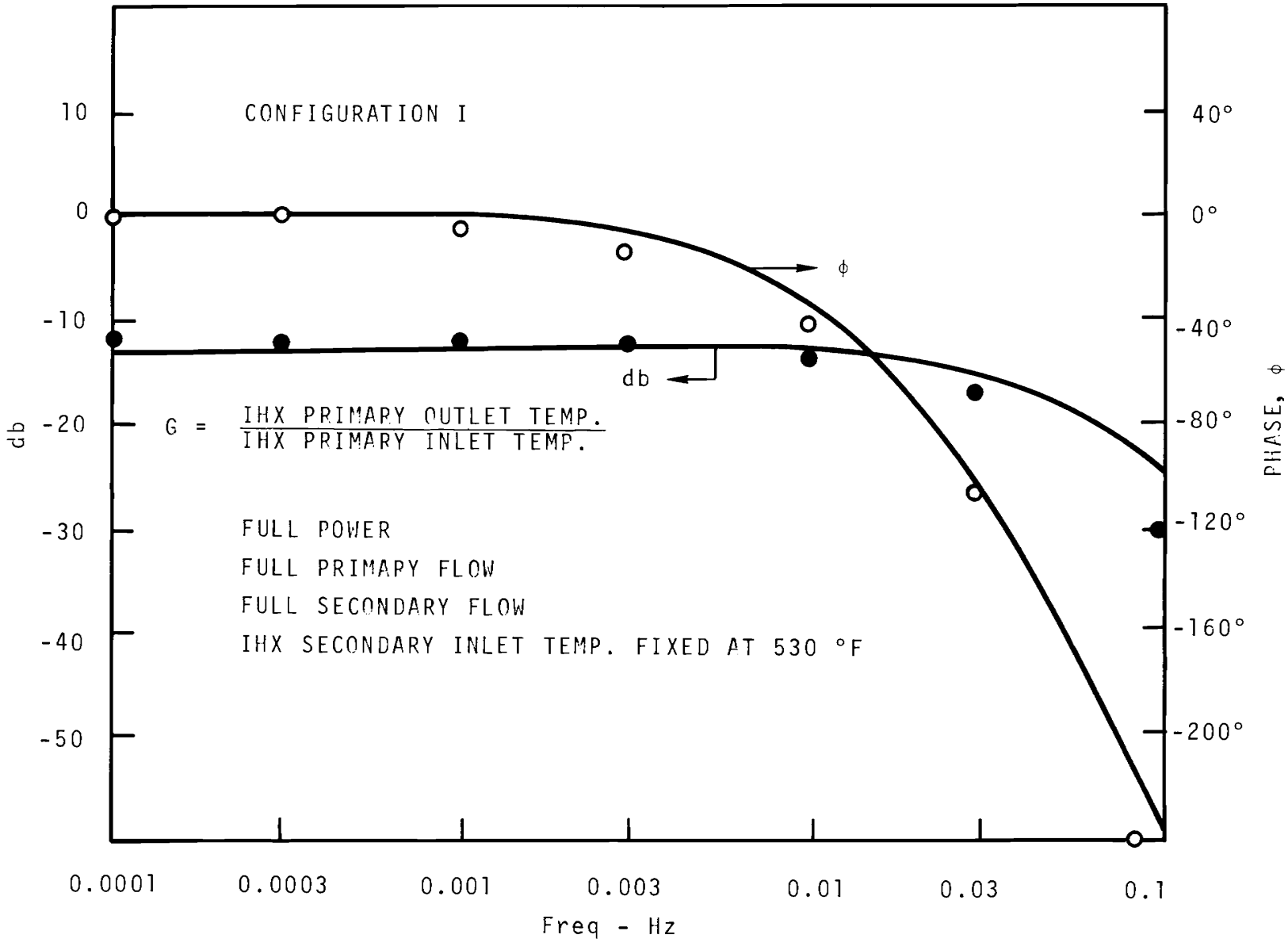

FIGURE A-7. IHX Frequency Response Characteristics

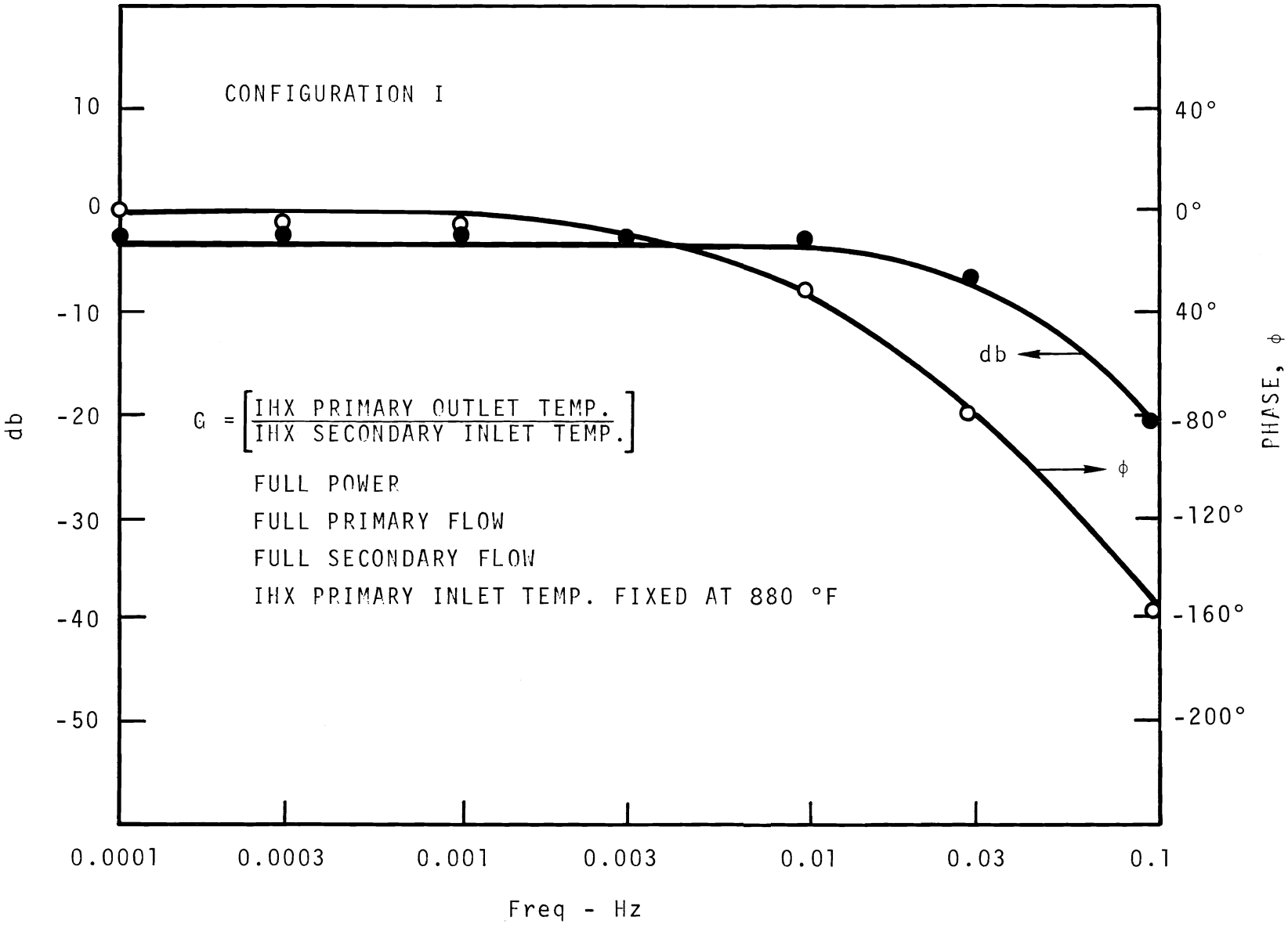

FIGURE A-8. IHX Frequency Response Characteristics

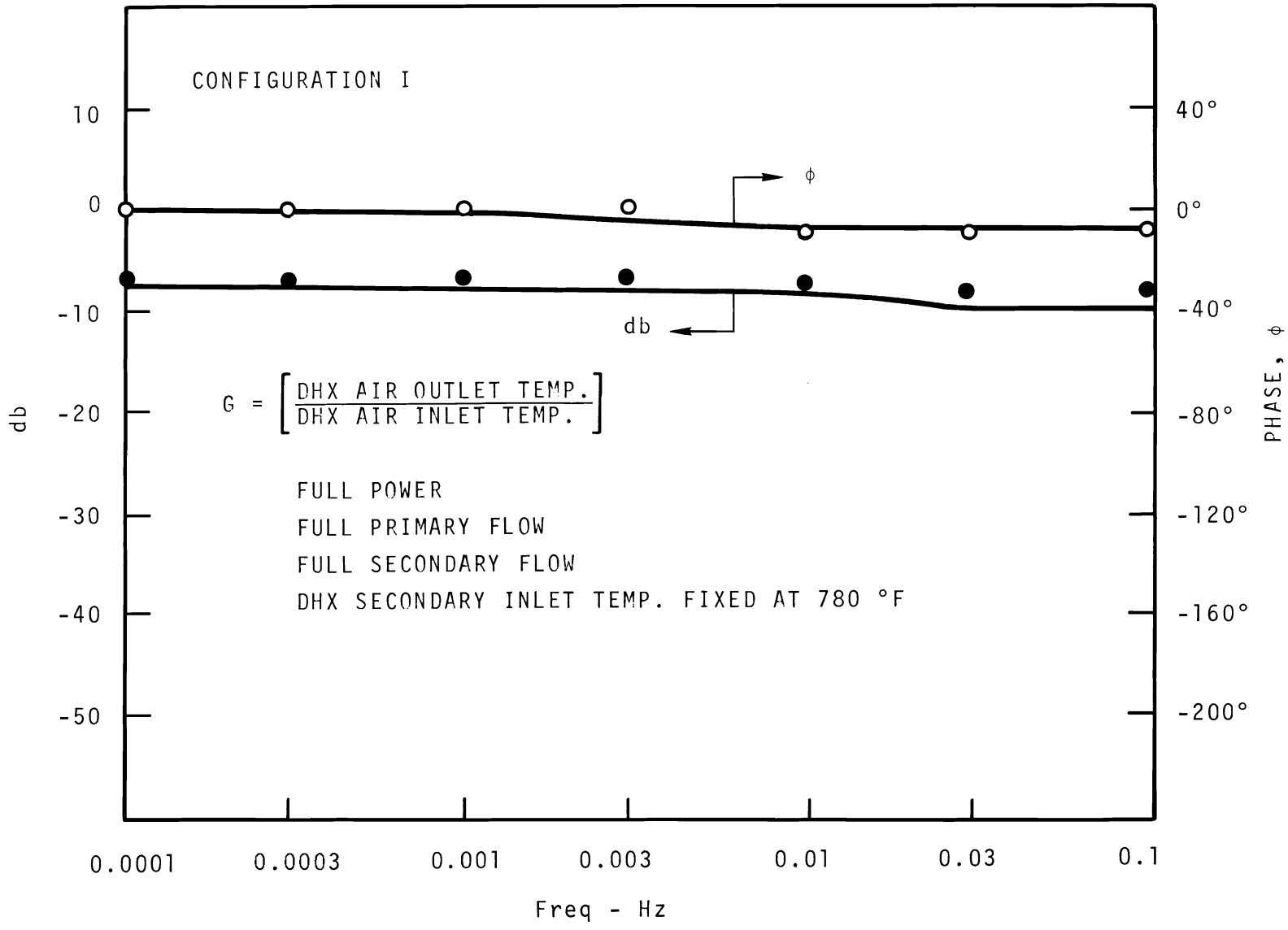

FIGURE A-9 DHX Frequency Response Characteristics

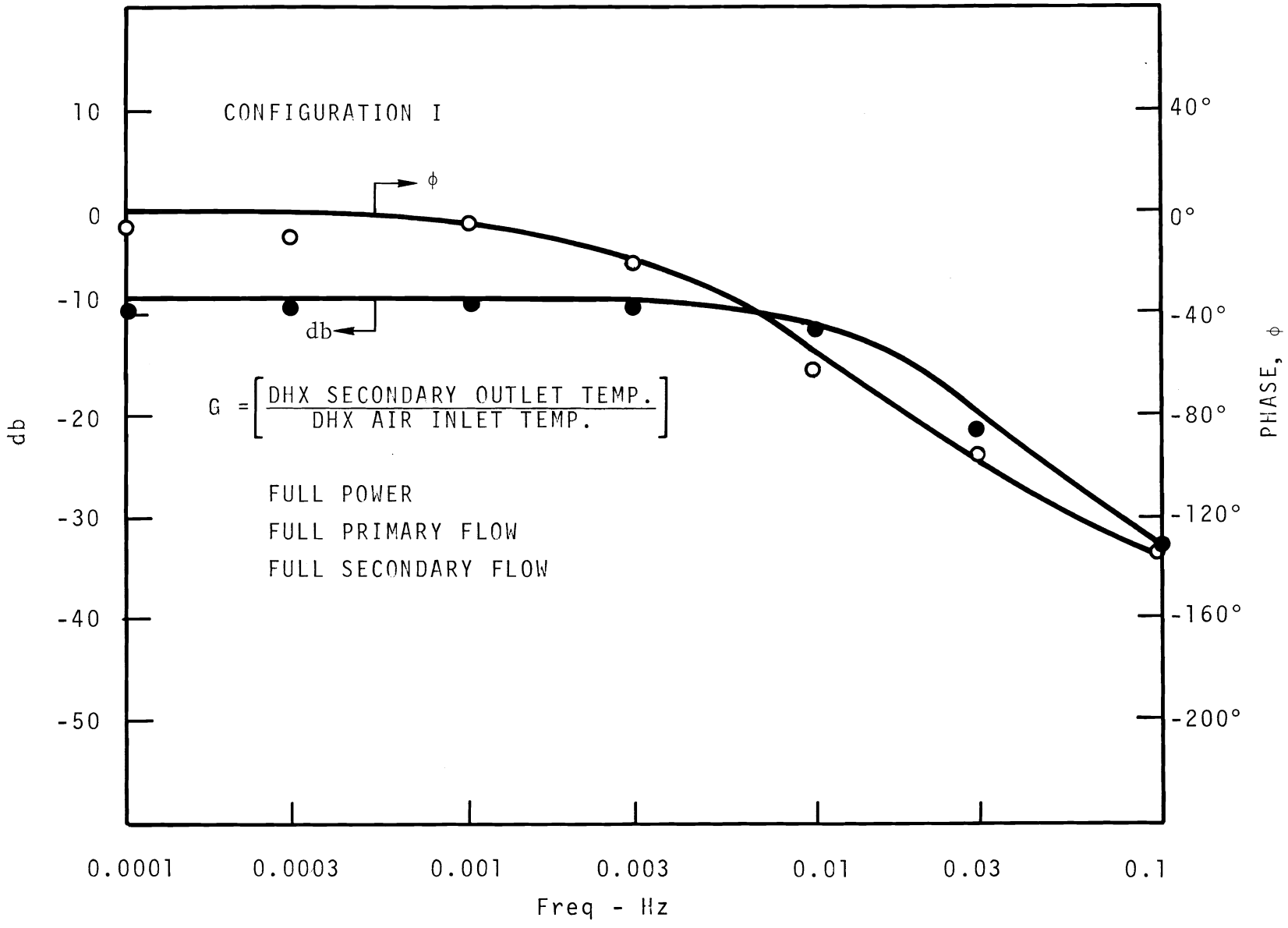

FIGURE A-10. DHX Frequency Response Characteristics

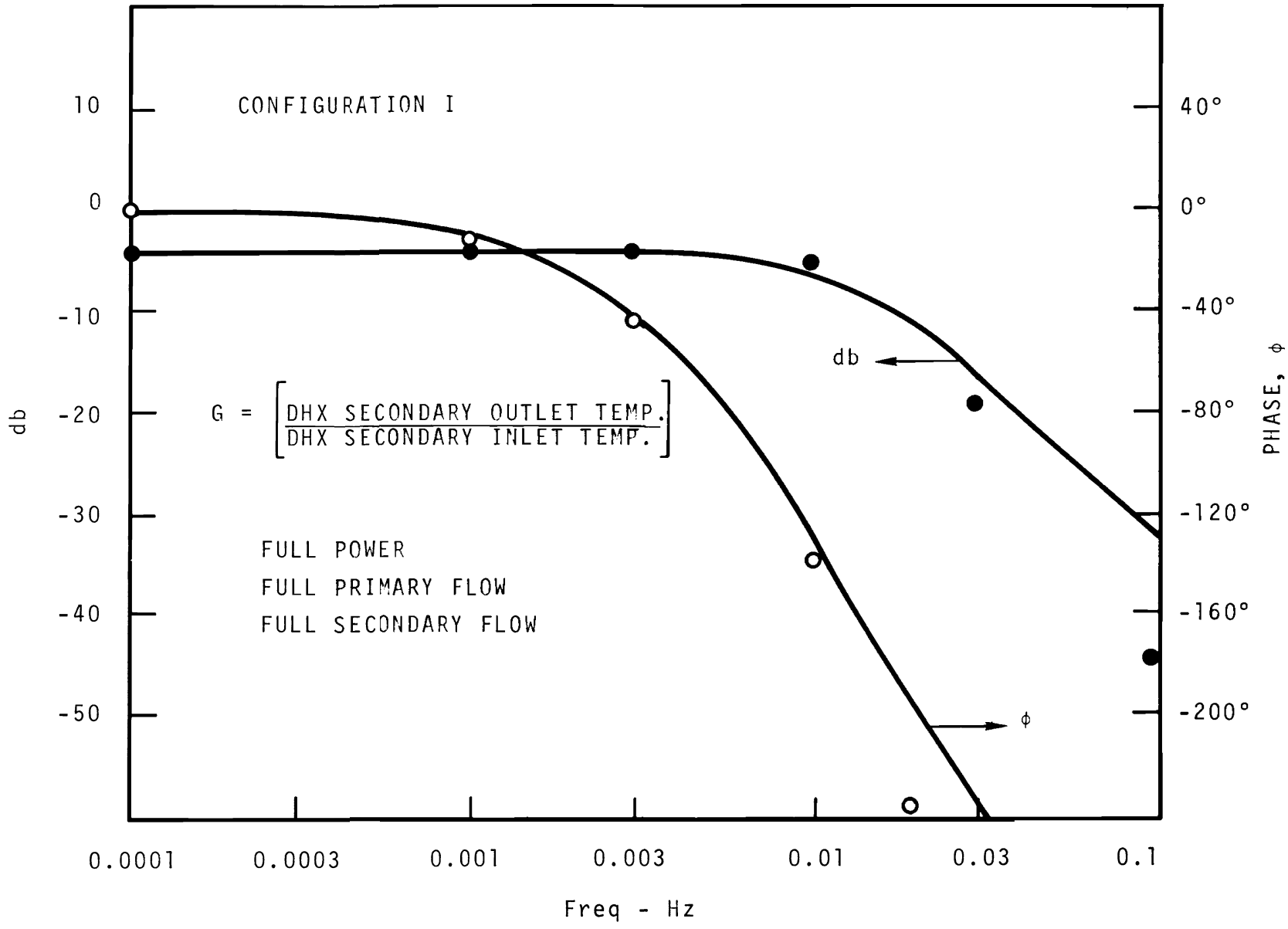

FIGURE A-11. DHX Frequency Response Characteristics

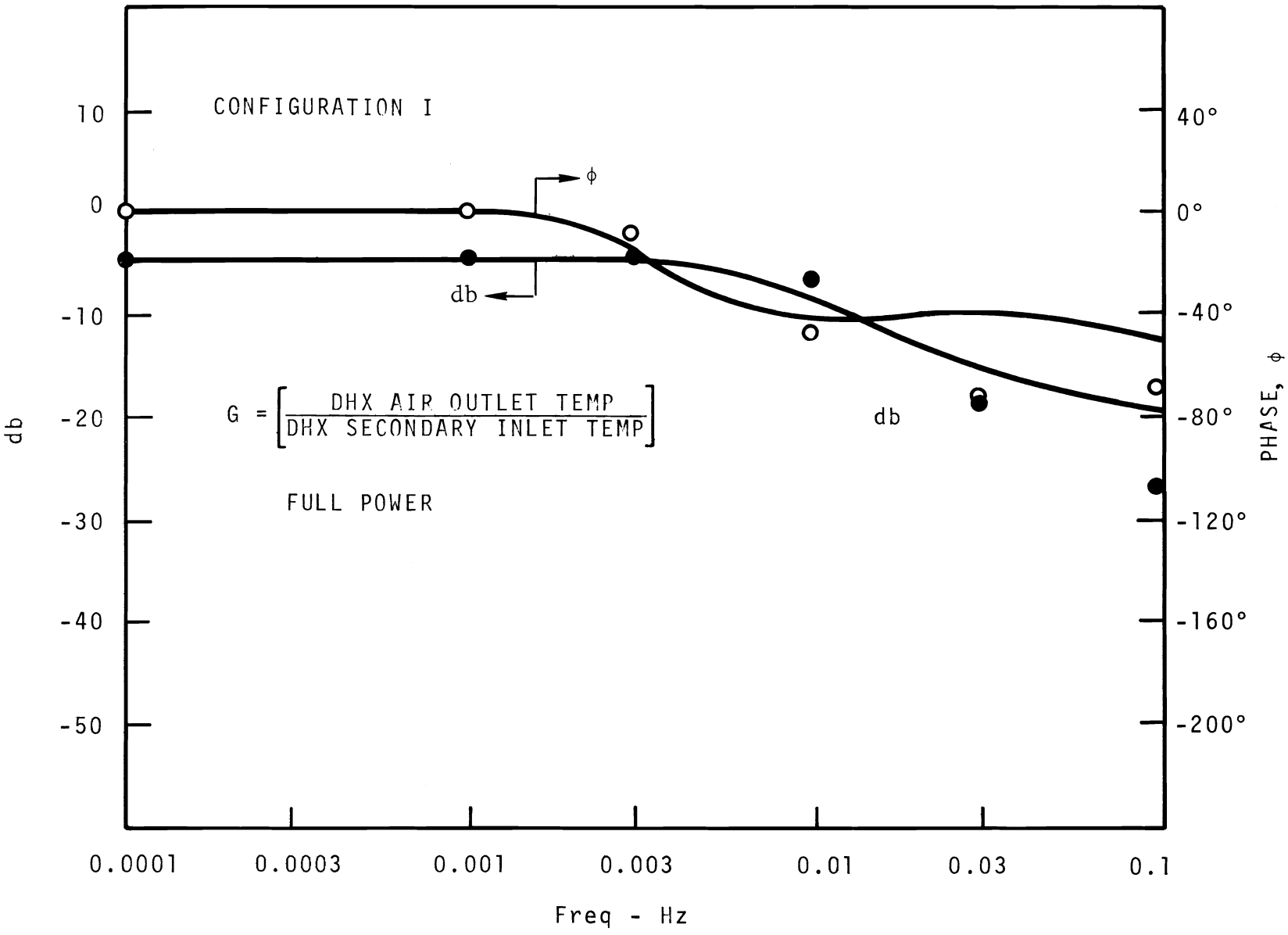

FIGURE A-12. DHX Frequency Response Characteristics

The reactor kinetics are calculated using an algebraic solution for the prompt neutrons (Equation 1).* The delayed neutrons are calculated by lumping the six groups into three groups (Equation 2). The method for determining the time constant for each of the three groups is described on page 10 of BNWL-707.[1] Reactivity changes for the kinetics equation are supplied from the Doppler equation or by the rod reactivity when the operator wishes to change power (Equation 3). The Doppler equation uses the average fuel temperature and is a linearization of the exact equation. Over the normal range of fuel temperatures there is almost no error introduced by linearizing the exact Doppler equation. Other reactivity terms are neglected because they are small and negative.

$$PL_N = \left[\frac{1}{\beta - \delta K}\right] \sum_{i=1}^{3} \ell^* \lambda_i C_i \qquad (1)$$

$$\left.\begin{aligned} \frac{dC_1}{dt} &= \frac{\beta_1}{\ell^*}(PL_N) - \lambda_1 C_1 \\ \frac{dC_2}{dt} &= \frac{\beta_2}{\ell^*}(PL_N) - \lambda_2 C_2 \\ \frac{dC_3}{dt} &= \frac{\beta_3}{\ell^*}(PL_N) - \lambda_3 C_3 \end{aligned}\right\} \qquad (2)$$

$$\delta K = \alpha_D (T_{AFR} - T_{AFRZ}) + \delta K_c \qquad (3)$$

Power is generated in several regions of the reactor and by several mechanisms. The power generated by each mechanism is calculated explicitly, then appropriate fractions are summed to calculate the power in each region. The calculation of neutron

---

* *See Table A-1 for explanation of symbols and parameter values.*

power (PL_N) has already been described in the kinetics section above. The fission product power (PL_{FP}) is calculated (see page 13 of BNWL-707)[2] using three groups with time constants chosen to best fit the post-scram fission product decay heat generation curve[3] (Equation 4 and 5). The first group was simulated with an infinite time constant since it has a time constant of nearly 10^4 sec. In cases other than post-scram, decay heat is of little consequence.

$$\left.\begin{aligned} \frac{d}{dt}(PL_{FP1}) &= \lambda_{FP1}(\beta_{FP1}\, PL_N - PL_{FP1}) \\ \frac{d}{dt}(PL_{FP2}) &= \lambda_{FP2}(\beta_{FP2}\, PL_N - PL_{FP2}) \\ \frac{d}{dt}(PL_{FP3}) &= \lambda_{FP3}(\beta_{FP3}\, PL_N - PL_{FP3}) \end{aligned}\right\} \quad (4)$$

$$PL_{FP} = PL_{FP1} + PL_{FP2} + PL_{FP3} \quad (5)$$

The neutron power and the decay heat power are summed in various ways to calculate total power (PL_{TOT}), closed loop power (PL_{CL}), radial reflector power (PL_{RR}), leakage region power (PL_{LR}), and fuel power (PL_F) (Equation 6 through 10). The closed loop power is removed by the closed loop heat transport system and thus is subtracted from the power removed by the main heat transport system.

$$PL_{TOT} = PL_N + PL_{FP} \quad (6)$$

$$PL_{CL} = \gamma_{CL}\, PL_{TOT} \quad (7)$$

$$PL_{RR} = \gamma_{RR}\, PL_N \quad (8)$$

$$PL_{LR} = \lambda_{LR} PL_N \quad (9)$$

$$PL_F = PL_{TOT} - PL_{CL} - PL_{RR} - PL_{LR} \quad (10)$$

The reactor thermal model accounts for the major sodium flow path through the reactor. All sodium entering the reactor flows through the inlet plenum. The sodium then splits and flows through the shroud tubes, the radial reflector region, or takes one of the several small flow paths bypassing the main heat generating regions. The sodium meets again when entering the outlet plenum. The sodium goes directly into the primary hot leg pipe upon leaving the outlet plenum. Figure 1 may aid in understanding the model of the FFTF.

The inlet plenum is approximated by a first order time lag; thus, perfect mixing is assumed (Equation 11). The time constant for the lag is a function of reactor flow. The volume of the inlet plenum is taken to be 975 ft^3. This inlet volume yields a time constant of about 10 sec at full reactor flow. T_{CIR} (Temperature Coolant Inlet Reactor) is the temperature at the inlet of the plenum and T_{CIP} (Temperature Coolant Inlet Plenum) is the temperature at the outlet of the plenum. The reactor flow rate, W_R, is calculated directly from primary flow since only one of the three heat transport circuits is simulated (Equation 12).

$$\frac{dT_{CIP}}{dt} = \frac{W_R C_{CIP}}{(\rho VC)_{IP}} (T_{CIR} - T_{CIP}) \quad (11)$$

$$W_R = W_P(3) \quad (12)$$

The majority of the reactor flow, about 80%, passes through the driver fuel ducts to cool the fuel. The fuel-to-coolant heat transfer is therefore the most significant reactor thermal calculation. The driver fuel coolant, W_{TR}, is calculated as a

percentage of the total reactor flow (Equation 13). The calculation of heat transferred between this coolant and the fuel uses two-axial coolant and two-axial fuel nodes. A nodal heat balance is performed to calculate the fuel and coolant temperatures (Equations 14 through 17). The double-primed parameters (A", V") are per driver element while the barred parameters ($\overline{\rho VC}$) are averaged over all materials. There is no axial heat conduction. Some cladding and duct metal is lumped with the coolant for the calculation of thermal inertia parameters. This method allows representation of the additional lag effects due to heat stored in the fission gas plenum metal. For this reason, the coolant temperature calculated, T_{CTR} (Temperature Coolant Tube Reactor), represents the temperature of the coolant leaving the fission gas plenum region rather than that leaving the active core region. The temperatures of the two fuel nodes are averaged and this average temperature, T_{AFR} (Temperature Average Fuel Reactor) is the fuel temperature used in the Doppler reactivity calculation (Equation 18).

$$W_{TR} = B_{TR}\, W_R \tag{13}$$

$$\frac{dT_{CT1}}{dt} = \frac{W_{TR}\, C_{CT}}{N_{ER}(\overline{\rho V''C})_{CT}} (T_{CIP} \quad T_{CT1}) + \frac{(UA'')_R}{(\overline{\rho V''C})_{CT}} \left[T_{f1} \quad T_{CT1}\right] \tag{14}$$

$$\frac{dT_{CTR}}{dt} = \frac{W_{TR}\, C_{CT}}{N_{ER}(\overline{\rho V''C})_{CT}} (T_{CT1} - T_{CTR}) + \frac{(UA'')_R}{(\overline{\rho V''C})_{CT}} \left[T_{f2} - T_{CTR}\right] \tag{15}$$

$$\frac{dT_{f1}}{dT} = \frac{b\alpha\, PL_F}{N_{ER}\,(\overline{\rho V''C})_f} - \frac{(UA'')_R}{(\overline{\rho V''C})_f} \left[T_{f1} - T_{CT1}\right] \tag{16}$$

$$\frac{dT_{f2}}{dt} = \frac{b\alpha\, PL_F}{N_{ER}\,(\overline{\rho V''C})_f} \quad \frac{(UA'')_R}{(\overline{\rho V''C})_f} \left[T_{f2} - T_{CTR}\right] \tag{17}$$

$$T_{AFR} = \frac{T_{f1} + T_{f2}}{2} \tag{18}$$

The purpose of the leakage calculation is to account for several sodium flow paths that are individually less significant to the vessel dynamics than either the tube coolant or the radial reflector coolant. The major contributors to what is called leakage flow are in-core leakage, hydraulic hold-down, vessel wall coolant, stored fuel coolant, and shield coolant flow. About 15% of the reactor flow falls into this category. The most significant factor that these flow paths have in common is that very little heat is transferred to the sodium. The temperature rise through the vessel for this stream is about 15" compared to a 250° ΔT for the overall vessel temperature rise. T_{CLR} (Temperature Coolant Leakage Reactor) is calculated assuming a first order equation with a variable flow coefficient. T_{CIP} and a small fraction of the neutron power are the inputs (Equation 19). The thermal properties used are essentially those of the sodium as the metal in the leakage region will have little effect on the dynamics. The leakage flow, W_{LR}, is calculated as a fixed percentage (about 15%) of reactor flow (Equation 20).

$$\frac{dT_{CLR}}{dt} = \frac{b\ PL_{LR}}{(\overline{\rho VC})_{LR}} - \frac{W_{LR}\ C_{CLR}}{(\overline{\rho VC})_{LR}} (T_{CLR} - T_{CIP}) \qquad (19)$$

$$W_{LR} = B_{LR}\ W_R \qquad (20)$$

The radial reflector flow, W_{RR}, is less than 5% of the total reactor flow (Equation 21). It is a significant flow path, however, as the radial reflector sodium carries almost as much energy per pound as the tube coolant. For this reason, a separate node is devoted to the radial reflector flow calculation. The radial reflector coolant outlet temperature, T_{CRR} (Temperature Coolant Radial Reflector), is calculated using a

first order equation with a coefficient that varies with flow. The input temperature is T_{CIP} and the input power is a fraction of neutron power (Equation 22). The heat capacity of the radial reflector metal is neglected in the calculation.

$$W_{RR} = B_{RR} W_R \tag{21}$$

$$\frac{dT_{CRR}}{dt} = \frac{b\ PL_{RR}}{(\overline{\rho VC})_{RR}} - \frac{W_{RR}\ C_{CRR}}{(\overline{\rho VC})_{RR}} (T_{CRR} - T_{CIP}) \tag{22}$$

The reactor outlet plenum is simulated as a first order lag, that is, perfect mixing is assumed. The time constant for this lag term is a function of reactor flow. Each of the three outputs from the reactor coolant temperature calculations is multiplied by the percentage of reactor flow in that particular stream. They are then added to form the input temperature to the outlet plenum (Equation 23). The volume used for the outlet plenum is 1000 ft^3. This volume gives an outlet plenum time constant of about 10 sec at full reactor flow.

$$\frac{dT_{COR}}{dt} = \frac{W_R\ C_{COR}}{(\rho VC)_{OR}} (B_{TR}\ T_{CTR} + B_{RR}\ T_{CRR} + B_{LR}\ T_{CLR} - T_{COR}) \tag{23}$$

T_{COR} (Temperature Coolant Outlet Reactor), the temperature of the coolant when it leaves the reactor, is the input to the primary hot leg pipe. The pipe is simulated as a pure distance/velocity lag. The simulation assumes no mixing and no heat transfer while the coolant is in the pipe. The calculation is performed on the digital part of the hybrid computer. The distance/velocity lag is calculated by setting up a table and letting each location in this table represent a block of

sodium moving along the pipe. The temperature input to the pipe is placed in a location in the table. Another temperature, which is to be the output from the pipe, is taken from its location in the table and sent to the analog computer for the IHX calculation. The rate at which the temperatures are put in and taken from the table is a function of primary flow rate. Each location in the table represents an equal volume of pipe such that the volume of a single node times the number of nodes equals the total volume of the pipe. In this way, a coolant temperature is entered into the table and taken from the table every time the integrated flow rate equals the nodal volume. To accomplish this, the primary flow is integrated with time and a check is performed to see if the integrated value has exceeded the nodal volume. When this occurs the flow integration is re-initialized and the time delay table is updated. The primary hot leg pipe is simulated as 20 nodes. The distance velocity lag of the primary hot leg pipe is nearly 36 sec at full primary flow. The output from this calculation is T_{CPXI} (Temperature Coolant Primary IHX Inlet).

T_{CPXI}, the temperature of the sodium entering the IHX, is the input to a plenum calculation. The plenum is simulated as a first-order time delay with the delay being a function of the primary flow (Equation 24). At full flow the time constant of this plenum is 1.5 seconds.

$$\frac{dT_{CPX1}}{dt} = \frac{1-\beta_P}{(\rho V)_{PXI}} (W_P)(T_{CPXI} - T_{CPX1}) \qquad (24)$$

Because of the design of the IHX, it is felt that some of the primary hot leg sodium will leak into the primary cold leg stream at the point where the hot leg and cold leg pipes join the IHX. Some of the secondary cold leg sodium may leak into the secondary hot leg sodium in the same way. Thus, some sodium,

both primary and secondary, will bypass the heat exchange surfaces. This bypass flow is accounted for in the heat transfer and the plenum calculations. It is simulated with the assumption that a percentage of the sodium is diverted just before it enters the inlet plenum and mixes with the main stream again when they enter the outlet plenum. The bypass flow is taken to be 5% of the total flow for the primary side and 2.5% of the total flow for the secondary side.

The exact equations for heat transfer in the IHX include partial derivatives with respect to distance (Equations 25 and 26). To solve these equations, the IHX heat transfer surfaces were simulated with two primary and two secondary nodes. A finite differencing technique was used to calculate the $\frac{\delta T}{\delta x}$ term for each node. The node nearest the flow inlet uses a central difference technique to calculate the temperature gradient (Equations 27 and 28). The node at the flow outlet uses a three point back technique to calculate this term (Equations 29 and 30). The primed parameters are per unit length (V', A'). The tube metal was not simulated as a separate node, but the thermal inertia that the tubes contribute was lumped with the sodium. One-half of the tube metal goes with the primary coolant and the other half goes with the secondary. The heat transfer coefficients and metal properties are simulated as being constant. Coefficients and properties applicable to full-power steady-state operation are used.

$$(\rho V' C)_P \frac{\partial T_P}{\partial t} = - W_P C_{CP} \frac{\partial T_P}{\partial x} - (UA')(T_P - T_S) \qquad (25)$$

$$(\rho V' C)_S \frac{\partial T_S}{\partial t} = - W_S C_{CS} \frac{\partial T_S}{\partial x} - (UA')(T_S - T_P) \qquad (26)$$

$$(\rho V'C)_{PX} \frac{dT_{CPX2}}{dt} = \frac{-C_{CPX}(1-\beta_P)(W_P)}{L_X} (T_{CPX3} - T_{CPX1})$$

$$- (UA')_X(T_{CPX2} - T_{CSX2}) \quad (27)$$

$$(\rho V'C)_{SX} \frac{dT_{CSX2}}{dt} = \frac{C_{CSX}(1-\beta_S)W_S}{L_X} (T_{CSX3} - T_{CSX1})$$

$$- (UA')_X(T_{CSX2} - T_{CPX2}) \quad (28)$$

$$(\rho V'C)_{PX} \frac{dT_{CPX3}}{dt} = \frac{-C_{CPX}(1-\beta_P)}{L_X} (W_P)(3T_{CPX3} - 4T_{CPX2} + T_{CPX1})$$

$$- (UA')_X(T_{CPX3} - T_{CSX3}) \quad (29)$$

$$(\rho V'C)_{SX} \frac{dT_{CSX1}}{dt} = \frac{C_{CSX}(1-\beta_S)}{L_X} W_S(4T_{CSX2} - 3T_{CSX1} - T_{CSX3})$$

$$- (UA')_X(T_{CSX1} - T_{CPX1}) \quad (30)$$

The temperature output from this primary heat transfer calculation is an input to the IHX primary outlet plenum calculation. The other input to the outlet plenum calculation is the bypass flow temperature which is the IHX primary inlet temperature. Each temperature is multiplied by the percentage of flow in its respective path. The sum of these products forms the input to a first-order time lag calculation which represents mixing in the plenum (Equation 31). The time constant for the plenum is a function of primary flow. At full flow, the tine constant for the primary outlet plenum is about 2 sec. The resultant temperature from the plenum calculation is T_{CPXO} (Temperature Coolant Primary IHX Outlet).

$$\frac{dT_{CPXO}}{dt} = \frac{1}{(\rho V)_{PXO}} (W_P) \left[(1-\beta_P)(T_{CPX3} - T_{CPXO}) + \beta_P (T_{CPXI} - T_{CPXO}) \right] \quad (31)$$

The primary cold leg pipe, with input T_{CPXO}, is simulated in the same way as the primary hot leg pipe. The time delay for the primary cold leg pipe at full flow is about 14 sec. Eight nodes are used for the primary cold leg pipe simulation. The outlet temperature from this pipe feeds into the reactor and is called T_{CIR} (Temperature Coolant Inlet Reactor).

The mixing plenums for the secondary side of the IHX are calculated in the same way that the primary plenums are (Equations 32 and 33). The time constant for the inlet plenum is about 4 sec, while that for the outlet plenum is about 2 sec. The inlet temperature for the secondary side of the IHX is T_{CSXI} (Temperature Coolant Secondary IHX Inlet) and the outlet temperature is T_{CSXO} (Temperature Coolant Secondary IHX Outlet).

$$\frac{dT_{CSX3}}{dt} = \frac{(1-\beta_S)}{(\rho V)_{SXI}} (W_S)(T_{CSXI} - T_{CSX3}) \qquad (32)$$

$$\frac{dT_{CSXO}}{dt} = \frac{1}{(\rho V)_{SXO}} W_S \left[(1-\beta_S)(T_{CSX1} - T_{CSXO}) + \beta_S (T_{CSXI} - T_{CSXO}) \right] \qquad 33)$$

The secondary hot leg pipe, with input T_{CSXO}, is simulated in the same way as the primary hot leg pipe. The time delay for the pipe is about 41 sec. Twenty-two nodes are used. The output from the pipe is T_{CSYI} (Temperature Coolant Secondary DHX Inlet). As the name specifies, this temperature forms the input to the secondary side of the DHX calculation.

The secondary side DHX calculation has the same form and the same approximations as the primary side IHX calculation, except that the DHX has no bypass flow. However, the parameters for

the DHX, such as the heat transfer coefficient, are significantly different from those of the IHX. The time constants for the secondary DHX plenums, both inlet and outlet, are about 1.5 sec (Equations 34 and 35). The output from the DHX secondary side calculation is T_{CSYO} (Temperature Secondary DHX Outlet).

$$\frac{dT_{CSY1}}{dt} = \frac{W_S}{(\rho V)_{SYI}} (T_{CSYI} - T_{CSY1}) \tag{34}$$

$$\frac{dT_{CSYO}}{dt} = \frac{W_S}{(\rho V)_{SYO}} (T_{CSY3} - T_{CSYO}) \tag{35}$$

T_{CSYO} is the input to the secondary cold leg pipe calculation. This calculation is performed in the same manner as the primary hot leg calculation. The time delay at full flow is about 47 sec. Twenty-five nodes simulate the pipe.

The tertiary (air) side of the DHX has an inlet temperature called T_{CTYI} (Temperature Coolant Tertiary DHX Inlet). This is the ambient air temperature and is determined by the requirements of the run being made. Unless specified otherwise, this temperature is taken to be 100 °F. There are no mixing plenums in the air side of the DKX. The heat transfer calculation uses the same finite differencing method explained previously (Equations 36, 37, 38, and 39). The parameters are such that the air side of the DHX has very short time constants in relation to the rest of the process.

$$(\rho V'C)_{SY} \frac{dT_{CSY2}}{dt} = \frac{C_{CSY}}{L_Y N_{MY}} (W_S)(T_{CSY1} - T_{CSY3}) - (UA')_Y (T_{CSY2} - T_{CTY2}) \tag{36}$$

$$(\rho V'C)_{TY} \frac{d_{CTY2}}{dt} = \frac{-C_{CTY}W_T}{L_Y} (T_{CTYO} - T_{CTYI})$$

$$- (UA')_Y(T_{CTY2} - T_{CSY2}) \quad (37)$$

$$(\rho V'C)_{SY} \frac{dT_{CSY3}}{dt} = \frac{C_{CSY}(W_S)}{L_Y N_{MY}} (4T_{CSY2} - 3T_{CSY3} - T_{CSY1})$$

$$- (UA')_Y(T_{CSY3} - T_{CTYI}) \quad (38)$$

$$(\rho V'C)_{TY} \frac{dT_{CTYO}}{dt} = \frac{C_{CTY}W_T}{L_Y} (4T_{CTY2} - 3T_{CTYO} - T_{CTYI})$$

$$- (UA')_Y(T_{CTY1} - T_{CSY1}) \quad (39)$$

The coolant flow dynamics are simulated with less accuracy than the rest of the process. Since the flow response is considerably faster than the response of the other components of the system, the system response is determined primarily by factors other than the flow response.

The primary flow dynamics were determined by performing a frequency response analysis using HYSIM-2A, which solves the dynamic flow and pump equations explicitly. HYSIM-2A simulates wound-rotor motor-driven pump. The frequency response was performed by varying the pump controller setpoint with a sine wave and measuring the primary flow. The frequency response showed that a first order lag would represent the portion of the flow dynamic range that coincided with the system dynamic range. A time constant of 2.27 sec was used for the first order lag as this gave the best fit of the frequency response data in the region of interest.

The response characteristics of the secondary flow were determined by analyzing the flow decay upon loss of power to the pump and by using information gained from the primary flow study. As in the case of primary flow, a first-order time lag provides adequate accuracy. The time constant for the lag is 4.5 sec.

The tertiary flow or air flow is not simulated dynamically. The calculation is purely algebraic; hence, the air flow setpoint determines the air flow instantaneously. There is not sufficient information available on the components that determine air flow dynamics to simulate this process accurately. The lack of a dynamic simulation of air flow may be a deficiency for secondary cold leg controller studies because the air flow response may be a significant part of the loop dynamics. For all the other studies performed, however, the algebraic air flow simulation will not cause a loss of accuracy. The air flow has been limited so that it cannot exceed 115% of its full-power, steady-state flow. This is done to simulate expected blower characteristics.

To provide a complete description of the simulation, it is necessary to furnish some detail concerning computational techniques. The division of responsibility between the analog and digital is such that each machine has partial control of the operating mode. The digital computer controls the problem time scale and puts the problem in initial condition (IC) during the initialization phase of the program. The analog computer controls the operate, hold, and IC parts of the mode after the initialization phase.

The highest speed that the problem can run in is X1000. Time scales of X10 and X100 are also available. Programming care was especially required for the fastest time scale of X1000 so that the digital computer was not included in a fast problem loop, even for digital calculations that required little time. At the highest speed, the time to convert the signal from analog to digital and back again can cause a significant phase shift in the system. However, the analog-to-digital and digital-to-analog conversions are rather a small portion of the distance/velocity lags, even in X1000; thus, these lags are a good application for the digital computer.

The pots labeled DCU on Figure A-19 (see page A-35) are digital coefficient units. They are special pots that can be updated from the digital computer while the problem is running. These pots are used in the mixing plenum calculations. The pot setting is proportional to the flow in that plenum.

The digital flow integration is performed using a rectangular integration routine. At uniform time intervals, this program multiplies the flow by a constant factor which includes the size of the time step and the integration gain. The product is added to the result from previous integration steps (Equation 40). The summation is then checked to see if it equals or is greater than the mass of sodium in one node. If the integration has filled the node it is time to update the time delay and initialize the integration. The integration is initialized by subtracting the nodal mass from integrated flow value that was just found to cause the node to overflow. The difference represents sodium that spilled over into the next node in the last integration step. It is saved and added to the first integration for the next node.

$$\int_o^T W_p dt = \sum_{t=o}^{t=T} W_p \Delta t \qquad (40)$$

The analog circuit diagrams have been included to provide additional detail concerning the simulation (Figures A-13 through 21). Several points need to be explained for the diagrams to be understood thoroughly. Most of the inputs to amplifiers on the analog used must be current inputs as there are very few input resistors associated with the amplifiers. Since the pots are current pots, inputs to an amplifier are often fed through a pot, even though the coefficient on the input is one. In these cases, a V-to-I designation has been used for that pot, specifying that the function of the pot is to convert a voltage signal to an equivalent current signal. All of the

analog amplifiers used are bipolar amplifiers, meaning that these amplifiers have an inverted and a noninverted output signal. The mode of the amplifiers can be changed so that they behave as conventional single pole amplifiers. A designation system to show the polarity of the output in relation to the input has been used for the circuit diagrams. A minus sign by an output from the amplifier designates that a phase inversion occurs in the amplifier. A plus sign by the output indicates that there is no inversion. When an amplifier has a noninverted output there must also be an inverted output. This is represented by two wires leading from the amplifier, one marked (+) and the other marked (-). The pots that set the initial conditions for the integrators have not been shown to conserve space on the circuit diagrams.

It was necessary to develop a method to show continuity when a diagram used more than one sheet. Hexagonal boxes with numbers in them were used. Any boxes with the same number are connected directly or are connected through a time delay in the digital computer. Those boxes that are directly connected have the same symbol beside them while those connected through a time delay have different symbols. The reason for this is that a different designation is used for a temperature entering a time delay than for a temperature leaving the time delay. In cases where boxes have the same number, numbers specifying figures are provided.

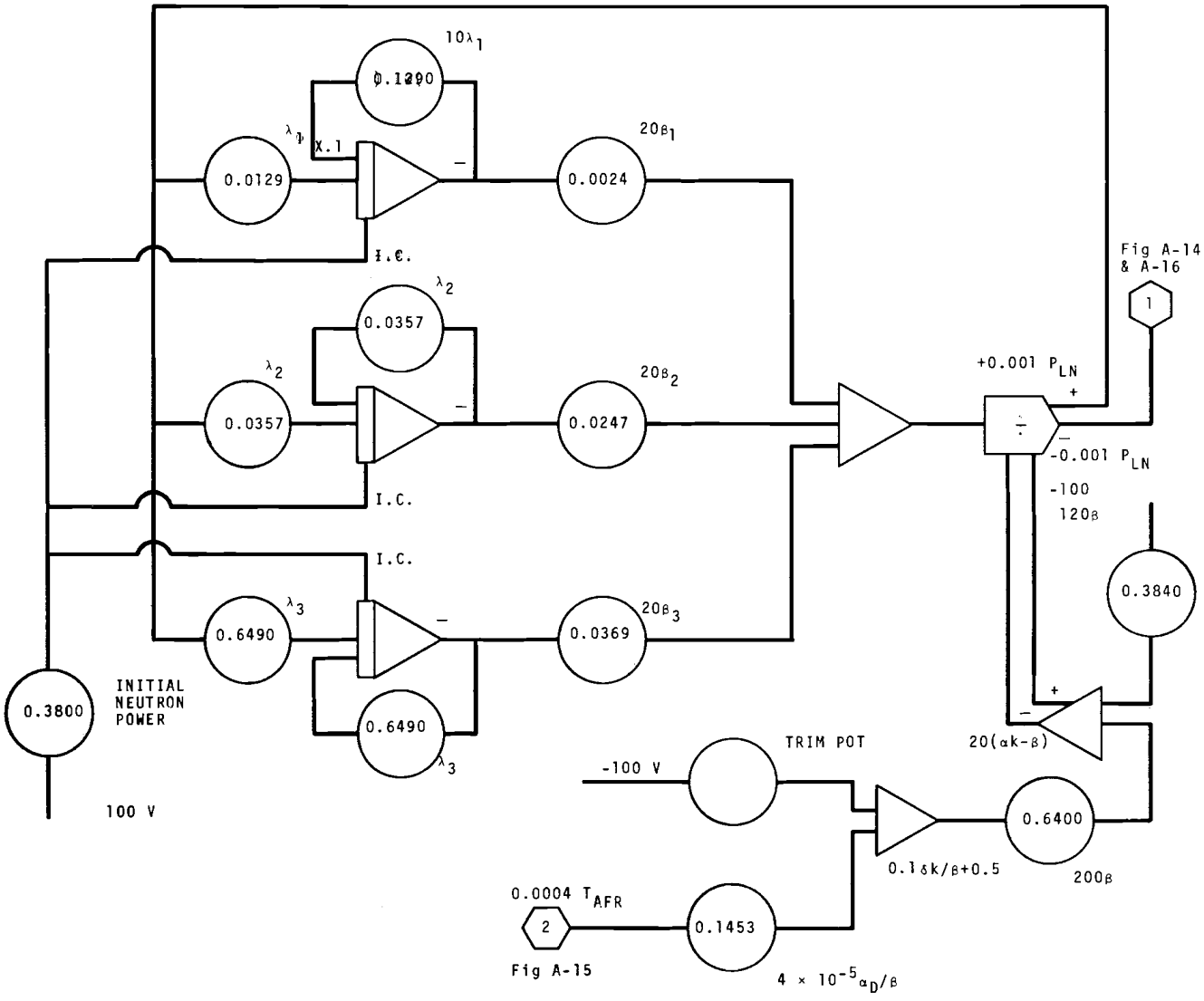

FIGURE A-13. Reactor Kinetics

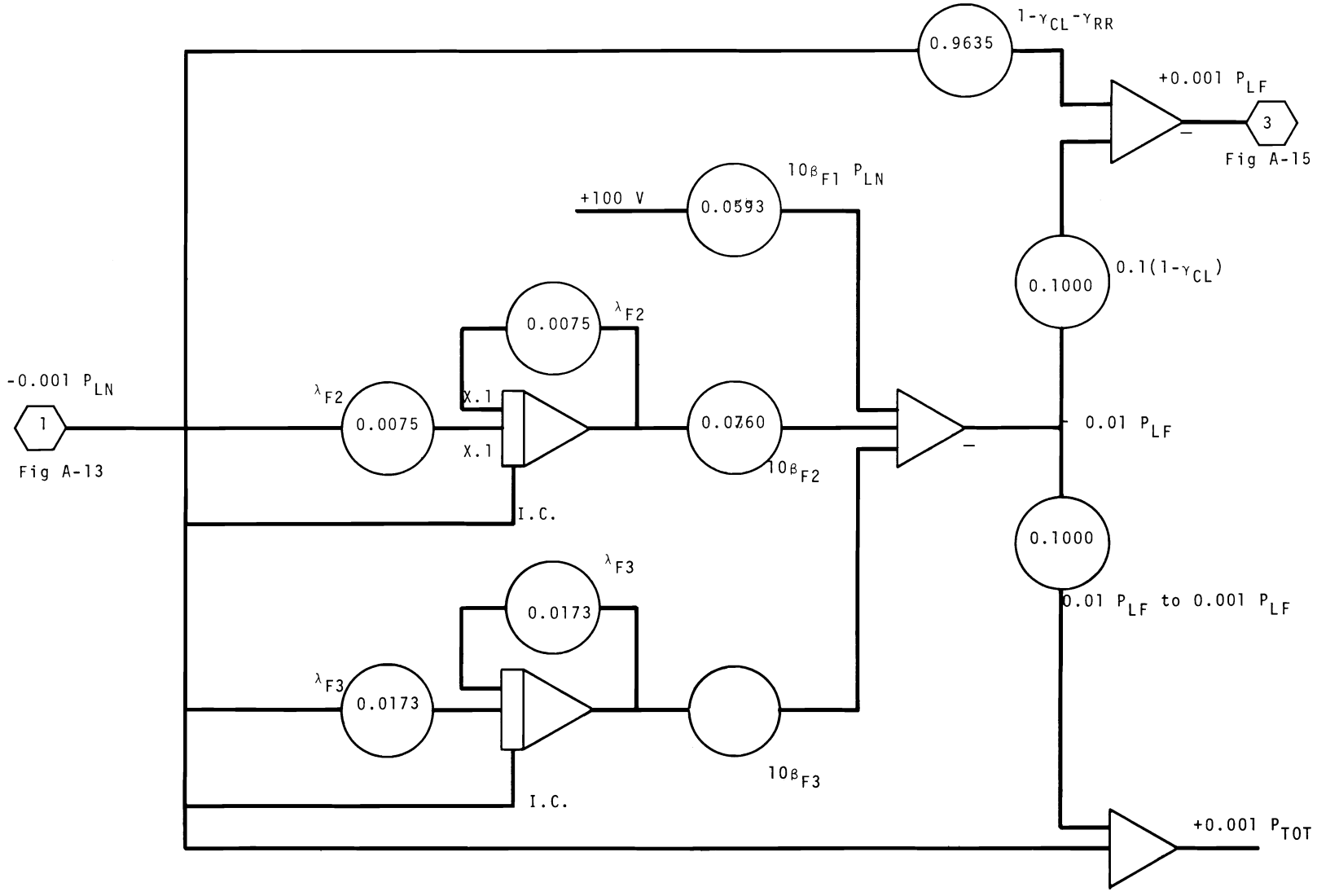

FIGURE A-14. Reactor Kinetics

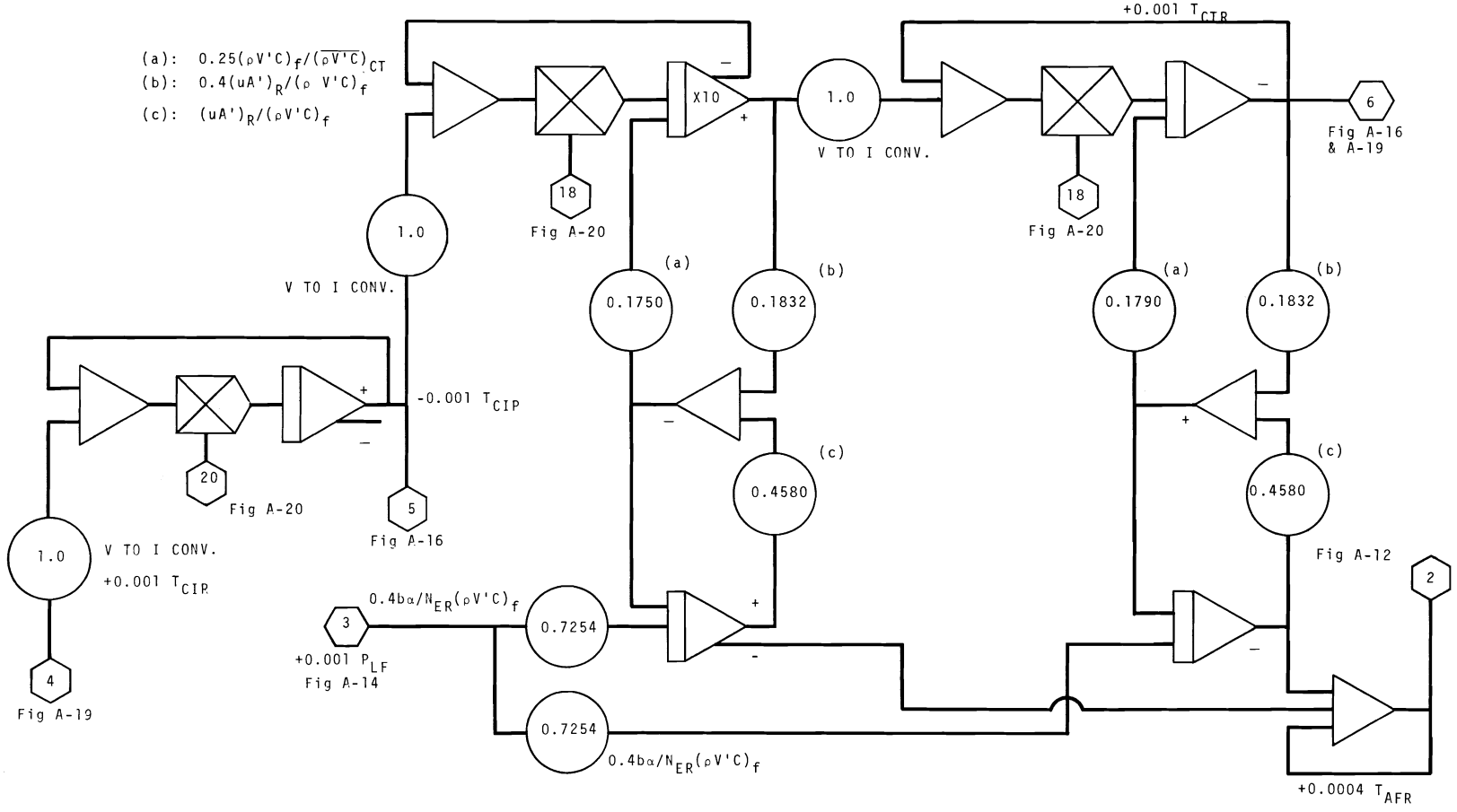

FIGURE A-15. Reactor Dynamics

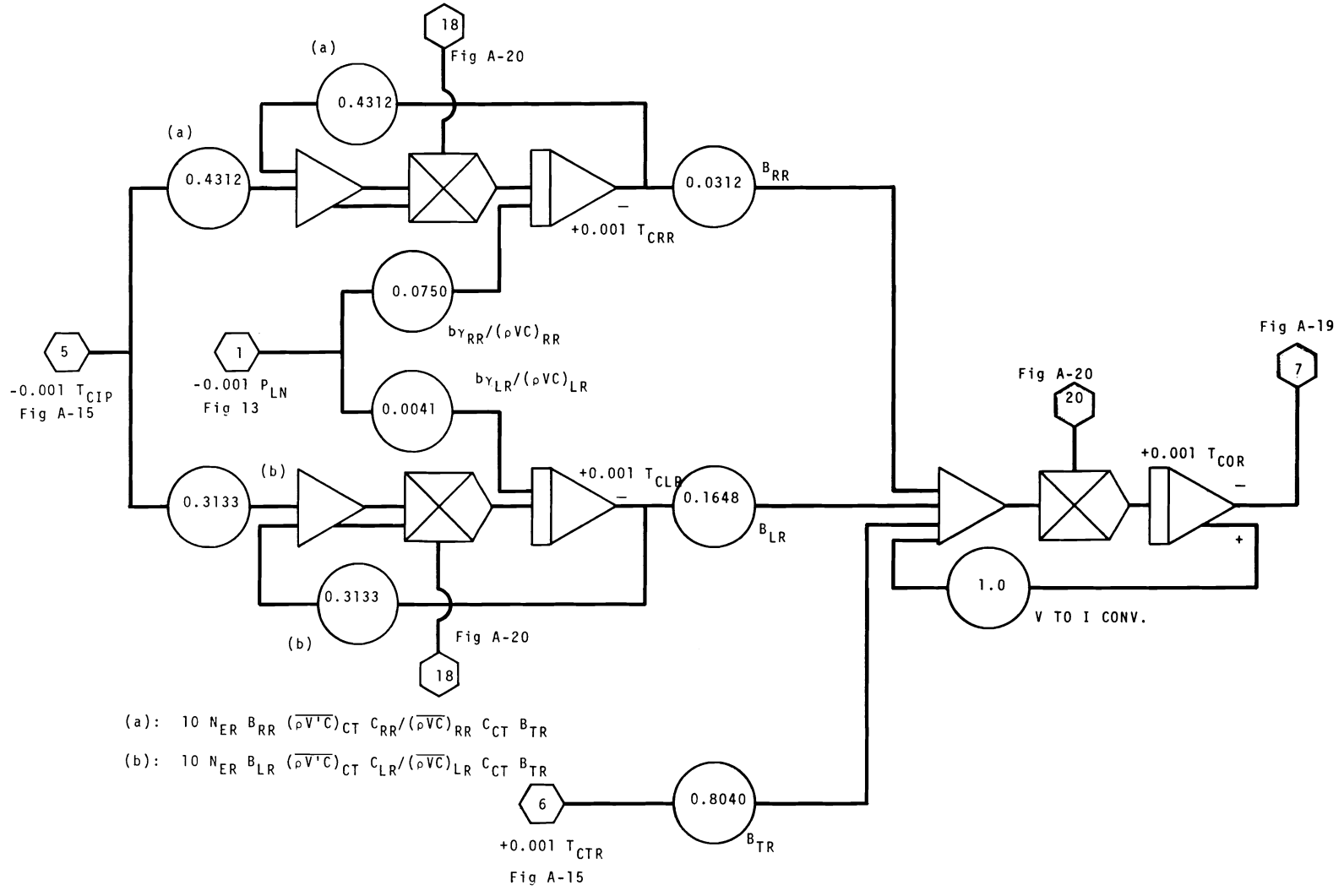

FIGURE A-16 Reactor Dynamics

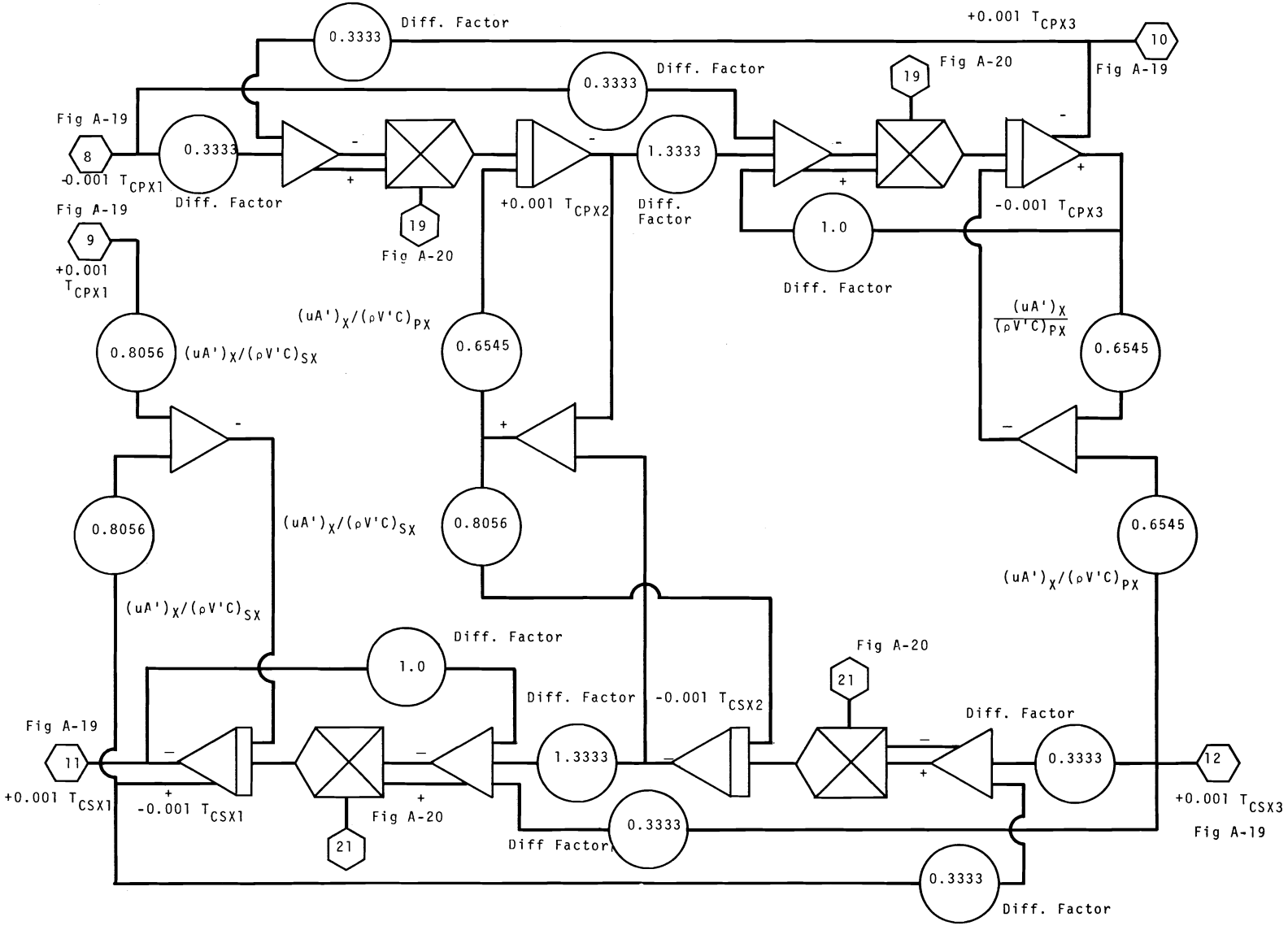

FIGURE A-17 IHX

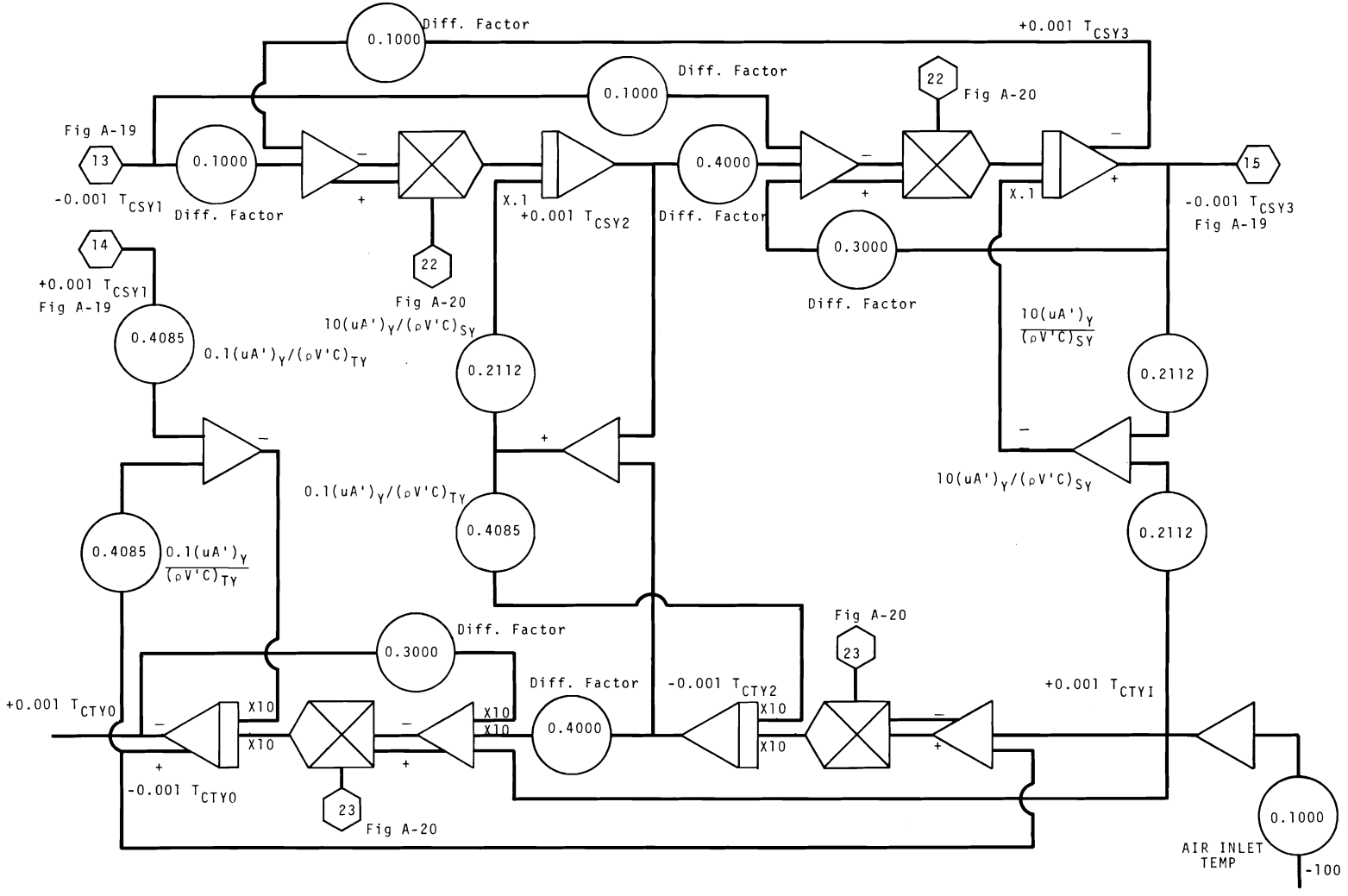

FIGURE A-18. DHX

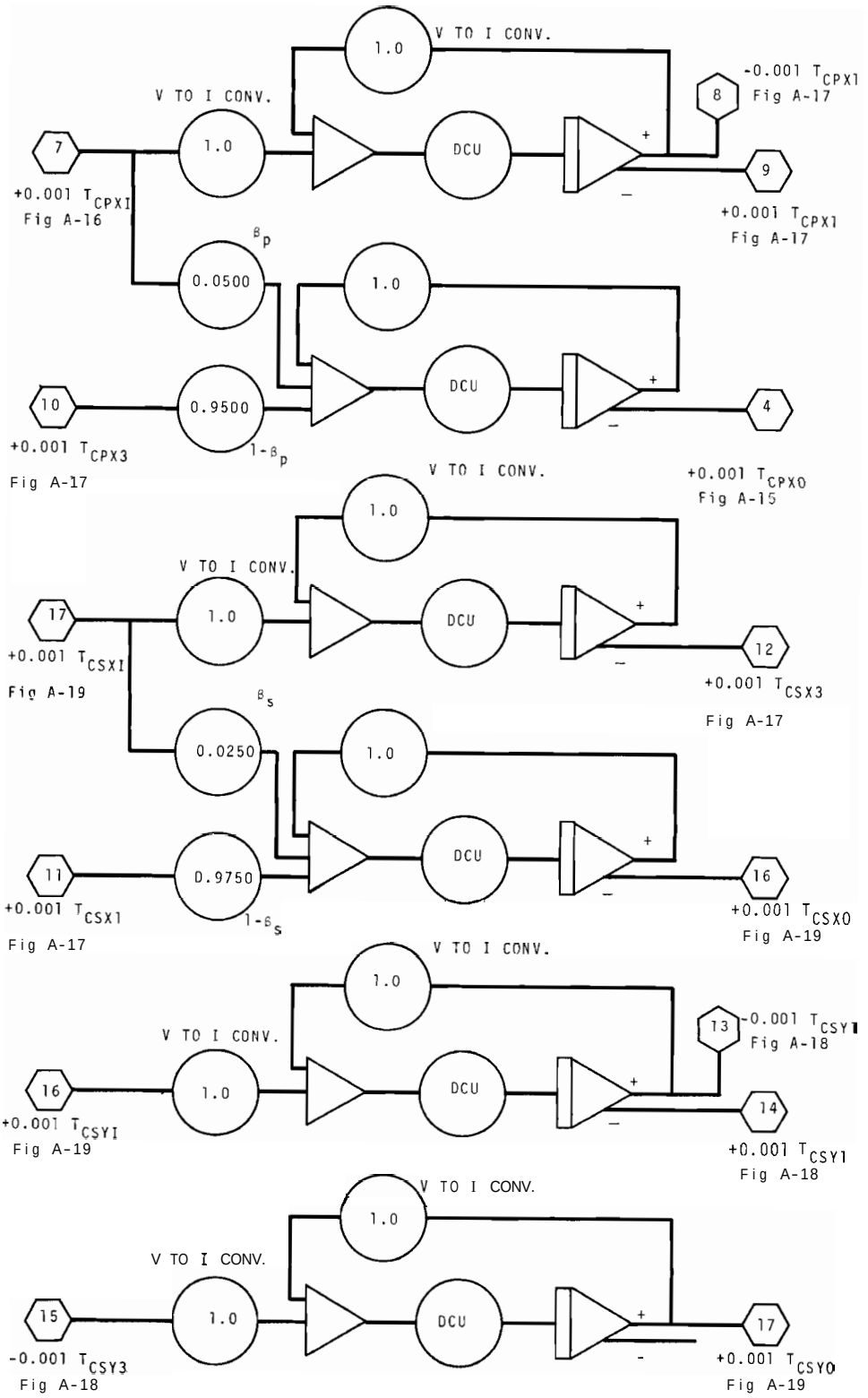

FIGURE A-19. Mixing Plenums

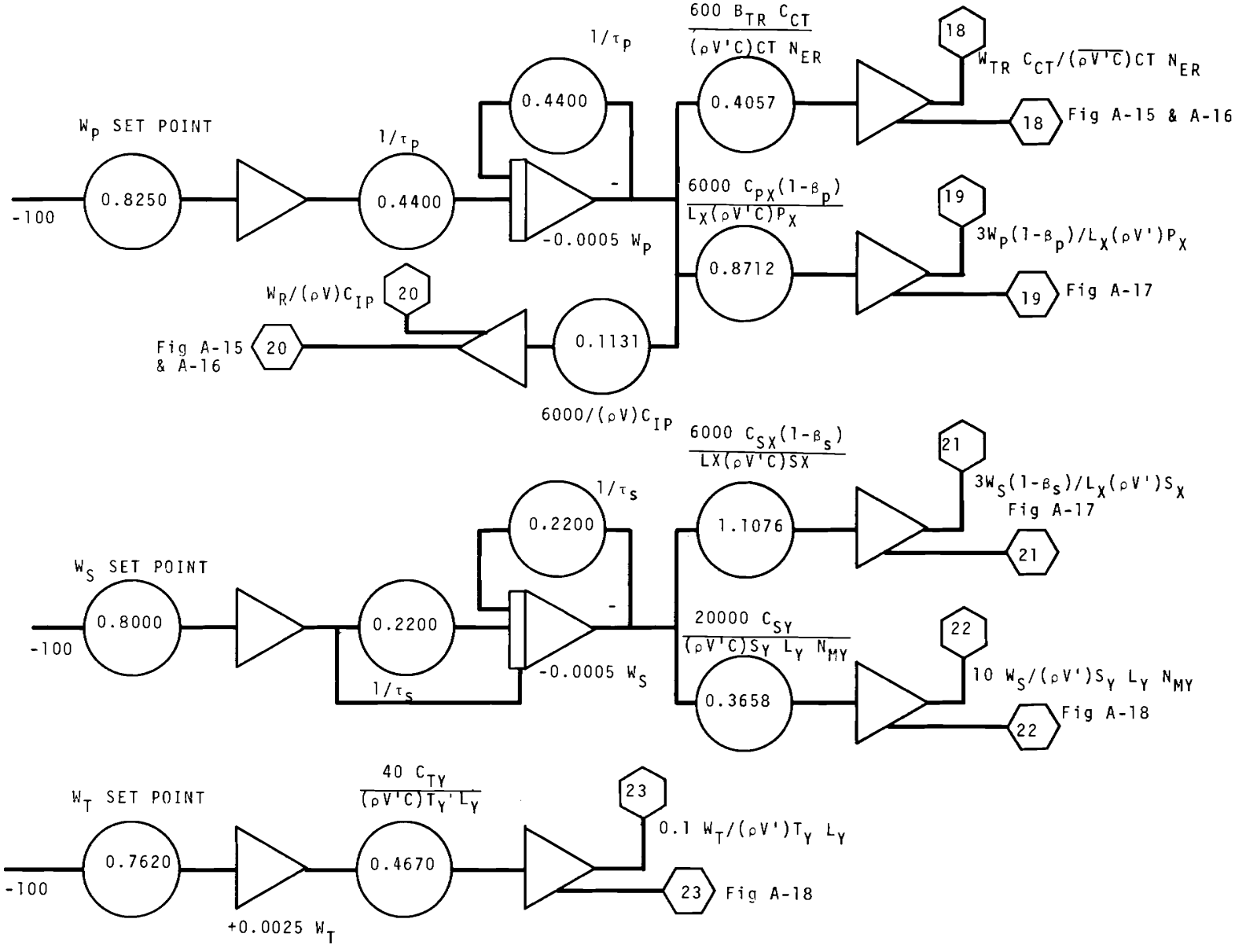

FIGURE A-20 Flow Calculation

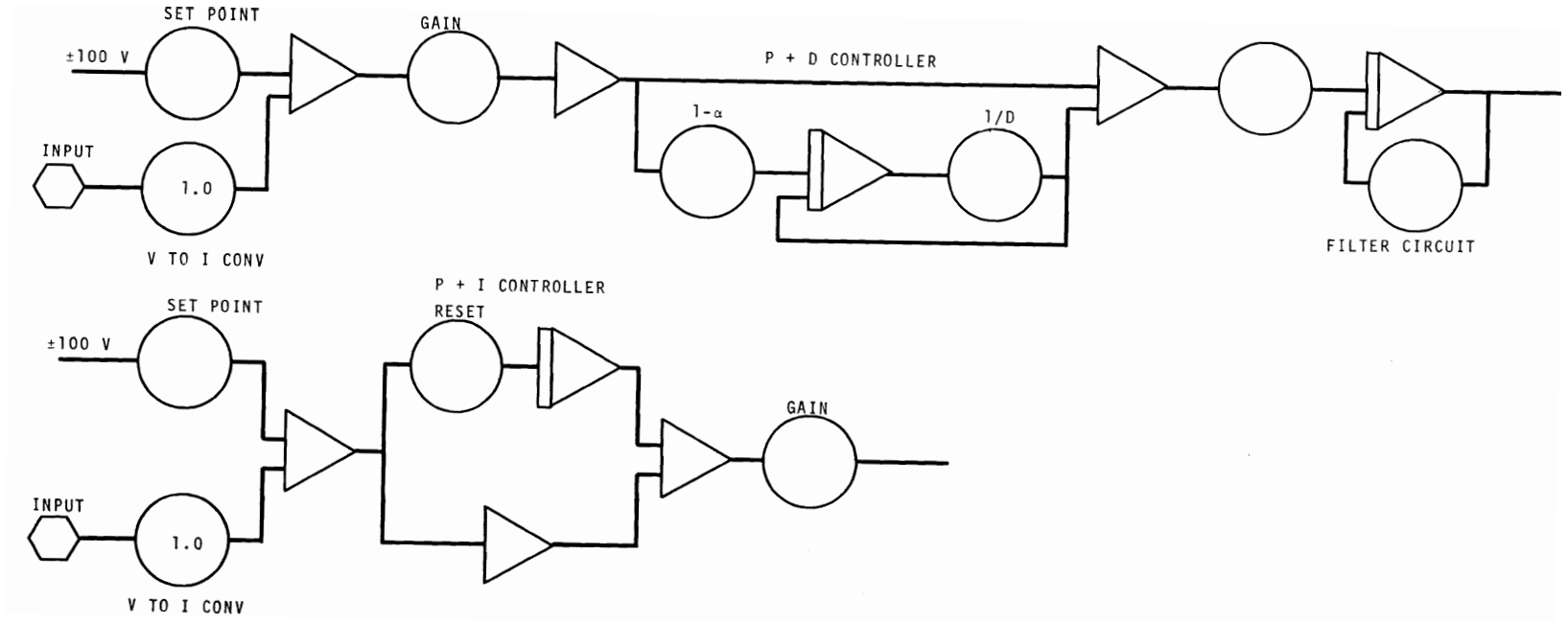

FIGURE A-21. Controllers

The scaling used for the variables on the analog circuit diagrams treats 100 V as unity. The units for the values shown are given in Table A-1.

TABLE A-1.

Symbol	Explanation	Value	
b	Conversion from MW to Btu/sec	948 Btu/sec-MW	
B_{LR}	Ratio of leakage flow to reactor flow	0.1648	
B_{RR}	Ratio of radial reflector flow to reactor flow	0.0312	
B_{TR}	Ratio of Driver Fuel (Tube) Coolant flow to reactor flow	0.804	
$C_{1,2,3}$	Delayed Neutron Precursor Concentration		
C_{CIP}	Specific heat of reactor inlet plenum sodium	0.311	Btu/lb-°F
C_{CLR}	Specific heat of the leakage coolant sodium	0.311	Btu/lb-°F
C_{CP}	Specific heat of primary sodium in the general heat transfer equation		Btu/lb-°F
C_{CPX}	Specific heat of primary **IHX** sodium	0.307	Btu/lb-°F
C_{COR}	Specific heat of reactor outlet plenum	0.304	Btu/lb-°F
C_{CRR}	Specific heat of the radial reflector coolant sodium	0.307	Btu/lb-°F
C_{CS}	Specific heat of secondary sodium in the general heat transfer equation		Btu/lb-°F
C_{CSX}	Specific heat of secondary **IHX** sodium	0.309	Btu/lb-°F
C_{CSY}	Specific heat of secondary **DHX** sodium	0.309	Btu/lb-°F
C_{CT}	Specific heat of Driver Fuel (Tube) coolant sodium	0.307	Btu/lb-°F

TABLE A-1 (contd)

Symbol	Explanation	Value
C_{CTY}	Specific heat of DHX air	0.255 Btu/lb-°F
G	Flow integration gain factor	
ℓ^*	Neutron lifetime	3.5×10^{-7} sec
L_X	Effective IHX tube length	15 ft
L_Y	Effective DHX tube length	120 ft
P_{LCL}	Power generated in the closed loops	MW
P_{LF}	Power generated in the driver fuel	MW
P_{LFP}	Power generated by decaying fission products	MW
$P_{LFP1,2,3}$	Power generated by the individual fission product groups	MW
P_{LLR}	Power generated in the leakage region	MW
P_{LN}	Power generated immediately by fission	MW
P_{LRR}	Power generated in the radial reflector	MW
P_{LTOT}	Total power generated in the reactor	MW
N_{ER}	Number of equivalent reactor channels**	78.25
N_{MY}	Number of DHX modules per circuit	4
t	Time	sec
T	Time at the end of one flow integration	sec
T_{AFR}	Average Fuel Temperature	°F
T_{AFRZ}	Steady state average fuel temperature	°F

** *N_{ER} includes driver fuel channels and open test positions. Each open test position contributes three fourths to N_{ER} while each driver fuel channel contribute one. It is expected that an open test position will generate about three fourths the power of a driver fuel assembly.*

TABLE A-1. (contd)

Symbol	Explanation	Value
T_{CIP}	Temperature of the coolant leaving the inlet plenum	°F
T_{CIR}	Temperature of the coolant entering the reactor	°F
T_{CLR}	Temperature of the coolant leaving the leakage region	°F
T_{COR}	Temperature of the coolant leaving the reactor	°F
T_{CPX1}	Temperature of the coolant entering the 1st primary IMX heat transfer node**	°F
T_{CPX2}	Temperature of the coolant entering the 2nd primary IHX heat transfer node	°F
T_{CPX3}	Temperature of the coolant leaving the 2nd primary IHX heat transfer node	°F
T_{CPXI}	Temperature of the coolant entering the primary side of the IHX	°F
T_{CPXO}	Temperature of the coolant leaving the primary side of the IHX	°F
T_{CRR}	Temperature of the coolant leaving the radial reflector region	°F
T_{CSX1}	Temperature of the coolant leaving the 2nd secondary IHX heat transfer node	°F
T_{CSX2}	Temperature of the coolant entering the 2nd secondary IHX heat transfer node	°F
T_{CSX3}	Temperature of the coolant entering the 1st secondary IHX heat transfer node	°F
T_{CSXI}	Temperature of the coolant entering the secondary side of the IHX	°F
T_{CSXO}	Temperature of the coolant leaving the secondary side of the IHX	°F
T_{CSY1}	Temperature of the coolant entering the 1st secondary DHX heat transfer node	°F
T_{CSY2}	Temperature of the coolant entering the 2nd secondary DHX heat transfer node	°F
T_{CSY3}	Temperature of the coolant leaving the 2nd secondary DHX heat transfer node	°F

** *The nodes are numbered in the direction of flow.*

TABLE A-1. (contd)

Symbol	Explanation	Value
T_{CSYI}	Temperature of the coolant entering the secondary side of the DHX	°F
T_{CSYO}	Temperature of the coolant leaving the secondary side of the DHX	°F
T_{CT1}	Temperature of the driver fuel (tube) coolant leaving the 1st node	°F
T_{CTR}	Temperature of the driver fuel (tube) coolant leaving the driver ducts	°F
T_{CTY2}	Temperature of the coolant entering the air DHX heat transfer node	°F
T_{CTYI}	Temperature of the coolant entering the air side of the DHX	°F
T_{CTYO}	Temperature of the coolant leaving the air side of the DHX	°F
T_{f1}	Radially averaged fuel temperature at the outlet of the 1st fuel node	°F
T_{f2}	Radially averaged fuel temperature at outlet of the 2nd fuel node	°F
T_p	Temperature of the primary coolant for the general heat transfer equation	°F
T_S	Temperature of the secondary coolant for the general heat transfer equation	°F
(UA')	Heat transfer coefficient times heat transfer area for the general heat transfer equation	Btu/°F-sec ft
$(UA'')_R$	Heat transfer coefficient times heat transfer area per driver element per node for fuel to coolant heat transfer	1.53 Btu/°F-sec node element
$(UA')_X$	Heat transfer coefficient times heat transfer area per axial foot for IHX heat transfer	87.6 Btu/°F-sec ft
$(UA')_Y$	Heat transfer coefficient times heat transfer area per axial foot for DHX heat transfer	0.744 Btu/°F-sec ft
W_{LR}	Leakage Flow	lb/sec

TABLE A–1. (contd)

Symbol	Explanation	Value
W_P	Primary Flow	lb/sec
W_R	Reactor Flow	lb/sec
W_{RR}	Radial Reflector Flow	lb/sec
W_S	Secondary Flow	lb/sec
W_T	Air (tertiary) Flow	lb/sec
W_{TR}	Driver Fuel duct (tube) flow	lb/sec
X	Axial distance along heat exchange surface	ft
	Fraction of power generated in a fuel node	0.5
α_D	Doppler coefficient	-1.86×10^{-6}/°F
β	Fraction of total neutrons that are delay neutrons	0.0032
β_1	Delay neutron fraction for the 1st group	0.000122
β_2	Delay neutron fraction for the 2nd group	0.00123
β_3	Delay neutron fraction for the 3rd group	0.001845
β_{FP1}	Fraction of total power contributed by 1st fission product group	0.0156
β_{FP2}	Fraction of total power contributed by 2nd fission product group	0.0076
β_{FP3}	Fraction of total power contributed by 3rd fission product group	0.0158
β_P	Fraction of primary flow that bypasses the IHX	0.05
β_S	Fraction of secondary flow that bypasses the IHX	0.025
γ_{CL}	Fraction of total power generated in the closed loops	0
γ_{LR}	Fraction of total power generated in the leakage region	0.0105

TABLE A-1. (contd)

Symbol	Explanation	Value
γ_{RR}	Fraction of total power generated in the radial reflector	0.026
δK	Total change in reactivity	¢
δK_C	Change in reactivity introduced by the operator	¢
λ_1	Decay constant for the 1st delay neutron group	0.0129/sec
λ_2	Decay constant for the 2nd delay neutron group	0.0357/sec
λ_3	Decay constant for the 3rd delay neutron group	0.649/sec
λ_{FP1}	Decay constant for the 1st fission product group	1.02×10^{-4}/sec
λ_{FP2}	Decay constant for the 2nd fission product group	7.5×10^{-4}/sec
λ_{FP3}	Decay constant for the 3rd fission product group	1.73×10^{-2}/sec
$(\rho V)_{PXI}$	IHX primary inlet plenum volume times sodium density	2092 lb
$(\rho V)_{PXO}$	IHX primary outlet plenum volume times sodium density	3536 lb
$(\rho V)_{SXI}$	IHX secondary inlet plenum volume times sodium density	5775 lb
$(\rho V)_{SXO}$	IHX secondary outlet plenum volume times sodium density	2915 lb
$(\rho V)_{SYI}$	DHX secondary inlet plenum volume times sodium density	2650 lb
$(\rho V)_{SYO}$	DHX secondary outlet plenum volume times sodium density	2750 lb
$(\overline{\rho V''C})_{CT}$	Averaged density, volume, specific heat term for the driver fuel coolant, calculated per driver element per node	4.67 Btu/°F node element
$(\overline{\rho V''C})_f$	Density, volume, specific heat term for the driver fuel, calculated per driver element per node	3.34 Btu/°F node element

TABLE A-1. (contd)

Symbol	Explanation	Value
$(\rho VC)_{IP}$	Density, volume specific heat term for the inlet plenum calculation	16,500 Btu/°F
$(\overline{\rho VC})_{LR}$	Averaged density, volume, specific heat term for the leakage region calculation	2420 Btu/°F
$(\rho VC)_{OR}$	Density, volume, specific heat term for the outlet plenum calculation	15,900 Btu/°F
$(\rho V'C)_{P}$	Density, volume, specific heat term for the general primary IHX equation	Btu/°F f t
$(\rho V'C)_{PX}$	Density, volume, specific heat term per axial foot for primary IHX heat transfer region	134 Btu/°F ft
$(\overline{\rho VC})_{RR}$	Averaged density volume specific heat term for the radial reflector region	328 Btu/°F
$(\rho V'C)_{S}$	Density, volume, specific heat term for the general secondary IMX equation	Btu/°F ft
$(\rho V'C)_{SX}$	Density, volume specific heat term per axial foot for secondary IHX heat transfer region	109 Btu/°F ft
$(\rho V'C)_{SY}$	Density, volume, specific heat term per axial foot for secondary DHX heat transfer region	32.2 Btu/°F ft
$(\rho V'C)_{TY}$	Density, volume, specific heat term per axial foot for tertiary (air) DMX heat transfer region.	0.182 Btu/°F ft

REFERENCES

1. C. D. Flowers and L. H. Gerhardstein. Analog-Hybrid Dynamic Simulation of the FFTF Reactor and Heat Transport System, BNWL-707. Battelle-Northwest, Richland, Washington, April 1968.

2. A. L. Gunby and G. A. Worth. "Hybrid Simulation in FFTF System Conceptual Design," The Effective Use of Computers in the Nuclear Industry, Knoxville, April 21-23, 1969, CONF-690401, pp. 415-432. Division of Technical Information Extension, Oak Ridge, Tennessee, 1969.

3. W. L. Bunch and L. D. O'Dell. Fission Product Inventory and Decay Heat Associated with FTR Fuel, BNWL-961. Battelle-Northwest, Richland, Washington, February 1969.

DISTRIBUTION

No. of Copies

OFFSITE

1 AEC Chicago Patent Group
G. H. Lee, Chief

27 AEC Division of Reactor Development and Technology
Director, RDT
Asst Dir for Nuclear Safety
Analysis & Evaluation Br, RDT:NS
Asst Dir for Plant Engrg, RDT
Facilities Br, RDT:PE
Components Br, RDT:PE
Instrumentation & Control Br, RDT:PE
Liquid Metal Systems Br, RDT:PE
Asst Dir for Program Analysis, RDT
Asst Dir for Project Mgmt, RDT
Liquid Metals Projects Br, RDT:PM
G. J. Mishko
FFTF Project Manager, RDT:PM
Asst Dir for Reactor Engrg, RDT
Control Mechanisms Br, RDT:RE
Core Design Br, RDT:RE (2)
Fuel Engineering Br, RDT:RE
Fuel Handling Br, RDT:RE
Reactor Vessels Br, RDT:RE
Coolant Chemistry Br, RDT:RT
Fuel Recycle Br, RDT:RT
Fuels & Materials Br, RDT:RT
Reactor Physics Br, RDT:RE
Special Technology Br, RDT:RT
Asst Dir for Engrg Standards, RDT
Manager, RDT:PM
LMFBR Program

212 AEC Division of Technical Information Extension

1 AEC Idaho Operations Office
Nuclear Technology Division
C. W. Bills, Director

1 AEC San Francisco Operations Office
Director, Reactor Division

No. of Copies	
5	AEC Site Representatives Argonne National Laboratory - CH Argonne National Laboratory - ID Atomics International General .Electric Co. Westinghouse Electric Corporation
3	Argonne National Laboratory R. A. Jaross LMFBR Program Office N. J. Swanson
1	Atomic Power Development Assoc. Document Librarian
5	Atomics International FFTF Program Office
2	Babcock & Wilcox Co. Atomic Energy Division S. H. Esleeck G. B. Garton
1	Bechtel Corporation J. J. Teachnor
1	Combustion Engineering 1000 MWe Follow-On Study W. P. Staker, Project Kanager
1	Combustion Engineering Mrs. Nell Iiolder, Librarian
3	General Electric Company Advanced Products Operation Karl Cohen

No. of Copies

1 General Electric Company
Nucleonics Laboratory
Dr. H. W. Alter, Mgr.
P.O. Box 846
Pleasanton, Calif. 94566

2 Gulf General Atomic Inc.
General Atomic Division
D. Coburn

1 Idaho Nuclear Corporation
J. A. Buckham

1 Liquid Metal Engineering Center
R. W. Dickinson

2 Liquid Metal Information Center
A. E. Miller

1 Oak Ridge National Laboratory
W. O. Harms

1 Stanford University
Nuclear Division
Division of Mechanical Engrg
R. Sher

1 United Nuclear Corporation
Research and Engineering Center
R. F. DeAngelis

1 WADCO Representative
R. M. Fleishman (ZPPR)

4 Westinghouse Electric Corporation (AEC)
W. Frisch
F. M. Heck
T. B. McCall
R. Span

15 Westinghouse Electric Corporation
Atomic Power Division
Advanced Reactor Systems
D. C. Spencer

No. of Copies

ONSITE-HANFORD

1 AEC Chicago Patent Group

R. K. Sharp

2 RDT Assistant Director for Pacific Northwest Laboratories

3 AEC Richland Operations Office

J. B. Kitchen
J. M. Shivley (2)

3 Gattelle Memorial Institute

1 Bechtel Corporation

W. A. Smith (Richland)

84 WADCO Corporation

G. J. Alkire
H. J. Anderson
S. O. Arneson
J. M. Atwood
J. M. Batch
A. L. Bement Sr.
D. C. Boyd
C. P. Cabell
J. R. Carrel1
W. L. Chase
J. C. Cochran
G. S. Cochrane
W. Dalos
W. H. Esselman
E. A. Evans
W. M. Gajewski
A. L. Gunby
L. D. Gustafson
J. W. Hagen
K. M. Harmon
R. A. Harvey (10)
E. N. Heck
R. E. Heineman
R. J. Hennig
S. A. Hunt (5)
H. G. Johnson
J. N. Judy
F. J. Leitz
W. B. McDonald
J. S. McMahon
J. W. Mitchell
J. Muraoka
J. M. Norris
R. E. Peterson
B. G. Rieck
W. E. Roake
G. J. Rogers
P. F. Shaw
W. F. Sheely
J. R. Sheff (2)
D. E. Sinpson (3)
D. D. Stepnewski (4)
C. D. Swanson
K. G. Toyoda
L. D. Turner
J. H. Westsik
B. Wolfe
G. A. Worth
W. R. Wykoff
WADCO Document Control (15)
WADCO Tech Pubs (703)

No. of Copies

39 Battelle-Northwest

F. W. Albaugh
J. L. Bates
A. L. Bement
D. C. Boyd
T. D. Chikalla
P. D. Cohn
G. M. Dalen
J. M. Davidson
F. G. Dawson
D. R. de Halas
G. E. Driver
K. Drumheller
L. M. Finch
J. C. Fox
W. L. Hampson
H. Marty
G. M. Hesson
D. C. Lehfeldt
C. W. Lindenmeier
R. P. Marshall
R. E. Nightingale
L. T. Pederson
W. D. Richmond
L. C. Schmid
G. L. Tingey
R. G. Wheeler
F. G. Williams
N. G. Wittenbrock
F. W. Woodfield
Technical Information (5)
Technical Publication (3)
Legal - 703 Bldg.
Legal - ROB